GOETHE UNIVERSITÄT FRANKFURT AM MAIN

Engineering and stabilization of the heterodimeric ABC exporters TAP and TmrAB for functional and structural studies

Dissertation
zur Erlangung des Doktorgrades
der Naturwissenschaften

vorgelegt beim Fachbereich
Biochemie, Chemie und Pharmazie
der Johann Wolfgang Goethe-Universität
in Frankfurt am Main

von

Valentina Herbring
aus Münster (NRW)

Frankfurt am Main 2019
(D30)

vom Fachbereich Biochemie, Chemie und Pharmazie der Johann Wolfgang Goethe-Universität als Dissertation angenommen.

Dekan: Prof. Dr. Clemens Glaubitz

1. Gutachter: Prof. Dr. Robert Tampé
2. Gutachter: Jun. Prof. Dr. Inga Hänelt

Datum der Disputation:

Results and parts of this work were published in the following articles:

- Valentina Herbring, Anja Bäucker, Simon Trowitzsch and Robert Tampé (2016)
  A dual inhibition mechanism of herpesviral ICP47 arresting a conformationally thermostable TAP complex.
  Sci Rep 6: 36907, DOI: 10.1038/srep36907

- Anne Nöll*, Christoph Thomas*, Valentina Herbring*, Tina Zollmann, Katja Barth, Ahmad Reza Mehdipour, Thomas M. Tomasiak, Stefan Brüchert, Benesh Joseph, Rupert Abele, Vincent Oliéric, Meitian Wang, Kay Diederichs, Gerhard Hummer, Robert M. Stroud, Klaas M. Pos, and Robert Tampé (2017)
  Crystal structure and mechanistic basis of a functional homolog of the antigen transporter TAP.
  Proc Natl Acad Sci USA 114: E438-E447, DOI: 10.1073/pnas.1620009114

- Andreas Hinz, Johanna Jedamzick, Valentina Herbring, Hanna Fischbach, Jessica Hartmann, David Parcej, Joachim Koch and Robert Tampé (2014)
  Assembly and function of the major histocompatibility complex (MHC) I peptide-loading complex are conserved across higher vertebrates.
  J Biol Chem 289: 33109-33117, DOI: 10.1074/jbc.M114.609263

- Markus Braner, Nicole Koller, Julia Knauer, Valentina Herbring, Susanne Hank, Ralph Wieneke, Robert Tampé (2019)
  Optical control of the antigen translocation by synthetic photo-conditional viral inhibitors.
  Chem Sci 10: 2001-2005, DOI: 10.1039/C8SC04863K

* contributed equally to this work

Declaration

Except where stated otherwise by reference or acknowledgment, the work presented was generated by myself under the supervision of my advisors during my doctoral studies. All contributions from colleagues are explicitly referenced in the thesis. The material listed below was obtained in the context of collaborative research:

Figure 3.4 D: Free ICP47 constructs and SR mutants. In-gel analysis was done by practical bachelor student Carolina Kuge (Institute of Biochemistry, Goethe University Frankfurt) under my supervision. I assembled the figure.

Figure 3.10: The stabilizing region of ICP47 is essential for interaction with coreTAP. ICP47/coreTAP expression, purification and SEC analysis were done by practical bachelor student Carolina Kuge (Institute of Biochemistry, Goethe University Frankfurt) under my supervision. Melting temperature calculation was performed by Carolina Kuge and myself. I assembled the figure.

Figure 3.11: CoreTAP melting temperature determined by nanoDSF. ICP47/-coreTAP expression, purification, and melting temperature determination was performed by myself with the support of Nano-Temper Technologies, München. Nano-Temper Technologies provided the raw data. I processed the data and assembled the figure.

Figure 3.14: ICP47-coreTAP complexes arrest a conformation excluding viral proteins from binding. Co-immunoprecipitation and in-gel analysis performed by practical master student Anja Bäucker (Institute of Biochemistry, Goethe University Frankfurt) under my supervision. I assembled the figure.

Figure 3.15: ICP47 stabilizes coreTAP. Negative-stain EM analysis was done by Susanne Hofmann (Institute of Biochemistry, Goethe University, Frankfurt). Equipment was provided by Werner Kühlbrandt (Max Planck Institute of Biophysics, Frankfurt). I prepared the samples and assembled the figure.

Figure 3.27: TmrA/TMD02-TmrB partially colocalizes with ER marker PDI. Immunofluorescence microscopy was done by Philipp Graab (Institute of Biochemistry, Goethe University, Frankfurt). Cell transfection, staining and the calculation of Pearson's correlation coefficients was done by myself. I assembled the figure.

Whenever a figure, table or text is identical to a previous publication, it is stated explicitly in the thesis that copyright permission and/or co-author agreement has been obtained.

The following parts of the thesis have been previously published:

section	**figure**	**publication**
3.1.1 - 3.1.5, 3.1.8, 4.1, 4.2, 4.3	3.1, 3.2, 3.3A, 3.4B, 3.5B, 3.6B, 3.7, 3.8A-C, 3.10, 3.13, 3.14, 4.1	Herbring *et al.* 2016 [1]
3.4.2	3.26	Nöll *et al.* 2017 [2]
	3.21B	V. Herbring, Master Thesis [3]

Contents

Summary

As central component of the peptide loading complex, the ABC transporter TAP is a key player in the adaptive immune response. By recognizing and translocating antigenic peptides derived from proteasomal degradation into the ER lumen it connects the processing of harmful intruders and the marking of an infected cell for elimination. This work focused mainly on the interaction between TAP and one of its viral inhibitors. Of the five known TAP inhibitors, ICP47 is the only one that is not anchored in the ER membrane and has a nonomolar affinity to TAP. These properties and its specific architecture make it an interesting protein engineering tool that can be used in a variety of ways to generate functionally arrested TAP complexes. Different lengths of ICP47 were chosen to map the optimal distance between the binding pocket and the N-terminal elbow helix of either TAP1 or TAP2. I demonstrated that the interaction of fused ICP47 with coreTAP inhibits antigen presentation via MHC I. Interestingly, the loss of MHC I surface expression only depended on the presence of the active domain and not on the length of the fused ICP47 fragments. Summarizing it can be said that TAP complexes containing an intact active domain of ICP47 successfully suppressed MHC I surface expression. Considering the MHC I surface expression in the use of free ICP47 fragments it was revealed that the active domain may not be sufficient. All free constructs, except the one that contains exclusively the active domain (1-35), were able to fully arrest peptide translocation, while the fragment 1-35 partially restored MHC I surface expression. This was the first evidence suggesting that more residues might be present in the ICP47 sequence that contribute to the interaction with TAP.

Further characterization of the ICP47-coreTAP fusion complexes comprised the determination of their thermostability and melting temperatures. The ICP47-coreTAP fusion complexes revealed a preferred orientation for ICP47. The ICP47(1-65) fragment led to a stable complex only if fused to TAP2, highlighting an interesting asymmetry at the TAP1/TAP2 interface, which suggests a shorter distance of the C-terminus of the stabilizing region to the elbow helix of TAP2 than of TAP1. The shorter fragments 1-35 and 1-50, and the ICP47-linker fragments, which inhibited, but did not trigger any thermostabilizing effects on TAP, revealed a second hint for the presence of other residues important for the ICP47/TAP interaction. To define the thermostability in more detail, the melting temperature of complexes with fused or freely bound ICP47 fragments was determined. Short fused fragments of ICP47 (residues 1-35 or 1-50) did not fully stabilize the TAP complex. Only ICP47 fragments longer than residues 1-50 raised the melting temperature to the full extent and led to a completely stabilized complex, suggesting that the critical melting temperature, which determines whether a complex is fully stabilized or not, is about 44-45 °C. By comparing different ICP47 proteins from the herpesviral clade, I further noticed that the 21 residues following the active domain are highly conserved. The residues in this region were exchanged by glycines and alanines to study their impact on the thermostabilization of TAP. I demonstrated that several

charged residues, an alanine rich, and a proline rich sequence were mainly responsible for the preservation of high melting temperatures. In summary, these findings reveal a dual inhibition mechanism of ICP47. While the active domain of ICP47 is wedged at the TAP1/2 interface and arrests the complex in an open-inward facing conformation, the highly conserved C-terminal region stabilizes the ICP47/TAP interaction and generates a thermostabilized TAP complex.

The second part of this thesis deals with two alternative expression and stabilization strategies for coreTAP, designed to provide a 1:1 ratio of TAP subunits during protein biosynthesis. Different glycine-serine (GS) linkers and a self-cleaving 2A site were implemented into the TAP sequence and used for comparison with the classical coreTAP. Despite their functionality in antigen translocation, the utilization of GS-linkers proved to be unsuitable due to low expression and scarce purification efficiency caused by the unfeasible orthogonal purification. In contrast, the use of a 2A site allowed orthogonal His_{10}- and SBP-tag purification and yielded comparable amounts to the classical coreTAP. However, the ICP47/coreTAP interaction appeared to be hampered by the modified N-terminus of ICP47, due to the cleavage process.

The third and last part of this work deals with the *Thermus thermophilus* ABC transporter TmrAB, which was identified to be part of the same ABC subfamily as TAP. The structure of TmrAB is similar to that of coreTAP and includes a TMD and an NBD for each subunit. In comparison to TAP, TmrAB has a broader substrate range, but it can transport peptides, which are also transported by TAP. Since the natural substrate, and thus the actual function, of TmrAB has not yet been identified, it is counted among the multidrug resistance ABC transporters, from where it also takes its name. In this work, the question was investigated whether TmrAB can be utilized as a TAP substitute. To compare the function of TmrAB and TAP in a natural cell environment, the N-terminal domains of the TAP subunits called TMD0s were fused to the TmrAB subunits and subsequently expressed as different combinations. I found that especially the hybrid complexes containing a TMD0 of TAP2 were functional in terms of MHC I surface expression. Furthermore, TmrAB with TMD0 co-localized prevalently with the ER marker PDI while complexes without TMD0 did not co-localize. Interestingly, the analysis of the interaction with components of the PLC revealed that interaction with tapasin could only occur when a TMD0 was present. In turn, calreticulin, MHC I, and ERp57 were bound, regardless of the presence of a TMD0. It is remarkable that a bacterial protein, sharing only 27-30% sequence identity with human TAP is able to take over a key function of our adaptive immune system. Yet, TmrAB originates from a hyperthermophilic bacterium and may have assembly and folding difficulties that the human cell seeks to overcome by recruiting chaperones like calreticulin and ERp57. Although further experiments will be necessary to analyze the interaction of TmrAB with the PLC components in more detail, TmrAB appears to be homologous to coreTAP, not only in terms of sequence and structure, but also in terms of function.

Deutsche Zusammenfassung

ABC-Transporter (von engl. *ATP-binding cassette transporters*) repräsentieren eine der größten und diversesten Membranprotein-Superfamilien. Zugehörige Transporter findet man in allen drei großen Lebensformen dieser Erde, von Archaeen, über Bakterien bis hin zu den Eukaryoten. Sie schleusen ein sehr weitläufiges Spektrum an Substraten durch biologische Membranen, was dazu führt, dass viele dieser ABC-Transporter an essentiellen vitalen Prozessen teilhaben. Mutationen oder Deletionen dieser Transporter führen zu deren Fehlfunktion und werden mit diversen Krankheiten in Verbindung gebracht. Beispiele solcher Erkrankungen sind die zystische Fibrose, die Entstehung von Multiresistenz bei Krebserkrankungen und ein Subtyp des *bare lymphocyte* Syndrome Typ I, auch Syndrom der nackten Lymphozyten genannt. Obwohl ABC-Transporter abhängig von ihrem Ursprungsorganismus, ihrer Funktion oder ihrem Aufbau unterschiedlich gruppiert werden können, verbindet sie doch alle das Verwenden der Energie aus ATP-Hydrolyse und ATP-Bindung für den Transport ihrer jeweiligen Substrate. Diese finden in den beiden "Motordomänen", auch NBDs genannt (für engl. *nucleotide bindind domain*), statt. Die NBDs befinden sich an der zytosolischen Seite von zwei homo- oder heterotypischen hydrophoben Transmembrandomänen (TMD). Zusammen bilden diese vier Domänen die Translokationseinheit, die auch als "*Core*"-Einheit bezeichnet wird. ABC-Transporter können noch zusätzliche Domänen oder Proteine besitzen, die oftmals regulatorischen oder funktionalen Zwecken dienen.

Der Antigentranslokationskomplex TAP (von engl. *transporter associated with antigen processing*) ist ein ABC-Transporter der B-Unterfamilie und ist ausschließlich in der ER-Membran und dem *cis*-Golgi von bekieferten Wirbeltieren zu finden. TAP bildet zusammen mit Calreticulin, MHC I/β_2m, ERp57 und Tapasin den Peptidbeladungskomplex PLC (von engl. *peptide loading complex*). Die Aufgabe von TAP ist es durch proteasomale Degradation entstandene Peptide über die ER-Membran ins ER-Lumen zu transportieren. Dort angekommen, werden die Peptide im PLC weiter prozessiert und stabil an MHC I Moleküle gebunden, die dann zur Zelloberfläche wandern, um dem Immunsystem präsentiert zu werden.

Der PLC stellt ein Schlüsselelement des adaptiven Immunsystems dar und wurde im Laufe der Evolution mehrfach von Viren anvisiert. Es sind insgesamt fünf virale Inhibitoren bekannt, die TAP auf unterschiedliche Art und Weise arretieren. Vier davon werden von Viren, die zur Familie der *Herpesviridae* gehören (ICP47, US6, UL49.5 and BNLF2a) und einer von Orthopoxviren kodiert (CPXV12). Alle TAP-Inhibitoren, außer dem zytosolischem ICP47, besitzen eine in der ER verankerte α-Helix, die mit zytosolischen oder ER-luminalen Domänen verbunden ist. ICP47 ist ein 88 Aminosäuren langes Polypeptid, dessen Region 3-34 die aktive Domäne bildet, die maßgeblich an der Inaktivierung von TAP beteiligt ist. Bei Membrankontakt formt die aktive Domäne zwei kurze α-Helices,

die die Peptidbindetasche von TAP mit hoher Affinität (K_d=50 nM) blockieren. Diese Eigenschaften von ICP47 wurden ausgenutzt um ICP47-TAP Hybride zu generieren. Unterschiedlich lange Fragmente von ICP47 wurden an die N-terminale *Elbow*-Helix der coreTAP-Untereinheiten fusioniert, um den optimalen Abstand zur Bindungstasche zu identifizieren. Auf diese Art und Weise konnte gezeigt werden, dass die Interaktion des fusionierten ICP47 mit coreTAP die Antigenpräsentation über den MHC I-Pfad verhindert. Interessanterweise war das Ausbleiben der MHC I-Oberflächenexpression ausschließlich von der Präsenz der aktiven Domäne und nicht von der Länge des ICP47-Fragments abhängig. Das Ersetzen der ICP47-Aminosäurereste 35-88 durch drei unterschiedliche flexible Glycin-Serin-*Linker* führte ebenfalls zum Arretieren der TAP-Funktion. Wurde dagegen eine selbst-schneidende 2A-Schnittstelle verwendet, um die TAP-Untereinheiten voneinander zu trennen, wurde die MHC I-Oberflächenexpression minimal erhöht, obwohl die überwiegende Mehrheit der Zellen keine MHC I-Oberflächenexpression zeigte.
Zusammenfassend kann man sagen, dass alle TAP-Komplexe, die eine intakte aktive Domäne von ICP47 enthielten, TAP inhibierten. Des Weiteren bestätigten diese Ergebnisse die beiden Studien, die gezeigt hatten, dass die aktive Domäne eine vergleichbare Inhibition bewirkt wie ICP47 in voller Länge [4, 5]. Die coreTAP-Komplexe, die jedoch fusionierte inaktive ICP47-Varianten enthielten (ΔH1 und ΔH2), waren in der Lage die MHC I-Oberflächenexpression zu 50-100% wiederherzustellen.
Basierend auf diesen Daten, wurde zunächst angenommen, dass die ICP47-Aminosäurereste 36-88 keine Funktion besitzen und das Fusionskonstrukt mit einer optimalen Inhibierungskapazität lediglich ICP47(1-35) enthalten müsste. Dabei wäre es auch denkbar gewesen, dass das Ersetzen der nicht benötigten Sequenz durch Glycin-Serin-*Linker* die Interaktion mit TAP erleichtert und das Positionieren der aktiven Domäne in der Peptidbindetasche begünstigt. Vergleicht man allerdings fusionierte ICP47-Fragmente mit freien, erhält man einen ersten Hinweis darauf, dass die aktive Domäne möglicherweise zwar den wichtigsten Teil zur Inhibition beiträgt, aber für eine komplette Inhibierung nicht ausreicht. Alle Konstrukte, außer dem einen, das nur die aktive Domäne enthielt, waren in der Lage die MHC I-Oberflächenexpression vollständig zu unterbinden, während das freie ICP47-Fragment 1-35 die MHC I-Oberflächenexpression teilweise wiederherstellen konnte.
Die weitere Charakterisierung der ICP47-coreTAP-Fusionskonstrukte beinhaltete die Bestimmung ihrer Thermostabilität und Schmelztemperaturen. Das Verwenden von transient transfizierten HEK-Suspensionszellen erlaubte es in einem relativ kleinem Maßstab ausreichende Mengen an gereinigtem Protein zu erhalten, ohne über einen zeitaufwändigeren Prozess *P. pastoris*-Klone generieren zu müssen. Die ICP47-coreTAP Fusionskonstrukte zeigten eine bevorzugte Orientierung von ICP47. So führte das ICP47(1-65)-Fragment nur bei Fusionierung an TAP2 zu einem stabilen Komplex, der

eine einstündige Inkubation bei 40 °C überstand, und dadurch eine interessante Asymmetrie an der TAP1/TAP2-Schnittstelle enthüllte. Dies bedeutete, dass der C-Terminus des Fragments näher an der *Elbow*-Helix von TAP2 als an der von TAP1 positioniert sein musste. Da die kürzeren Fragmente ICP47(1-35) und ICP47(1-50), sowie die Konstrukte mit Glycin-Serin-*Linkern* zwar TAP inhibieren konnten, aber keine Thermostabilisierung auslösten, stellten sie den zweiten Hinweis dar, dass ICP47 sehr wahrscheinlich auch außerhalb der aktiven Domäne Aminosäurereste besitzt, die die Interaktion beinflussen. Weiterhin wurde deutlich, dass die Bestimmung der Thermostabilität, zwar neue Erkenntnisse liefern konnte, doch die feinen Unterschiede zwischen den unterschiedlichen Fusionskonstrukten nicht zu Genüge hervorheben konnte.
Um die Thermostabilität präziser beschreiben zu können, wurden die Schmelztemperaturen der TAP-Komplexe mit fusionierten oder freien ICP47-Fragmenten bestimmt. Die kürzeren fusionierten Fragmente (Reste 1-35 und 1-50) konnten TAP nicht komplett stabilisieren, lieferten aber Schmelztemperaturen, die über der von Wildtyp-TAP lagen (36.3 ±1.5 °C). Nur die ICP47-TAP-Komplexe, die mindestens die ICP47-Aminosäurereste 1-65 enthielten, zeigten eine volle Stabilisierung der Komplexe. Interessanterweise war mit Hilfe der Schmelztemperaturbestimmung die Asymmetrie des TAP-Komplexes nicht so deutlich zu beobachten wie mit dem vorangegangenen Versuch. Das Fragment ICP47(1-65) zeigte eine Schmelztemperatur von 44.2 °C, wenn es an coreTAP1 fusioniert war und 45.7 °C bei der Fusion an coreTAP2. Dies könnte darauf hinweisen, dass die kritische Schmelztemperatur zwischen 44-45 °C liegt und nur die Kombination mit einer Inkubation über längere Zeit bei höheren Temperaturen Aufschluss darüber gibt, ob ein Fusionskomplex komplett stabilisiert ist.
Die freien viralen Fragmente zeigten, dass die ICP47-Aminosäurereste 1-55 benötigt werden, um eine komplette Interaktion mit TAP zu gewährleisten. Die Kombination mit dem kürzeren Fragement, das nur die Reste 1-35 enhielt, führte sowohl mit als auch ohne Reporter-GFP zu einer Destabilisierung und senkte die Schmelztemperatur auf ca. 26 °C. ICP47 interagiert über eine relativ große Grenzfläche mit den TAP-Untereinheiten, wobei sich die aktive Domäne wie ein Keil zwischen sie schiebt. Dies könnte erklären, warum eine aktive Domäne, die nicht die optimale Position in der Bindetasche erreicht, trotzdem die korrekte Funktion von TAP verhindern kann. Um dies zu bestärken, konnte ich zudem zeigen, dass nicht perfekt positionierte fusionierte ICP47-Fragmente von freiem ICP47(1-88) verdrängt werden können. Der funktionale Arrest wurde dadurch gezeigt, dass ICP47-coreTAP-Komplexe, unabhängig von der ICP47-Fragmentlänge, den freien TAP-Inhibitor US6 nicht binden konnten.
Die aktive Domäne wurde als die kürzeste ICP47 Sequenz definiert, die eine vergleichbare Aktivität zu ICP47 in voller Länge aufweist. Dennoch sind die 20 Aminosäuren, die C-terminal zur aktiven Domäne gelegen sind, höher konserviert. Vergleicht man die ICP47 Sequenzen des humanen *Herpes simplex* Virus 1 und 2 miteinander, fällt auf, dass sich

die Aminosäuren 1-55 zu 67% gleichen, während die Aminosäuren 56-88 keine signifikante Konservierung zeigen. Ein weiterer Vergleich der Sequenz 35-55 der unterschiedlichen ICP47-Proteine verschiedener Herpesviren zeigt, dass in diesem Abschnitt geladene Aminosäuren besonders häufig vorkommen. Außerdem befinden sich dort eine alanin- und eine prolinreiche PxxPLLxPP Sequenz. Da letztere dafür bekannt ist in Protein-Protein Interaktionen involviert zu sein, ist es denkbar, dass sich ein ähnliches Motiv auch in der ICP47/TAP-Interaktion herausgebildet haben könnte, um den Transporter in einer peptidabweisenden Konformation zu halten. Um die Bedeutung dieser Region weiter zu charakterisieren, wurde die Sequenz in sieben Teile zu je drei Aminosäuren unterteilt und gegen Alanine und Glycine ausgetauscht. Durch das anschließende Bestimmen der Schmelztemperatur konnten sowohl die geladenen Aminosäurereste, als auch die alanin- und prolinhaltigen Sequenzen als relevant für die ICP47/TAP Interaktion definiert werden. Des Weiteren konnte belegt werden, dass die am höchsten konservierten Aminosäurereste auch am relevantesten für die vollständige Stabilisierung von TAP sind. Das in dieser Arbeit verwendete ICP47 ist leider das einzige mit nicht konservierten Aminosäureresten 53-55 (RSP), die auch keinen Einfluss auf die Stabilität von TAP zu haben schienen. Dennoch wurde in Anbetracht der hohen Konservierung dieser Aminosäurereste in anderen Sequenzen und der größtenteils stabilisierenden Eigenschaft der übrigen Teilsequenz, die ICP47-Region 35-55 als die stabilisierende Region benannt. Zusammenfassend kann man sagen, dass TAP auf zwei Art und Weisen von ICP47 inhibiert wird: Während sich die aktive Domäne an der TAP1/2-Schnittfläche verkeilt, um den Komplex in einer *open-inward facing* Konformation zu arretieren, sorgen die Aminosäurereste der stabilisierenden Region dafür, dass die aktive Domäne ihre Position beibehält.

Der zweite Teil dieser Arbeit befasst sich mit zwei alternativen Expressions- und Stabilisierungsstrategien für coreTAP, die bereits während der Proteinbiosynthese für ein 1:1 Verhältnis der TAP-Untereinheiten sorgen sollen. Im *P. pastoris* Expressionssystem ist es theoretisch möglich zwei Proteinsequenzen auf einem Plasmid ins Hefegenom zu überführen, um sie gleichzeitig zu exprimieren. Frühere Versuche dies für TAP zu etablieren scheiterten jedoch. So wurden in einem neuen Experiment coreTAP1 und coreTAP2 über drei verschieden lange Glycin-Serin-*Linker* mit jeweils 40, 50 oder 60 Aminosäuren miteinander fusioniert, um nur einen einzigen Proteinstrang, ähnlich dem von P-Glycoprotein, zu erhalten. Alle Konstrukte konnten in humanen Zellen exprimiert werden, doch nur in geringen Mengen. Weiterhin erwiesen sich hauptsächlich nur die Konstrukte mit N-terminalem coreTAP1 als funktional in Bezug auf die MHC I-Oberflächenexpression. Der Versuch coreTAP1-L60-coreTAP2 in *P. pastoris* zu exprimieren, führte leider nicht zu einer erhöhten Ausbeute. Die Reinigung im größeren Maßstab zeigte außerdem, dass die ausschließliche Reinigung über das His_{10}-Tag nicht genügte um eine hohe Reinheit zu erlangen. Folglich wurde dieses Konstrukt im Rahmen dieser Arbeit nicht weiter charakterisiert.

Die zweite Alternative zur Co-Expression der coreTAP-Untereinheiten beinhaltete die Verwendung einer selbst-schneidenden 2A-Schnittstelle. Diese wurde in den Konstrukten zwischen den coreTAP-Untereinheiten positioniert um drei Konstrukte zu generieren: coreTAP1-2A-coreTAP2, ICP47-coreTAP2-2A-coreTAP1 und coreTAP1-2A-ICP47-coreTAP2. Da die Untereinheiten in diesem Ansatz nicht miteinander verbunden waren, konnten wieder zwei unterschiedliche Reinigungs-Tags eingesetzt werden, um eine orthogonale Reinigung über His_{10}- und SBP-Tag zu ermöglichen. Die 2A-Sequenz war in der Lage die Untereinheiten effizient voneinander zu trennen und führte nach orthogonaler Reinigung zu einer Ausbeute, die mit coreTAP, das auf zwei separaten Plasmiden kodiert war, verglichen werden konnte. Im Vergleich zu den gleichartigen Konstrukten ohne 2A-Schnittstelle, zeigte coreTAP alleine eine ähnliche Funktionalität, während die ICP47-Fusionskonstrukte eine geringfügig höhere MHC I-Oberflächenexpression aufwiesen. Diese Abweichung könnte durch fehlerhaft geschnittene Komplexe oder durch Rückstände der 2A-Schnittstelle verursacht sein. Die anschließende Bestimmung der Schmelztemperaturen der beiden ICP47-Konstrukte bewies, dass die aktive Domäne mit TAP nur dann optimal interagieren konnte, wenn der N-Terminus nicht durch Rückstände der 2A-Schnittstelle modifiziert wurde. Ob eine hohe Ausbeute dieser Komplexe durch Expression in *P. pastoris* erreicht werden kann, wird sich in zukünftigen Versuchen zeigen.

Der dritte und letzte Teil dieser Arbeit handelt von dem aus *Thermus thermophilus* stammendem ABC-Transporter TmrAB, der basierend auf seiner Sequenz zur selben Unterfamilie wie TAP gezählt werden kann. Der Aufbau von TmrAB ähnelt dem von coreTAP und beinhaltet für jede Untereinheit eine TMD und eine NBD. Im Vergleich zu TAP hat TmrAB ein breiteres Substratspektrum, kann aber Peptide transportieren, die in dem Peptidrepertoire von TAP enthalten sind. Da das natürliche Substrat, und somit die eigentliche Funktion, von TmrAB noch nicht identifiziert worden ist, wird es zu den *multidrug resistance* ABC-Transportern gezählt und bezieht daher auch seinen Namen. In dieser Arbeit wurde der Frage nachgegangen, ob TmrAB tatsächlich die Funktion des humanen TAPs ersetzen kann. Um die Funktion von TmrAB und TAP in einer natürlichen Zellumgebung vergleichen zu können, wurden die N-terminalen Domänen der TAP-Untereinheiten, genannt TMD0s, an die TmrAB-Untereinheiten fusioniert und anschließend als unterschiedliche Kombinationen exprimiert. Dabei zeigte sich, dass besonders die Hybridkomplexe, die eine TMD0 von TAP2 enthielten, in Bezug auf MHC I-Oberflächenexpression funktional waren. Weiterhin co-lokalisierte TMD0-TmrAB vermehrt mit dem ER-Marker PDI, während das Fehlen der TMD0 zur Folge hatte, dass die Co-Lokalisierung stark reduziert wurde. Die Analyse der Interaktion mit Komponenten des PLCs ergab, dass die Interaktion mit Tapasin nur Zustande kommen konnte, wenn eine TMD0 vorhanden war. Calreticulin, MHC I und ERp57 konnten dagegen auch ohne TMD0 mit TmrAB interagieren. Die Interaktion mit diesen drei PLC-Komponenten ist

recht erstaunlich, da die Sequenzen von TmrAB und TAP nur zu 27-30% identisch sind. Allerdings könnte TmrAB, das ursprünglich aus einem hyperthermophilen Bakterium stammt, in humanen Zellen leichte Assemblierungs und Faltungsprobleme haben, die die Zelle durch das Rekrutieren von Chaperonen, darunter Calreticulin und ERp57, zu beheben versucht. Weitere Versuche sind notwendig, um die Interaktionen genauer analysieren zu können. Dennoch zeigten diese Experimente, dass TmrAB nicht nur aufgrund seiner Sequenz, Struktur oder Substratspezifität als TAP-Ersatz dienen kann. Es wurde bewiesen, dass TmrAB in der Lage ist in menschlichen Zellen die Funktion einer Kernkomponente der adaptiven Immunantwort zu übernehmen.

Chapter 1

Introduction

1.1 ABC transporters - an overview

The ATP-binding cassette (ABC) transporter superfamily is considered one of the largest and most diverse transporter superfamilies. Members can be found in all kingdoms of life, moving a large variety of substrates across biological membranes. These substrates range from relatively small molecules like ions, sugars, amino acids, vitamins, lipids, antibiotics and drugs to larger molecules such as oligosaccharides, oligopeptides and even high molecular weight proteins. Accordingly, ABC transporters are associated with various important biological processes in bacteria and eukarya that range from energy supply to osmoregulation, detoxification, and virulence. Furthermore, several ABC transporters are known as principal actors in different clinical diseases such as cystic fibrosis, multidrug resistance of cancers, and antigen presentation [6–9].

Although ABC transporters can be mainly divided into uptake and export systems, which have in turn a wide range of substrates, a few functional and architectural features are shared by most members of the ABC family. Their main function consists in converting the energy released by ATP binding and hydrolysis into conformational changes to move substrates across the membrane. Furthermore, ABC transporters usually consist of two "motor domains", the nucleotide binding domains (NBD), which are connected to the cytosolic face of two homo- or heterotypic hydrophobic transmembrane domains (TMD). These domains build together the substrate translocation unit, also known as "core" unit. Accessory domains or proteins, which often assume regulatory or functional tasks, can be additionally part of the ABC transporters [6, 10, 11].

1.1.1 Classification of ABC transporters

The members of the ABC transporter family can be classified and subdivided in different ways, depending on which properties are in focus. So, ABC transporters can be divided by their phylogenetic origin of the transmembrane domains, by their function as importers or exporters, or by the organism they originate from. The following sections will briefly outline possible ABC transporter classifications, focusing on relevant parts for the characterization of the human TAP and the bacterial TmrAB transporters.

1.1.1.1 ABC importers

Depending on their structural assembly and functionality, ABC importers can be grouped into type I, type II and type III energy coupling factor (ECF) transporter systems (Fig. 1.1) and are mostly found in prokaryotes and rarely in plants or mammals [12–14]. Compared to type II importers, type I importers usually contain fewer transmembrane (TM) helices. The homodimer MetNI for instance, has a set of 2 x 5 TM helices, and in MalFGK the heterodimers MalF and MalG have 8 and 6 TM helices, respectively [12, 15, 16]. Type I importers transport their substrates by the alternating access model, switching between inward- and outward-facing conformation [17]. Type II importers are characterized by larger transmembrane regions, composed of 10 helices per half-transporter (denominated TM 1-10). The conformational change they undergo during transport is presumably limited to TM helices 3, 4, 5, 5a, 10 and the loop between TM 2 and 3. Since the access through the periplasmic gate apparently correlates with the size of the respective substrate, it was suggested that the substrate selectivity filter mechanism is comparable to channels [12]. Both, type I and II importers rely on soluble substrate-binding domains or proteins, which capture the respective substrate and deliver it to the TMDs, while exporters and ECF importers do not require this components [18]. ECF transporters play an essential role in micronutrient uptake in bacteria and Archaea and were only recently included into the ABC transporter family, although they were discovered already 40 years ago [19]. Their modular composition slightly differs from the classical architecture of ABC transporters: ECF transporters are composed of two ABC ATPase domains, one conserved transmembrane component and a variable transmembrane substrate-capture protein, with a distinct substrate specificity [7, 20].

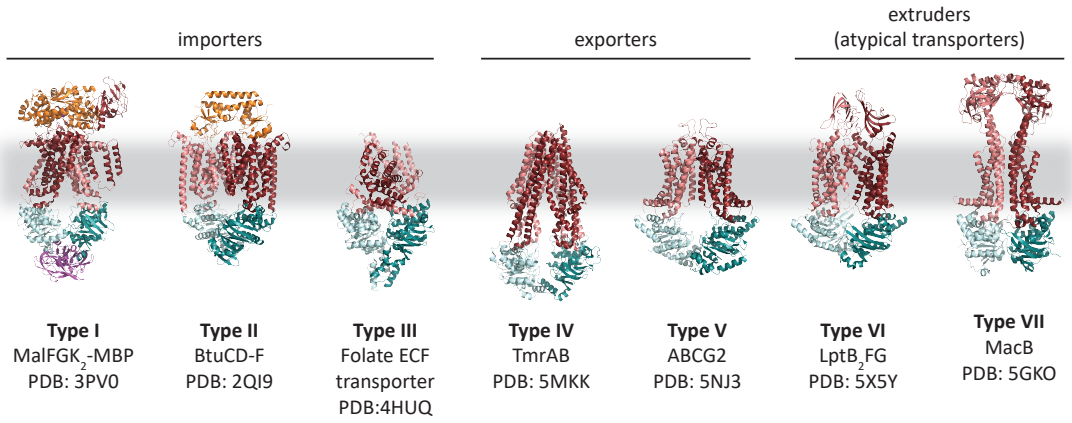

Figure 1.1: ABC transporter classes.
According to current knowledge, ABC transporters can be grouped in seven classes, comprising importers, exporters and extruders (atypical transporters) [21, 22]. All transporters consist of two TMDs (red and pink) and two NBDs (cyan and light blue). Some transporters have auxiliary domains, for example substrate-binding proteins (orange) or regulatory domains (purple). From the left to the right the following transporters are: As representative of type I class, the X-ray structure of maltose importer $MalFGK_2$ in complex with maltose-binding protein form *E. coli* is shown [16]. The X-ray structure of the vitamin B_{12} importer BtuCD *form E. coli* in complex with its substrate-binding protein BtuF depicts the type II importer class [23]. The ECF transporter type III class is represented by the X-ray structure of the folate transporter from *L. brevis* [24]. The X-ray structure of TmrAB from *T. thermophilus* is exemplarily shown for the type IV exporter class [2] and type V exporter class is represented by the cryo-EM structure of human ABCG2 [25]. The two new ABC transporter classes type VI and VII are depicted by the X-ray structures of the LPS-extracting $LptB_2FG$ from *P. aeruginosa* and by MacB from the MacAB-TolC multidrug efflux-pump derived from *A. baumannii* [26, 27].

1.1.1.2 ABC exporters

ABC efflux systems can be subdivided into two classes, depending on the phylogenetic origin of their transmembrane domains. Although a third class of exporters was proposed based on phylogenetic analyses [28, 29], these ABC transporters are not exporters comparable to the other two classes, and will be described more in detail in the next section.

Several structures have been solved for type IV exporters [30–34], whereas only recently structures of class V exporters were determined [25, 35] (Fig. 1.1). Apart their differing architectures, exporters can be found in prokaryotes and eukaryotes, and translocate their substrates mainly by the alternating access model switching between inward- and outward-facing conformations. For a few ABC exporters (ABCA1 and PglK) an outward-only translocation mechanism with lateral substrate access was proposed [36, 37].

The TMDs are mainly fused to the NBDs, so that the transporter can consist of only one polypeptide containing all the domains or of two homo- or heterodimers, each of which includes a TMD and a NBD. ABC exporters can transport various hydrophobic

substrates, such as lipids, fatty acids, cholesterol, drugs, and also larger molecules such as proteins (toxins, hydrolytic enzymes, S-layer proteins, lantibiotics, bacteriocins, and competence factors) [38]. Since most drug exporters are able to translocate a vide range of drugs, differing in size and shape out of the cells, they are termed multidrug-resistant (MDR) transporters and are particularly in focus of medical research

1.1.1.3 Novel atypical ABC transporters

Only recently structures of ABC transporters were solved, that do not operate as importers or exporters and exhibit an unprecedented noncanonical ABC transporter fold (Fig. 1.1). These transporters belong to a functionally diverse and monophyletic group of ABC transporters, previously termed ABC3 porters [28]. $LptB_2FG$ for instance, extracts lipopolysaccharide (LPS) from the external leaflet of the inner membrane of bacteria via a still unknown mechanism. LPS is further propelled through the periplasm along a filamentary construction composed of LptC and LptA to be then inserted into the extracellular leaflet of the outer membrane by LptD/E [39, 40]. So, in contrast to all other known ABC transporter translocation mechanisms, the substrate is not transported by $LptB_2FG$ across the membrane. It was suggested that $LptB_2FG$ utilizes alternating lateral gates in open or closed conformations to translocate LPS.
Gram-negative bacteria mediate the export of toxic molecules, antibiotics, and virulence factors by tripartite efflux pumps (TEPs) that span the inner and outer membrane [41]. The homodimeric ABC transporter MacB, resident in the inner membrane, forms a TEP with the adaptor protein MacA and the exit duct TolC, and confers resistance to macrolide antibiotics [42]. A MacB halftransporter consists of a N-terminal NBD, a TMD formed by 4 helices, and a large periplasmic domain located between TM1 and TM2. Nucleotide-free and ATP bound conformations lack the characteristic cavities, that can be observed in inward- or outward-facing conformations, typical for the alternating-access mechanism of other ABC transporters. It was suggested that MacB acts as a molecular bellows, driving the efflux of substrates from the periplasm out of the cells. This mechanism was termed mechanotransmission and proposes, that the substrate interacts mainly with a cavity formed by the periplasmic domain and is pushed out of the cavity towards TolC upon NBD dimerization. It was furthermore proposed, that PvdT, AatP, LolC, LolE, and FtsX, which all have the same transmembrane topology as MacB could operate with similar mechanisms [21].

1.1.1.4 ABC transporters in humans

The Human Genome Organization lists 51 human ABC transporters, which subdivide into the 7 subfamilies ABCA to ABCG (Fig. 1.2) [43]. The division into subfamilies is based on sequence homology of the TMDs and NBDs, the order of these domains and similarity in gene structures, forming half- or full-transporters. Not all members of these subfamilies can be found in humans. So, for example, ABCG3 was found only in rodents and ABCA14 to ABCA16 were lost in all primates. Moreover, it was found that zebrafishes possess a member of an eight ABCH family [44]. Human ABC transporters are mainly exporters and translocate a variety of compounds from the cytoplasm out of the cell or from the cytoplasm into cellular compartments like the ER, mitochondria or peroxisomes.

ABCA

The ABCA subfamily is composed of 12 members, all featuring full-transporter architecture, and two members classified by HGNC as pseudogenes (ABCA11P and ABCA17P) [43]. Depending on their phylogenetic origin, the subfamily can be further divided into two groups. The first group comprises ABCA1, ABCA2, ABCA3, ABCA4, ABCA7, ABCA11P, ABCA12, ABCA13 and ABCA17P, the second group ABCA5, ABCA6, ABCA8, ABCA9 and ABCA10 [45]. This subfamily includes some of the largest ABC transporters consisting of more than 2200 amino acids. Since several severe diseases are caused by genetic defects of ABCA members, some of them attracted considerable attention in recent years. The cholesterol efflux pump ABCA1 is known to be mutated in Tangier's disease. ABCA4 is localized to outer segment disk edges of rods and cones, and flipps N-retinylidene-phosphatidylethanolamine and phosphatidylethanolamine from the lumen to the cytoplasmic leaflet of the disc membrane [14]. Mutations of this gene are known to cause severe retinal degenerative diseases like Stargardt macular degeneration, cone-rod dystrophy, retinitis pigmentosa, and age-related macular degeneration [14, 46, 47]. ABCA12 is a keratinocyte transmembrane lipid transporter, localized at the lamellar granule. Dysfunction causes the reduction of epidermal ceramides, malformation of the epidermal lipid barrier, and ichthyosis phenotypes [48, 49].

ABCB

The ABCB subfamily is composed of 11 members, which are divided in 4 full-transporters (ABCB1, ABCB4, ABCB5 and ABCB11) and 7 half-transporters (ABCB2/ABCB3, ABCB6, ABCB7, ABCB8, ABCB9 and ABCB10). ABCB1, also named MDR1, PGY1 or CLCS, can be found at the blood-brain barrier and in the liver, where it protects the cells from toxic compounds. It causes multidrug resistance in cancer cells and was the first human ABC transporter cloned and characterized, whereas the structure of human ABCB1 was only recently solved in ATP-bound outward-facing conformation [50].

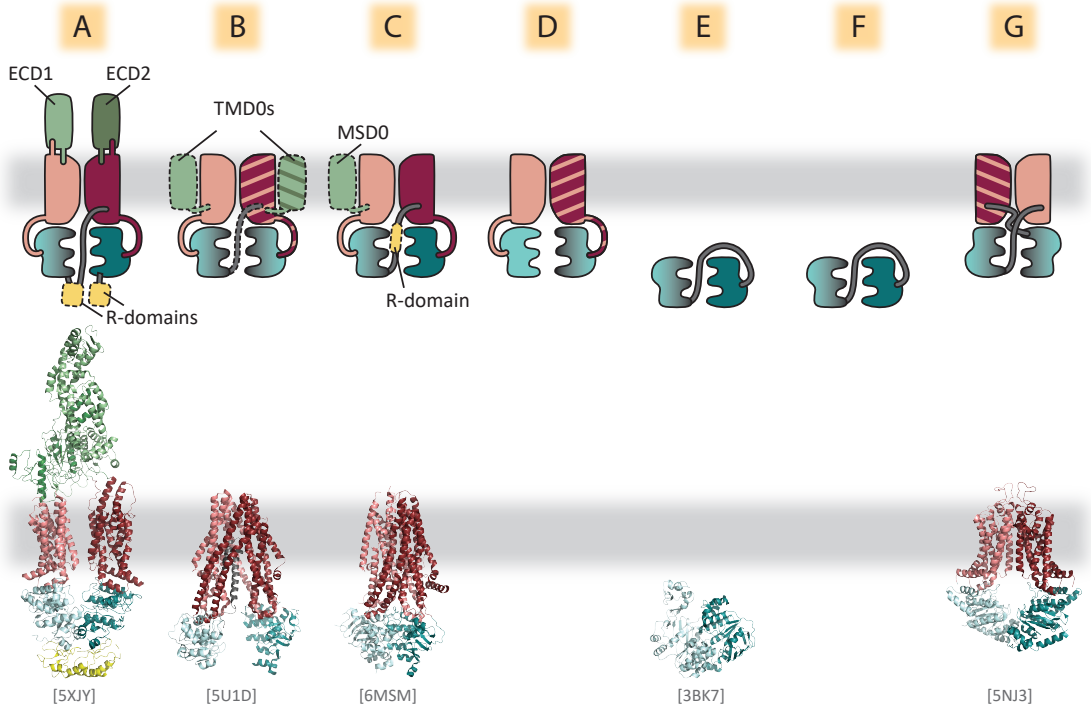

A	B	C	D	E	F	G
ABCA1	ABCB1	ABCC1	ABCD1	ABCE1	ABCF1	ABCG1
ABCA2	TAP1	ABCC2	ABCD2		ABCF2	ABCG2
ABCA3	TAP2	ABCC3	ABCD3		ABCF3	ABCG4
ABCA4	ABCB4	ABCC4	ABCD4			ABCG5
ABCA5	ABCB5	ABCC5				ABCG8
ABCA6	ABCB6	ABCC6				
ABCA7	ABCB7	CFTR				
ABCA8	ABCB8	ABCC8				
ABCA9	ABCB9	ABCC9				
ABCA10	ABCB10	ABCC10				
(ABCA11P)	ABCB11	ABCC11				
ABCA12		ABCC12				
ABCA13		(ABCC13P)				
(ABCA17P)						

Figure 1.2: Human ABC transporter subfamilies.
The human ABC transporters can be divided into seven subfamilies termed ABCA to ABCG. NBDs are shown in blue, TMDs in pink and magenta, and auxiliary domains in green and yellow. Extra domains with dotted borders can be found only in a subset of subfamily members. Half-transporters can be identical (same color), different (other shade) or both variations can be found within one family (striped colors). Non-canonic NBDs are depicted with dark color gradient (adapted from Seyffer *et al.* 2015 [51]). Below the schematic representation of each subfamily structures of subfamily representatives can be found. The respective denotations are marked in orange in the list of the subfamily members below.

ABCB4, also named MDR3 or PGY3, is an ABCB1 homolog located in the liver, where it translocates phosphatidylcholine [52, 53]. ABCB11, also named BSEP (bile salt export pump), resides as well in the liver and is involved in bile salt secretion. Mutations in human ABCB11 cause progressive familial intrahepatic cholestasis type 2 [54]. ABCB5 is mainly expressed in physiological skin and human malignant melanoma and is presumably involved in multi drug resistance of cancer cells [55, 56].
The heterodimeric ABCB2/ABCB3, also named TAP (transporter associated with antigen processing), is involved in antigen presentation by translocating antigentic peptides derived from proteasomal degradation out of the cytosol into the ER lumen. TAP is part of the supramolecular peptide loading complex (PLC), that, assisted by tapasin, ERp57 and calreticulin, selectively loads high-affinity peptides onto MHC I [57]. In most cases, TAP1 or TAP2 deficiency, a subtype of the bare lymphocyte syndrome type I, leads to chronic bacterial infections of the respiratory tract and 50% of patients also have granulomatous skin lesions [9, 58, 59]. ABCB9, also named TAPL, is the closest human homolog of TAP and functions as lysosomal polypeptide transporter [60]. The remaining ABCB6, ABCB7, ABCB8, and ABCB10 are localized at the mitochondrial membrane, where they are involved in biogenesis of cytosolic ironsulfur clusters, heme biosynthesis, iron homeostasis, multidrug resistance, and protection against oxidative stress [61].

ABCC

The ABCC subfamily comprises 13 full-transporters with rather diversified functionalities. The most prominent member is ABCC7, or CFTR (cystic fibrosis transmembrane conductance regulator), a chloride channel, that regulates the epithelial fluid transport in several tissues and organs, especially those of the gastrointestinal and respiratory tracts. Mutations of the CFTR gene lead to cystic fibrosis, a disease causing frequent and destructive lung infections [62, 63]. ABCC8 and ABCC9, also named SUR1 and SUR2 (sulphonylurea receptor) respectively, are part of ATPsensitive potassium K_{ATP} channels, which are composed of four inwardly-rectifying potassium ion pore-forming subunits (Kir6.2) and four high-affinity sulphonylurea receptor subunits. SUR1 and SUR2 sense the intracellular ADP concentration and link thereby the electrical activity of cell membranes to cellular metabolism. $(SUR1/Kir6.2)_4$ channels are broadly distributed in the neuroendocrine system and are involved in insulin secretion. Isoform A of SUR2, paired with Kir6.2 forms the K_{ATP} channels found in cardiac and skeletal muscle cells. Isoform B of SUR2 assembles with Kir6.1 and can be found in smooth muscles [64]. The remaining members of this subfamily are mainly involved in multi drug resistance. ABCC1, ABCC2, and ABCC3 translocate drugs and organic anions. ABCC4, ABCC5, ABCC11 and ABCC12 lack an N-terminal domain that is not required for transport

of organic or lipophilic anions, glutathione conjugates or nucleotide analogs [45, 65]. ABCC13 is classified as pseudogene by HGNC [43].

ABCD

The ABCD subfamily comprises only four members, which are all half-transporters. ABCD1 to 3 are localized at the human peroxisome membrane and are involved in the transport of fatty acids [66–69]. ABCD1 and the closely related ABCD2 transport free very-long-chain fatty acids as well as their CoA-esters [69, 70]. Mutations in ABCD1 cause X-linked adrenoleukodystrophy, the most common inherited peroxisomal disorder characterized by abnormal accumulation of saturated, very long chain fatty acids predominantly in brain white matter, adrenal cortex and testis [71]. ABCD3 is involved in the transport of branched-chain fatty acids and C27 bile acids into peroxisomes [72]. ABCD4 is localized at the ER and lysosomal membranes and is involved in the release of vitamin B_{12} from lysosomes [73]. Mutations in ABCD genes can occur in Zellweger syndrome [66].

ABCE and ABCF

The ABCE and ABCF subfamilies are the smallest subfamilies with one and three members, respectively. Both subfamilies lack the transmembrane part of ABC transporters and consist only of NBDs. While ABCE1 is the key factor for the recycling process of ribosomes [74], ABCF1 interacts with eukaryotic initiation factor 2, which plays a key role in translation initiation and control [75].

ABCG

The ABCG subfamily is composed of five 'reverse' half-transporters with inverse domain topology, having N-terminal NBDs and C-terminal TMDs. ABCG1 is involved in macrophage lipid export processes, regulating cholesterol and phospholipid transport [76]. ABCG4 is a homolog of ABCG1 with 72% identity at amino acid level, and probably has a similar function [77, 78]. ABCG2, also named BCRP (breast cancer resistance protein), operates as multidrug transporter and has physiological roles in several tissues including the mammary gland and the blood-brain, blood-testis, and maternal-fetal barriers [79]. ABCG5 and ABCG8 form a heterodimeric transporter located in apical membranes of bile ducts and intestinal enterocytes, that mediate the efficient excretion of neutral sterols [80]. Mutations of ABCG5/8 are the cause of sitosterolemia, an autosomal recessive disorder characterized by the accumulation of both plant-derived (primarily sitosterol) and animal-derived (cholesterol) sterols in plasma and tissues [81].

1.1.1.5 Bacterial ABC exporters

Bacterial ABC exporters are involved in a wide range of biological processes, including the regulation of substrate efflux, that ranges from small inorganic ions, drugs, and antibiotics to large protein toxins and other macromolecules. Some can also function as mediators and regulators in transmembrane processes, without being involved in any direct transport reaction. FtsEX for example, was identified as a regulator of cell-wall hydrolysis at the division site. The cell wall material, mostly consisting of peptidoglycal (PG), that is initially shared by daughter cells, has to be processed by amidases before the daughter-cells can separate. These amidases are activated by EnvC, a divisome-associated protein with PG-cleaving LytM domains, that interacts with FtsEX via a periplasmic loop of the transmembrane component FtsX. ATP hydrolysis mediated by FtsE induces conformational changes, that are transmitted to EnvC to control the amidase activity [82, 83].

Unlike in humans, bacterial ABC transporters are not subdivided into A-G subfamilies and are mostly named after the organism they originate from and/or their function. However, many mammalian ABC exporters, especially those of the B subfamily, have bacterial homologs or precursors, that are mostly involved in multidrug resistance processes. P-glycoprotein (ABCB1) for example, has several homologs, of which the homodimeric MsbA and LmrA are the most well-known. While it was demonstrated several times, that MsbA is involved in flipping Lipid A from the inner leaflet of the cytoplasmic membrane to the outer membrane, glycerophospholipid export function is controversially discussed [84, 85]. LmrA is an efflux transporter for various amphiphilic cationic compounds and can partially replace MsbA function [86]. Both, MsbA and LmrA have a similar selectivity for cytotoxic drugs and modulators as ABCB1.

Several other homo- or heterodimeric exporters that do not have close relatives in humans or mammalians can confer resistance to various drugs. Examples are Sav1866 from *Staphylococcus aureus*, PatAB from *Streptococcus pneumoniae*, LmrCD from *Lactococcus lactis* and BmrCD from *Bacillus subtilis*. Although TmrAB from *Thermus thermophilus* also belongs to the bacterial MDR exporters, a structural genomics screen identified it as a TAP homolog [87].

While most of the well-known bacterial exporters are involved in multidrug resistance and are therefore in focus of medical research, many others are involved in lipid translocation. PglK for example, behaves similar to ABCA1 and flips lipid-linked oligosaccharides from the cytoplasmic side to the periplasmic side of the membrane. For such flippases a lateral substrate access mechanism was proposed, although the complete mechanism is still elusive [22, 36].

Bacterial ABC exporters usually consist of four domains, comprising two TMDs and two NBDs. In some transporters the TMDs are fused to the NBDs and can form homo-

or heterodimers. Since they have a wide range of substrates, the NBDs are usually conserved while the similarities of the TMDs are mostly confined to structural analogy. Substrate translocation occurs, as for other ABC transporters, mostly via the alternating access mechanism [82].

1.1.2 Translocation mechanisms of B-subfamily and related exporters

The majority of ABC B-subfamily exporters and their related bacterial exporters translocate their substrates via the 'alternating access mechanism' that was presented more than 50 years ago as a general substrate translocation mechanism for membrane pumps [88]. Although many structures of B-subfamily ABC transporters were already solved, many more are missing to understand all transitions of the transport cycle. Especially structures with bound substrates would particularly contribute to close the transport cycle gaps. Though, these structures are difficult to obtain, since properties and binding affinities of the substrates are altered in detergents. Moreover, transporters in detergents tend, in the absence of ATP, to adopt an inward facing conformation without substrate bound [89].

The alternating access mechanism implies that the transporter switches between two major states, the inward- and the outward facing conformations. Both, importers and exporters use this mechanism, although it is shifted which state binds the substrate tightly or weakly. Exporters have separated NBDs in the inward-facing conformation and

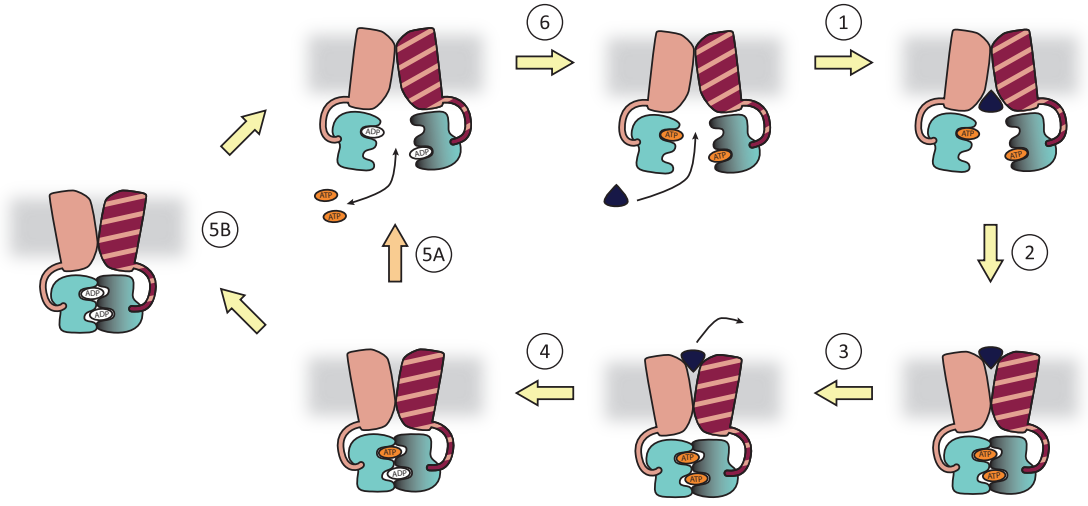

Figure 1.3: ABC exporter transport mechanism.
Substrate binding during the resting state induces a conformational change (1), that leads to NBD dimerization (2). The conformation changes thereby to the outward-facing state with bound substrate and ATP (orange). Substrate release (3) induces ATP hydrolysis of the first ATP (4). Transporter with a degenerated NBD now return to the resting state (5A) and ADP (white) is exchanged by ATP. All other exporters undergo a second ATP hydrolysis step (5B) before returning to the resting state. Adapted from Grossmann *et al.* [90].

tightly dimerized NBDs in the outward-facing state. The current translocation model (Fig. 1.3) states that ATP is bound in the resting state and the NBDs are separated. Upon substrate binding (1) a conformational change is induced. The NBDs dimerize and translocate the substrate to the other side of the membrane (2). An intermediate occluded conformation with closed NBDs and substrate enclosed in the central cavity can potentially occur. Substrate release (3) triggers ATP hydrolysis (4), which is essential to disassemble the NBDs, so that the transporter can return to the inward-facing conformation. ABC exporters with a degenerate ATPase site directly return to the resting state (5A), where ADP is exchanged by ATP. Transporters with two canonical ATPase sites undergo a second ATP hydrolysis step (5B) before returning to the resting state, although it is still unclear weather the second hydrolysis step can occur simultaneously with the first [89–91].

For other ABC exporters the alternating access mechanism could not be proven. The antibacterial peptide transporter McjD for example, appears to utilize a novel translocation mechanism that requires only a transient opening of the cavity for peptide release [92]. For ABC exporters operating as flippases an outward-only mechanism with lateral substrate access was proposed. In contrast to the alternating access mechanism, the outward-only mechanism does not require a large separation of the NBDs. However, a certain opening is needed for phosphate release and nucleotide exchange. The mechanism is thought to begin with an ATP-bound outward-facing conformation. In the next step the pyrophosphate-glycan headgroup of the substrate is transferred into the outward-facing cavity, while the lipidic polyprenyl tail probably remains attached to the lipid-facing surface of the transporter. ATP hydrolysis and inorganic phosphate release induce the separation of the NBDs and the closure of the outward-facing gate, adopting a conformation of insufficient size to fit a substrate. So the substrate dissociates and ADP is exchanged for ATP, thereby resetting the system [36, 89].

1.1.3 The human TAP transporter

The genes of the human antigen translocation complex reside in the genomic region encoding the class II proteins of the major histocompatibility complex (MHC) and code for two heterodimeric half-transporters, TAP1 (ABCB2) and TAP2 (ABCB3) [93, 94]. The TAP subunits can both be divided into three functional modules: an N-terminal transmembrane domain (TMD0) formed by four helices, the central transmembrane domain (TMD) formed by six helices, and a cytosolic nucleotide-binding domain [95, 96]. TMD and NBD form the coreTAP complex, which is connected by a short α-helix, named elbow helix, to the TMD0 (Fig. 1.4). TAP is assembled at the ER membrane, where it becomes part of the peptide loading complex. The biogenesis of functional TAP depends

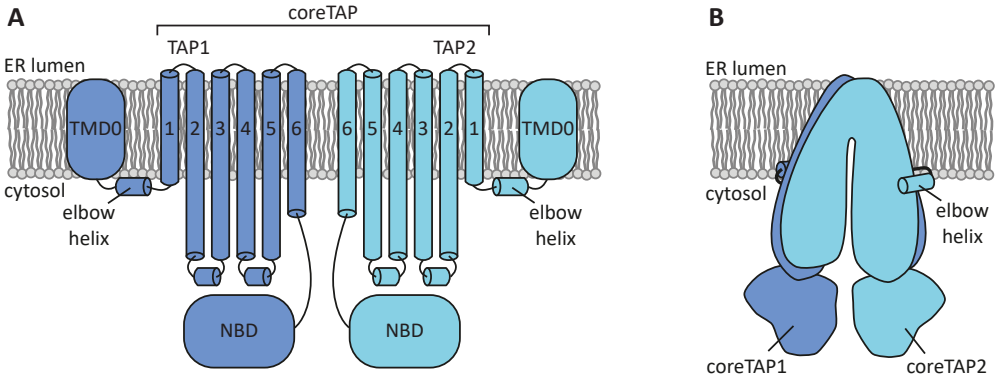

Figure 1.4: Schematic representation of the TAP transporter.
(A) The human antigen translocation complex TAP comprises the two half-transporters TAP1 (blue) and TAP2 (light blue), which are both composed of an N-terminal transmembrane domain (TMD0), a central transmembrane domain (TMD), and a cytosolic nucleotide-binding domain (NBD). The TMD0 is formed of 4 helices that are connected by the elbow helix to the six helices of the transmembrane domain. The coreTAP complex comprises the two TMDs and the two NBDs. (B) Schematic representation of coreTAP subunit arrangement. Adapted from Oldham *et al.* [32].

on the assembly of preexisting TAP1 with newly synthesized TAP2, but not vice versa [97]. Both subunits contribute to peptide binding [98], whereas the coreTAP complex is essential and sufficient for peptide binding and transport [95], while the TMD0s are necessary for assembly of the peptide loading complex [99]. The cryo-EM structure of coreTAP arrested by the herpesviral inhibitor ICP47 was recently revealed [32, 33], confirming the classical fold of ABC type I exporters. Although this is the first known TAP structure, it only partially contributes to the understanding of the peptide transport cycle: Being blocked by ICP47, peptides cannot accommodate into the binding cavity and TAP is forced to adopt a nonfunctional conformation. Furthermore, the structure lacks the highly flexible TMD0s, so that no conclusions about the TMD0-TAP interface and interactions with the peptide loading complex could be drawn.

TAP preferentially binds and translocates peptides derived from proteasomal degradation with a length of 8-16 amino acids, although 8-12 amino acid peptides are transported most efficiently [98, 100]. In addition to the preferred peptides, peptides with a length of up to 40 residues as well as sterically restricted peptides can be transported [101]. Peptide binding is defined by the first three N-terminal and the C-terminal amino acid residues. Lysine, arginine and asparagine are favored at the first N-terminal position, while arginine is favored at the second position and tryptophan and tyrosine at the third. At the C-terminus basic and hydrophobic residues are preferred [102]. The combination of NMR data and molecular modeling recently revealed the location of the peptide-binding cavity [103].

TAP possesses two different ATPase sites at the NBDs: the canonical site contains all consensus residues, whereas the degenerate site contains non-consensus substitutions

[104]. This single canonic ATPase site in TAP is sufficient to control NBD dimerization and disassembly, thereby inducing all conformational changes in the TMDs needed during peptide translocation.

1.1.4 TmrAB, a bacterial ABC transporter

The hyperthermophilic *Gram*-negative eubacterium *Thermus thermophilus* HB27, originally isolated from a hot spring in Japan, grows optimally at temperatures in the range of 65 to 72 °C [105]. Organisms growing at high temperatures often encode proteins, which own natural thermostability properties, disclosing optimal targets for biochemical assays and structural analysis. *T. thermophilus* holds the genes TTC0976 and TTC0977, which are arranged in one operon with overlapping open reading frames and encode the multidrug resistance ABC exporter TmrAB. A structural genomic screen identified TmrAB as potential TAP homolog. Similarly to TAP, TmrAB is also obligatory heterodimeric and possesses a degenerate ATPase site [87]. The heterodimers consist of one polypeptide chain, each containing a TMD formed by 6 helices and a NBD. The first structure of TmrAB in an inward-facing conformation was solved by cryo-EM with the help of the antigen-binding fragment AH5, which helped to overcome the pseudosymmerty of the two subunits. At the time, this structure of about 135 kDa was the smallest protein structure solved by single-particle cryo-EM [106]. The second structure of TmrAB was recently solved by X-ray crystallography at an significantly improved resolution of 2.7 Å, compared to the previous 8.2 Å structure [2].
TmrAB mediates the ATP-dependent uptake of the multidrug model compound Hoechst 33342 in inside-out oriented vesicles, which could be specifically inhibited by verapamil [87]. Later it was demonstrated, that TmrAB has a broader substrate specificity, covering the substrate spectrum of TAP [2], although its natural substrate is still elusive. It was also hypothesized that TmrAB can potentially act as flippase, since during delipidation of the transporter only lipid A was retained and prolonged delipidation further led to reduced ATPase activity [107].

1.2 The human adaptive immune response

Since their origin, organisms have had to fight against viruses, bacteria, fungi, and numerous other pathogens. So, all multicellular plants and animals possess an innate, antigen-unspecific immune response, that comprises humoral and cellular defenses and has been developed quite early during evolution. However, this immune response reflects only a first line of defense, limited to physiological and mechanical barriers, like mucous tissues, cilia, macrophages, natural killer cells, granuolcytes, and the complement system.

Most pathogens have developed often unique and sophisticated strategies to escape this first line of defense and need more flexible and adaptable defense mechanisms.
Jawed vertebrates have evolved a second line of defense, called the adaptive or acquired immune system, which cooperates with the innate immune system to eliminate pathogens more efficiently. In contrast to the innate system, this defense is highly specific to the pathogen assaulting the organism and can provide long-lasting protection through immunological memory. Cells of the adaptive immune system are able to remember antigens for tens of years, which is also the basis for the development and efficiency of vaccines.
The induction of an adaptive immune response begins with the ingestion of a pathogen by an immature dendritic cell surveying the local environment. Its primary function is not to destroy pathogens, but to carry pathogenic antigens to the peripheral lymph nodes, in order to present them to T lymphocytes. Dendritic cells become activated upon pathogen uptake and travel then to nearby lymph nodes. The activation induces the maturation of the dendritic cell into a highly effective antigen-presenting cell (APC) that can now activate pathogen-specific lymphocytes in the lymph node. Cytokines secreted by the activated dendritic cells influence both innate and adaptive immune responses. In the lymphoid tissues, naive lymphocytes that have yet to encounter their specific antigen, and APCs can come together. Upon recognition of their specific antigens, the naive lymphocyte stops migrating and enlarges, differentiating to a lymphoblast. The lymphoblast then starts to divide and creates around 1000 cells of identical specificity, which then differentiate into effector cells. In the case of B cells, the differentiated effector cells form antibody-secreting plasma cells. In the case of T cells, the effector cells have the possibility to destroy infected cells or to activate other cells of the immune system. The life-span of effector cells is limited and once the antigen is removed, most of the antigen-specific cells resulting from the clonal expansion of small lymphocytes undergo apoptosis. Only few of these cells survive, forming the memory cells that represent the basis of immunological memory.
The effectiveness of T lymphocytes depends on the interaction with infected cells. Antigens are produced by pathogens that have infected a target cell or that have been ingested by it and are recognized by T and T_H1 cells. In contrast, helper T cells recognize and interact with B cells. Antigenic peptides are presented on the cell surface by particular membrane glycoproteins named major histocompatibility complex (MHC). There are two types of MHC molecules: class I molecules can be found on the cell surface of all nucleated cells, presenting peptides derived from cytosolic degradation, and can thus display fragments of viral proteins. Class II molecules can be found only on antigen-presenting cells, presenting peptides derived from proteins in intracellular vesicles. Thus, the displayed peptides derive from pathogens living in macrophage vesicles or internalized by phagocytic cells and B cells. [108]

1.2.1 The MHC I antigen processing pathway

The peptide loading complex (PLC, Fig. 1.5) resides at the ER membrane and comprises several proteins fulfilling central and critical steps in antigen presentation via MHC I molecules (Fig. 1.6). The PLC is composed of one TAP complex and two each, tapasin, ERp57s, MHC I/β_2m and calreticulin. The MHC I peptide loading process starts with TAP translocating antigenic peptide precursors derived from proteasomal degradation into the ER lumen. After transport, these peptides are then further trimmed by the aminopeptidases ERAP1/2 [109]. The type I membrane glycoprotein tapasin acts as

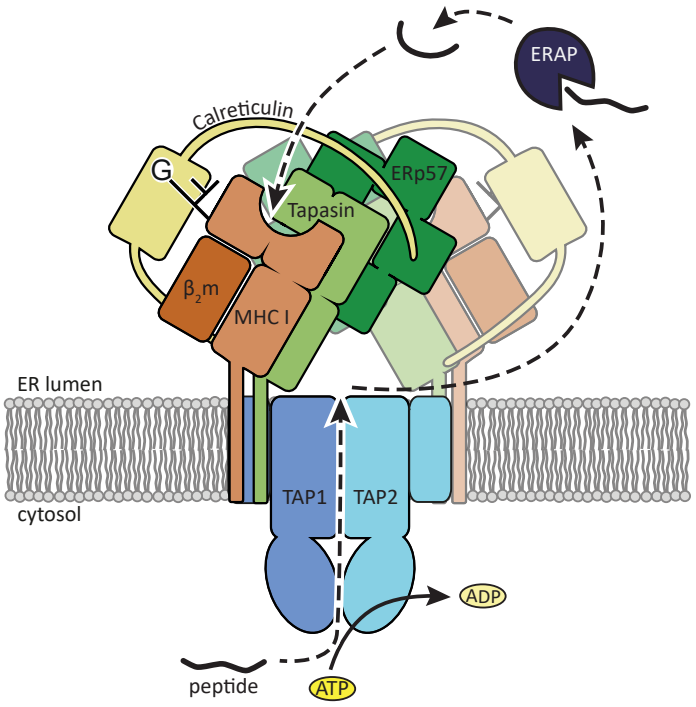

Figure 1.5: Schematic representation of the PLC function.
The PLC is composed of TAP, tapasin, ERp57, MHC I/β_2m and calreticulin. TAP translocates proteasomal degradation derived peptide precursors into the ER lumen, which are further trimmed by ERAP1/2 before loading onto MHC I. Tapasin is involved in MHC I/peptide complex proofreading, while ERp57 and calreticulin assist the correct folding and assembly of the PLC [110]. Adapted from Blees *et al.* [111].

a bridge between the TAP transporter and MHC I, binding to both components at the same time [99]. Furthermore, tapasin is able to distinguish MHC I loaded with optimal or with suboptimal peptides [112–114]. MHC I molecules comprise two subunits, the heavy chain with the α 1 to 3 domains and the $\beta_2$microglobulin chain, which are non-covalently bound via interaction of β_2m with the α3 domain. β_2m is invariant while the α-subunit is polymorphic and encoded by the human leukocyte antigen (HLA)-A, -B, or -C gene. These HLA alleles differ in their dependency for tapasin regarding surface expression. Tapasin interacts also with ERp57, a protein of the PDI (protein disulfide isomerase) family. ERp57 functions specifically with calreticulin and supports the correct

formation of disulfide bonds in folding glycoproteins [110]. Calreticulin is a glycoprotein folding chaperone, and consists of three domains: the globular domain, the P-loop and a C-terminal acidic helix. Since it recognizes monoglucosylated N-linked glycans, it binds to the N-linked glycan at Asn86 of MHC I with an affinity of $\sim$1 μM. The interaction of its P-loop with ERp57 stabilizes the association of MHC I and calreticulin within the PLC [110]. The 7.2 Å structure of the fully assembled endogenous human PLC was recently solved by single-particle cryo-EM [111].

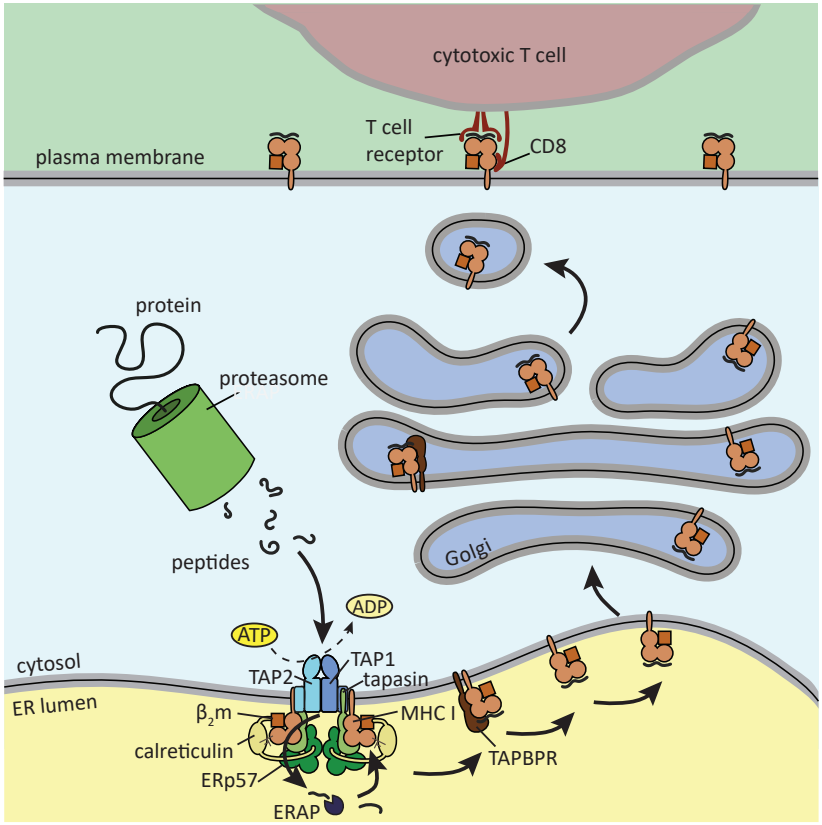

Figure 1.6: The MHC I antigen presentation pathway.
Antigenic peptides derived from proteasomal degradation are transported by TAP into the ER lumen. After beeing processed by ERAP1/2 the peptides are loaded onto MHC I molecules. Tapasin and TAPBPR sense the quality of the peptides, so that only high-affinity peptides remain bound to MHC I. Stable MHC I/peptide complexes dissociate from PLC and traffic through the secretory pathway to the cell surface to be presented to cytotoxic T cells.

Despite an efficient translocation of antigenic peptides into the ER, the second most important step for the activation of the adaptive immune response is to ensure that only high-affinity epitope peptides are bound to MHC I molecules. The first selection takes place in the peptide binding pocket of TAP, which translocates only a subset of all peptides present in the cytosol. The optimal length of these peptides is 8 to 12 residues, a near-ideal length for the binding to MHC I molecules [98, 100, 101]. A second selection takes place after translocation, when ERAP1/2 optimize the length of the peptides

[115, 116]. However, the actual selection step involves tapasin to proofread and select stable MHC I/peptide complexes [110, 117, 118]. TAPBPR (TAP-binding protein-related) was also found to be involved in proofreading of stable MHC I/peptide complexes. In contrast to tapasin, TAPBPR does not interact with ERp57 and calreticulin, and is hence not considered part of the PLC. Furthermore TAPBPR does not contain a ER-retention signal like tapasin and can accompany MHC I/peptide through the *Golgi* [119, 120]. TAPBRP can interact with UGT1 (UDP-glucose:glycoprotein glucosyltransferase 1), which can reglucosylate the glycan on MHC I and thereby facilitate the recognition by calreticulin [121].
Once a stable peptide has been found, the MHC I/peptide complexes leave the ER and travel through the *Golgi* to be presented on the cell surface. During the transport, the MHC I molecules undergo several posttranslational modifications. Peptides that fail the proofreading quality control are removed from MHC I to allow the binding of high-affinity peptides [110]. All these quality controls and optimizations of the antigentic peptides will ensure the recognition by $CD8^+$ T cells, allowing the adaptive immune system to monitor and remove pathogens.

1.2.2 Viral immune evasion

The antigen presentation pathway offers several possibilities to be manipulated and circumvented. Especially TAP, a central component of this pathway, appears to be a perfect target for viral immune evasion strategies. Although viruses evolved to interfere with the proteins involved in MHC I presentation in many different ways, some of them have evolved sophisticated strategies that specifically target key processes of the peptide transport cycle. Currently five proteins of viral origin are known to interfere with the TAP function (Fig. 1.7). Four of them are encoded by viruses belonging to the *Herpesviridae* family (ICP47, US6, UL49.5 and BNLF2a) and one is encoded by Orthopoxvirus (CPXV12). Although most the TAP inhibitors belong to one virus family, they are unrelated to each other, suggesting that the inhibition of TAP has evolved independently several times. Many herperviruses can establish long-term infections within their hosts, which underlie an enormous immunological pressure and thereby favor the evolution of different inhibition mechanisms [122, 123]. All inhibitors, except for the cytosolic ICP47, own a membranespanning helix and cytosolic or ER-lumenal domains. US6 and UL49.5 are type I membrane proteins, CPXV12 represents a type II membrane protein and BNLF2a belongs to the tail-anchored proteins [124].

A

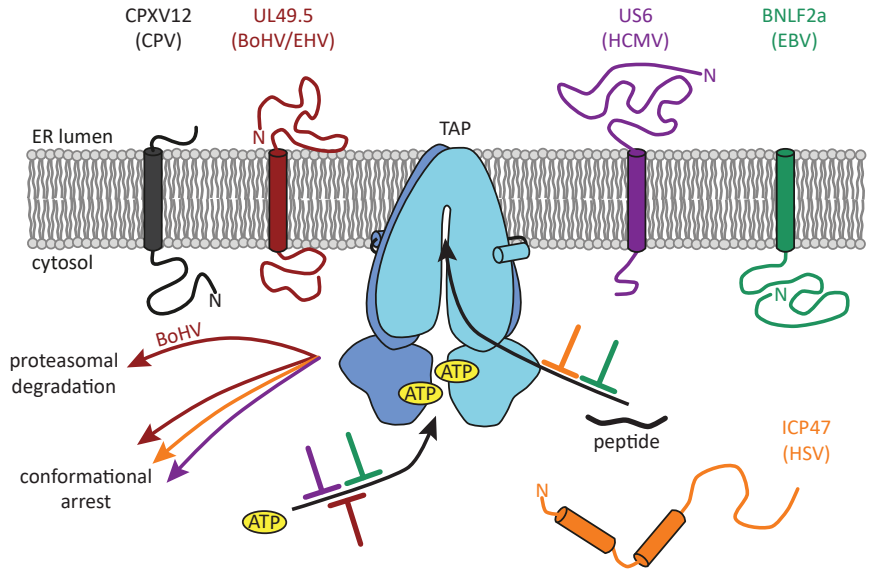

B

Inhibitor	Virus	Structure	#aa	Degradation of TAP1/2	Interference with binding of peptide	ATP	Conforamtional alterations
ICP47	HSV1/2	cytosolic	88/86	-	+	-	+
UL49.5	BoHV	type I MP	96	+	-	-	+
UL49.5	EHV1/4	type I MP	100	-	-	+	+
UL49.5	PRV	type I MP	98	-	-	-	+
US6	HCMV	type I MP	182	-	-	+	+
BNLF2a	EBV	TA protein	60	-	+	+	?
CPXV12	CPXV	type II MP	69	- (TAP1)	?	?	?

Figure 1.7: Viral evasion mechanisms.
(A) TAP can be inhibited by five viral inhibitors: ICP47 (orange) prevents peptide binding from the cytosolic side. UL49.5 (red) utilizes different mechanisms, depending on the species of the virus. UL49.5 from bovine herpes virus marks TAP for proteasomal degradation, while UL49.5 from equine herpes virus impedes ATP binding. UL49.5 from bovine and equine herpes virus and from pseudorabies virus induce a conformational arrest of TAP. US6 (purple) prevents ATP binding by interacting with TAP on its ER-lumenal interface. BNLF2a (green) interferes with both, ATP and peptide binding. CPXV12 (black) obstructs the formation of the peptide loading complex. Its precise inhibition mechanism is still elusive. Adapted from Hinz *et al.* [125]. (B) Comparison of structural and mechanistic features of the viral inhibitors of TAP. Adapted from Ressing *et al.* [124].

ICP47

Herpes simplex virus 1 (HSV1) is a common human pathogen, which first infects mucosa and then spreads via sensory neurons into ganglia where it achieves a lifelong persistence [126]. Post infection, the cell starts to synthesize infected cell polypeptides (ICPs). Five of the more than 50 ICPs are immediately-early polypeptides: ICP0, 4, 22, 27 and 47 [127, 128]. These polypeptides are needed to regulate the production of the other ICPs or to evade the hosts immune system.

ICP47, a small 88 amino acid protein (also known as IE12, Vmw12 or IE5), interacts with the TAP complex at its cytosolic interface thereby arresting its function [129]. As a

consequence the MHC I antigen presentation pathway is blocked and the virus can escape the immune surveillance. More precisely, ICP47 inhibits the TAP-dependent peptide translocation into the ER but not the ATP binding by interacting with TAP at a high affinity of 50 nM [4]. The viral factor needs both TAP subunits to bind to the TAP complex [130]. Within 2 h after infection with HSV, cells are lacking functional TAP molecules. Thus MHC I molecules cannot be loaded with peptides and are retained in the ER. This causes the assignment of peptide-deficient MHC I molecules for proteasomal degradation [131, 132]. The ICP47 residues 3-34 are known to be the most important for TAP inactivation, since they show nearly the same activity as the full length protein [4]. Hence these residues constitute the active domain of ICP47. By replacing each non-alanine residue in the active domain by alanines, three regions (8-12, 17-24 and 28-31) appeared to be the most critical for inhibition [5]. In aqueous solutions ICP47 does not present a secondary structure, whereas the contact with cell membranes or lipid-like solvents, induces the active domain to adopt a helix-loop-helix conformation [133, 134]. Although the structure of TAP arrested by ICP47 was recently solved [32, 33], the precise inhibition mechanism, and especially the thereby involved TAP-residues were not investigated in detail and remained partially elusive.
HSV2, a human pathogen, which produces genital herpes, encodes a 86 residues long ICP47 that shares 42% amino acid sequence identity with ICP47 from HSV1, although similarity is mostly limited to their N-terminal active domain sequence. Binding affinities to TAP do not significantly differ [135].

US6

The human cytomegalovirus encodes various genes that target MHC I molecules at different points in their assembly procedure. One of these genes encodes a 22 kDa glycoprotein that resides at the ER membrane and binds to TAP, thereby inhibiting peptide translocation into the ER [136–138]. In contrast to ICP47, US6 interacts with TAP inside the ER. Thereby peptide binding remains unaffected, while ATP binding is prevented [139, 140]. Although US6 interacts with several ER-lumenal loops of TAP, both TAP subunits are required for full interaction [141].

UL49.5

UL49.5 is encoded by the varicellovirus and blocks TAP in different ways, depending on the species of the virus. Few UL49.5 variants, for example UL49.5 from human herpesvirus 3 or varicella-zoster virus (VZV) and canid herpesvirus 1 (CaHV-1) fail to inhibit TAP. In some other cases UL49.5 possesses a dual role, acting both as molecular chaperone and as an immune evasion protein [142].
In case of bovine herpes virus-1 (BoHV-1) TAP is arrested in a translocation-incompetent state and marked for proteasomal degradation. This proteasomal degradation of both

TAP subunits is induced by the last two C-terminal residues of the viral inhibitor. The process strictly requires additional signaling of an upstream regulatory element in the ER lumenal domain of UL49.5 [143–145]. In contrast, UL49.5 from equine herpes-virus (EHV) 1 and 4 prevents ATP binding to TAP. Pseudorabies virus does not affect peptide or ATP binding. All variants arrest TAP in a translocation-incompetent state [144].

BNLF2a

BNLF2a is encoded by the Epstein-Barr virus and blocks both, peptide and ATP binding to TAP by arresting coreTAP in a transport-incompetent state [146–148]. The binding mechanism of BNLF2a differs from other inhibition mechanisms and prevents the binding of other inhibitors [149]. BNLF2a comprises two domains: a C-terminal tail anchor enables membrane integration and ER retention, whereas its cytosolic N-terminus inhibits TAP function [150]. Despite naturally occurring sequence polymorphisms of BNLF2a, the mutations did not affect MHC I surface presentation [151].

CPXV12

CPXV12 is encoded by cowpox virus, which interferes with the formation of the peptide loading complex, inhibiting peptide translocation by TAP. In contrast to the other TAP inhibitors CPXV12 is less species specific, reflecting the ability of cowpox virus to infect many mammalian species [123, 152]. The precise inhibition mechanism remains to be determined.

1.3 Motivation and aims

The ABC transporter TAP is a key player in the adaptive immune response. By recognizing and translocating antigenic peptides derived from proteasomal degradation into the ER lumen it constitutes a bridge between the processing of harmful intruders and the marking of an infected cell for elimination. This puts TAP also in focus of medical research, especially in the fields of infectious and genetic diseases, and cancer research. While TAP function was already well studied, there were still many open questions, especially regarding the inhibition mechanisms of viral inhibitors, the structure of TAP, and the interaction with PLC components. Being a membrane protein resident at an intracellular membrane, and moreover part of a large protein complex, the access to TAP is inherently complicated, which makes also targeting quite difficult. Furthermore, ABC proteins are highly flexible, which often makes them ungrateful targets for structure determination.

A novel fusion approach was established in this work, allowing to position the viral TAP inhibitor ICP47 with a predefined orientation with regard to the heterodimeric TAP complex. The effects of ICP47 fragments of different lengths were compared towards transport inhibition and thermal stabilization of the TAP complex. This was aimed at finding optimally arrested ICP47-TAP complexes that could constitute possible candidates for future structural studies. Moreover, these ICP47-TAP hybrids allowed to gain new insights into the inhibition mechanism of ICP47.

Different glycine-serine linkers and a self-cleaving 2A site were further implemented into the TAP sequence to enable an imposed 1:1 stoichiometry of the two TAP subunits during protein biosynthesis. In addition to the identification of an optimally expressing construct, these efforts may also serve as proof of principle for future construct design of other proteins that require a specific stoichiometry.

The third part of this work deals with the bacterial ABC transporter TmrAB, which was described to be a potential TAP homolog. It owns the classical architecture shared by ABC transporters of the B subfamily and is able to translocate the peptide repertoire of TAP. In order to prove that TmrAB is an actual TAP homolog, various TAP-TmrAB hybrids were generated to disclose the function and localization of TAP-TmrAB hybrids in mammalian cells.

Chapter 2

Methods

2.1 Microbiology

2.1.1 Working with *Escherichia coli (E. coli)*

2.1.1.1 Cultivation of *E. coli* strains

MC1061 cells were used for all cloning experiments except those with pInitial. This special vector requires DB3.1 cells which are *ccdb*-resistant. *E. coli* (strains MC1061 and DB3.0) were grown in LB-Medium containing the appropriate antibiotic (100 μg/ml ampicillin, 70 μg/ml kanamycin or 25 μg/ml zeocin) at 37 °C and 180 rpm.

LB Medium	
10 g/L	Tryptone
5 g/L	Yeast extract
10 g/L	NaCl
15 g/L	Agar (only for plates)

2.1.1.2 Preparation of competent cells with rubidium chloride

3 ml of LB w/o antibiotic were inoculated with 0.1 ml *E. coli* (strains MC1061 or DB3.0) and grown at 37 °C and 180 rpm. This overnight culture was used to inoculate 200 ml of LB w/o antibiotic. The culture was grown at 37 °C and 180 rpm to an OD_{600} of 0.4 and subsequently cooled down on ice. All further steps were carried out on ice. Cells were harvested 10 min at 2000 g and 4 °C and carefully resuspended in 35 ml cold TFBI. The suspension was kept one hour on ice and then centrifuged 10 min at 2000 g and 4 °C.

The cells were carefully resuspended in 10 ml cold TFBII. 0.1 ml aliquots were frozen in liquid nitrogen and stored at -80 °C.

Transformation buffer I pH 5.8 (TFBI)	
30 mM	K-acetate
100 mM	RbCl
50 mM	$MnCl_2$
10 mM	$CaCl_2$
15 %	Glycerol

Transformation buffer II pH 6.8 (TFBII)	
10 mM	MOPS
10 mM	RbCl
75 mM	$CaCl_2$
15 %	Glycerol

2.1.1.3 Transformation of RbCl competent *E. coli*

An aliquot of frozen competent cells was thawed on ice. 0.1-1.0 μg of plasmid DNA or 10-20 μl of ligation mix were added to the cells and incubated 10 min on ice. The cells were heat-shocked for 3 min at 37 °C and subsequently kept on ice for 2 min. After adding 750 μl of LB, the cells were incubated 30 min at 37 °C and 400 rpm. For re-transformation of plasmid DNA, 20 μl of cell suspension was plated on LB agar plates containing the appropriate antibiotic. For transformation of a ligation, the cells were harvested 10 s at 10,000 g, resuspended in 0.1 ml LB and plated on LB agar plates containing the appropriate antibiotic. The plates were incubated overnight at 37 °C.

2.1.2 Working with *Pichia pastoris* (*P. pastoris*)

2.1.2.1 Cultivation of *P. pastoris*

The protease-deficient *P. pastoris* strain SMD1163-His^+ (Invitrogen) was cultured in YPD (full medium) or MGY (minimal medium) at 30 °C and 180 rpm.

YPD (Yeast Extract-Peptone-Dextrose) medium	
20 g/L	Glucose
10 g/L	Yeast extract
20 g/L	Peptone

MGY (Glycerol-complex Medium)	
3.4 g/L	Yeast Nitorgen Base
10 g/L	Ammonium sulphate
0.4 mg/L	Biotin
10 g	Glycerol 99.5%

2.1.2.2 pPICZ vectors

The *P. pastoris* strain SMD1163-His$^+$ retains the functional HIS4 gene, which is essential for histidine biosynthesis and allows the use of the pPICZA, B and C vectors (Invitrogen), which do not carry the HIS4 gene and can be selected on zeocin. All TAP-constructs were introduced into the pPICZC-vector by Bsp119I (N-terminal) and XmaJI (C-terminal) restriction sites.

2.1.2.3 Transformation of *P. pastoris*

100 μg of Plasmid DNA were digested 3 h with 100 U of MssI in a total volume of 200 μl at 37 °C. The reaction was stopped by incubating the sample 20 min at 65 °C. The restriction efficiency was verified with 5 μl of the reaction product loaded onto an 1% agarose-gel by electrophoresis and subsequent staining in an ethidium bromide solution. Purification of the linearized Plasmid-DNA was performed with a Nucleospin Gel and PCR Clean-up kit (Macherey-Nagel). 700 μl of NTI buffer were added to the reaction to obtain a total volume of 900 μl. Then 300 μl a time were loaded onto three columns and the supernatant again onto three columns. Further washing steps were performed according to the manual. Each column-bound DNA was eluted with 30 μl MilliQ-water. 30 μg of linearized DNA were concentrated to a total volume of 20 μl in a SpeedVac centrifuge.

100 ml of MGY medium were inoculated with fresh *P. pastoris* (SMD1163-His$^+$) culture and grown at 30 °C and 180 rpm until an OD_{600} of 1-2 was reached. An OD_{600} of 1 corresponds to 5x10^7 cells/ml. For each transformation 8x10^8 cells were used. The cells were resuspended in 8 ml lithium acetate/DTT buffer and incubated 30 min at room temperature. After 10 min centrifugation at 1,500 g, the cells were resuspended in 1.5 ml 1 M sorbitol and washed three times in 1.5 ml 1 M sorbitol. The cells were resuspended in 50 μl of 1 M sorbitol, mixed with 5 μg of purified DNA linearized by MssI and transferred to a 0.2 cm gap vial. After 5 min incubation on ice the electroporation was performed by a genepulser XCell (Bio-rad) using the fungal program 4 (25 μF, 200 Ω, 1.5 kV). Immediately after electroporation 1 ml of 1 M sorbitol was added to the cells which were transferred to a 15 ml falcon tube and incubated 1 h at 30 °C. 200 μl were

plated on 0, 100, 400, 700, 1000 μg zeocin/ml YPDS and incubated at 30 °C. 2-4 days after electroporation colonies appeared and were used for further clone selection.

2.1.2.4 Selection of *P. pastoris* clones

Lithium acetate/DTT buffer (pH 7.5)	
100 mM	LiAc
10 mM	DTT
0.6 M	Sorbitol
10 mM	Tris/HCl

YPDS	
20 g/L	Glucose
10 g/L	Yeast extract
20 g/L	Peptone
15 g/L	Agar

MMY	
3.4 g/L	Yeast Nitorgen Base
10 g/L	Ammonium sulphate
0.4 mg/L	Biotin
10 ml/L	Methanol

Breaking buffer pH 7.4	
50 mM	KH_2PO_4
1 mM	EDTA
5 mM	Aminocaproic acid
5%	Glycerol

2x SEC buffer pH 7.4	
40 mM	HEPES
200 mM	NaCl
50 mM	KCl

For each construct 24 colonies (possibly growing on high zeocin concentrations) were transferred to 50 ml tubespin bioreactors (TPP) in 5 ml MGY with appropriate zeocin concentration. After incubating 48 h at 30 °C and 180 rpm, 4 ml MGY were inoculated with the previously grown cultures to an OD_{600} of 6 and incubated over night at 30 °C

and 180 rpm. The cells were centrifuged 10 min at 3,500 g and resuspended in 10 ml MMY. After 24 h incubation at 30 °C and 180 rpm the cells were harvested 10 min at 6,000 g and used for membrane preparation. The pelleted cells were resuspended in 1 ml breaking buffer and transferred to a 2 ml tube with screw-cap. 0.5 ml acidic prewashed glass beads, 18 μl of 1 mM PMSF and 18 μl of 2.5 mM benzamidine were added. The cells were disrupted using a FastPrep (MP Biomedicals) with MP24x2 rotor and the program 20 s and 5 m/s at 4 °C. Cell disruption was repeated five times with 2 min cooling steps on ice in between. The tubes were centrifuged 5 min at 1,500 g and the upper suspension containing the cell membranes was collected. The lower part containing the glass beads and remaining cells was resuspended in 1 ml breaking buffer containing 18 μl of 1 mM PMSF and 18 μl of 2.5 mM benzamidine. This procedure was repeated two more times and the membranes were then harvested 30 min at 100,000 g using an Optima TLX ultracentrifuge (Beckman Coulter). The supernatant was discarded and the membranes were solubilized in 50 μl water, 15 μl 10% detergent (FOS-choline 12 or GDN, Affimetrix) and 75 μl 2x SEC buffer. After 1.5 h rotating at 4 °C, the solubilized membranes were centrifuged 30 min at 100,000 g. The supernatant was collected and used for further gelfiltration, in-gel fluorescence or western blot analysis.

To determine whether the *P. pastoris* clones contain equal amounts of each subunit, the membranes were solubilized with FOS-choline 12, which is a relatively harsh detergent that disrupts the interaction of the two TAP subunits. In the subsequent size exclusion chromatography each subunit fused to a GFP variant appears as a single peak. The best clone, that was selected for further studies, eluted in monodisperse peaks with similar peak intensities for both subunits. In case *P. pastoris* was selected for a TAP variant containing only one fluorescent protein, GDN was used. The best clone eluted as monodisperse peak with highest peak intensity among the other tested clones.

2.1.2.5 High density fermentation of *P. pastoris*

Trace salt solution (sterile filtered)	
233.8 mM	$FeSO_4$ x 7 H_2O
24.1 mM	$CuSO_4$ x 5 H_2O
0.5 mM	NaI
17.8 mM	$MnSO_4$
8.3 mM	Na_2MoO_4 x 2 H_2O
0.3 mM	H_3BO_3
2.1 mM	$CoCl_2$
146.7 mM	$ZnCl_2$
0.49 % (v/v)	H_2SO4
0.8 mM	Biotin

Basal salts[153]	
14.4 g	$(NH_4)_2SO_4$
1.5 g	$CaSO_4$ x 2 H_2O
29.1 g	K_2SO_4
23.9 g	$MgSO_4$ x 7 H_2O
74 g	Glycerol (86 %)
to 1.6 l	Distilled water

Large-scale fermentation was carried out in a Labfors 3 bench-top bioreactor (Infors HT) equipped with 7.5 l vessel, microprocessor control of dissolved oxygen, pH, temperature, agitation, nutrient and methanol feed. Methanol concentration was monitored on-line by an external sensor (Raven Biotech). Basal salts [153] with 2 ml Antifoam 204 (Sigma) were autoclaved within the vessel. Before inoculation the medium was supplemented with 200 ml sodium hexametaphosphate (250 g/l sterile filtered) and 9 ml Trace salt solution. The fermentor was inoculated with 400 ml pre-culture as soon as a constant temperature of 30 °C was reached. pH was adjusted using 25% ammonium hydroxide solution.

Fermentation was performed in three phases. First, the cells were grown until the initial glycerol was completely consumed (glycerol batch phase), which is indicated by the dropping dissolved oxygen (from 100% to ∼35%). Subsequently, glycerol-feed phase started, feeding the cells continuously with 50% glycerol solution supplemented with 12 ml/l Trace salt solution. The feed-rate was increased stepwise from 2 to 12 (device specific parameter) to ensure an exponential-like feed until cells reached a density of ∼200 g/l. Dissolved oxygen was automatically adjusted to 35% for the remaining fermentation by the addition of pure oxygen. Following, in a time range of approximately

6 h, the feed-rate was stepwise reduced to 0 in order to ensure a complete consumption of the glycerol in the medium. After a short starving, the methanol-feed phase was started, feeding the cells with methanol supplemented with 12 ml/l Trace salt solution. The methanol feed was performed in three steps: First, a methanol-adaptation phase with a methanol concentration of 0.2%. Then the concentration was increased to 0.5% and later for the induction phase to 1%. 24 h after induction cells were harvested 35 min at 4500 g and 4 °C with yields of up to 260 g/l and stored in plastic bags at -80 °C. The detailed fermentation sequence is annotated in the supplements.

2.2 Molecular biology

2.2.1 Polymerase chain reaction (PCR)

DNA sequences were amplified using *Pfu* (*Pyrococcus furiosus*) DNA polymerase using the following protocol:

1 μl	plasmid DNA (30 ng/μl)
1 μl	forward primer (20 pmol/μl)
1 μl	reverse primer (20 pmol/μl)
2.5 μl	*Pfu* Buffer with $MgSO_4$
2.5 μl	dNTPs (2 mM each)
0.75 μl	DMSO
1 μl	*Pfu* DNA polymerase (2.5 U/μl)
Ad 20 μl	MilliQ water

If larger amounts of PCR product were needed, the reaction mixture was scaled up to a total volume of 50 μl. The following PCR program was used:

1 x	Intial denaturation	95 °C	120 s
30x	Denaturation	95 °C	30 s
	Primer annealing	58 °C *	30 s
	Elongation	72 °C	2 min/kb for products up to 2 kb, for larger products prolonged by 1 min/kb
1x	Final elongation	72 °C	1.25 x the elongation time used above

* Most of the primer were designed to have melting temperatures in the range of 60 °C to 64 °C, operating with a primer annealing temperature of 58 °C. If this was not possible, the primer annealing temperature was adjusted to the primer melting temperature.

2.2.2 Primer phosphorylation

PCR products that were used for blunt-end ligation were amplified with phosphorylated primers. These primers were phosphorylated 30 min at 37 °C using the following approach and subsequently heath deactivated 10 min at 72 °C.

2 μl	primer [100 pmol/μl]
2 μl	10x kinase buffer A
2 μl	ATP [10 mM]
1 μl	T4 polynucleotide kinase [10u/μl]
13 μl	dH_2O

2.2.3 Colony PCR

A colony PCR permits to preselect bacterial colonies before DNA purification and sequencing by verifying if one or more genes of interest were inserted into a backbone. Most commonly it was used for complex cloning, involving at least three DNA fragments. The primer used for this reaction must cover the sequence of interest, ideally annealing with the backbone at the 5 and 3 ends of the sequence. An overnight grown bacterial colony was picked with a pipette tip, dissolved in 20 μl MilliQ water and incubated for 10 min at 95 °C. The pipette tip was transferred to a tube containing 5 ml fresh LB medium with the appropriate antibiotic for further cultivation. Subsequently, the DNA sequences were amplified with Dream Taq DNA polymerase (Thermo Scientific) using the following protocol and PCR program:

3.75 μl	DNA (colony in MilliQ water)
0.375 μl	forward primer (20 pmol/μl)
0.375 μl	reverse primer (20 pmol/μl)
1.5 μl	Dream Taq buffer
0.75 μl	dNTPs (2 mM each)
0.1 μl	Dream Taq (5 U/μl)
8.2 μl	MilliQ water

1 x	Intial denaturation	95 °C	120 s
25x	Denaturation	95 °C	30 s
	Primer annealing	57 °C	30 s
	Elongation	72 °C	1 min/kb
1x	Final elongation	72 °C	1.25 x the elongation time used above

2.2.4 Agarose gel electrophoresis

DNA fragments derived from PCR-reaction or enzymatic restriction were separated by agarose gel electrophoresis. DNA in 1x DNA loading dye was loaded onto an 1% agarose in 1x TAE gel and separated in 1x TAE at 140 V using a Sub-Cell GT electrophoresis chamber (BioRad) and a E143 power supply (Consort). Subsequently, the gel was stained 15 min in 0.004% ethidium bromide solution to be analyzed on a UV-transilluminator (UST-20M-8R, 312 nm, biostep).

10x loading dye	
3 ml	Glycerol 99%
7 ml	dH_2O
10 μg	Bromophenol blue
10 μg	Xylene cyanol
10 μg	Orange G

50x TEA buffer	
242 g	Tris
57.1 ml	Acetic acid
100 ml	EDTA 0.5M (pH8.0)
Ad 1 l	dH_2O

2.2.5 Purification of DNA fragments

DNA fragments derived from PCR-reaction or enzymatic restriction were separated by agarose gel electrophoresis. Then, the DNA-bands were cut out and purified by Nucleospin gel and PCR clean-up kit (Macherey-Nagel). Departing from the manual, the DNA was eluted in 20 or 50 μl MilliQ water.

2.2.6 FX-cloning

FX-cloning (fast exchange) is a cloning system based on the class IIS restriction enzyme SapI (or LguI) that allows a high-throughput generation of different expression vectors with the same gene of interest [154]. The SapI cleavage (Fig. 2.1, left) generates a three base pair overhang that can be designed individually, depending on the application. During cleavage the recognition site of SapI is removed, allowing a seamless ligation. 3 and 5 ends carry different overhangs, assuring an oriented insertion into the backbone vector. The gene of interest was amplified by PCR with primers generating the SapI restriction site with appropriate overhang sequences for transfer into the pInitial vector,

which carries the lethal *ccdB* gene in between its SapI restriction sites. This step does not remove the SapI restriction sites, it exchanges only the gene sequence in between these restriction sites. Clones were selected on kanamycin resistance. The correct insertion of the gene of interest was verified by sequencing. Once the gene of interest was inserted into pInitial, it could be easily transferred without further PCRs or restrictions to other bacterial or mammalian expression vectors suitable for FX-cloning system. Here, the genes of interest were transferred to vectors based on pcDNA3 carrying C-terminal mVenus-C8-His_{10} or mCerulean-myc-SBP [155] both with ampicillin resistance.
pInitial, carrying the gene of interest, and pExpression, carrying the ccdB gene, are mixed together, digested with SapI, subsequently ligated by T4-Ligase and then plated on LB-plates with 100 μg/ml ampicillin. On these plates only clones carrying a pExpression-gene of interest vector could survive.

2.2.7 Cloning with SapI

Most constructs in this study were generated by using exclusively the restriction enzyme SapI for cloning procedures, however, without following the FX-cloning protocol. As mentioned above, SapI generates three base pair overhangs that can be designed individually, based on the application. For point mutations or the exchange or insertion of up to three amino acids, the whole plasmid was amplified with primers carrying the SapI restriction site and the mutations. Subsequently, the PCR products were separated on an agarose gel. The DNA-fragment of the expected size was cut out of the gel and purified, digested by SapI and contemporaneously religated by T4-ligase. In case several fragments had to be ligated, all of them were amplified to carry unique overhangs, that matched the next fragments overhang. Since the recognition site of SapI is eliminated during the enzymatic digestion, the ligated product cannot be digested again, and the correct product accumulates over time (Fig. 2.1).
This cloning strategy allows to seamlessly fuse one ore more fragments without leaving behind parts of restriction sites in between the different gene fragments. Fusing one fragment was successful in approximately more than 95% and four fragments in more than 70% of the tested colonies.
Often, the amplification of the genes of interest by PCR yielded several side products. However, this did not affect the efficiency of the reaction if only the DNA-fragments at the expected height on an agarose gel were used. Because of this, a DpnI digestion of template plasmid DNA was not necessary. The decreased efficiency in case of the fusion of more than one fragment was non further investigated, but is probably due to ligation errors or a non-optimal molar ratio of the fragments. The created plasmids were sequenced to verify the correct insertion.

The following restriction-ligation mix was used for most of the constructs. The amount of DNA had to be adjusted to the number of DNA fragments. For each fragment min. 2 μl of DNA or plasmid (max. 1 μg/ μl) were used. The restriction-ligation mix was incubated 30 min at 35 °C and subsequently used for *E. coli* MC10611 transformation. Since the reaction is very specific, the exact amount of DNA is of minor importance.

Restriction-ligation mix	
5-10 μl	Purified DNA (200-600 ng/μl)
2 μl	FD buffer
1 μl	FD LguI
1 μl	10 mM ATP
1 μl	T4 DNA ligase
Ad 20 μl	dH_2O

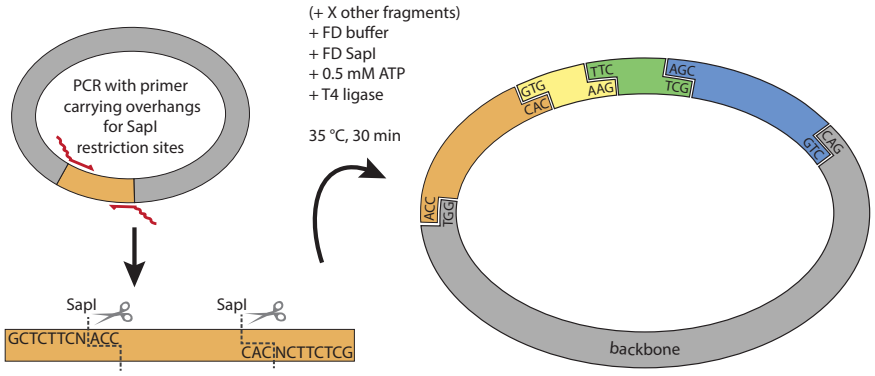

Figure 2.1: One-pot SapI cloning.
Genes of interest and a backbone are amplified by primers that attach SapI restriction sites to the 5'- and 3'-ends of the DNA fragments. Since the SapI recognition site is eliminated by SapI during the restriction, it is possible to design individual overhangs for the gene fragments to ligate several of them directionally into the backbone-vector. The simultaneous addition of fast digest SapI, T4-ligase and ATP in fast digest buffer allows to assemble these fragments in a one-pot reaction.

2.2.8 Restriction digestion with other enzymes

All other cloning steps or test restrictions after cloning that had to be performed using other restriction enzymes than LguI were performed using enzymes purchased from Thermo Fisher Scientific according to the manual. For double digestions the most compatible buffer according to the manual was used. The following restriction-digestion mix was incubated 2 h at 37 °C for normal enzymes and 15 min for fast digest enzymes. The reaction was stopped 20 min at 60 °C. In case of test restrictions the DNA was directly loaded onto an agarose gel.

5-10 μl	Purified DNA (200-600 ng/μl)
2 μl	Compatible buffer
1 μl	Enzyme 1
1 μl	(Enzyme 2)
Ad 20 μl	dH_2O

2.2.9 DNA ligation

Restricted DNA was purified by Gel and PCR Clean-up kit (Macherey-Nagel) and eluted in 20 or 50 μl MillyQ water. The ligation mix was incubated 2 h at 25 °C and then used directly for *E. coli* MC1061 transformation. The following protocol was used for ligation:

5-15 μl	Purified DNA (200-600 ng/μl)
2 μl	T4-ligase buffer
1 μl	T4-ligase
Ad 20 μl	dH_2O

2.2.10 Preparation of plasmid DNA

For small scale plasmid DNA isolation, the Nucleo Spin Plasmid Easy Pure kit (Macherey-Nagel) was used, starting with 5 ml bacterial overnight culture. The DNA was eluted in 50 μl of MilliQ water. For large scale plasmid DNA isolation, the Nucleobond AX kit (Macherey-Nagel) was used, starting with 200-500 ml bacterial overnight culture, depending on the needed DNA amount. The precipitated DNA was resuspended in 300 μl MilliQ water to measure the concentration by NanoDrop microvolume spectrophotometer ND-1000 (Peqlab). DNA concentration was adjusted to 1 μg/μl.

2.2.11 Sequencing and DNA analysis

The sequence of all generated plasmids was verified by sequencing the plasmid DNA (MWG Eurofins or Seqlab). 1500 ng of plasmid DNA were mixed with 40 pmol of sequencing primer in a total volume of 15 μl. All constructs were designed using Serial Cloner 2.6.1 and Snap Gene Viewer. Sequencing results were analyzed by Serial Cloner 2.6.1.

2.2.12 Design and cloning of used constructs

2.2.12.1 Backbone vectors

Plasmids used for transfection of mammalian cells were based on pcDNA vektors and were compatible with FX-cloning [154, 155]. A typical backbone vector contained ampicillin as selection marker, CMV promotor and a C-terminal tag composed of C3 cleavage-site, a GFP variant (mVenus, mCerulean or eGFP), C8- or myc-tag and His_{10}- or SBP-tag (Fig. 2.2).

Plasmids used for *P. pastoris* were based on pPICZ vectors which allow a high-level, methanol inducible expression. pPICZ contains zeocin as a selection marker and a AOX1 promotor. The gene of interest was transferred from a pcDNA vector to a pPICZ vector.

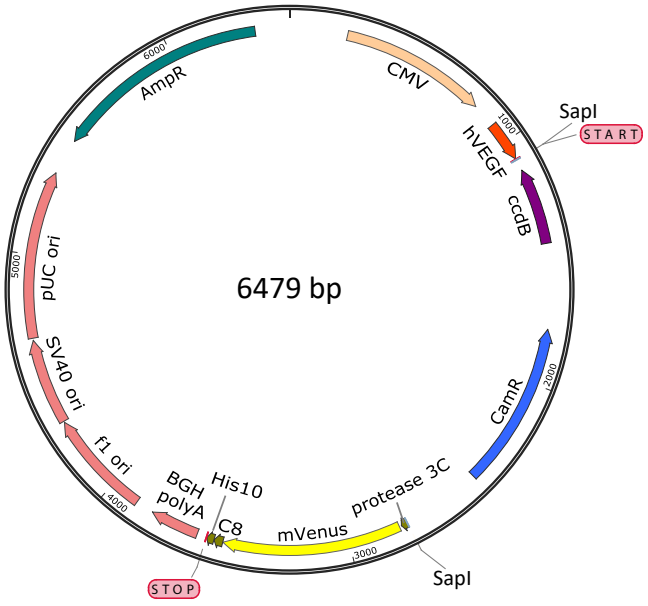

Figure 2.2: Backbone vector for mammalian expression. A typical FX-cloning compatible backbone vector for expression in mammalian cells contains a CMV-promotor, two SapI restriction sites to introduce a gene of interest that replaces the *ccDB* cassette, expression- and purification-tags and an ampicillin resistance.

2.2.12.2 Design and cloning of ICP47 and ICP47-coreTAP fusion constructs

Fusing the viral inhibitor ICP47 to the elbow helix of the coreTAP subunits allows to arrest the TAP transporter by simulating a defined high local concentration of ICP47 similar to a ball-and-chain inactivation of voltage-gated ion channels [156]. The polypeptide was systematically truncated in order to understand the function of the conserved regions and the orientation of ICP47 inside the binding pocket. These truncations were made at different time points or by different cloning strategies and were subdivided here into several parts.

ICP47-coreTAP fusions part I

Four fusion constructs harboring the active domain of ICP47 (residues 1-35, 1-50, 1-65 or 1-78) and two with an impaired active domain (residues 12-88 (ΔH1) and 1-22, 34-88 (ΔH2)) as negative control were generated with either coreTAP1 or coreTAP2. To compare their expression levels and to allow purification of heterodimeric complexes, the TAP subunits were fused to the fluorescent proteins mVenus or mCerulean, followed by a C8-His_{10} tag and a myc-SBP tag, respectively. These fusion constructs were created using ICP47(1-88) fused on coreTAP1 or coreTAP2 as template, which was generated by Anja Bäucker during her bachelor thesis [157]. The whole plasmid was PCR amplified using phosphorylated primers, which generate blunt ends at the desired fragment size (primer pairs 1/3, 1/4, 1/5, 1/6, 7/8 and 9/10, for ICP47 1-35, 1-50, 1-65, 1-78, ΔH1 and ΔH2 on coreTAP1 respectively. Primer pairs 2/3, 2/4, 2/5, 2/6, 7/8, 9/10 for ICP47 1-35, 1-50, 1-65, 1-78, ΔH1 and ΔH2 on coreTAP2 respectively). The DNA was digested by DpnI, purified and subsequently ligated and transformed into *E. coli* MC1061 (Fig. 2.3). Since this cloning method was successful in less than 50%, all further cloning procedures were performed with SapI-cloning. These fusion constructs, except for the two ΔH2 variants, were generated during my master thesis [3], but are listed here to keep the overview of all ICP47 constructs.

ICP47-coreTAP fusions part II

Flow cytometry experiments made it necessary to avoid the fluorophore mCerulean, as the cytometers used did not have the appropriate laser/filter settings for optimal detection. In all ICP47-TAP2-mCerulean fusion constructs, the mCerulean-myc-SBP tag was replaced by mVenus-C8-His_{10} tag. The constructs with an intact active domain and ΔH2 were PCR-amplified by primer pair 11/12, ΔH1 was amplified by primer pair 13/12, and coreTAP without ICP47 was amplified by primer pair 14/12. The resulting DNA fragments were ligated into pInitial, then transferred to an empty pExpression backbone with mVenus-C8-His_{10} tag by FX-cloning [154] (Fig. 2.4).

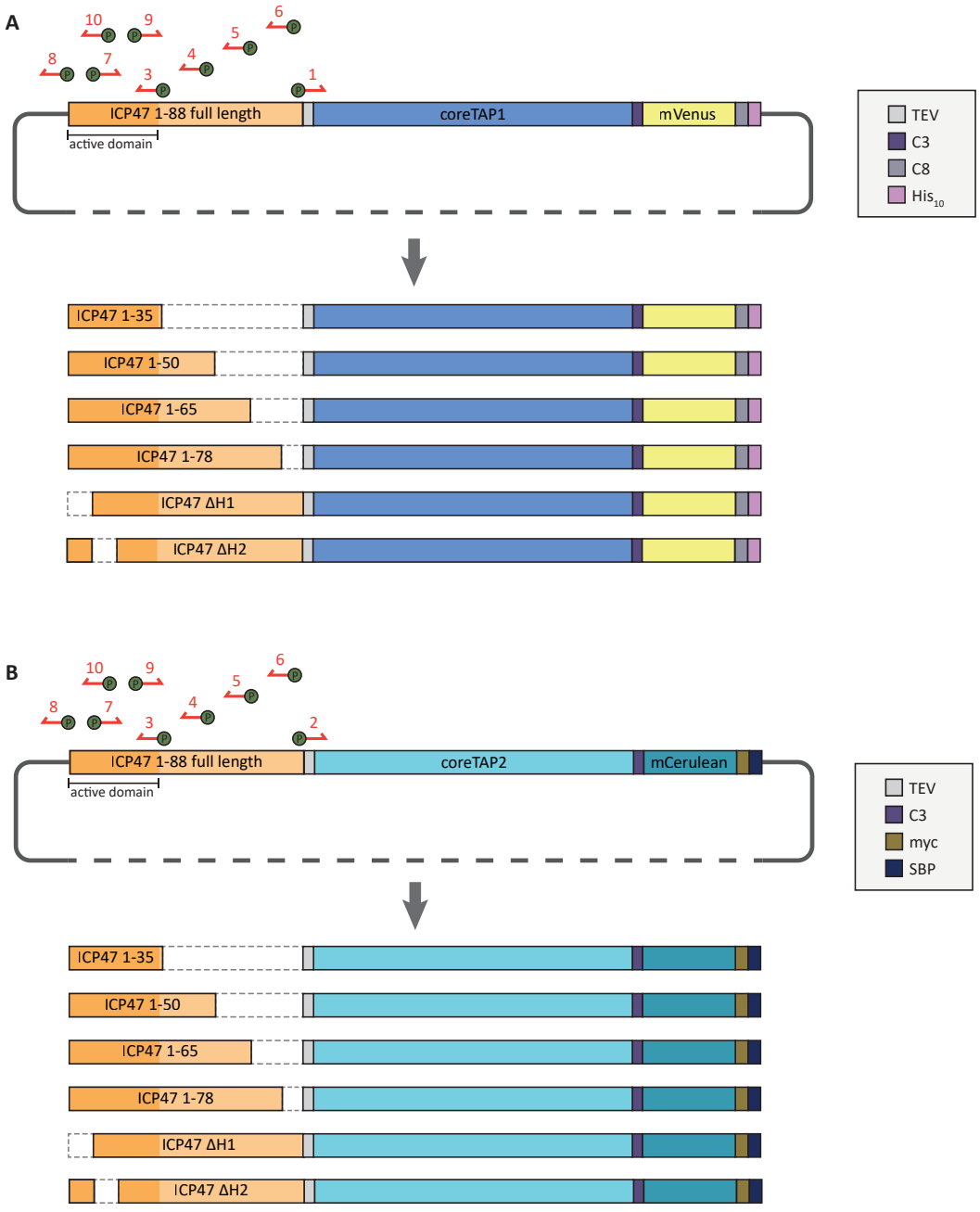

Figure 2.3: Cloning of ICP47-TAP fusions I.
Starting from the fusion constructs ICP47-TEV-coreTAP1-C3-mVenus-C8-His_{10} (A) and ICP47-TEV-coreTAP2-C3-mCerulean-myc-SBP (B), 12 constructs with shortened ICP47 were generated (6 for each TAP subunit). The whole plasmid was amplified by phosphorylated primer pairs 1/3, 1/4, 1/5, 1/6, 7/8 and 9/10 for TAP1 constructs and by primer pairs 2/3, 2/4, 2/5, 2/6, 7/8 and 9/10 for TAP2 constructs. After PCR amplification the DNA-fragments were religated. Altogether, this resulted in seven different ICP47 fragments fused to the TAP subunits: five potentially functional (ICP47 residues 1-35, 1-50, 1-65, 1-78 and 1-88) and two impaired (ICP47 residues 12-88 and 1-22, 34-88).

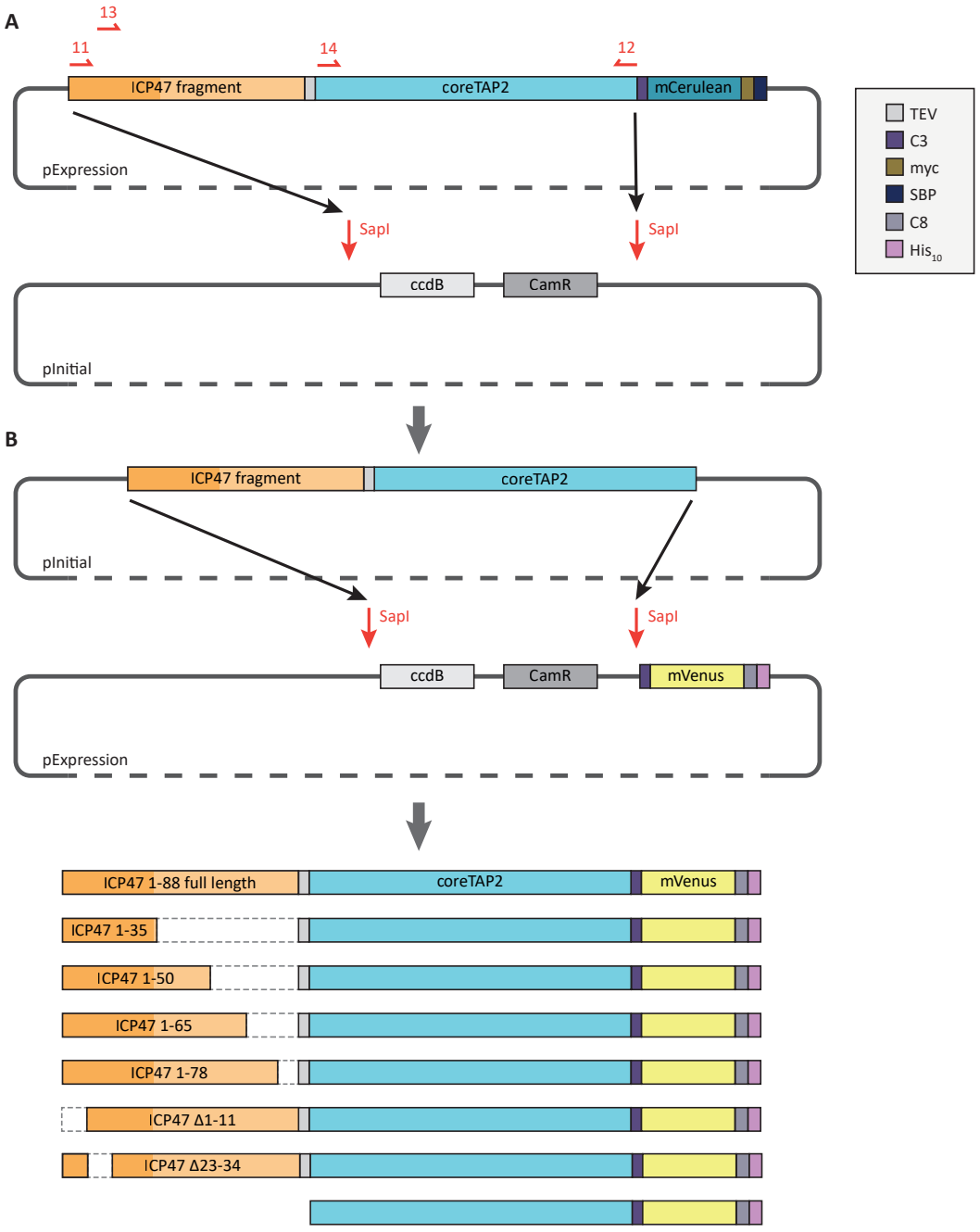

Figure 2.4: Cloning of ICP47-TAP fusions II.
The previously described ICP47-TAP fusion constructs carrying the mCerulean-myc-SBP tag (Fig. 2.4) were PCR amplified by primer pairs 11/12 (ICP47 1-35, 1-50, 1-65, 1-78, 1-88 and ΔH2), 13/12 (ΔH1) and 14/12 (coreTAP2). Subsequently, all DNA fragments were ligated into pInitial [154] (A) to be then transferred into a pExpression vector carrying a mVenus-C8-His_{10} tag (B) by FX-cloning [154].

ICP47-coreTAP fusions part III

Since previous studies defined the active domain as the only essential part of ICP47 needed for the interaction with the TAP complex [4, 5], five more constructs were designed using flexible glycine-serine linker to bypass the distance between the C-terminus of the active domain of ICP47 (residue 34) and the elbow helix of the TAP subunits. These five constructs represented an alternative to various ICP47 fragments fused to the TAP subunits and served as controls. Three synthetic linker based on G_4S repeats ($(G_4S)_4G_4$, $(G_4S)_6G_4$ and $(G_4S)_8G_4$) were amplified by forward primer 15 and reverse primer 16, 17 and 18, respectively. The backbones with ICP47(1-34)-coreTAP1 or -coreTAP2 were amplified by forward primer 19 and 20, respectively and reverse primer 21. The two fragments were religated by one-pot SapI cloning (Fig. 2.5).

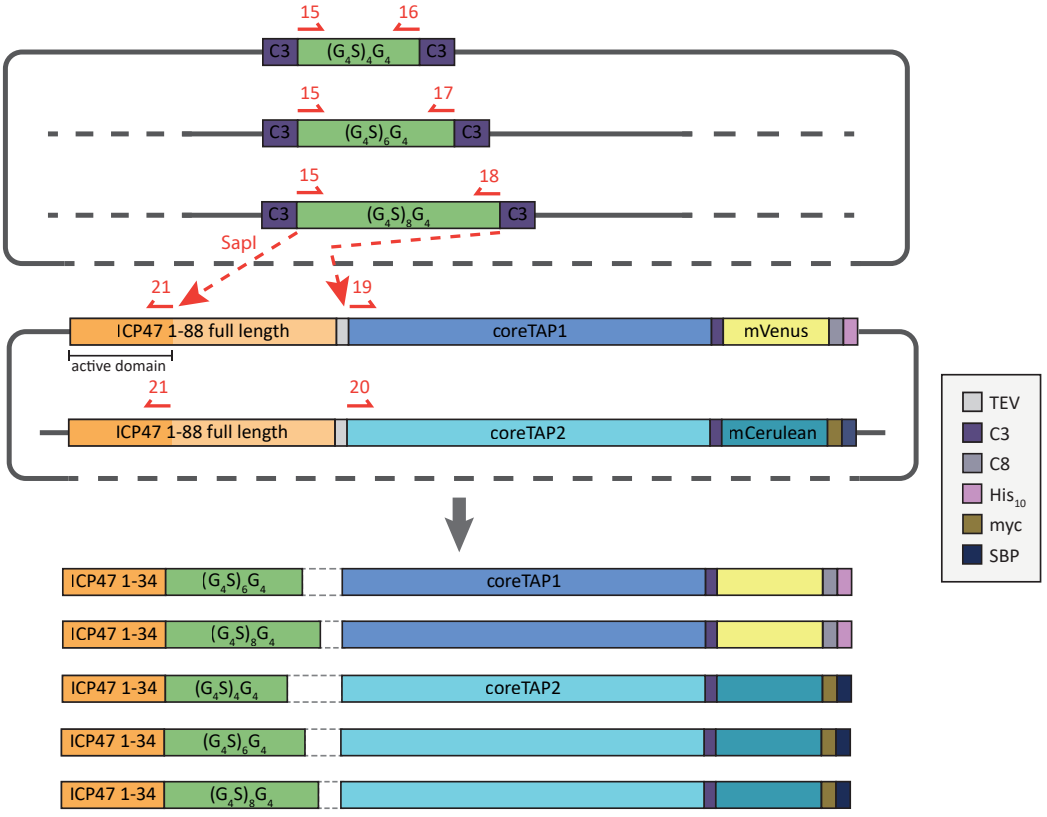

Figure 2.5: Cloning of ICP47-TAP fusions III.
Three synthetic linkers based on G_4S repeats were amplified by forward primer 15 and reverse primer 16, 17 and 18, respectively. The backbones with ICP47(1-34)-coreTAP1 or -coreTAP2 were amplified by forward primer 19 and 20, respectively and reverse primer 21. The two fragments were religated by one-pot SapI cloning.

ICP47-coreTAP for expression in *P. pastoris*

ICP47(1-88)-TEV-coreTAP2-mCerulean-StrepII was cloned into pPICZ vector by Anja Bäucker during her bachelor thesis [157]. Unfortunately, thereby the serine at position 2 in ICP47 was mutated to glycine. In this project, the vector was used as template to create the construct ICP47(1-72)-TEV-coreTAP2-mCerulean-StrepII. First, the residues 73-88 and the TEV cleavage site were removed by PCR-amplifying the vector with primer pair 22/23. The resulting DNA was then religated by one-pot SapI cloning. This step replaced the seven residues of the TEV-cleavage site by seven residues of ICP47 so that the total distance between the C-terminus of the active domain of ICP47 and the elbow helix of coreTAP2 remained the same when compared to the optimal ICP47(1-65)-TEV-coreTAP2 construct. In a second step, the S2G mutation was removed by PCR-amplifying the vector with primer pair 24/25. The resulting DNA was religated by one-pot SapI cloning (Fig. 2.6).

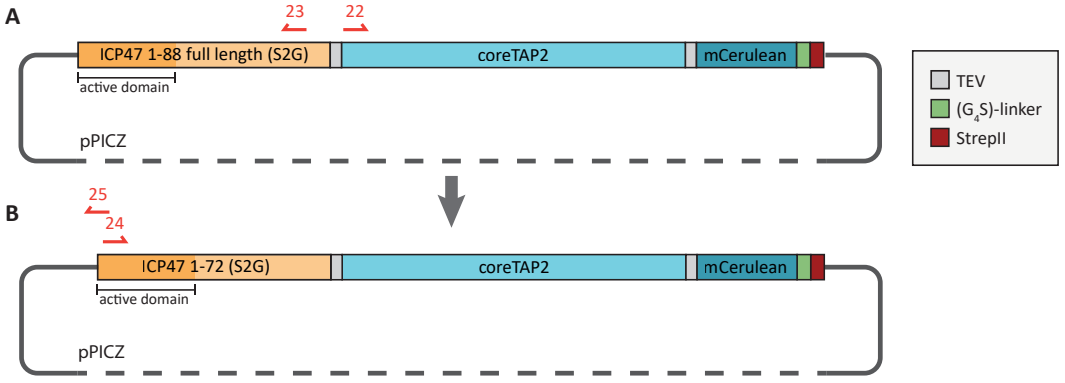

Figure 2.6: ICP47-coreTAP for expression in *P. pastoris*.
Starting from ICP47(1-88)-TEV-coreTAP2-mCerulean-StrepII, the TEV-cleavage site and 15 residues of ICP47 were removed by amplifying the whole plasmid with primer pair 22/23 (A). Subsequently, the DNA fragment was religated by one-pot SapI cloning. In a second step, the glycine at position two was mutated back to the original serine by amplifying the plasmid with primer pair 24/25 and then religating it by one-pot SapI cloning (B).

ICP47 constructs

ICP47(1-88) was cloned by Anja Bäucker into pInital during her bachelor thesis [157]. For this project, ICP47 was transferred by FX-cloning [154] from pInitial into a pExpression for mammalian cells carrying an mVenus-myc-His_{10} tag (Fig. 2.7A). Using this ICP47(1-88)-mVenus-myc-His_{10}, three shorter variants were created by amplifying the whole plasmid and subsequently religating it using the forward primer 26 and reverse primer 27, 28 or 29 to generate the ICP47 fragments 1-35, 1-55 and 1-73 respectively. One more construct was generated by primer pair 30/31 leading to ICP47(1-35)-myc-His_{10} without mVenus (Fig. 2.7B).

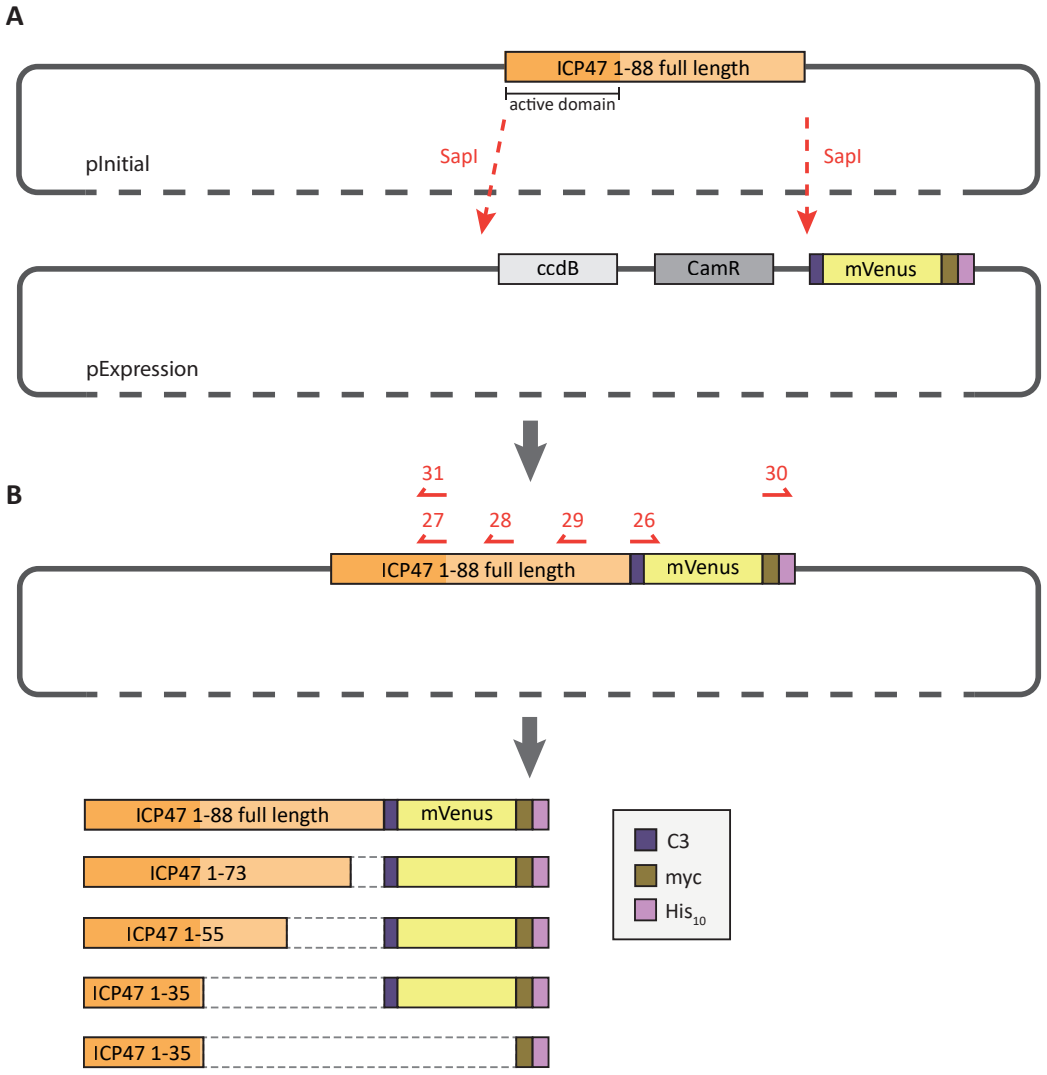

Figure 2.7: Free ICP47 constructs.
ICP47 was transferred from pInitial to a pExpression carrying a mVenus-myc-His_{10} tag (A). In a second step the whole plasmid was amplified by primer pairs 26/27, 26/28, 26/29 and 30/31 to be then religated by one-pot SapI cloning. ICP47 fragments 1-35, 1-55 and 1-73 with mVenus-myc-His_{10} tag and ICP47(1-35) without mVenus were generated respectively (B).

Mutations in the stabilizing region of ICP47

To define the residues involved in the stabilization of TAP more precisely, the putative stabilizing region of ICP47 (residues 35-55) was dissected into seven segments of three residues each (SR1-7). Using ICP47(1-88)-mVenus-myc-His_{10} as template, the whole plasmid was amplified with primer pairs 32/33, 34/35, 36/37, 38/39, 40/41, 42/43 and 44/45 (Fig. 2.8A). The DNA fragments were religated by one-pot SapI cloning to create SR mutations 1-7 respectively. All triplets were exchanged for glycine-alanine-glycine, except for SR2, where alanine-glycine-glycine was used (Fig. 2.8B).

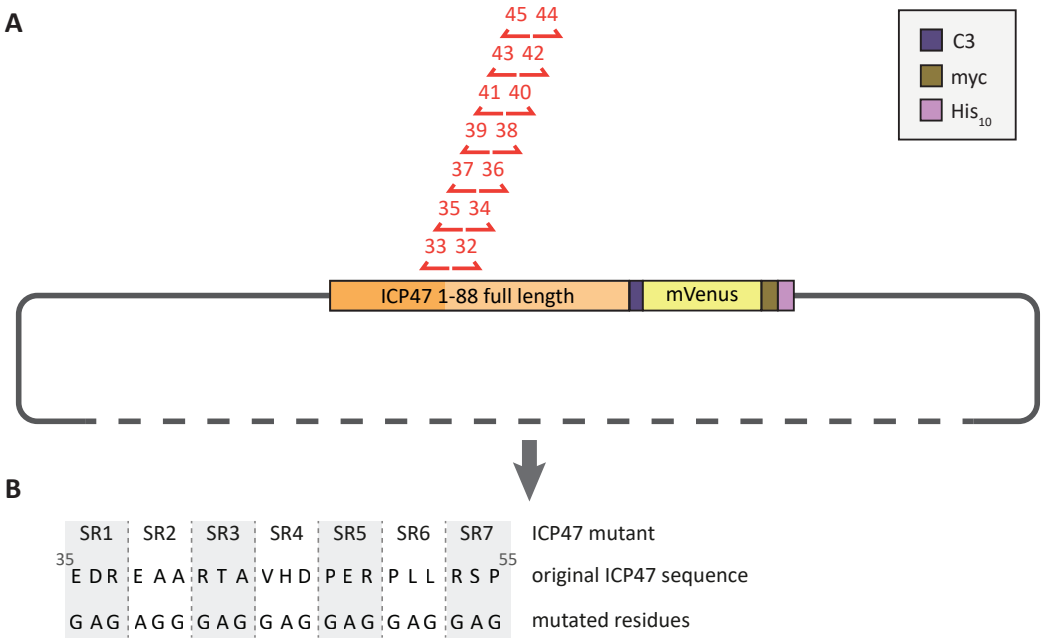

Figure 2.8: Mutations in the stabilizing region of ICP47.
ICP47(1-88)-mVenus-myc-His_{10} was amplified with primer pairs 32/33, 34/35, 36/37, 38/39, 40/41, 42/43 and 44/45 (A) and religated by one-pot SapI cloning to generate mutations in the putative stabilizing region of ICP47 (residues 35-55). This sequence was dissected into seven segments of three residues each. All triplets were exchanged for glycine-alanine-glycine, except for SR2, where alanine-glycine-glycine was used (B).

2.2.12.3 Design and cloning of 2A-site constructs

The foot-and-mouth disease virus (FMDV) encodes a short sequence (2A site) that mediates a cotranslational "ribosome skipping" event, allowing to cleave a protein at a defined position during its biosynthesis [158]. So, placing a 2A-site in between two proteins, which have to be expressed in similar amounts, can significantly improve the 1:1 stoichiometry of these proteins. In the FMDV genome, the 2A site is originally located in between the capsid protein 1D (CP1D) and the nonstructural protein 2B (Fig. 2.9A) [159]. Since there are hints that the C-terminus of CP1D could influence the cleavage efficiency of the 2A site, 39 residues of CP1D were attached to the 19 residues of the F2A site [160]. This "long" 2A-site was synthesized with flanking SapI restriction sites by Eurofins, so that it can be directly ligated in between two proteins of interest. coreTAP1-C3-mVenus-C8-His_{10} on pExpression was "opened" in between coreTAP1 and C3 by amplifying the whole plasmid with primer pair 46/47. ICP47(1-88)-coreTAP2 was amplified with primer pair 48/49 and the myc-SBP tag was amplified with primer pair 50/51 (Fig. 2.9B). These fragments were reassembled together with the 2A-site fragment by one-pot SapI cloning to coreTAP1-myc-SBP-2A-ICP47-coreTAP2-C3-mVenus-C8-His_{10} (Fig. 2.9C), abbreviated coreTAP1-2A-ICP47-coreTAP2.

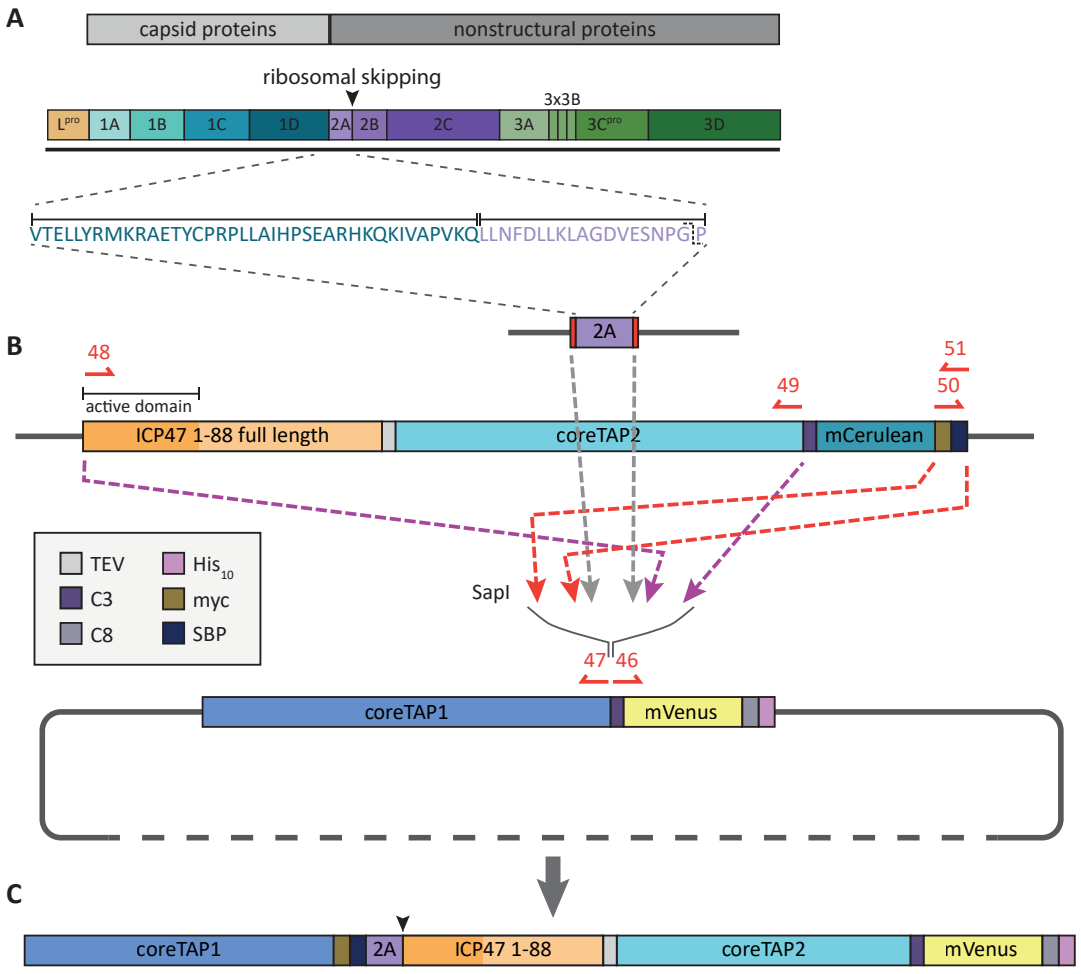

Figure 2.9: Design of coreTAP1-2A-ICP47-coreTAP2.
The C-terminus of CP1D (39 residues) and the 2A-site were synthetized with flanking SapI restriction sites by Eurofins (A). coreTAP1-C3-mVenus-C8-His_{10} on pExpression was "opened" in between coreTAP1 and C3 by amplifying the whole plasmid with primer pair 46/47. ICP47-coreTAP2 was amplified with primer pair 48/49 and the myc-SBP tag was amplified with primer pair 50/51 (B). These fragments were reassembled together with the 2A-site fragment by one-pot SapI cloning to coreTAP1-myc-SBP-2A-ICP47-coreTAP2-C3-mVenus-C8-His_{10} (C), abbreviated coreTAP1-2A-ICP47-coreTAP2.

A second 2A-site construct was designed to have ICP47-coreTAP2 placed in front of the 2A-site so that ICP47 cannot be potentially hindered by the remaining residues of the cleaving process. ICP47-coreTAP2 on pExpression was "openend" behind the purification tags by amplifying the whole plasmid with primer pair 51/52. coreTAP1-mVenus was amplified with primer pair 53/54 (Fig. 2.10A). These two fragments were reassembled together with the 2A-site fragment by one-pot SapI cloning to ICP47-coreTAP2-C3-myc-SBP-2A-coreTAP1-C3-mVenus-C8-His_{10} (Fig. 2.10B), abbreviated ICP47-coreTAP2-2A-coreTAP1.

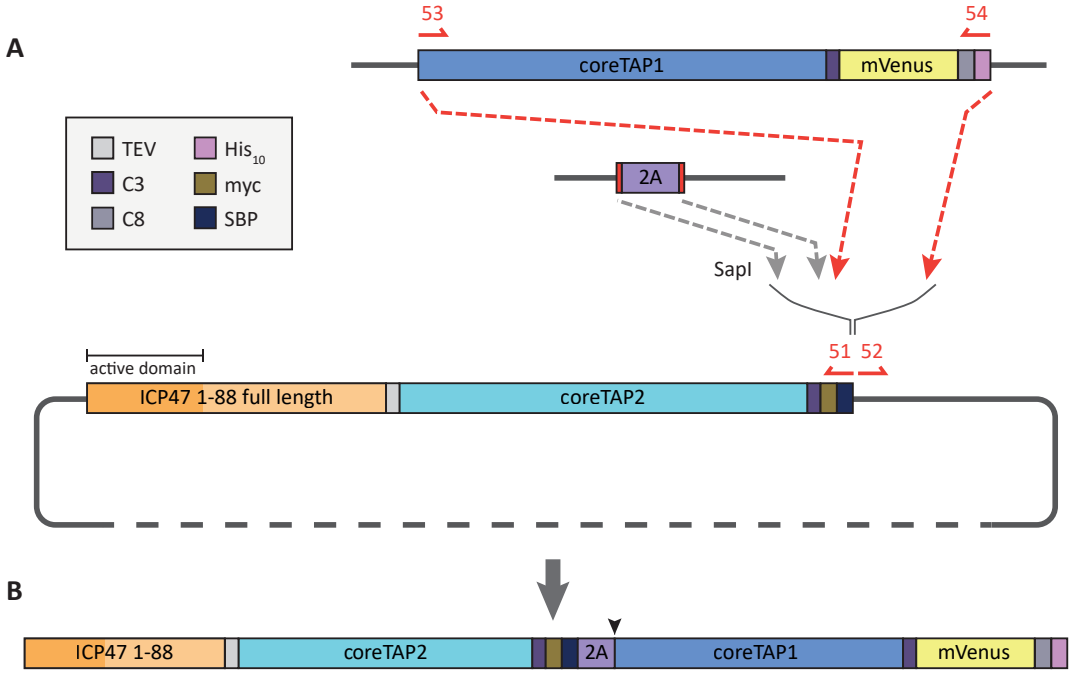

Figure 2.10: Design of ICP47-coreTAP2-2A-coreTAP1.
ICP47-coreTAP2 on pExpression was "opened" behind the purification tags by amplifying the whole plasmid with primer pair 51/52. coreTAP1-mVenus was amplified with primer pair 53/54 (A). These two fragments were reassembled together with the 2A-site fragment by one-pot SapI cloning to ICP47-coreTAP2-C3-myc-SBP-2A-coreTAP1-C3-mVenus-C8-His_{10} (B), abbreviated ICP47-coreTAP2-2A-coreTAP1.

A third 2A-site construct was created without ICP47 as active control for coreTAP1-2A-ICP47-coreTAP2 and ICP47-coreTAP2-2A-coreTAP1. coreTAP1-mVenus on pExpression was "opened" at the C-terminus of TAP1 by amplifying the whole plasmid with primer pair 46/47. coreTAP2 was amplified with primer pair 55/49 and the myc-SBP tag was amplified with primer pair 50/51 (Fig. 2.11A). These three fragments were reassembled together with the 2A-site fragment by one-pot SapI cloning to coreTAP1-myc-SBP-2A-coreTAP2-C3-mVenus-C8-His_{10} (Fig. 2.11B), abbreviated coreTAP1-2A-coreTAP2.

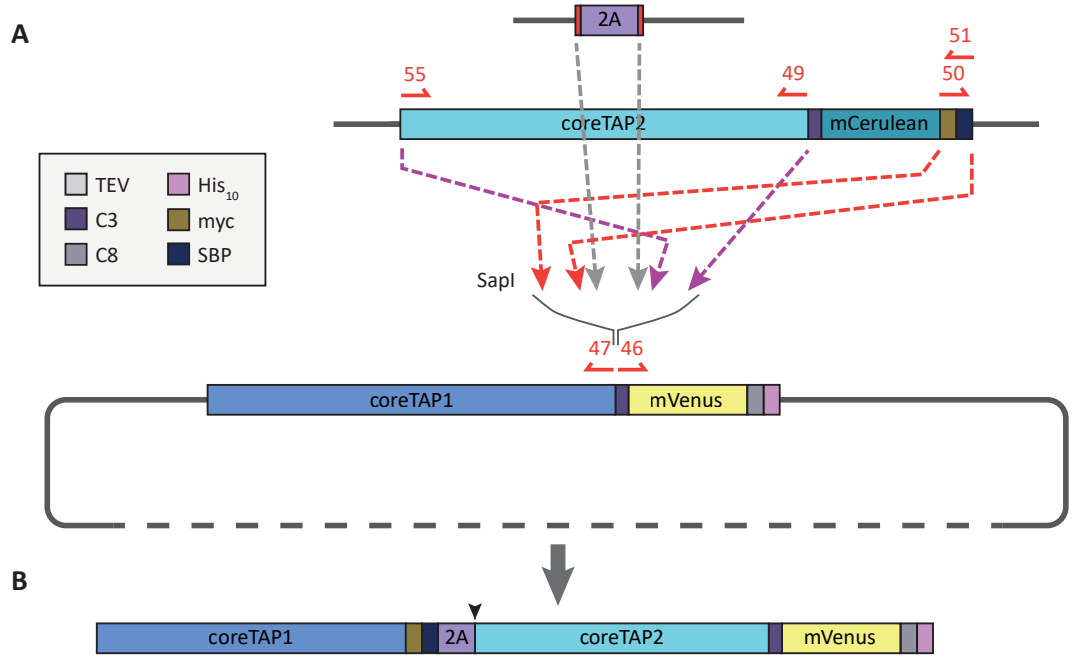

Figure 2.11: Design of coreTAP1-2A-coreTAP2.
coreTAP1-mVenus on pExpression was "opened" at the C-terminus of TAP1 by amplifying the whole plasmid with primer pair 46/47. coreTAP2 was amplified with primer pair 55/49 and the myc-SBP tag was amplified with primer pair 50/51 (A). These three fragments were reassembled together with the 2A-site fragment by one-pot SapI cloning to coreTAP1-myc-SBP-2A-coreTAP2-C3-mVenus-C8-His_{10} (B), abbreviated coreTAP1-2A-coreTAP2.

2.2.12.4 Design and cloning of linker-coreTAP constructs

An alternative to ensure a 1:1 stoichiometry of the TAP subunits during expression is to synthesize both subunits linked as one protein. The linear distance between the C-terminus of one subunit and the N-terminus of the other subunit was estimated to be 60-70 Å using Pymol. Considering that the linker cannot pass through the NBDs and should not be located in the cavity formed by the subunits, the minimal length for the linker was set to be 40 amino acids.

The coreTAP subunits were fused by three different glycine-serine linkers. These linkers were based on a G_4S repeat and were designed with N- and C-terminal C3-protease cleavage site (LEVLFQGP) and SapI restriction sites. The shortest linker comprised 40 amino acids (C3-$(G_4S)_4G_4$-C3), the middle 50 (C3-$(G_4S)_6G_4$-C3) and the longest 60 amino acids (C3-$(G_4S)_8G_4$-C3). The linkers were designed by Andreas Hinz for the bachelor thesis of Claudia Rehwald [161] and were ordered as a synthetic gene form Eurofins. On this plasmid, the different linkers were separated from each other by restriction with BamHI/XhoI, with XhoI/KpnI and with KpnI/HindIII to generate the

short linker L40, the middle linker L50 and the long linker L60, respectively (Fig. 2.12A). The coreTAP1 subunit was amplified with primer pair 56/57 and 60/61 for N- or C-terminal positioning respectively. Similarly, the coreTAP2 subunit was amplified with primer pair 58/59 and 62/63 (Fig. 2.12B). The DNA fragments and the different linkers were then inserted into pInitial vector by FX-cloning and subsequently into pExpression containing a eGFP-myc-SBP tag (Fig. 2.12C). Cloning of these fusion constructs started during my master thesis [3].

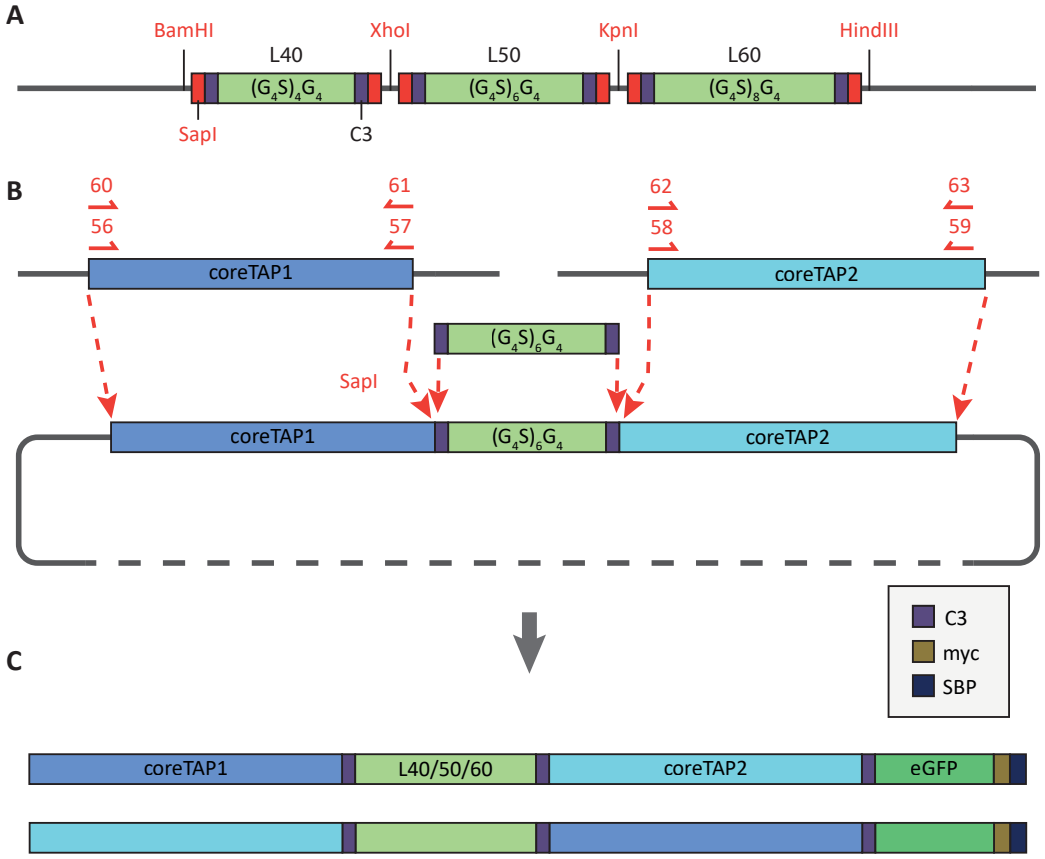

Figure 2.12: Design of coreTAP-linker-coreTAP constructs.
Three glycine serine linkers with flanking C3-protease cleavage sites and SapI restriction sites were encoded on one plasmid and could be separated by restriction with BamHI/XhoI, XhoI/KpnI and KpnI/HindIII (A). This results in the short linker C3-$(G_4S)_4G_4$-C3 (L40), the middle linker C3-$(G_4S)_6G_4$-C3 (L50) and the long linker C3-$(G_4S)_8G_4$-C3 (L60). coreTAP1 was amplified with primer pair 56/57 for N-terminal positioning and with primer pair 60/61 for C-terminal positioning. Similarly, coreTAP2 was amplified with primer pair 58/59 for N-terminal positioning and with primer pair 62/63 for C-terminal positioning (B). The coreTAP subunits and the linker fragments were reassembled by FX-cloning into pInitial to six coreTAP fusion constructs with varying orientation of the subunits and three different linker lengths. These coreTAP fusion constructs were then transferred by FX-cloning into a pExpression vector containing a GFP-myc-SBP tag (C).

2.2.12.5 Design and cloning of coreTAP-TmrAB hybrids

In order to analyze the functionality and potential similarity of TmrAB to TAP, TmrAB had to be adapted for expression in human cells. In a first step the overlapping A and B subunits of TmrAB were transferred to pExpression vector for mammalian expression systems with C3-mVenus-C8-His_{10} tag by amplifying TmrAB with primer pair 64/65. pExpression was "opened" by amplifying the whole plasmid with primer pair 66/67 (Fig. 2.13A). The two DNA fragments were reassembled by one-pot SapI cloning to form TmrAB-C3-mVenus-C8-His_{10} (Fig. 2.13B). Using this construct as template, the A and B subunits were separated from each other. The whole plasmid was amplified with primer pair 68/69 to delete TmrA-C3-mVenus-C8-His_{10} and with primer pair 70/67 to delete TmrB and subsequently religated by one-pot SapI cloning (Fig. 2.13B, C). The catalytic base of TmrAB, a glutamic acid at position 523 in the A subunit was mutated to glutamine to create an inactive TmrAB variant [87]. The whole plasmid was amplified with primer pair 82/83 and religated by one-pot SapI cloning (Fig. 2.13C).
Since there was no knowledge about the functionality and the localization of the bacterial transporter TmrAB in mammalian cells, TAP-TmrAB hybrids were generated, which contained the TMD0s of TAP and as core-complex the TmrAB subunits. All possible combinations of TAP-TmrAB hybrids had to be created to find the complex that could be used to replace TAP.
Full length TAP1-C3-mVenus-C8-His_{10} in pExpression was amplified with primer pair 71/74, so that TmrA, amplified with primer pair 76/77, could be inserted by one-pot SapI cloning instead of coreTAP1 (Fig. 2.14A). Similarly, full length TAP1-C3-mVenus-C8-His_{10} in pExpression was amplified with primer pair 73/74 to remove coreTAP1-C3-mVenus-C8-His_{10}, so that TmrB amplified with primer pair 79/80 could be inserted by one-pot SapI cloning (Fig. 2.14A). These cloning steps led to TMD01-TmrA-C3-mVenus-C8-His_{10} and TMD01-TmrB (Fig. 2.14B).
Flull length TAP2-C3-mCerulean-myc-SBP in pExpression was amplified with primer pair 73/75 to generate the backbone for the hybrids containing only the TMD0 of TAP2 (Fig. 2.14C). Due to the significantly different melting temperatures of TmrA and mVenus, this fusion construct could not be amplified as one and was dissected into TmrA and mVenus. TmrA was amplified with primer pair 78/77, mVenus with primer pair 71/72 and TmrB with primer pair 81/80 (Fig. 2.14C). These DNA fragments were reassembled by one-pot SapI cloning to TMD02-TmrA-C3-mVenus-C8-His_{10} and TMD02-TmrB in pExpression (Fig. 2.14D).

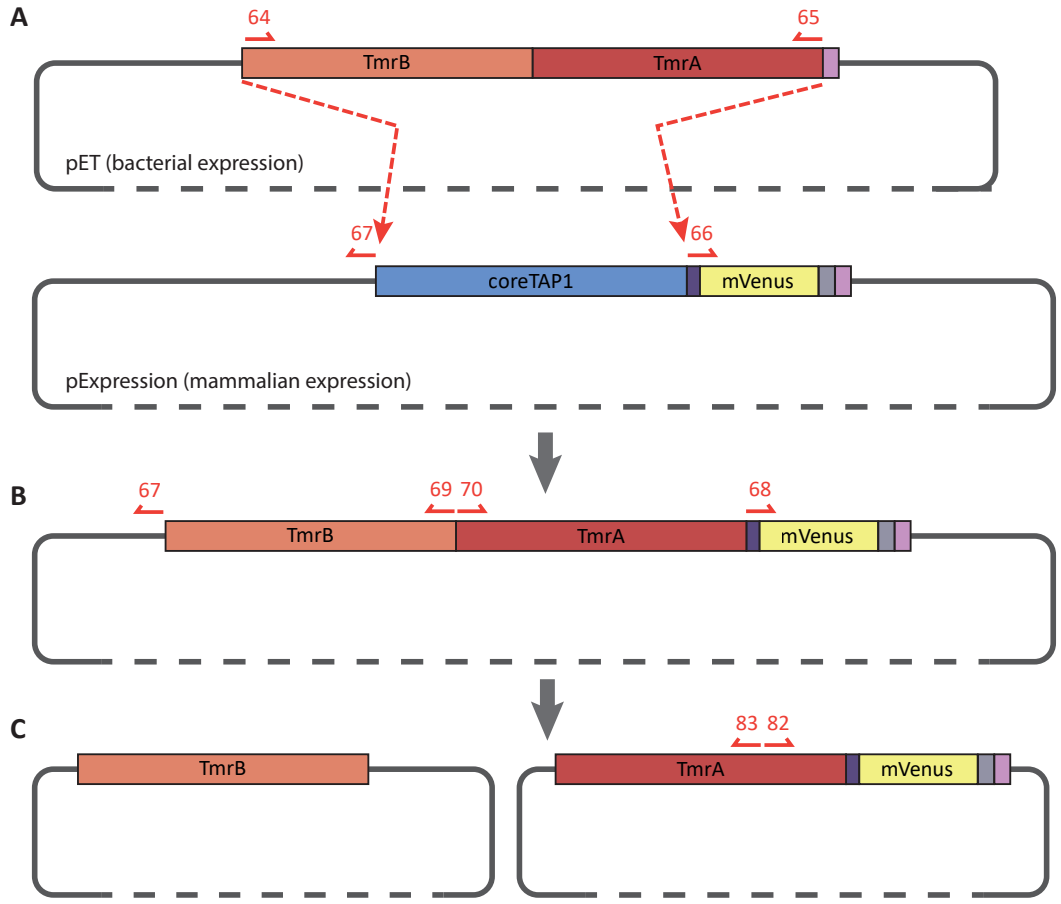

Figure 2.13: Design of TmrAB constructs.
TmrAB was transferred from pET vector for bacterial expression to pExpression for mammalian expression. The backbone vector was amplified with primer pair 66/67 and TmrAB was amplified with primer pair 64/65 (A). The two DNA fragments were reassembled by one-pot SapI cloning to TmrAB-C3-mVenus-C8-His_{10} (B). TmrA-C3-mVenus-C8-His_{10} was generated by amplifying the previously obtained plasmid with primer pair 67/70 and by subsequently religating it by one-pot SapI cloning. Similarly, TmrB was obtained with primer pair 68/69 (B, C). To create an inactive TmrAB variant (EQ-mutant), the whole plasmid was amplified with primer pair 82/83 and religated by one-pot SapI cloning (C).

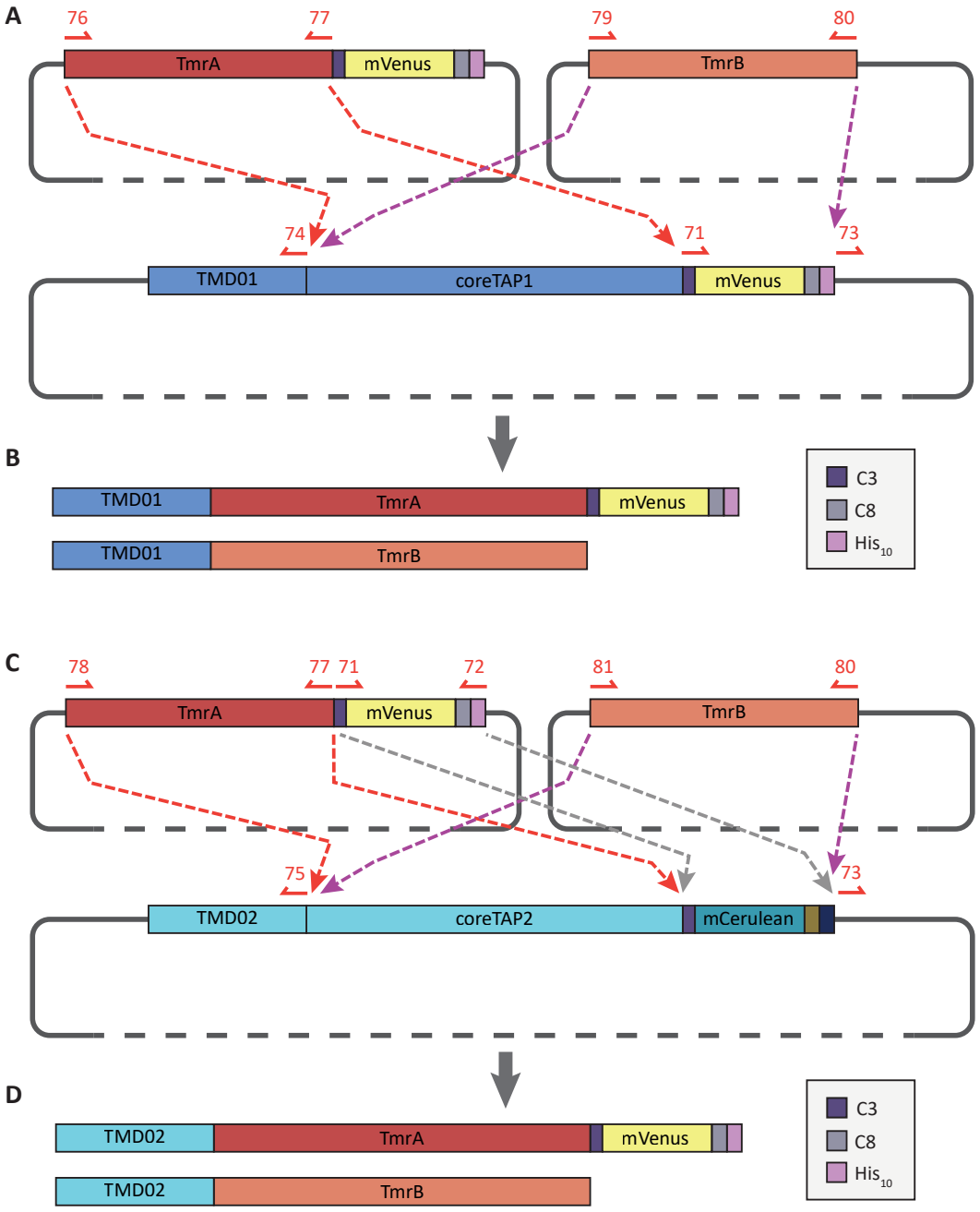

Figure 2.14: Design of TMD0-TmrAB constructs.
Full length TAP1-C3-mVenus-C8-His_{10} in pExpression was amplified with primer pair 71/74, so that TmrA, amplified with primer pair 76/77, could be inserted by one-pot SapI cloning instead of coreTAP1 (A). Similarly, full length TAP1-C3-mVenus-C8-His_{10} in pExpression was amplified with primer pair 73/74 to remove coreTAP1-C3-mVenus-C8-His_{10}, so that TmrB amplified with primer pair 79/80 could be inserted by one-pot SapI cloning (A). These cloning steps led to TMD01-TmrA-C3-mVenus-C8-His_{10} and TMD01-TmrB (B). Full length TAP2-C3-mCerulean-myc-SBP in pExpression was amplified with primer pair 73/75 to generate the backbone for the hybrids containing only the TMD0 of TAP2 (C). TmrA was amplified with primer pair 78/77, mVenus with primer pair 71/72 and TmrB with primer pair 81/80 (C). These DNA fragments were reassembled by one-pot SapI cloning to TMD02-TmrA-C3-mVenus-C8-His_{10} and TMD02-TmrB in pExpression (D).

2.2.12.6 Primer

The following table lists all the previously described cloning primers used in this work.

Primer No.	construct	Sequence
1	ICP47-coreTAP1 for	GAGAATCTTTATTTTCAGGGCGGCGG
2	ICP47-coreTAP2 for	GAGAATCTTTATTTTCAGGGCGGCGC
3	ICP47(1-35) rev	CTCACGCCCCCTTTTATTGATCTCATCG
4	ICP47(1-50) rev	GGGACGCTCCGGGTCGTGC
5	ICP47(1-65) rev	TGCGTTGGGGGCGATTTCGG
6	ICP47(1-78) rev	CACGGTCCCGCCGGTTCTTC
7	ICP47(ΔH1) for	CTGGACAACATGCGGGTTGGG
8	ICP47(ΔH1) rev	CATGGTTTCGGAGGCCGTCC
9	ICP47(ΔH2) for	GAGGACCGGGAGGCGGC
10	ICP47(ΔH2) rev	GTACGTCCTGGGCCCAACCC
11	ICP47 for	tatataGCTCTTCTagtTGGGCCCTGGAAAT
12	coreTAP2 rev	tatataGCTCTTCTtgcGTCCATCAGTCTCTG
13	ICP47(ΔH1) for	tatataGCTCTTCTagtCTGGACAACATGCGGGTTG
14	coreTAP2 for	tatataGCTCTTCTagtGGCGCTCAGGAAAAG
15	G4S-L24/34/44 for	tatataGCTCTTCTggtGGAGGCGGG
16	G4S-L24 rev	atatatGCTCTTCTcccGCCCCCTCCGG
17	G4S-L34 rev	atatatGCTCTTCTcccTCCACCGCC
18	G4S-L44 rev	atatatGCTCTTCTcccCCCACCGCCAG
19	G4S-cTAP1 for	tatataGCTCTTCTgggGGCGGTCAGGG
20	G4S-cTAP2 for	tatataGCTCTTCTgggGGCGCTCAGGAAAAG
21	G4S-cTAP1/2 rev	atatatGCTCTTCTaccACGCCCCCTTTTATTG
22	ICP47-coreTAP2 ΔTEV for	tatataGCTCTTCTggcGCTCAGGAAAAG
23	ICP47-coreTAP2 ΔTEV rev	atatatGCTCTTCTgccTCGATGTGCCAC
24	ICP47(G2S) for	tatataGCTCTTCTagtTGGGCCCTGGAAATG
25	ICP47(G2S) rev	tatataGCTCTTCTactCATCGTTTCGAATAATTAGTTG
26	ΔICP47 for	tatataGCTCTTCTgggGCATTAGAAGTTTTGTTTC
27	ΔICP47(1-35) rev	tatataGCTCTTCTcccCTCACGCCCCCTTTTATTG
28	ΔICP47(1-55) rev	tatataGCTCTTCTcccGGGAGAGCGCAGCAG
29	ΔICP47(1-73) rev	tatataGCTCTTCTcccTCTTCGATGTGCCACACC
30	ΔICP47(1-35)ΔmV for	tatataGCTCTTCTgagCTCGAGGAACAAAAACTCATCTC
31	ΔICP47(1-35)ΔmV rev	tatataGCTCTTCTctcACGCCCCCTTTTATTG
32	ICP47 SR1 for	tatataGCTCTTCTgctGGGGAGGCGGCCAGAAC
33	ICP47 SR1 rev	tatataGCTCTTCTagcTCCACGCCCCCTTTTATTG
34	ICP47 SR2 for	tatataGCTCTTCTggaGGGAGAACCGCCGTGCAC
35	ICP47 SR2 rev	tatataGCTCTTCTtccAGCCCGGTCCTCACGCCC
36	ICP47 SR3 for	tatataGCTCTTCTgctGGGGTGCACGACCCGGAG
37	ICP47 SR3 rev	tatataGCTCTTCTagcTCCGGCCGCCTCCCGGTC
38	ICP47 SR4 for	tatataGCTCTTCTgctGGGCCGGAGCGTCCCC
39	ICP47 SR4 rev	tatataGCTCTTCTagcTCCGGCGGTTCTGGCCGC
40	ICP47 SR5 for	tatataGCTCTTCTgctGGGCCCCTGCTGCGCTCT
41	ICP47 SR5 rev	tatataGCTCTTCTagcTCCGTCGTGCACGGCGGT
42	ICP47 SR6 for	tatataGCTCTTCTgctGGGCGCTCTCCCGGGCTG
43	ICP47 SR6 rev	tatataGCTCTTCTagcTCCACGCTCCGGGTCGTGCAC
44	ICP47 SR7 for	tatataGCTCTTCTgctGGGGGGCTGCTGCCCGAAATC
45	ICP47 SR7 rev	tatataGCTCTTCTagcTCCCAGCAGGGGACGCTCCGG
46	C3-mV for	tatataGCTCTTCTagcAAGGGCGAGGAGCTG
47	coreTAP1 rev	tatataGCTCTTCTggtACCTTGTGGACCTTG

48	ICP47 for	tatataGCTCTTCTttcAGTTGGGCCCTGGAAATG
49	coreTAP2 rev	tatataGCTCTTCTgctCACGGTACCTTGTGGACC
50	Myc for	tatataGCTCTTCTaccGAACAAAAACTCATCTCAGAAG
51	SBP rev	tatataGCTCTTCTcacTGGTTCACGTTGACCTTG
52	Backbone for	tatataGCTCTTCTtaaTCTAGAGGGCCCGTTTAAAC
53	coreTAP1 for	tatataGCTCTTCTttcAGTGGCGGTCAGGGC
54	His_{10} rev	tatataGCTCTTCTttaGTGATGGTGGTGATGATGATG
55	coreTAP2 for	tatataGCTCTTCTttcGGCGCTCAGGAAAAGGAAC
56	coreTAP1 N-term for	tatataGCTCTTCTagtGGCGGTCAGGGCGGCTCC
57	coreTAP1 N-term rev	atatatGCTCTTCTtaaTTCAGGAGCGTCAGCAGGAGC
58	coreTAP2 C-term for	tatataGCTCTTCTccaGGCGCTCAGGAAAAGGAACAAGATC
59	coreTAP2 C-term rev	tatataGCTCTTCAtgcGTCCATCAGTCTCTGCTGGACCAG
60	coreTAP1 C-term for	tatataGCTCTTCTccaGGCGGTCAGGGCGGCTC
61	coreTAP1 C-term rev	tatataGCTCTTCAtgcTTCAGGAGCGTCAGCAGGAGC
62	coreTAP2 N-term for	tatataGCTCTTCTagtGGCGCTCAGGAAAAGGAACAAGATC
63	coreTAP2 N-term rev	atatatGCTCTTCTtaaGTCCATCAGTCTCTGCTGGACCAG
64	TmrB for	tatataGCTCTTCTatgAGTACCGGTCGGTCA
65	TmrA rev	tatataGCTCTTCTtaaTGCACCACCACCACCAAG
66	C3-mV for	tatataGCTCTTCTttaGAAGTTTTGTTTCAAGGTCC
67	pExpr rev	tatataGCTCTTCTcatGGTTTCGGAGGCCGTC
68	ΔTmrA for	tatataGCTCTTCTtaaTCTAGAGGGCCCGTTTAAAC
69	ΔTmrA rev	tatataGCTCTTCTttaCGCTTCCACCTCCTTCTG
70	ΔTmrB for	tatataGCTCTTCTatgGTGACGGAGGACACCTACAG
71	C3-mVenus for	tatataGCTCTTCTttaGAAGTTTTGTTTCAAGGTCC
72	C8-His_{10} rev	tatataGCTCTTCTttaGTGATGGTGGTG
73	Backbone for	tatataGCTCTTCTtaaTCTAGAGGGCCCG
74	TMD01 rev	tatataGCTCTTCTgggCACCCAGAG
75	TMD02 rev	tatataGCTCTTCTcttCTCCTGGGCTCC
76	TmrA for	tatataGCTCTTCTcccGTGACGGAGGACACCTAC
77	TmrA rev	tatataGCTCTTCTtaaTGCACCACCACCACCAAG
78	TmrA for	tatataGCTCTTCTaagGTGACGGAGGACACCTAC
79	TmrB for	tatataGCTCTTCTcccAGTACCGGTCGGTCAG
80	TmrB rev	tatataGCTCTTCTttaGCTTCCACCTCCTTCTGC
81	TmrB for	tatataGCTCTTCTaagAGTACCGGTCGGTCAG
82	TmrA EQ for	tatataGCTCTTCTcagGCCACGGCCAGCGTG
83	TmrA EQ rev	tatataGCTCTTCTctgGTCCAGGATGAGGAGGATG

2.3 Mammalian cell culture

2.3.1 Cell lines and cultivation conditions

2.3.1.1 Adherent cell lines

Adherent cell lines were cultured in T75 or T175 flasks (Sarstedt) at 37 °C and 5% CO_2. The cell lines HEK293-T, FreeStyle^{TM} 293-F, HeLa Kyoto, BRE-169 and STF1-169 were cultured in DMEM (Gibco) supplemented with 10% fetal calf serum (FCS, Capricorn Scientific). BRE-169 and STF1-169 cell lines were kindly provided by H. de la Salle, Strasbourg, France [58, 59]. The MelJuSo and MelJuSo TAP1/2$^{-/-}$ cell lines (kindly

provided by E. J. H. J. Wiertz, UMC Utrecht, [162]) were cultured in RPMI 1640 (Gibco) supplemented with 10% FCS. At 80-90% confluence the cells were washed in DPBS (Gibco) and then detached with 1.5 ml trypsin-EDTA solution (Sigma Aldrich). After adding medium to a total volume of 10 ml, the cells were resuspended and 2-3 ml of the suspension was carried over to a new flask. Medium was added to a total volume of 12 ml (T75) or 24 ml (T175).

2.3.1.2 Suspension cell lines

Raji cells were cultured in RPMI 1640 supplemented with 10% FCS in T175 flasks (upright) at 37 °C and 5% CO_2. Twice a week the cells were passaged in a ratio of 1:10 and diluted with fresh medium. FreeStyle^{TM} 293-F cells were cultured in FreeStyle^{TM} 293 expression medium (Gibco) to a maximal density of 3 x 10^6 cells/ml in 1 l shaking flasks in a maximal volume of 300 ml. Cells were passaged two times a week seeding 0.5 x 10^6 cells/ml into a new flask. Cells were cultured shaking at 125 rpm, 37 °C and 8% CO_2.

2.3.1.3 Freezing and thawing of mammalian cells

For long term storage, the cells were washed in DPBS, detached with trypsin-EDTA solution and harvested 4 min at 1,000 g. Cells were resuspended to a density of 2-4 x 10^6 cells/ml in FCS containing 10% DMSO and transferred to 1 ml cryogenic vials (Corning). The vials were shifted to a Cool Cell FTS30 and stored for 1-2 days at -80 °C. Afterwards, the cells were stored in liquid nitrogen. To take frozen cells back in culture, a frozen vial was rapidly heated up in a water bath at 37 °C and immediately mixed with 10 ml fresh medium. Cells were harvested 4 min at 1,000 g, resuspended in 12 ml medium and transferred to a T75 flask. Medium was exchanged after 12-24 h.

2.3.1.4 Transfection of mammalian cells

HEK293-T cells

For small scale transfection, 24 h before transfection, 2 x 10^5 cells/well were seeded into 6-well plates. 4 μg of purified plasmid DNA and 15 μl polyethylenimine (PEI, 18 mM) were dissolved separately in 200 μl DMEM without FCS (per well). The two solutions were mixed, incubated 30 min at room temperature, and then added dropwise to the cells. Cells were harvested 24 h after transfection. For large scale transfection, 72 h before transfection 2 x 10^6 cells/dish were seeded into 15 cm dishes. 30 μg of purified plasmid

DNA and 90 μl PEI (18 mM) were dissolved separately in 700 μl DMEM without FCS (per dish). The two solutions were mixed, incubated 30 min at room temperature and then added dropwise to the cells. The cells were harvested 24 h after transfection.

FreeStyle^{TM} 293-F cells

24 h before transfection 5 x 10^5 cells/ml were seeded into 300 ml FreeStyle^{TM} 293 expression medium. 300 μg of purified plasmid DNA were dissolved in 12 ml Opti MEM (Gibco) and 1.2 ml PEI (18 mM) were dissolved in 11 ml Opti MEM. The two solutions were mixed, incubated 30 min at room temperature and then added to the cells. The cells were harvested 48 h after transfection 10 min at 1,500 g.

HeLa Kyoto cells

24 h before transfection 2 x 10^6 cells/dish were seeded into 15 cm dishes. 30 min before transfection the medium was exchanged and supplemented with 1000 U of recombinant human interferon-γ (Peprotech) to trigger immunostimulatory effects, increasing the PLC amount in the cells. 30 μg of purified plasmid DNA and 225 μl PEI (18 mM) were dissolved separately in 700 μl OptiMEM (per dish). The two solutions were mixed, incubated 30 min at room temperature and then added dropwise to the cells. The cells were harvested 24 h after transfection.

TAP-deficient cells

For transfection of TAP-deficient cell lines BRE-169 and STF1-169 2 x 10^5 cells/well were seeded into 6 well plates. 2 μg of purified plasmid DNA and 6 μl X-treme GENE HP (Roche) were dissolved separately in 200 and 100 μl DMEM without FCS, respectively (per well). The two solutions were mixed, incubated 30 min at room temperature and then added dropwise to the cells. Cells were harvested 48 h after transfection.

2.3.2 MHC I surface expression assay

MHC I surface expression was analyzed by flow cytometry. TAP1-deficient BRE-169 cells, TAP2-deficient STF1-169 cells, or TAP1/2-deficient MelJuSo cells were complemented each with the missing TAP subunit(s). Raji cells were used as positive control. After harvesting the cells, all further steps were carried out on ice. The cells were washed in FACS-buffer (2% FCS in DPBS, ice-cold) and centrifuged 3 min at 300 g and 4°C. After discarding the supernatant, cells were washed twice in FACS-buffer. Cells were then blocked 20 min by 5% BSA in FACS-buffer. After two more washing steps, the

cells were stained 20 min with 125 ng anti-human HLA-A,B,C (clone W6/32; BioLegend) conjugated to PE or APC/Cy7 in 100 μl FACS-buffer. The non-bound antibody was removed by washing with FACS-buffer. The cells were fixed with 0.25% formaldehyde in FACS-buffer and stored at 8°C or used immediately for cytometry. Data were recorded by an Attune (Invitrogen) or a Celesta (BD) flow cytometer and processed using FlowJo V10 software (TreeStar, Inc.).

By plotting FSC-A against SSC-A the living cells population was determined (cells gate, Fig. 2.15A) and subsequently used to discriminate doublets by plotting FSC-A against FSC-H (P2 gate, Fig. 2.15B). The mVenus positive or eGFP positive population out of P2 gate (mVenus gate, Fig. 2.15C) was utilized to determine PE or APC/Cy7 fluorescence of this population.

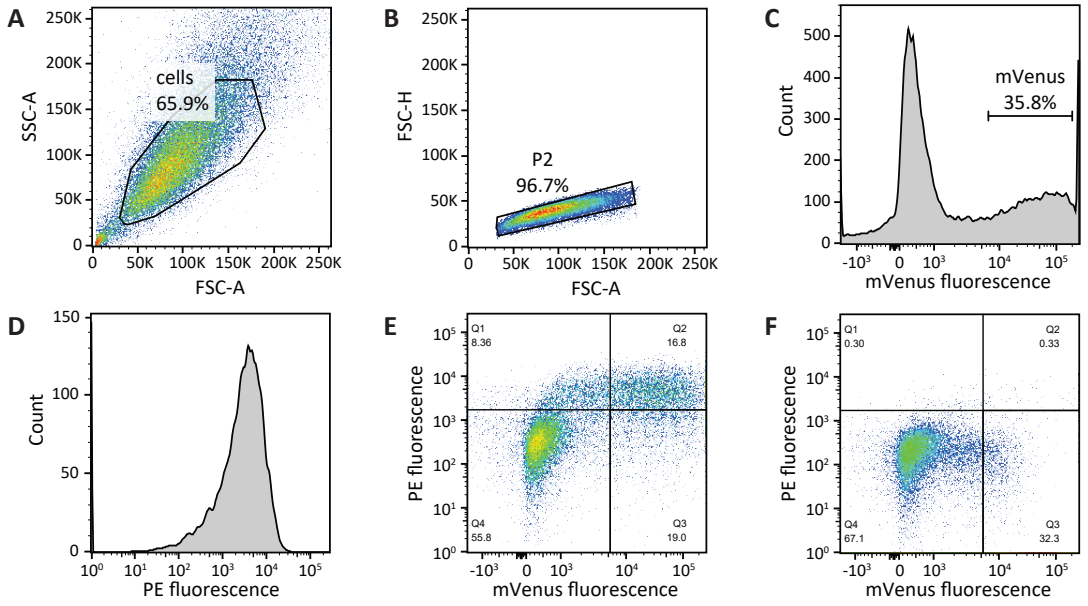

Figure 2.15: Gating strategy for MHC I surface expression.
Flow cytometry gating strategy is exemplarily shown for coreTAP1 expressed in BRE-169 cells. The living cell population (A, cells gate) was used for doublet discrimination (B, P2 gate). mVenus positive cells out of this population (C) were utilized to display the PE fluorescence. The dot-plots show mVenus fluorescence plotted against PE fluorescence (P2 gate) of BRE-169 cells expressing coreTAP1 (D) and ICP47(1-88)-coreTAP1 (E).

2.3.3 Immunofluorescence microscopy

Confocal laser scanning microscopy allows to create high resolution images of single subcellular compartments and organelles. The visualization was performed at a ZEISS LSM 880 confocal laser scanning microscope by using cells expressing fluorescently tagged proteins or by staining cells with fluorescently labeled antibodies. 2 x 10^4 cells per well were seeded into 8-well on cover glass II plates with 0.8 cm^2 chambers and transfected after 24 h. Staining was performed 24 h after transfection. The growth medium was

removed and cells were washed in DPBS. 4% paraformaldehyde in DPBS were added to fix the cells. After 20 min the cells were washed with DPBS and 0.1% triton X100 in DPBS were added. After 10 min incubation, the cells were washed in DPBS. 5% BSA in DPBS was added and removed immediately. Subsequently, the cells were blocked 1 h in 5% BSA in DPBS. The primary antibodies were appropriately diluted in 250 μl 1% BSA in DPBS and incubated overnight at 4°C. Before applying the secondary antibody, the cells were washed in DPBS. The secondary antibodies were appropriately diluted in 500 μl 1% BSA in DPBS and incubated 1 h at room temperature. After staining, the cells were washed three times in 5% BSA and once in DPBS. 2% paraformaldehyde were added to the cells and removed after 20 min. The cells were stored in DPBS at 8 °C in the dark.
Pearson's coefficient was calculated with Coloc2 Plugin of ImageJ 1.48 v.

antibody	**organism**	**dilution**	**source**
α-PDI	mouse	1:200	Abcam ab2792
α-LAMP1	mouse	1:100	Biolegend 328602
α-mouse-AF647	goat	1:500	Life technologies A21235

2.4 Biochemical methods

2.4.1 Preparation of HEK293-T, HeLa and FreeStyle^{TM} 293-F membranes

5 g HEK293-T or FreeStyle^{TM} 293-F cells were resuspended in 50 ml of 20 mM HEPES pH 7.4, 1% PI Mix HP (Serva) and 1 mM DTT, and incubated 10 min on ice. HeLa Kyoto cells were processed in smaller quantities (∼0.5 g) with adjusted buffer volumes and without DTT. The cell suspension was transferred to a Wheaton 357546 tight glass dounce homogenizer and pressed 40 times. After 5 ml of 2.5 M sucrose were added, the cells were pressed 4 more times. The homogenate was centrifuged 4 min at 200 g and 8 min at 700 g and 4 °C. The supernatant was ultracentrifuged 45 min at 100,000 g and 4 °C. The pelleted membranes were resuspended in 2 ml 20 mM HEPES pH 7.4, 1% PI Mix (Serva) and 1 mM DTT and homogenized using a 5 ml dounce homogenizer. Protein concentration was determined by Bradford assay and adjusted to 20 mg/mg. The membranes were frozen in liquid nitrogen and stored at -80°C.

2.4.2 Preparation of *P. pastoris* membranes

25 g *P. pastoris* cells were resuspended in breaking buffer to a total volume of 75 ml. After 12 ml activated glass beads were filled into 50 ml falcon tubes, cell suspension was

added to 40 ml total volume. The cells were disrupted using a FastPrep (MP Biomedicals) with MP2x50 rotor and the program 45 s and 5 m/s at 4°C. Cell disruption was repeated five times with 2 min cooling steps on ice in between. The tubes were centrifuged 15 min at 3,500 g and the upper suspension containing the cell membranes was collected. The lower part containing the glass beads and remaining cells was resuspended in a total volume of 40 ml breaking buffer. This procedure was repeated two more times and the membranes were then harvested 45 min at 100,000 g using an XE 90 or L-90K ultracentrifuge (Beckman Coulter). The supernatant was discarded and the membranes were homogenized in 20 ml TAP buffer. Protein concentration was determined by Bradford assay and adjusted to 20 mg/mg. The membranes were frozen in liquid nitrogen and stored at -80°C.

Glass beads

0.25-0.5 mm glass beads (Roth) were incubated 30 min in 30% HCl. Then washed with MilliQ water to neutral pH and dried. Activated glass beads were stored at 8°C.

Breaking buffer pH 7.4		
50 mM	KH_2PO_4	
1 mM	EDTA	
5 mM	Aminocaproic acid	Dissolve separately in water
5%	Glycerol	
1 mM	PMSF	
2.5 mM	Benzamidine	

TAP buffer pH 7.4	
20 mM	HEPES
200 mM	NaCl
50 mM	KCl
15%	Glycerol

2.4.3 Determination of protein concentration

2.4.3.1 Bradford assay

Bradford assay was used to spectroscopically determine the total protein concentration of HEK293-T, FreeStyle^{TM} 293-F or *P. pastoris* membranes. Bovine serum albumin (BSA, Thermo Fisher) was diluted to 0.125, 0.25, 0.5, 0.75 and 1.0 mg/ml in DPBS. Membranes were diluted 1:50 and 1:100 in DPBS. 3 times 10 μl of MilliQ water, BSA solutions and diluted membranes were transferred to a round bottom 96 well Rotilabo microtiter plate

(Roth). 290 μl of Pierce Coomassie Plus (Bradford) Assay Reagent (Thermo Fisher) were added to each well and incubated 10 min at room temperature. After air bubbles were removed from the surface, the absorbance at 595 nm was analyzed by a CLARIOstar spectrometer (BMG Labtech). Mean values of triplicates were calculated. The BSA samples were used to backcalculate the total protein amount of the membranes.

2.4.3.2 NanoDrop protein quantification

The absorption at 280 nm of 1-2 μl of purified protein solution was measured by NanoDrop Spectrophotometer ND-1000. Extinction coefficients of measured proteins were calculated by ProtParam tool (ExPASy.org) and protein concentration was calculated by Beer-Lambert law.

$$c\left[\frac{mg}{ml}\right] = \frac{A_{280}}{\epsilon\left[\frac{l}{mol \times cm} \times d[cm]\right]} \times MW\left[\frac{g}{mol}\right]$$

c: protein concentration
A_{280}: absorbance at 280 nm
ϵ: extinction coefficient
d: pathlength (here 1 cm)
MW: molecular weight

2.4.4 Protein purification

2.4.4.1 Small scale purification

Proteins purified by orthogonal small scale purification carried a C-terminal His_{10}-tag on one subunit and SBP-tag on the other subunit. In case of non-orthogonal purification (TAP1-TAP2 fusions or TmrAB) only His_{10}-tag was present. Small scale purification was used for fast parallel screening of different constructs, where the protein amount was not relevant. Pelleted HEK293-T, FreeStyle^{TM} 293-F or HeLa cells were directly lysed without membrane preparation. The following amounts refer to 1 ml pelleted cells. 1 ml frozen cells were dissolved and homogenized in 3 ml solubilisation buffer. Cells were incubated 90 min rotating at 8 °C and then centrifuged 30 min at 100,000 g. 200 μl Ni-Sepharose 6 Fast Flow slurry (GE Healthcare Life Sciences) was washed two times with 1 ml MilliQ water and two times with 1 ml IMAC wash buffer before incubation with the ultracentrifuged supernatant. After incubating 2 h at 8 °C on an over-head rotor, the beads were harvested 5 min at 500 g. Subsequently, 1 ml IMAC wash buffer was added and the beads were incubated 15 min rotating at 8 °C. After harvesting the

beads, 1 ml IMAC elution buffer was added. The beads were incubated 30 min rotating at 8 °C, then the supernatant was collected and frozen at -80 °C or used for the next purification step. 150 μl high capacity streptavidin agarose resin slurry (Thermo Fisher) was washed two times with 1 ml MilliQ water and two times with 1 ml SBP wash buffer before incubation with the IMAC eluate. After 3 h rotating incubation at 8 °C, the beads were harvested 5 min at 500 g. Subsequently, 1 ml SBP wash buffer was added and the beads were incubated 15 min rotating at 8 °C. After harvesting the beads, 1 ml SBP elution buffer was added. The beads were incubated 40 min rotating at 8 °C, then the beads were removed by filtration with a 0.22 μm SpinX column (Costar) and the eluate was frozen at -80 °C.

2.4.4.2 Large scale purification

Proteins purified by orthogonal large scale purification carried a C-terminal His_{10}-tag on one subunit and StrepII-tag on the other subunit. In case of non-orthogonal purification of TAP1-TAP2 fusions, only His_{10}-tag was present. Large scale purification was used to obtain high amounts of purified protein derived from *P. pastoris* membranes. 25 ml *P. pastoris* membranes (20 mg/ml) were thawed in 12.5 ml 4x solubilisation buffer, 1.5 ml MilliQ water, 10 ml 10% GDN, 500 μl benzamidine and PMSF stock solutions. The membranes were solubilized 1.5 h rotating at 8 °C, then ultracentrifuged 45 min at 100,000 g. 2 ml Ni-Sepharose 6 Fast Flow slurry (GE Healthcare Life Sciences) were transferred to an empty Econo-Pac® chromatography column (Bio-Rad) and washed with 10 ml MilliQ water and then with 10 ml IMAC wash buffer at gravity flow. Subsequently, the ultracentrifuged solubilisate was run through the column at minimal flow rate by a Minipuls 2 (Gilson) peristaltic pump. Beads were washed with 20 ml IMAC wash buffer at minimal flow rate. Protein was eluted with 10 ml IMAC elution buffer at minimal flow rate. 2 ml strep-tactin resin (Strep-Tactin® Superflow® 50% suspension, iba) were transferred to an empty Poly-Prep® chromatography column (Bio-Rad) and washed with 10 ml MilliQ water and then with 10 ml StrepII wash buffer at gravity flow. Subsequently, the IMAC eluate was run through the column at minimal flow rate. Beads were washed with 5 ml StrepII wash buffer at minimal flow rate. Protein was eluted with 5 ml StrepII elution buffer at minimal flow rate. The eluate was concentrated using 100K Amicon Ultra-15 centrifugal filter (Merck Millipore). Final protein concentration was determined by NanoDrop microvolume spectrophotometer ND-1000 (Peqlab).

2.4.4.3 Co-immunoprecipitation

To analyze the binding behavior of the ICP47-fusion constructs to free ICP47 and US6 (both carrying a C-terminal mVenus-tag), HEK293-T cells were transfected in 15 cm dishes (1 dish per construct) as described for the protein purification but with an excess of free expressed viral factor. For transfection a molar ratio of 1:1:5 (coreTAP1:coreTAP2:viral factor) was applied using 30 μg total DNA per dish. Transfection was performed as described before. The cells were harvested and solubilized 1 h rotating in 1 ml of solubilization buffer supplemented with 2% digitonin (MerckMillipore) instead of GDN. All steps were carried out on ice. An aliquot of every step was stored in SDS buffer (50 mM Tris/HCL pH 7.5, 10% glycerol, 2% SDS, 0.7% β-mercaptoethanol). The samples were centrifuged 30 min at 120.000 g and 4 °C. The supernatant was incubated 1 h with 50 μl prewashed streptavidin agarose beads (#20361 High Capacity Streptavidin Agarose Resin, Thermo Scientific). For washing, the beads were incubated 15 min with 1 ml of SBP wash buffer supplemented with 0.1% digitonin. Bound proteins were eluted 15 min in 1 ml of SBP wash buffer supplemented with 2.5 mM biotin and 0.1% digitonin. 8 μg of anti-C8 antibody (purified from Chessie 8 supernatant) were bound 1 h to 50 μl of sheep anti-mouse IgG Dynabeads (Novex^{TM}, Life-Technologies) and washed two times with SBP wash buffer supplemented with 0.1% digitonin. The eluted proteins were added to the antibody-coated Dynabeads and incubated 90 min rotating. The beads were washed five times 15 min with 1 ml of SBP wash buffer supplemented with 0.1% digitonin and then eluted 30 min at 37 °C in SDS buffer.

2.4.4.4 PLC pulldown

The membranes of five 15 cm dishes per construct of HeLa Kyoto cells were solubilized 1 h at 8 °C on an over-head rotor in 20 mM HEPES, 150 mM NaCl, 8.6% glycerol, 1% GDN and 1% PI-Mix, adjusting the volume to a final protein concentration of 10 mg/ml. The solubilisate was ultracentrifuged 30 min at 100.000 g and 4 °C. 100 μl Dynabeads for His-tag pulldown (Invitrogen) were washed twice in 1 ml 20 mM HEPES, 150 mM NaCl, 8.6% glycerol, and 0.1%GDN before incubation with the ultracentrifuged supernatant. After incubating 3 h at 8 °C on an over-head rotor, the beads were harvested and washed in 1 ml 20 mM HEPES, 150 mM NaCl, 8.6% glycerol, and 0.1% GDN. Then, 200 μl elution buffer (20 mM HEPES, 150 mM NaCl, 8.6% glycerol, 0.1% GDN and 300 mM imidazole) was added and the beads were incubated 30 min rotating at 8 °C. The eluate was frozen in liquid nitrogen and stored at -80 °C.

2.4.4.5 Purification of anti-C8 antibody

C8 antibody was purified from Chessie 8 supernatant (HIV-1 gp41 Hybridoma, [163]). Chessie 8 produce a monoclonal antibody of isotype IgG1, which reacts with gp160. It is specific for gp41 and recognizes the epitope PDRPEG. Cells were cultivated in RPMI 1640 supplemented with 50 μM β-mercaptoethanol, 100 U/ml penicillin, 100 μg/ml streptomycin, and 10% FCS. To obtain the antibody cells were overgrown until they died. For antibody purification, a ÄKTA Prime plus and a HiTrap™Protein G HP affinity column (GE Healthcare) were used. The column was washed with 20 ml DPBS, then 50 ml sterile filtered hybridoma supernatant were loaded. After washing with DPBS, the antibody was eluted with 25 mM glycine (pH 2.0) and neutralized with 1 M Tris/HCl pH 9.0. Pooled fractions were dialyzed in DPBS supplemented with 0.02% NaN_3.

2.4.4.6 Purification buffers

Solubilisation buffer pH 7.4	
20 mM	HEPES
200 mM	NaCl
50 mM	KCl
15% v/v	Glycerol
2% w/v	GDN
20 mM	Imidazol
1% v/v	PI-Mix

4x Solubilisation buffer pH 7.4	
80 mM	HEPES
800 mM	NaCl
200 mM	KCl
60% v/v	Glycerol

IMAC wash buffer	
20 mM	HEPES
200 mM	NaCl
50 mM	KCl
15% v/v	Glycerol
0.01% w/v	GDN
40 mM	Imidazol

IMAC elution buffer

20 mM	HEPES
200 mM	NaCl
50 mM	KCl
15% v/v	Glycerol
0.01% w/v	GDN
200 mM	Imidazol

SBP and StrepII wash buffer

20 mM	HEPES
200 mM	NaCl
50 mM	KCl
15% v/v	Glycerol
0.01% w/v	GDN

SBP elution buffer

20 mM	HEPES
200 mM	NaCl
50 mM	KCl
15% v/v	Glycerol
0.01% w/v	GDN
10 mM	Biotin

StrepII elution buffer

20 mM	HEPES
200 mM	NaCl
50 mM	KCl
15% v/v	Glycerol
0.01% w/v	GDN
10 mM	Desthiobiotin

Benzamidine stock solution

250 mM dissolved in MilliQ water

PMSF stock solution

100 mM dissolved in isopropanol

2.4.5 SDS-PAGE

Sodium dodecyl sulfate polyacrylamide gel electrophoresis (SDS-PAGE) was used as standard method for protein separation on a gel as purification or expression control [164].

Purified protein was directly mixed with 10x sample buffer to 1x final concentration. Pelleted cells were first lysed 1-2 h at room temperature in Ripa-buffer (Thermo Scientific) supplemented with 1% PI-Mix (Serva) and 1% benzonase (Sigma). 10x sample buffer was added to 1x final concentration. For immunoblot and instant blue staining the samples were denatured 10 min at 60-75 °C, while in-gel fluorescence does not require denaturation. Gels were casted using 0.75/1.0/1.5 mm gels chambers (BioRad). Separation gel (10% or 12%) was poured into the chamber and coated with isopropanol. As soon as the gel firmed up, stacking gel was added and the comb (10 or 15 slots) was inserted. Gel chambers were mounted into Mini-PROTEAN® Tetra electrophoresis chamber (Bio-Rad) and filled with 1x running buffer. Proteins were separated 1.0-1.5 h at 125 V. After removing the gel chamber, gels were further used for immunoblot, instant blue staining or in-gel fluorescence.

10x sample buffer (pH 7.4)

6 M	β-mercaptoethanol
30% w/v	SDS
20% w/v	Sucrose
100 mM	Tris-HCl
0.25% w/v	Bromophenol-blue
10 mM	EGTA

Separation gel (1 gel)

10%	12%	
2.08 ml	2.5 ml	Acrylamide solution (30% acrylamide / 0.8% N,N'-methylenbisacrylamide)
1.56 ml	1.56 ml	1.5 M Tris, 0.4% w/v SDS, pH 8.8
2.48 ml	2.06 ml	MilliQ water
62.5 μl	62.5 μl	10% w/v APS
10 μl	7 μl	TEMED

Stacking gel (1 gel)	
333 μl	Acrylamide-solution
	(30% acrylamide / 0.8% N,N'-methylenbisacrylamide)
208 μl	1.5 M Tris, 0.4% w/v SDS, pH 6.8
1.09 ml	MilliQ water
20.83 μl	10% w/v APS
2.33 μl	TEMED

Running buffer pH 8.3	
30 g	Tris
10 g	SDS
144 g	Glycine
Ad 1l	MilliQ water

2.4.6 InstantBlue staining

InstantBlue (Sigma) is a ready-to-use solution to visualize proteins directly after SDS-PAGE. The gels were washed one time in MilliQ water and then incubated 15-30 min in 20 ml InstantBlue solution.

2.4.7 In-gel fluorescence

In-gel fluorescence allows to visualize fluorescently tagged proteins previously separated by SDS PAGE. To obtain reliable signals it is important to load the protein solutions on the gel without denaturing them. In-gel fluorescence was detected using an ImageQuant LAS 4000 (GE Healthcare Life Sciences). Excitation and emission wavelengths are listed below.

Filter settings for LAS 4000		
	excitation (nm)	emission (nm)
eGFP	515	575
mVenus	515	575
mVenus*	460	520
mCerulean	460	520
mCherry	630	670

*mVenus can be visualized with two filter settings

2.4.8 Immunoblotting

Western blotting is a method that allows to transfer proteins from an acrylamide gel to a nitrocellulose or PVDF (polyvinylidene fluoride) membrane and to detect them by specific antibodies. Here, proteins were transferred to PVDF membranes by semi-dry or wet blot technique.

2.4.8.1 Buffers and antibodies

Transfer buffer	
25 mM	Tris/HCl pH 7.5
192 mM	Glycin
0.03% w/v	SDS
20% v/v	Methanol

1x TBS-T pH 8.0	
20 mM	Tris
1.5 M	NaCl
0.0005% v/v	Tween 20

Blocking Buffer

3% w/v milk powder in 1x TBS-T

Antibodies

antibody	**organism**	**dilution**	**source**
α-TAP1	mouse	1:10	Hybridoma
α-TAP2	mouse	1:10	Hybridoma
α-His-tag	mouse	1:3000	Sigma H1029
α-Calreticulin	rabbit	1:2000	Sigma C4606
α-HLA A, B, C	mouse	1:200	Hybridoma
α-Tapasin	rat	0.8 mg/ml	Hybridoma
α-ERP57	rabbit	1:2000	Abcam ab10287
α-mouse	goat	1:20,000	Sigma A2554
α-rat	goat	1:20,000	Sigma A9037
α-rabbit	goat	1:20,000	Anaspec AS-28177

2.4.8.2 Semi-dry blot

Protein solution was separated by SDS-PAGE and then transferred by semi-dry western blot [165] onto a PVDF membrane (Trans Blot Turbo, Bio-Rad). One layer of Whatman paper (1 mm) soaked with transfer buffer, followed by a methanol activated PVDF membrane, the gel and a second layer of Whatman paper were placed onto the anode of the cassette, which was then closed with the cathode-lid. Proteins were blotted 30 min at 25 V.

2.4.8.3 Wet blot

Protein solution was separated by SDS-PAGE and then transferred by wet western blot onto a PVDF membrane (2.5 L Trans Blot, Bio-Rad). During assembly, the cassette and all components were immerged in at least 2 cm of transfer buffer. A filter, followed by two layers of Whatman paper (1 mm), the methanol activated PVDF membrane, the gel, two layers Whatman paper and a second filter were placed onto the bottom of a cassette. After closing the cassette, the bottom of the cassette was placed towards the anode and the chamber was filled with approximately 2.5 L transfer buffer. Proteins were blotted 15 h overnight at 30 V in the cold room at 8 °C.

2.4.8.4 Protein detection

After removing the gel and the whatman paper, the PVDF membrane was transferred to a 50 ml falcon tube and washed 5 min in 10 ml TBS-T. Subsequently, the membrane was incubated 20 min in 15 ml blocking buffer and then washed three times 5 min with 10 ml TBS-T. 10 ml of primary antibody solution was added. After overnight incubation at 4 °C or 2 h incubation at room temperature the membrane was washed three times 5 min with 10 ml TBS-T. 10 ml of secondary antibody solution was added and incubated 1 h at room temperature. The membrane was washed three times 5 min in TBS-T and then stored in TBS-T till detection. Directly before detection, the membrane was coated with 1.5 ml ECL solution (Clarify™ Western ECL Substrate, Bio-Rad). The chemiluminescent signal was detected by a Lumi-Imager F1 (Roche). In case of weak signal, the membrane was treated with KPL LumiGLO Reserve™ Chemiluminescent Substrate Kit (Sera Care) to enhance the chemiluminescent signal.

2.4.9 Multi-color size exclusion chromatography and thermostability analyses

The monodispersity of the purified TAP complexes was analyzed by multicolor fluorescence based size exclusion chromatography (MC-FSEC) [166]. The fluorescent proteins mVenus or mCerulean were fused to TAP subunits or ICP47 and were detected by an Agilent 1200 series or Shimadzu high-performance liquid chromatography (HPLC) system using a Shodex semi-micro KW404-4 F (4.66 300 mm) column.
For the MC-FSEC analysis, 60 μl of the purified TAP complexes were filtered through 0.22 μm SpinX centrifuge filter (Costar). 50 μl of each sample were then injected by an autosampler. To determine the thermostability of the ICP47-TAP complexes, 60 μl of the protein solution were incubated for 1 h at 40 °C, then treated as described above, and compared by MC-FSEC with a sample stored for 1 h on ice.
The melting temperatures of the protein complexes were determined by incubating samples five min at 25-50 °C, treating them then as described above and injecting them for SEC analysis. Elution profiles were overlaid and the overlap area was calculated with ImageJ 1.48 v. The area of the profiles at 4 °C was normalized to 100%. Curve fit was calculated with GraphPad Prism 5 using the nonlinear regression "EC50 shift" fit. The bottom value of this fit was used to normalize the fit to a range of 0-100%.
In a second approach melting temperatures were determined via nano differential scanning fluorimetry (nanoDSF) with a Prometheus NT.48 (Nano Temper).

SEC running buffer	
20 mM	HEPES/NaOH, pH 7.4
200 mM	NaCl
50 mM	KCl
5%	Glycerol
0.05%	w/v GDN

2.4.10 Negative-stain EM

2 μl of orthogonally purified protein (3-10 μg/ml) were applied to a glow-discharged carbon-coated copper grid (400 mesh) and stained with 2% uranyl formate. Data were collected on a Tecnai G2 Spirit transmission electron microscope (FEI). These experiments were kindly carried out by Susanne Hofmann in collaboration with the group of Werner Kühlbrandt at the Max Planck Institute of Biophysics.

2.5 Materials

2.5.1 Chemicals and reagents

name	**supplier**
Agar	Roth
Aminocaproic acid	Roth
Ammonium sulfate	Roth
ATP	Thermo Scientific
D(+)Biotin	Roth
Bovine serum albumin	Thermo Fisher
$CaSO_4$ x 2 H_2O	Roth
D-Desthiobiotin	iba
Digitonin	Merck
FOS-choline 12	Affimetrix
GDN	Affimetrix
Yeast extract	Roth
Yeast Nitrogen Base	Difco
Zeocin	Thermo Fisher

2.5.2 Consumables and lab equipment

name	**supplier**
15 ml, 50 ml tubes	Sarstedt
Acrylamide solution	Roth
Amicon Ultra-15 centrifugal filter 100K	Merck Millipore
Benzonase	Sigma
Cell culture flasks and dishes	Sarstedt
Cell culture media	Gibco
dNTPs	Thermo Scientific
DPBS	Gibco
Dream Taq DNA polymerase	Thermo Scientific
Dynabeads for His-tag pulldown	Invitrogen
Dynabeads IgG sheep anti-mouse	Novex
ECL solution	Bio-Rad
Econo-Pac chromatography column	Bio-Rad
Enzymes	Thermo Scientific
FCS	Capricorn Scientific
Glass beads 0.25-0.5 mm	Roth

High capacity streptavidin agarose resin slurry	Thermo Fisher
HiTrap Protein G HP affinity column	GE Healthcare
InstantBlue	Sigma
KPL LumiGLO Reserve Chemiluminescent Substrate Kit	Sera Care
Ni-Sepharose 6 Fast Flow slurry	GE Healthcare
Nucleobond AX kit	Macherey-Nagel
NucleoSpin Gel and PCR Clean-up kit	Macherey-Nagel
NucleoSpin Plasmid Easy Pure kit	Macherey-Nagel
Pfu DNA polymerase	Thermo Scientific or Promega
Pierce Coomassie Plus (Bradford) Assay Reagent	Thermo Fisher
Primer	Eurofins Genomics
Protease inhibitor mix HP	Serva
PVDF (polyvinylidene fluoride) membrane 0.45 μm	Roth
Ripa-buffer	Thermo Scientific
Semi-micro KW404-4 F (4.66 300 mm) column	Shodex
SpinX column	Costar
Strep-Tactin Superflow 50% suspension	iba
T4 polynucleotide kinase kit	Thermo Scientific
Tubespin bioreactors	TPP
Trypsin-EDTA solution	Sigma Aldrich

2.5.3 Technical equipment

name	**supplier**
Benchtop bioreactor Labfors 3	Infors
Confocal laser scanning microscope LSM 880	Zeiss
Electrophoresis chamber Sub-Cell GT	Biorad
FastPrep	MP Biomedicals
Flow cytometer Attune	Invitrogen
Flow cytometer Celesta	BD
Genepulser Xcell	Bio-Rad
High-performance liquid chromatography (HPLC) system 1200 series	Agilent
High-performance liquid chromatography system	Shimadzu
ImageQuant LAS 4000	GE Healthcare
Lumi-Imager F1	Roche
Methanol sensor	Raven Biotech
Microvolume spectrophotometer NanoDrop ND-1000	Peqlab

Peristaltic pump Minipuls 2	Gilson
Power supply E143	Consort
Spectrometer CLARIOstar	BMG Labtech
Trans Blot	Bio-Rad
Trans Blot Turbo	Bio-Rad
Ultracentrifuge Optima TLX	Beckman Coulter
Ultracentrifuges XE 90 and L-90K	Beckman Coulter
Univapo 100H (SpeedVac)	UniEquip
UV-transilluminator UST-20M-8R, 312 nm	Biostep

Chapter 3

Results

3.1 Stabilizing the coreTAP transporter with fragments of the viral inhibitor ICP47

3.1.1 Design and expression of ICP47-coreTAP fusion constructs

The fusion of full length ICP47 fragments to the coreTAP subunits causes an arrest of the TAP transporter by simulating a defined high local concentration of the viral inhibitor, similar to a ball-and-chain inactivation of voltage-gated ion channels [156, 157]. In order to understand the function of the conserved regions in ICP47, this polypeptide was systematically truncated and fused to the elbow helix of the TAP subunits (Fig. 3.1). Five fusion constructs for each subunit were generated harboring the active domain of ICP47 (residues 1-35, 1-50, 1-65, 1-78 or 1-88) connected by a TEV protease cleavage site either to coreTAP1 or to coreTAP2 (Fig. 3.2). Two more fusion constructs, ΔH1 and ΔH2, contained an impaired active domain, where the first or the second helix of ICP47 was deleted. These constructs were composed of ICP47 residues 12-88 and 1-22/34-88 respectively, and served as negative control (Fig. 3.2).

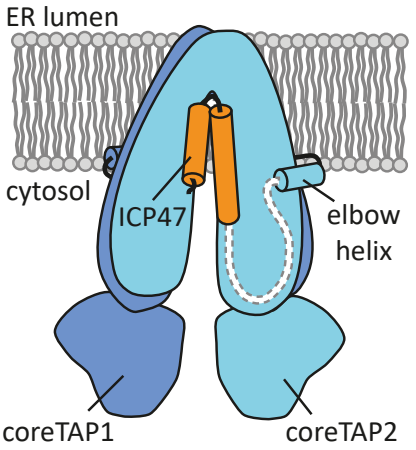

Figure 3.1: ICP47-coreTAP fusion complex. Schematic representation of an ICP47-fragment fused to the coreTAP2 subunit. The ICP47 polypeptide is highlighted in orange and core TAP1 and TAP2 subunits in blue and light blue, respectively.

Five more constructs were generated, with the active domain of ICP47 (residues 1-34) connected by three different glycine-serine (GS) linkers to the

coreTAP subunits. These GS-linkers of 40, 50 and 60 residues length, covered approximately the distance between the ICP47 binding pocket and the elbow helices of coreTAP. Three different linker lengths were chosen to find the construct, which behaves best biochemically and enables the correct positioning of the ICP47 active domain into the binding pocket (Fig. 3.2).

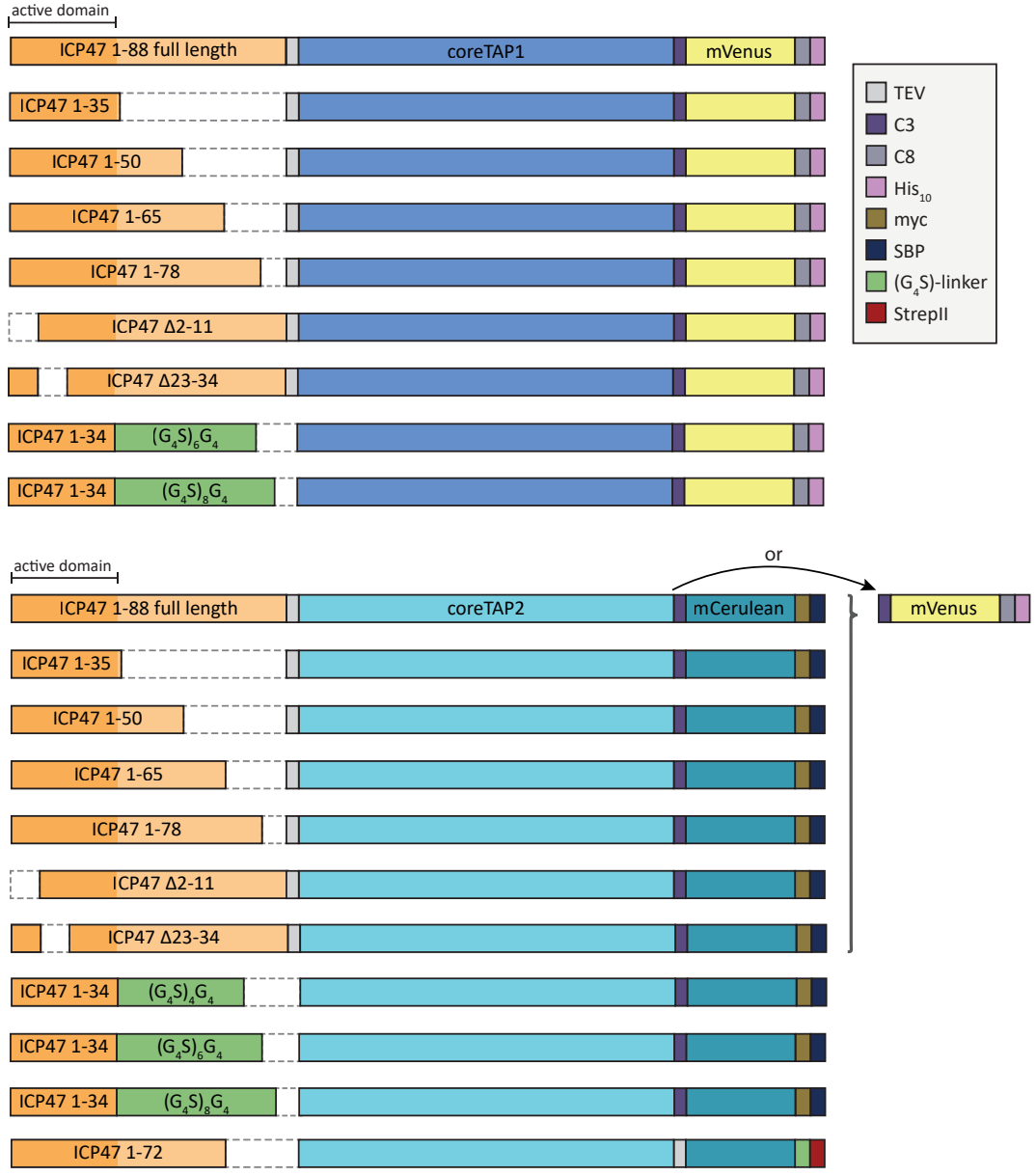

Figure 3.2: ICP47-coreTAP fusion constructs.
ICP47 residues 1-35, 1-50, 1-65, 1-78, 1-88, 12-88 and 1-22/34-88 (orange) were fused by a TEV-cleavage site to the elbow-helix of the TAP subunits (coreTAP1 blue, coreTAP2 light blue). The active domain of ICP47 (residues 1-34) was fused by three different glycine-serine linkers (green) to the elbow-helix of the TAP subunits. CoreTAP1 and coreTAP2 constructs were fused to a C3-mVenus-C8-His_{10} tag, coreTAP2 was also fused to C3-mCerulean-myc-SBP tag. ICP47(1-72)-coreTAP2 was fused to TEV-mCerulean-Linker-StrepII tag for expression in *P. pastoris*.

For comparison of expression levels and to allow an orthogonal purification of the heterodimeric coreTAP complex, both subunits and free ICP47 fragments were fused to the GFP derivatives mVenus or mCerulean, followed by a C8-His_{10} tag or a myc-SBP tag respectively. Constructs used for fermentation in *P. pastoris* were also fused to mVenus or mCerulean, but followed only by His_{10}- or StrepII-tag, respectively (Fig. 3.2).

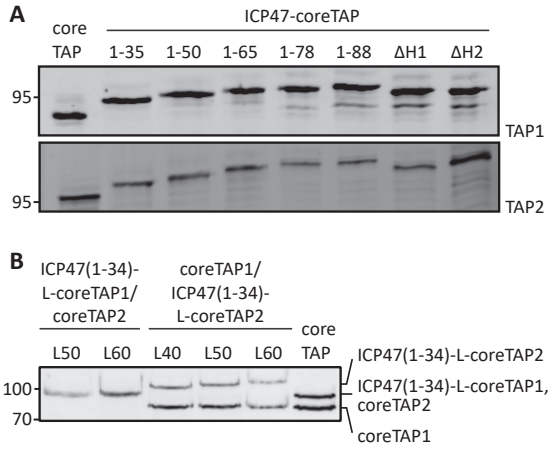

Figure 3.3: ICP47-coreTAP expression. coreTAP and ICP47-coreTAP (A) and ICP47(1-34)-L-coreTAP (B) fusion constructs expressed in HEK293-T cells analyzed by SDS-PAGE and in-gel fluorescence respectively.

The N-terminal fusion of ICP47 to the coreTAP subunits and, in particular, the varying lengths of the ICP47 fragments did not affect the expression levels of the fusion constructs in HEK cells (Fig. 3.3). Only ICP47(1-34)-L50-coreTAP1/coreTAP2 showed a slightly reduced expression level (Fig. 3.3B), suggesting that the fusion could lead to mispositioning of ICP47 resulting then in altered expression levels.

For comparison, four more ICP47 fragments (1-35, 1-55, 1-73 and 1-88) were fused directly to C3-mVenus-C8-His_{10} or C8-His_{10} tag (Fig. 3.4A). These "free" ICP47 variants were co-expressed with the coreTAP subunits to compare the properties of these coreTAP complexes to the fused variants, excluding that any effects could be exclusively attributed to the fusion. Previous studies defined the active domain as essential and sufficient for TAP inhibition, displaying the same inhibitory activity as the full-length protein [4, 5]. In this study, ICP47 residues that could be involved in TAP interaction were characterized more precisely with regard to the coreTAP melting temperature. Therefore, the putative stabilizing region of ICP47 (residues 35-55) was dissected into seven segments of three residues (SR1-7). These triplets were exchanged for glycine-alanine-glycine, except for SR2, where alanine-glycine-glycine was used (Fig. 3.4B).

The free ICP47 variants were co-expressed with coreTAP in HEK293-F cells and subsequently co-purified (first via His_{10}-tag, then via SBP-tag). The ICP47 fragments 1-55, 1-73 and 1-88 were co-purified in comparable amounts to the coreTAP subunits, while the shortest fragment ICP47(1-35) showed reduced intensity, indicating a possibly altered interaction of the short fragment to coreTAP (Fig. 3.4C). ICP47(1-88)SR/coreTAP variants were expressed and co-purified by practical student Carolina Kuge. All SR mutants were co-purified with coreTAP at similar ratios. The reduced intensity of ICP47(1-88)SR4/coreTAP is presumably due to handling variations and could be solved by repeating the experiment (Fig. 3.4D).

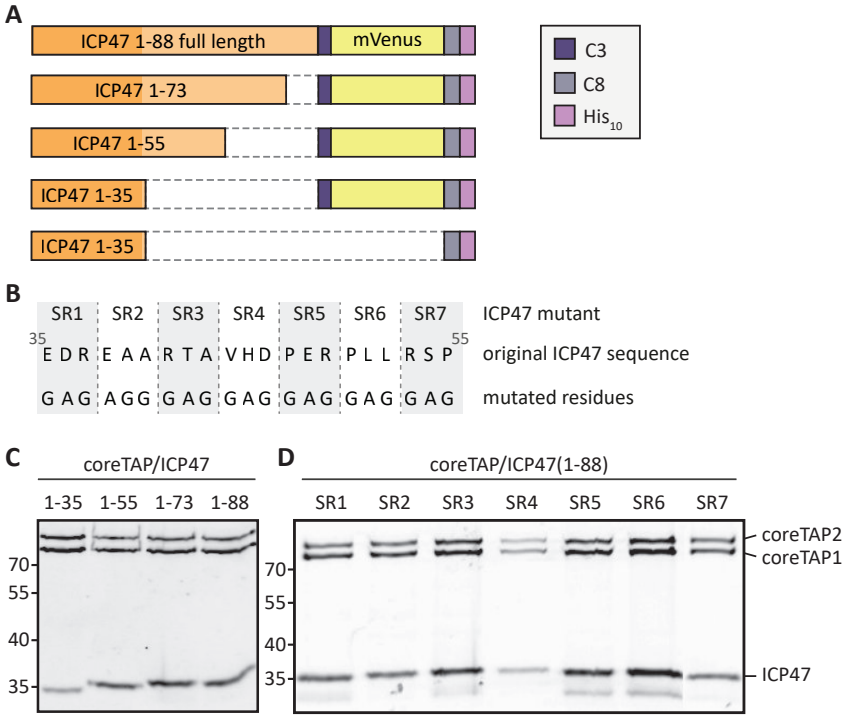

Figure 3.4: Free ICP47 constructs and SR mutants.
ICP47 residues 1-35, 1-55, 1-73 and 1-88 were fused to C3-mVenus-C8-His_{10} tag. ICP47(1-35) was furthermore fused to C8-His_{10} tag without mVenus (A). The putative stabilizing region of ICP47 (residues 35-55) was dissected into seven segments of three residues (SR1-7). These triplets were exchanged for glycine-alanine-glycine, except for SR2, where alanine-glycine-glycine was used (B). Free ICP47 fragments were co-expressed with coreTAP, orthogonally purified and analyzed by SDS-Page and in-gel fluorescence (C). ICP47-SR mutants were co-expressed with coreTAP, orthogonally purified and analyzed by SDS-Page and in-gel fluorescence (D).

3.1.2 ICP47-coreTAP complexes block the MHC I surface presentation

To test if peptide translocation is blocked by the ICP47 fusion constructs, the MHC I surface expression was monitored by flow cytometry. The TAP-deficient human cell lines BRE-169 and STF1-169, isolated from patients lacking TAP1 or TAP2, respectively [58, 59], were complemented with the missing subunit fused to different ICP47 fragments. The expression levels of the fusion constructs and the MHC I surface expression was quantified by flow cytometry. TAP-deficient cells transfected with a construct coding for mVenus only (mock control) display a background level of MHC I surface expression (Fig. 3.5A, B). A similar background level was observed for all ICP47-coreTAP fusion constructs containing the intact active domain of ICP47 (1-35, 1-50, 1-65, 1-78 and 1-88). In contrast, the constructs harboring an N- or C-terminally truncated ICP47 (ΔH1 and ΔH2) did not block MHC I surface expression in TAP-deficient cells (Fig. 3.5A, B). These changes in surface expression confirm that the active domain of ICP47 is necessary

and sufficient for an effective interaction of the fused viral factor with TAP. Interestingly, the distance between the active domain of ICP47 (residues 3-34) and the elbow helix of each TAP subunit can vary between one and 62 amino acids without affecting the inhibitory function of the active domain, reflecting its high degree of flexibility including several interactions of ICP47 at the TAP1/2 interface.

To analyze this apparently highly variable C-terminus of ICP47, constructs that bridged the distance between the active domain of ICP47 (residues 1-34) and the elbow helices of TAP by different glycine-serine linkers (40, 50 or 60 residues in total) were also tested for MHC I surface expression (Fig. 3.5C, D). Since these five constructs were fused to mCerulean instead of mVenus, the detection via flow cytometry was not optimal and the comparison with mVenus-fusions is impeded. Nonetheless, the coreTAP complexes with implemented linkers showed slightly elevated MHC I surface expressions compared to the complexes with an original ICP47 sequence. None exceeded values of mean fluorescence intensity 2-3 times above background (Fig. 3.5D), indicating that the proper function of the TAP complex is still impeded. Thus, these results confirmed the findings of previous studies demonstrating that the active domain of ICP47 is the only prerequisite for an effective interaction with TAP.

To gain deeper insights into ICP47-TAP interaction and to exclude any effects due to the fusion per se, four free ICP47 fragments were co-expressed with coreTAP1 in TAP1-deficient BRE-169 cells to be analyzed for MHC I surface expression. Notably, the ICP47 fragments 1-55, 1-73 and 1-88 did not display any MHC I surface presentation above background level (Fig. 3.6A, B). Only the fragment 1-35, which already demonstrated a reduced interaction to coreTAP during co-purification (Fig. 3.4C), showed a pronounced second peak towards higher MHC I surface presentation values in flow cytometry analysis (Fig. 3.6A) and a four times higher mean fluorescence intensity value (Fig. 3.6B).

This contrasting difference in the behavior of free ICP47 fragments represented a first evidence that the interaction of the viral inhibitor ICP47 and the TAP complex is not determined exclusively by the presence of the active domain of ICP47.

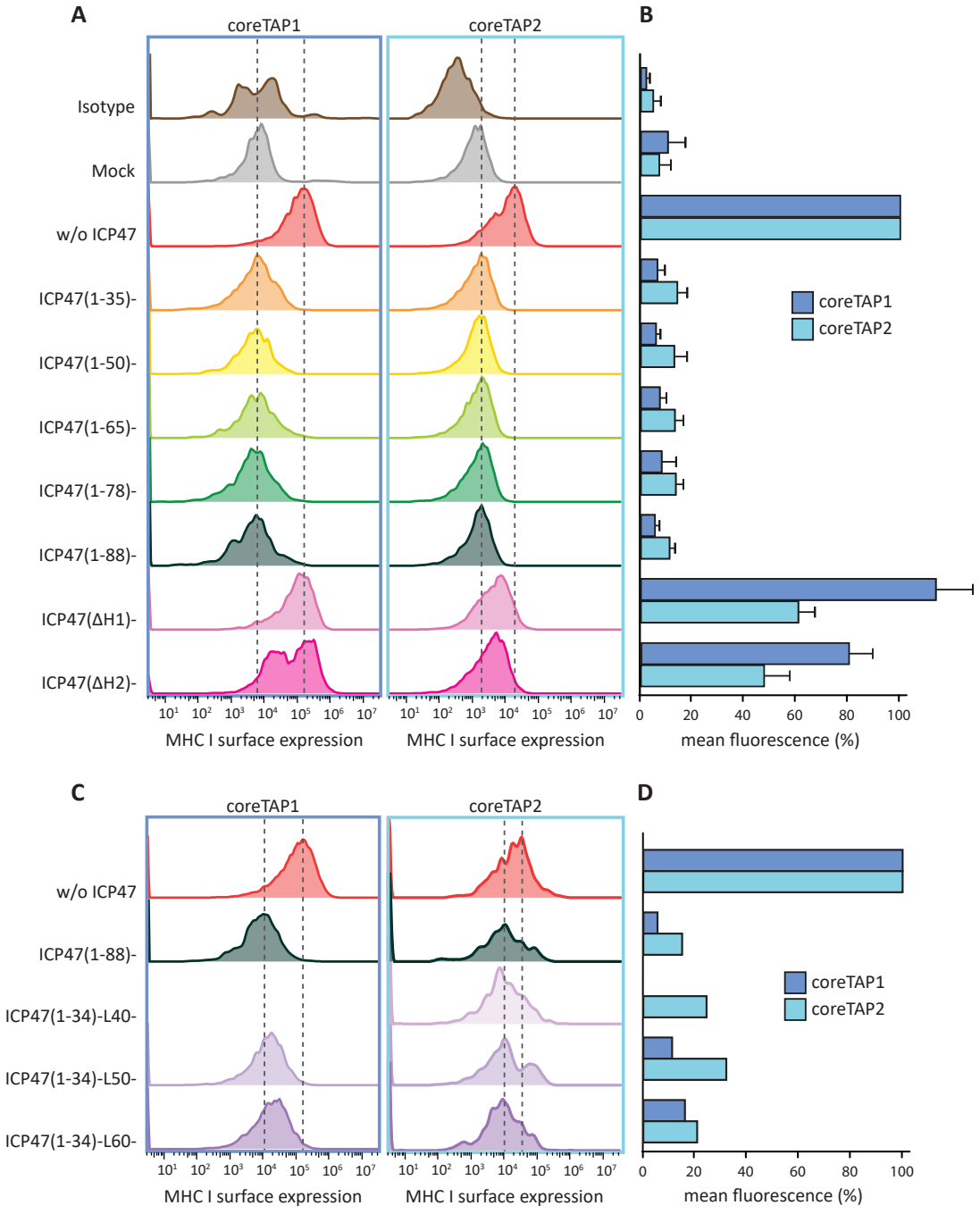

Figure 3.5: ICP47-coreTAP complexes indirectly block MHC I surface expression. ICP47-coreTAP1 and ICP47-coreTAP2 fusion variants were expressed in the TAP-deficient cells BRE-169 ($TAP1^{-/-}$) and STF1-169 ($TAP2^{-/-}$), respectively. MHC I surface expression was monitored by flow cytometry using a PE-labeled MHC I-specific antibody (A, C). The mean PE fluorescence was calculated for transfected cells (mVenus positive (B) and mCerulean positive (D)). The mean (±SD) fluorescence of MHC I presented on the cell surface of TAP1- or TAP2-deficient cells transfected with constructs coding for coreTAP1 or coreTAP2 without ICP47 was normalized to 100% (B: n=3; D: n=1).

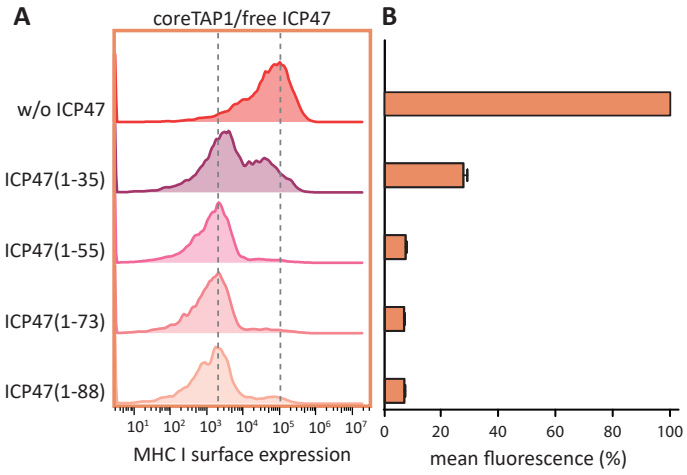

Figure 3.6: Free ICP47 fragments block MHC I surface expression.
Free ICP47 fragments were co-expressed with coreTAP1 in TAP1-deficient BRE-169 cells. MHC I surface expression was monitored by flow cytometry using a PE-labeled MHC I-specific antibody (A). The mean PE fluorescence was calculated for transfected cells (mVenus positive (B)). The mean fluorescence (±SD) of MHC I presented on the cell surface of TAP1-deficient cells transfected with a construct coding for coreTAP1 without ICP47 was normalized to 100% (n=3).

3.1.3 Asymmetric thermostability of ICP47-coreTAP complexes

ICP47-coreTAP fusion constructs were co-expressed with the complementary coreTAP subunit in HEK cells. Assembly of stoichiometrically defined coreTAP1/2 complexes was analyzed by multicolor fluorescence-based size exclusion chromatography (MC-FSEC) after orthogonal purification via His_{10}- and SBP-tag. The coreTAP complex and all functionally arrested ICP47-coreTAP complexes eluted as defined peaks (Fig. 3.7, blue peaks), corresponding to particles with an apparent molecular weight of approximately 360 kDa. This estimated size indicates that the ICP47 fusions did not negatively affect TAP assembly. In a next step the thermostability of the ICP47-coreTAP complexes was examined by FSEC after one hour incubation at 40 °C. Under these conditions, the coreTAP complex without fused ICP47 eluted as a double peak with reduced height, indicating that the complex is unstable at this temperature and eventually dissociated into its subunits (Fig. 3.7). As expected, ICP47-coreTAP complexes with an impaired active domain of ICP47 (ΔH1 and ΔH2) did not show thermal stabilization. CoreTAP1 and coreTAP2 complexes fused to active ICP47 fragments spanning residues 1-35 and 1-50 were likewise unstable and eluted as double peaks similar to coreTAP. The medium-length fragment ICP47(1-65) fused to coreTAP1 also resulted in an unstable complex. Yet, a thermostable complex was assembled in case of a fusion to coreTAP2. Both coreTAP subunits containing ICP47 fragments 1-78 and 1-88 (full-length) led to stable coreTAP complexes. These findings suggest that the ICP47 fragments 1-35 and 1-50 fused to the elbow helices of either TAP1 or TAP2 did not allow an optimal positioning

of the active domain in the binding cavity. The differences in thermal stabilization by ICP47(1-65) fusions suggest a directionality for optimal ICP47 binding that is dictated by the asymmetry of the TAP transporter.

Interestingly, ICP47-coreTAP complexes that had the active domain of ICP47 (residues 1-34) fused by different flexible glycine-serine linkers to the TAP elbow helices did not show thermal stabilization, independently of the linker lengths. This finding contradicts the previously observed behavior, which indicated that all these linker-constructs were able to arrest TAP function, but supports the assumption that the C-terminal ICP47 residues might play an important role in the interaction with TAP.

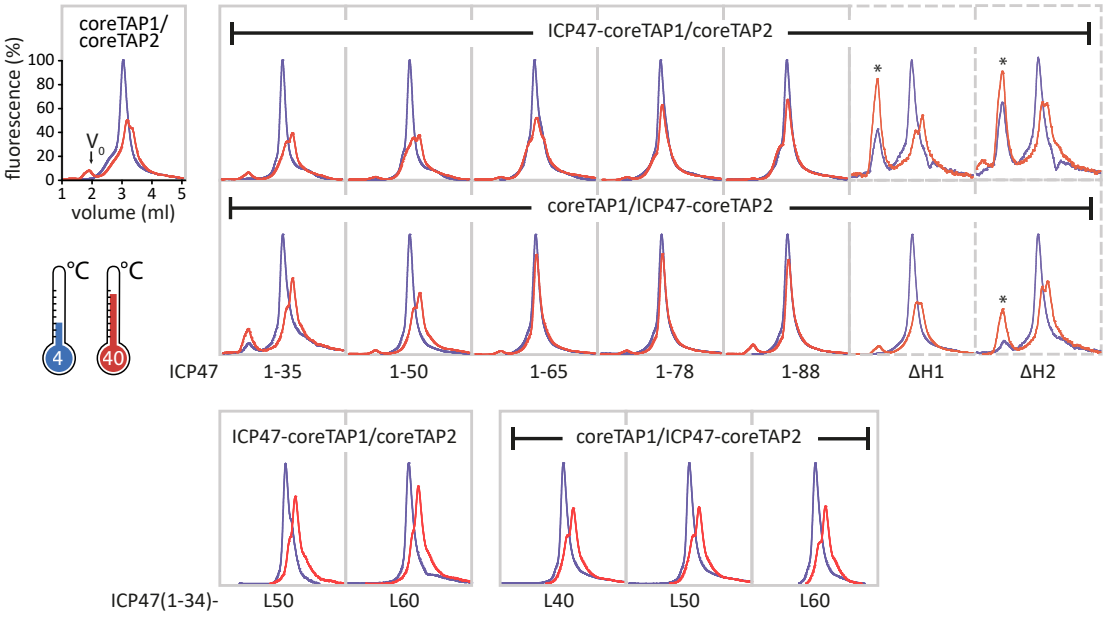

Figure 3.7: Fused ICP47 induces an asymmetric thermostability of coreTAP complexes. Purified coreTAP and ICP47-coreTAP complexes were incubated 1 h at 4 °C and at 40 °C. mVenus fluorescence was recorded by FSEC (blue, 4 °C; red, 40 °C). FSEC profiles at 4 °C were normalized to 100%. The fusion constructs containing inactive ICP47 (ΔH1 and ΔH2) are displayed in dashed boxes. The void volume is indicated in the first panel. The peaks denoted by an asterisk appear higher due to low purification yields.

3.1.4 ICP47-coreTAP complexes are largely thermostabilized

The determination of melting temperatures is a reliable method to characterize the thermostability of interacting proteins and gives more precise insights into their behavior at elevated temperatures compared to the thermostability assay used in the section before. The melting temperature of ICP47-coreTAP complexes exposed to increasing temperatures was determined by analyzing FSEC profiles of orthogonally purified coreTAP complexes, similar to a previously published method [167]. It was assumed that the

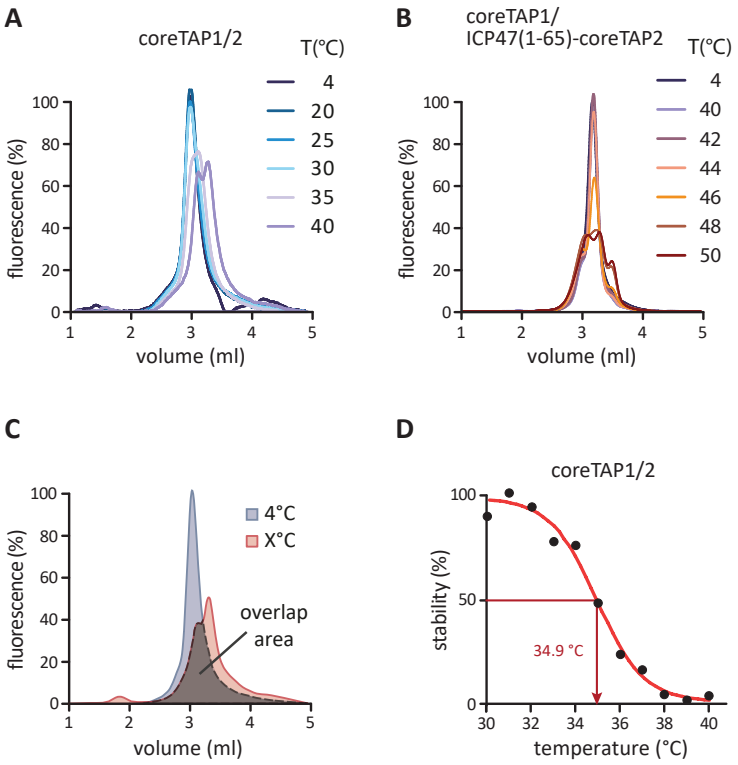

Figure 3.8: Melting temperature calculation by FSEC profiles.
Purified coreTAP (A) and coreTAP complex with ICP47(1-65) fused to TAP2 (B) were incubated 5 min at varying temperatures as indicated. FSEC profiles of mVenus fluorescence are shown. (C) Illustration of the overlap area calculation of TAP1/ICP47(1-50)-TAP2. (D) Melting curves were built using the overlap areas, here coreTAP1/2 and coreTAP1/ICP47(1-65)-coreTAP2 are shown exemplarily. Melting temperatures of the other constructs are depicted in Fig. 3.9 and summarized in Table 3.1.

coreTAP subunits disintegrate at increasing temperatures, while fluorescent reporter proteins stay intact. As set out above, ICP47 fragments have to be fused preferably to the coreTAP2 subunit to favor the formation of a thermostable coreTAP complex. Therefore, the following experiments were focused primarily on ICP47-coreTAP2 fusions, and not all ICP47-coreTAP1 fusions were analyzed in detail. Fig. 3.8A and B show exemplary FSEC thermostability profiles of heterodimeric coreTAP and coreTAP1/ICP47-coreTAP2 complexes, respectively. By overlaying the FSEC profiles with the reference peak at 4 °C, an overlap area can be calculated, which reflects the stability at defined temperatures (Fig. 3.8C). Next, the calculated overlap areas were used to build melting curves of coreTAP complexes (Fig. 3.8D).

While orthogonally purified coreTAP1/2 in GDN without fused ICP47 fragment already dissociated at 36.3 ±1.5 °C (Fig. 3.8D and Table 3.1), fusion of full length ICP47 raised the melting temperature of the coreTAP complexes to 47.1 ±0.1 °C (fusion to coreTAP2) and to 46.0 ±2.6 °C (fusion to coreTAP1) (Fig. 3.9 and Table 3.1). Surprisingly, the shorter fragments 1-35 and 1-50 fused to coreTAP2, without any stabilizing effect

on coreTAP1/2 in the thermostability assay, increased the melting temperature by 4-6 °C. The fusion of the shortest fragment 1-35 to coreTAP1 did not alter the melting temperature, while fragment 1-50 slightly raised the melting temperature to 39.9 °C. The fusion of the fragments 1-65 and 1-78 to both subunits raised the melting temperature by approximately 10 °C with a slight tendency to higher melting temperatures for longer ICP47 fragments (Fig. 3.9 and Table 3.1). Due to low purification yields it was not possible to determine reliable melting temperatures for the ΔH1 and ΔH2 mutants.

Table 3.1: Melting temperatures of ICP47-coreTAP complexes

construct	**melting temperature**
coreTAP1/coreTAP2	36.3 ±1.5 °C ***
coreTAP1/ICP47(1-35)-coreTAP2	41.4 ±0.2 °C **
coreTAP1/ICP47(1-50)-coreTAP2	43.6 ±0.2 °C **
coreTAP1/ICP47(1-65)-coreTAP2	45.7 ±0.2 °C **
coreTAP1/ICP47(1-78)-coreTAP2	46.1 ±0.6 °C **
coreTAP1/ICP47(1-88)-coreTAP2	47.1 ±0.1 °C **
coreTAP1/ICP47(1-34)-L50-coreTAP2	36.9 °C*
ICP47(1-35)-coreTAP1/coreTAP2	35.8 °C*
ICP47(1-50)-coreTAP1/coreTAP2	39.9 °C*
ICP47(1-65)-coreTAP1/coreTAP2	44.2 °C*
ICP47(1-78)-coreTAP1/coreTAP2	46.7 °C*
ICP47(1-88)-coreTAP1/coreTAP2	46.0 ±2.6 °C**
coreTAP/ICP47(1-35)	33.2 °C*
coreTAP/ICP47(1-55)	44.6 °C*
coreTAP/ICP47(1-73)	45.7 °C*
coreTAP/ICP47(1-88)	45.6 °C*
coreTAP/ICP47(1-35)ΔmVenus	26.2 °C*

* n=1; ** n=2; *** n=3

Although the previous thermostability assay demonstrated that constructs with the active domain of ICP47 (residues (1-34)) fused by different glycine-serine linkers to the coreTAP subunits did not thermo-stabilize coreTAP, coreTAP1/ICP47(1-34)-L50-coreTAP2 was exemplarily analyzed. As expected, this fusion did not raise the melting temperature (Fig. 3.9 and Table 3.1), proving again that the active domain of ICP47 is apparently essential for coreTAP inhibition but not sufficient for complete interaction with coreTAP. The distance that can be bridged by these 50 residues should ensure a correct positioning of the active domain inside the binding cavity. Although, it cannot be excluded that the linker was too flexible, and enabled the interaction with other coreTAP complexes.

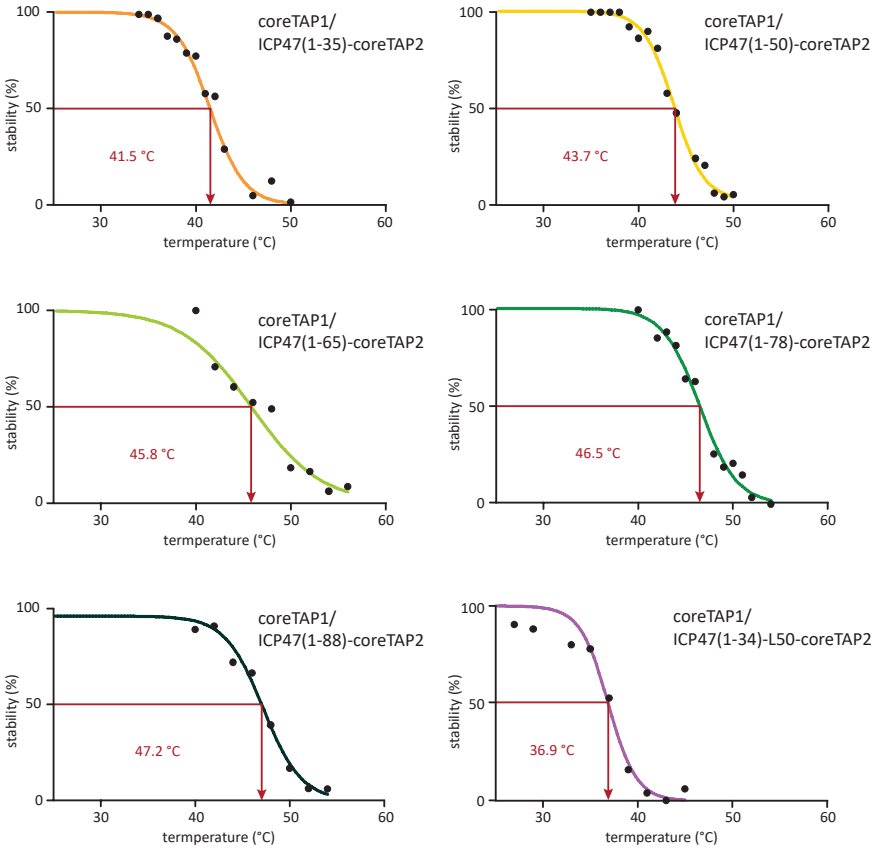

Figure 3.9: ICP47 fusion increases the melting temperature of coreTAP. Stability of orthogonally purified ICP47-coreTAP2 fusion complexes was determined by FSEC. The calculated melting temperatures are depicted under the respective construct (red arrow). Table 3.1 shows the average of calculated melting temperatures.

3.1.5 The stabilizing domain of ICP47

For comparison, the melting temperature of coreTAP co-expressed with non-fused ICP47 variants, containing ICP47 residues 1-35, 1-55, 1-73, and 1-88 (Table 3.1) was determined. Unexpectedly, the shortest fragment, ICP47(1-35), which has the same affinity as full-length ICP47 and is sufficient to block peptide binding and transport by TAP [4, 5], destabilized the coreTAP complex lowering the melting temperature to 33.2 °C. In contrast, ICP47(1-55), -(1-73), and -(1-88) raised the melting temperature to approximately 45 °C, suggesting that residues 35-55 have an extra function in stabilizing the TAP complex and cannot be replaced by other residues like glycine-serine linkers. Taking into account that the 1-35 fragment fused to the coreTAP2 subunit raised the melting point by few degree and the fragment 1-34 fused by a 50 residues long linker did not alter the melting temperature, it can be hypothesized that the fusion per se helps to stabilize the TAP complex, circumventing the absence of the residues 35-55 and bringing the active domain in close proximity to the binding cavity.

To avoid any steric hindrance or interaction effects caused by the fusion to the GFP

derivate mVenus, a fifth ICP47 variant was tested. ICP47(1-35)-C8-His_{10} without mVenus lowered the coreTAP melting temperature even further to 26.2 °C (Table 3.1), confirming the importance of the C-terminal ICP47 residues.

In order to define the residues involved in the stabilization of coreTAP more precisely, the putative stabilizing region of ICP47 (residues 35-55) was dissected into seven segments of three residues (SR1-7). These triplets were exchanged for glycine-alanine-glycine, except for SR2, where alanine-glycine-glycine was used (Fig. 3.10). The residues of SR2 were found to be the most critical for coreTAP stabilization. SR1, SR5, and SR6 lowered the melting temperature approximately to 36 °C, SR3 to 38 °C. In contrast, SR4 and SR7 did not significantly affect the melting temperature of the ICP47/coreTAP complex.

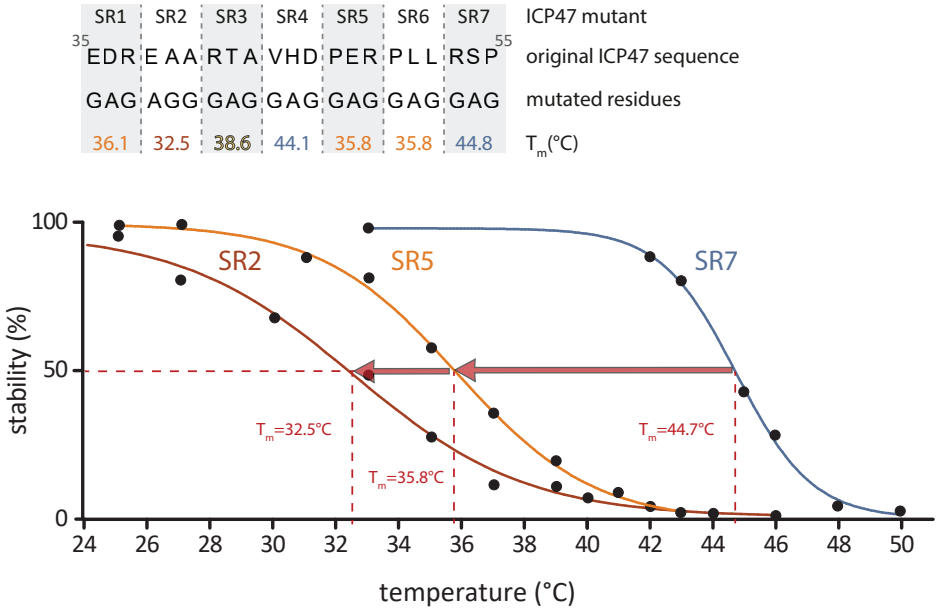

Figure 3.10: The stabilizing region of ICP47 is essential for interaction with coreTAP. The stabilizing region of ICP47 (residues 35-55) was dissected into seven fragments (SR1-7) of three amino acids, which were replaced by glycines or alanines in order to link a change in melting temperature of ICP47/coreTAP complexes to single residues of the stabilizing region. The calculated melting temperatures are depicted below the respective mutation. Melting curves of SR2, SR5, and SR7 are representatively shown.

3.1.6 Alternative methods to determine protein stability

Although the method for melting temperature determination has been published before [167], it includes multiple complex steps making it difficult for routine application. Therefore alternative methods had to be considered. At first, the well-established microscale fluorescent thermal stability assay was tested, which utilizes the thiol-specific fluorochrome N-[4-(7-diethylamino-4-methyl-3-coumarinyl)phenyl]maleimide (CPM) [168]. However, all TAP constructs used in this study were based on cys-less TAP, in which all cysteines

except C213 in TAP2 were replaced. This single cysteine in TAP was not sufficient to obtain interpretable stability profiles.

In a second approach melting temperatures were determined via nano differential scanning fluorimetry (nanoDSF). This dye-free assay allows to analyze protein folding as well as thermal and chemical stability by measuring changes in tryptophan fluorescence in a temperature range of 15-98 °C. Hydrophobic tryptophans are mostly embedded in the protein interior and become exposed during heat denaturation. This process alters their photo-physical properties, shifting the emission of tryptophan to longer wavelengths from 330 nm to 350 nm [169].

The purified ICP47-coreTAP complexes used to determine the melting temperatures via FSEC were re-analyzed by nanoDSF. Since in prior experiments the strong fluorescence signal of the GFP-derivates was read out, minimal protein amounts and a low protein concentration were sufficient to determine melting temperatures. The nanoDSF assay allows protein concentrations of 5 μg/ml to 150 mg/ml, however the appropriate concentration for the protein of interest has to be individually determined. Unfortunately, of all tested complexes only ICP47(1-65)-coreTAP1/coreTAP2, ICP47(1-88)-coreTAP1/coreTAP2, coreTAP1/ICP47(1-50)-coreTAP2 and coreTAP1/ICP47(1-88)-coreTAP2 could be measured, but only at minimal detection limit. The calculated melting temperatures were slightly higher, but comparable to those determined by FSEC measurements (Fig. 3.11). This demonstrates that determining the melting temperature of TAP complexes in detergent, available moreover only in minimal amounts, can be accomplished via FSEC with ±2 °C precision, in case other more common methods fail or are not available.

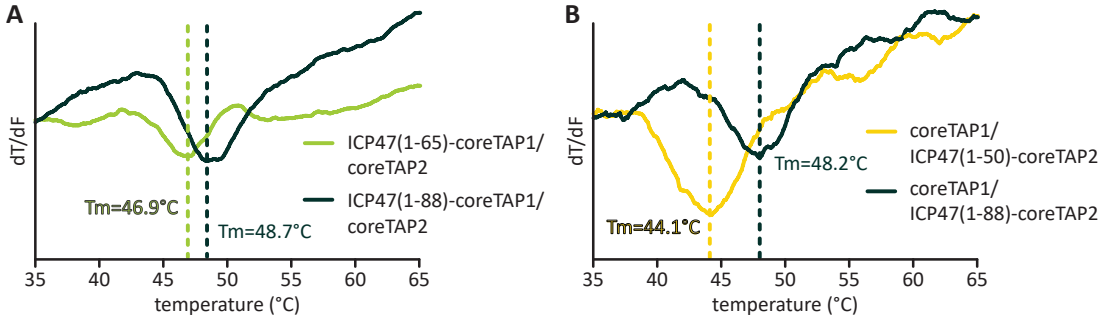

Figure 3.11: CoreTAP melting temperature determined by nanoDSF. Melting temperatures of orthogonally purified ICP47-coreTAP fusion complexes were analyzed via nanoDSF. The left panel (A) shows coreTAP with ICP47 fragments fused to coreTAP1, while the right panel (B) shows coreTAP with ICP47 fragments fused to coreTAP2. The first derivatives of tryptophan fluorescence emission at 350 nm were calculated to obtain the melting temperature, which corresponds to the minimal turning points (dotted lines). Melting temperatures are annotated in respective colors.

3.1.7 Thermostability depends on the detergent used for purification

Future structural analysis of TAP may include the utilization of ICP47-coreTAP complexes, and solubilization in other detergents besides GDN may become crucial. For this purpose, it was tested whether the stabilization of coreTAP by ICP47 can endure purification in a harsher detergent like n-dodecyl β_D-maltoside (DDM) that is commonly used in membrane protein crystallography [170] and was recently used to purify TAP [32, 33] and related ABC transporters [2, 106, 171]. At the same time I checked whether ICP47-coreTAP can be purified in a single step via SBP-tag instead of orthogonal purification. This aimed at speeding up the purification procedure for a faster thermostability screening.

CoreTAP1/2, coreTAP1/ICP47(1-72)-coreTAP2, and coreTAP1/2/ICP47 were expressed in HEK cells to be subsequently purified parallely in 2% GDN or 1% DDM, each by orthogonal purification via His_{10}- and SBP-tag, or by single purification via SBP-tag. For all conditions thermostability was analyzed by comparing the purified complexes via FSEC after 1 h incubation at 4 °C and 40 °C. The mCerulean fluorescence of orthogonally purified coreTAP1/ICP47(1-72)-coreTAP2 in GDN at 4 °C was normalized to 100% (Fig. 3.12, blue peak, yellow box) to adjust the purification yields of the other conditions. Heterodimeric coreTAP1/2 eluted as single peak solely after orthogonal purification in GDN. CoreTAP1/ICP47(1-72)-coreTAP2 could be purified via orthogonal purification

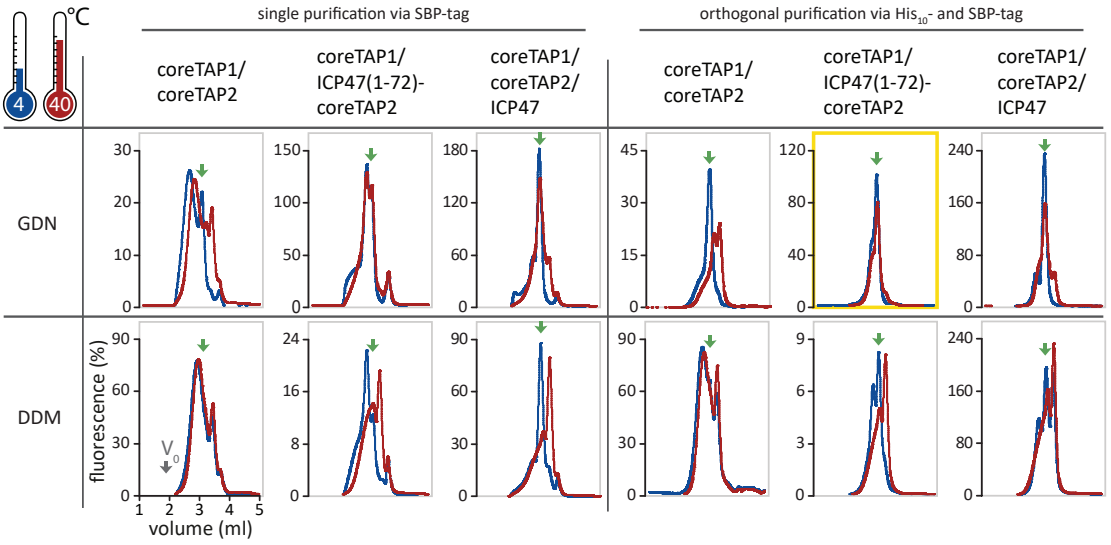

Figure 3.12: Purification in DDM prevents thermostabilization of coreTAP. CoreTAP1/2, coreTAP1/ICP47(1-72)-coreTAP2 and coreTAP1/2/ICP47 were expressed in HEK293-F cells and subsequently solubilized in 2% GDN or 1% DDM and purified via SPB-tag (single purification, left side) or via His_{10}- and SBP-tag (orthogonal purification, right side). Purified coreTAP complexes were incubated 1 h at 4 °C (blue) and at 40 °C (red) and analyzed via MC-FSEC. mCerulean fluorescence of coreTAP1/ICP47(1-72)-coreTAP2 purified in GDN and incubated at 4 °C was normalized to 100% (yiellow box). Elution volume and void volume are shown in the lower panel on the left side.

in both, GDN and DDM. However, in DDM coreTAP eluted with an additional peak at lower elution volume, supposedly corresponding to oligomerized complexes. Unfortunately, this construct proved to be thermostable only in GDN. Interestingly, coreTAP1/2 with free ICP47 eluted as a single peak with strongly increased yield for both, single and orthogonal purification in GDN. Purification in DDM was possible and the yield was comparable to coreTAP1/2. However, it proved to be thermostable only in GDN (Fig. 3.12).

Summarizing, none of the tested construct combinations and purification conditions led to a thermostabilized coreTAP complex in DDM, indicating that the high affinity of ICP47 and coreTAP or the integrity of coreTAP can only be preserved by purification in an adequately mild detergent like GDN. Moreover, the orthogonal purification procedure is essential to obtain a highly pure coreTAP complex in case ICP47 is fused. The utilization of free ICP47 however, appears to be an interesting tool for TAP purification, since it eluted with increased yield as almost monodisperse sample already after single purification by SBP-tag.

3.1.8 ICP47-coreTAP arrests TAP in a specific conformation

In order to link the stabilizing effect to a physiological function, the interaction of the ICP47-coreTAP fusion complexes with free viral factors was probed. US6 and ICP47 interact with TAP from opposite subcellular compartments, the cytosol and the ER lumen, and exclude each other (Fig. 3.13) [129, 140]. To prove that the ICP47-coreTAP fusion complexes were arrested in a defined conformation, the ICP47-coreTAP fusion complexes were co-expressed with the free viral inhibitors US6 and ICP47. After co-immunoprecipitation, the interaction partners were quantified by SDS-PAGE and in-gel fluorescence (Fig. 3.14).

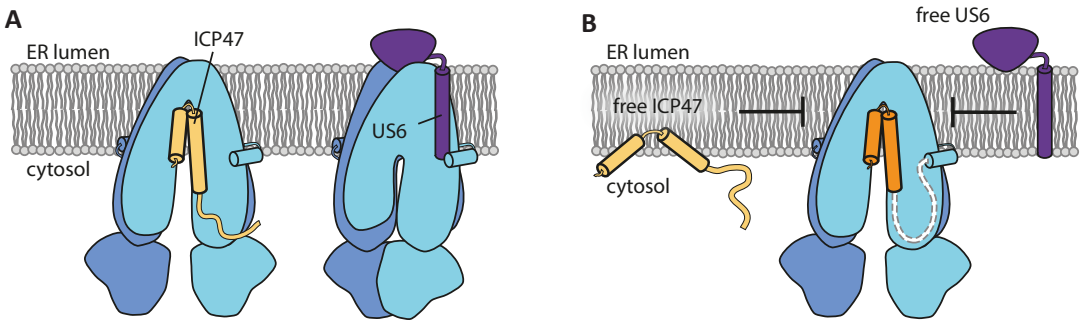

Figure 3.13: ICP47 and US6 interaction.
ICP47 and US6 mutually exclude each other from binding to TAP (A). TAP is conformationally arrested, probed by binding of free ICP47 and US6 (B).

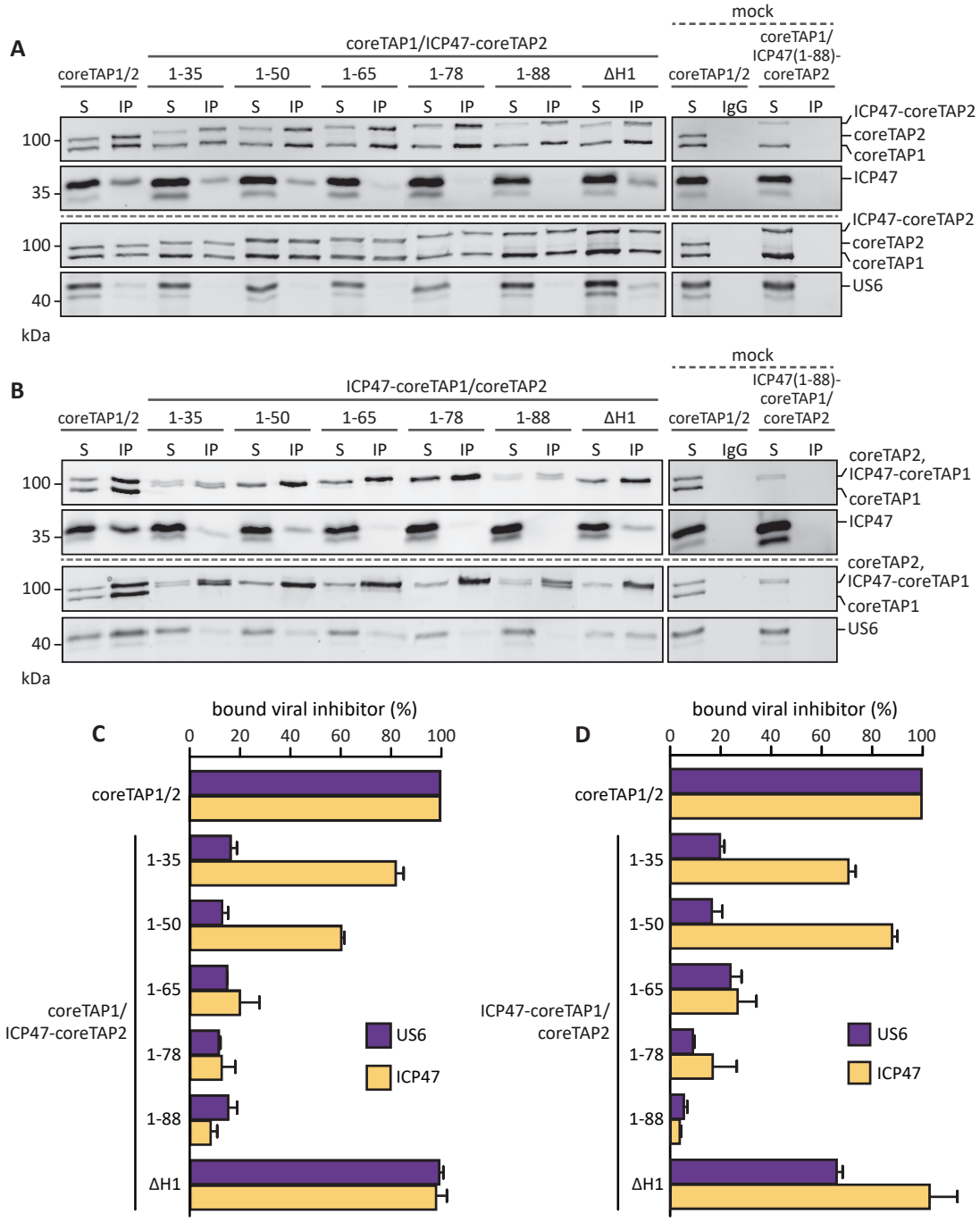

Figure 3.14: ICP47-coreTAP complexes arrest a conformation excluding other viral inhibitors from binding. In-gel fluorescence analysis of the viral proteins US6 and ICP47 co-expressed with ICP47-coreTAP complexes in HEK293-T cells after co-immunoprecipitation via SPB- and C8-tags. Samples of solubilized complexes from whole cell extracts (S) and co-immunoprecipitated complexes (IP) are shown (A and B). The co-precipitated viral factor was quantified in relation to the corresponding coreTAP complex lacking ICP47 (C and D). Error bars represent standard deviations from three independent experiments.

The coreTAP complex devoid of fused ICP47 presents maximal binding (100%) to the viral proteins (Fig. 3.14C, D). Notably, the interaction of non-fused ICP47 gradually decreased to background level with increasing size of the fused ICP47 fragments. The presence of the intact active domain is mandatory, since a truncation restored the amount of co-precipitated viral factor to 100%. Interestingly, a distinction can be made between the most thermostable complexes (ICP47 1-65, 1-78, and 1-88) and unstable complexes (ICP47 1-35 and 1-50). In contrast, all ICP47-coreTAP fusion complexes did not interact with US6. Only a coreTAP fusion with an impaired active domain of ICP47 (ΔH1) restored the interaction with US6, confirming that the entire active domain is required to arrest a defined conformation of TAP. Fused short fragments of ICP47 could be easily outcompeted by free full-length ICP47, although already a slight interaction with a fused short fragment caused the functional arrest. To conclude, an ICP47 fragment complying with all the requirements to generate a stably arrested coreTAP complex cannot be outcompeted by free viral factors.
This experiment was performed with the help of practical student Anja Bäucker.

3.1.9 Expression of ICP47-coreTAP in *Pichia pastoris*

At the beginning of this project I planned to utilize ICP47-coreTAP complexes also for the structural determination of coreTAP, which was unknown at that time. A *P. pastoris* clone that stably expressed coreTAP1/ICP47(1-72)-coreTAP2 was generated to ensure a high production of cell mass, and hence higher amounts of protein. After fermentation and orthogonal purification via His_{10}- and StrepII-tag, it was tested whether ICP47(1-72) fused on coreTAP can stabilize this complex 7 days at 18 °C. FSEC analysis (Fig. 3.15A) showed that the incubation did not negatively affect the protein sample. The peak width was comparable, although the front-peak, probably corresponding to oligomerized protein, appeared to be more pronounced. Yet, negative stain analysis of these samples revealed that the sample is not as homogeneous as the fluorescence signal in the SEC analysis suggested (Fig. 3.15B). Single particles that could be coreTAP1/ICP47(1-72)-coreTAP2 complexes in size were identified before and after incubation, but far more particles appeared to be aggregated. A 2D classification could not be made due to low quality of the sample, and thus low number of particles. However, it is worth mentioning that the negative-stain EM analysis was performed to evaluate the quality of coreTAP directly after orthogonal purification without further SEC purification. Negative-stain EM analysis was carried out by Susanne Hofmann.

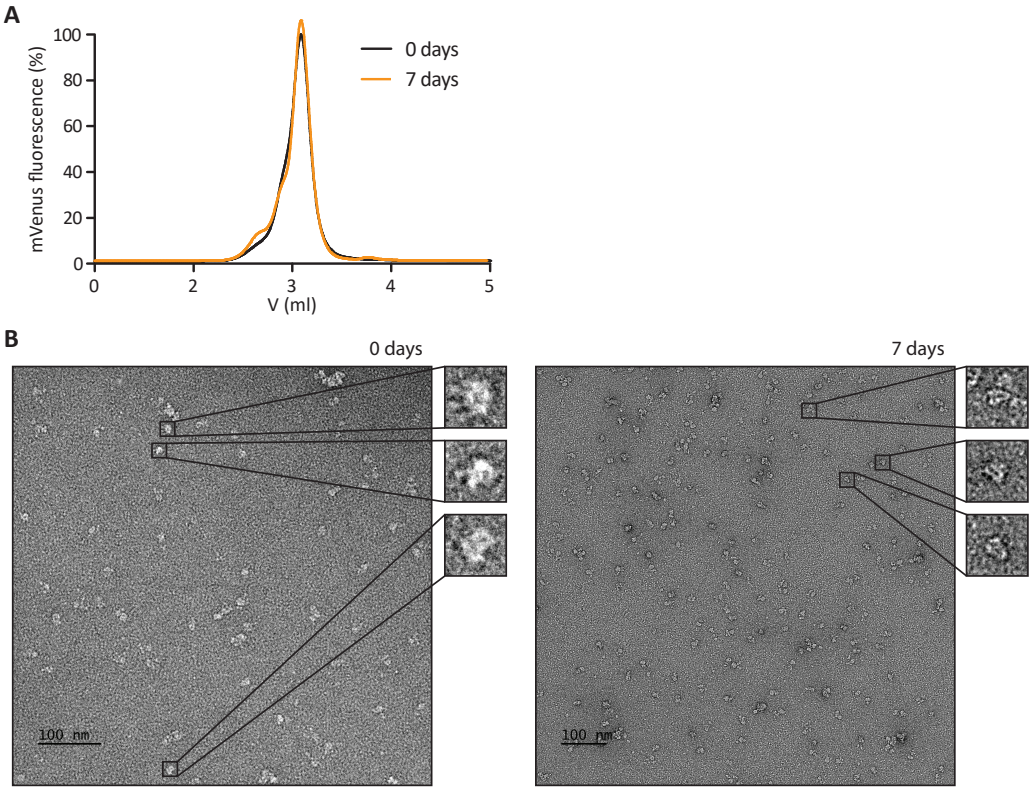

Figure 3.15: ICP47 stabilizes coreTAP.
CoreTAP1/ICP47(1-72)-coreTAP2, expressed in *P. pastoris* and orthogonally purified, was compared via FSEC (A) and negative stain (B) after 7 days incubation at 18 °C. Micrographs are displayed at different magnifications.

In a second approach, *P. pastoris* membranes were utilized to orthogonally purify coreTAP1/ICP47(1-72)-coreTAP2 (Fig. 3.16A). This time the GFP-derivates and purification tags (mVenus-His_{10} or mCerulean-StrepII) were removed via TEV-cleavage and the sample was subsequently fractionated (Fig. 3.16B). The peak fractions (blue) were concentrated to 3.7 mg/ml and utilized for an initial vapor diffusion crystallization screen with MemStart and MemSys kits (Molecular Dimensions). Unfortunately, this screening did not yield any crystals. The experiment was not repeated due to the high amount of used detergent (3 g) combined with the low yield of purified protein (approximately 185 μg). Several more attempts were made to generate a *P. pastoris* clone able to produce higher amounts of coreTAP, however, this clone could not be found.

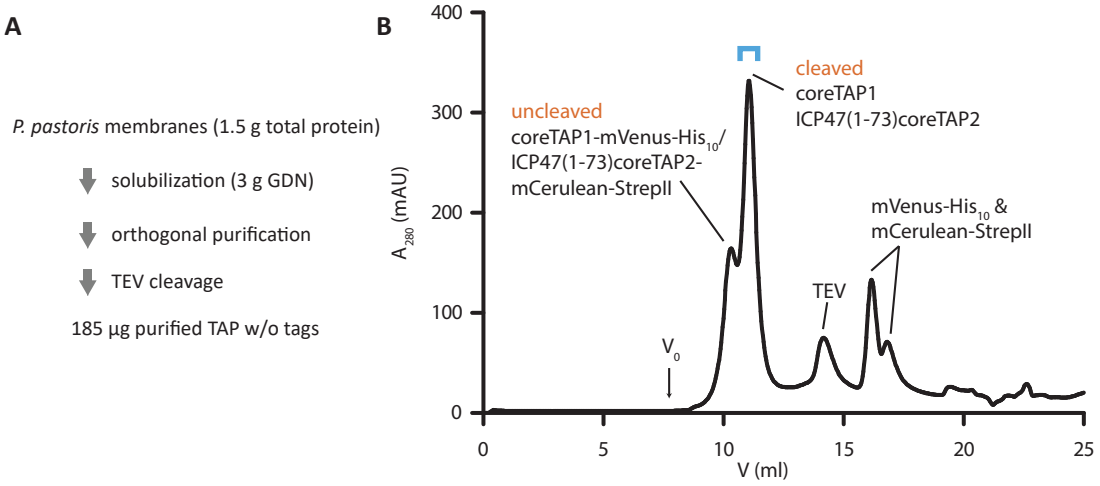

Figure 3.16: Purification of coreTAP1/ICP47(1-73)-coreTAP2.
CoreTAP1/ICP47(1-73)-coreTAP2 expressed in *P. pastoris* was orthogonally purified (A). The purification tags mVenus-His_{10} or mCerulean-StrepII were removed via overnight TEV-clavage at a molar ratio of 1:10 (TEV:coreTAP). The sample was subsequently fractionated on an Äkta purifier utilizing a Superdex 200 increase 10/300 GL column. The peak fraction (blue) was utilized for further experiments (B).

3.2 Self-cleaving ICP47-coreTAP

3.2.1 Introducing a 2A site into ICP47-coreTAP

One of the biggest issues with generating *Pichia pastoris* clones, which stably express coreTAP, is the screening process to find those clones that contain both subunits in a 1:1 stoichiometry. This process can be alleviated by placing both coreTAP subunits on one vector. Although the pPICZ-system is designed to optionally carry two genes of interest, previous attempts on coreTAP by former members of the laboratory failed. As an alternative, the two coreTAP subunits can be placed on one vector, separated by a self-cleaving 2A site [159, 160], enabling the expression of both subunits under the control of only one promoter. The F2A site is encoded by the foot-and-mouth disease virus (FMDV) and mediates a cotranslational "ribosome skipping" event, which cleaves a protein at a defined position during its biosynthesis [158].
Three different constructs were designed, two of these to ensure an optimal positioning of ICP47: coreTAP1-myc-SBP-2A-ICP47-coreTAP2-C3-mVenus-C8-His_{10}, ICP47-coreTAP2-C3-myc-SBP-2A-coreTAP1-C3-mVenus-C8-His_{10} and a third, coreTAP1-myc-SBP-2A-coreTAP2-C3-mVenus-C8-His_{10} as active control (Fig. 3.17). All combinations included only one C-terminal mVenus-tag as reporter for successful expression, but two tags for orthogonal purification as the previous constructs (Fig. 3.2). The orientation of the purification tags depended on the N- or C-terminal position of the coreTAP

subunits: the N-terminal subunit was fused to C3-myc-SBP, while the C-terminal subunit was fused to C3-mVenus-C8-His_{10}. For clarity, constructs will be named coreTAP1-2A-ICP47-coreTAP2, ICP47-coreTAP2-2A-coreTAP1 and coreTAP1-2A-coreTAP2 in the following.

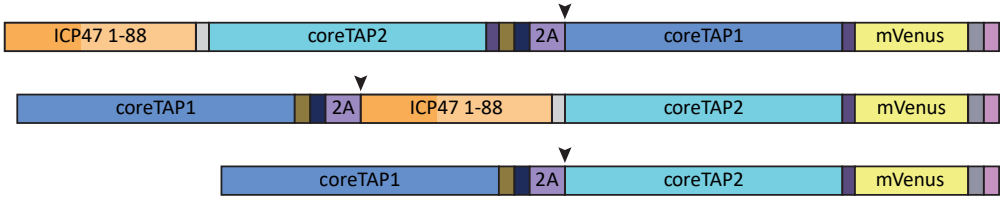

Figure 3.17: ICP47-coreTAP constructs with a F2A site.
The ICP47-coreTAP or coreTAP subunits were connected on one vector by a F2A site. ICP47-coreTAP2 was positioned N- or C-terminally of the F2A site. The orientation of the purification tags depended on the N- or C-terminal position of the coreTAP subunits: the N-terminal subunit was fused to C3-myc-SBP, while the C-terminal subunit was fused to C3-mVenus-C8-His_{10}.

3.2.2 Functionality of ICP47-coreTAP with F2A site is comparable to ICP47-coreTAP

Functionality of the new constructs with the F2A site was determined at first by monitoring the MHC I surface expression in TAP deficient cells by flow cytometry. The new constructs were compared to the previous ones to ensure a correct functionality or inhibition. The TAP2-deficient human cell line STF1-169 was complemented with the F2A-coreTAP constructs, coreTAP2 and coreTAP/ICP47. MHC I surface expression was monitored only for cells containing mVenus as reporter gene. TAP2-deficient cells transfected with a construct coding for mVenus only displayed background level of MHC I surface expression (Fig. 3.18). A similar background level was observed for coreTAP2 co-expressed with ICP47. Although both F2A constructs containing ICP47 fused to coreTAP2 blocked peptide translocation, they led to populations with different MHC I surface expressions: While the N-terminal ICP47 shifted the whole MHC I surface expression distribution to higher values (Fig. 3.18 dotted lines), the ICP47 placed behind the 2A site caused the appearance of two defined populations. The majority of these cells showed a low MHC I surface expression and was broadly distributed (Fig. 3.18 left dotted line), whereas a small population had a high MHC I surface expression (Fig. 3.18 right dotted line). Despite coreTAP with and without F2A site showed similar MFI values for MHC I surface presentation, the population with high MHC I surface expression (Fig. 3.18 right dotted line) appeared to be less widely distributed for the F2A construct.

This finding demonstrated, that coreTAP subunits, classically placed on two vectors, can be successfully replaced by coreTAP constructs separated by a F2A cleavage site. ICP47 appeared to be slightly more effective if positioned directly after the F2A site inside the construct. But, since both variations were not as efficient in TAP inhibition as coreTAP with co-expressed ICP47, further analysis was required to find the optimal, best inhibiting construct.

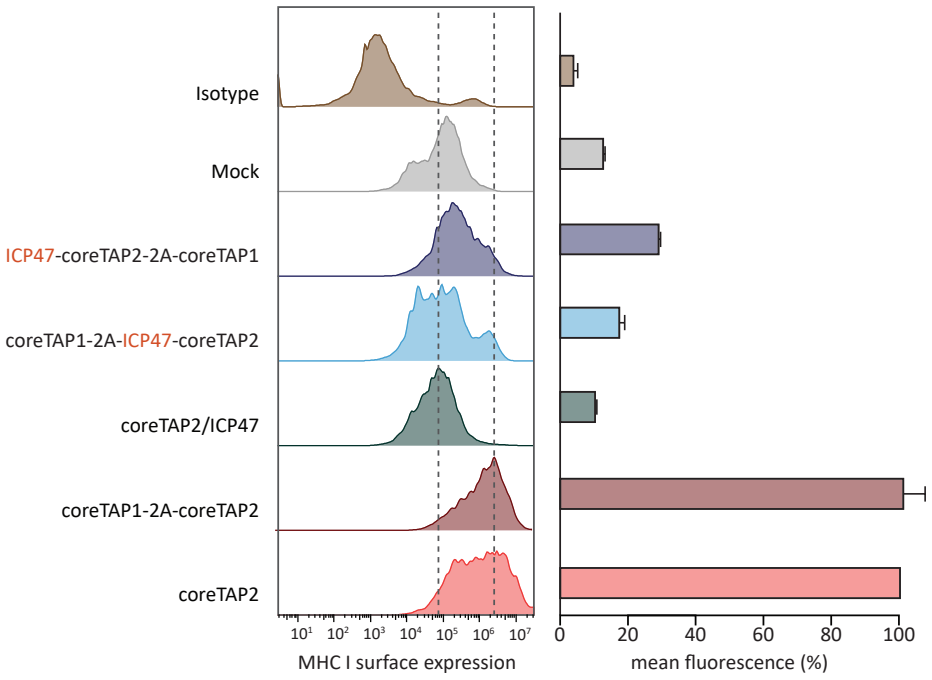

Figure 3.18: MHC I surface expression is not affected by F2A site.
TAP2-deficient STF1-169 were complemented with the F2A constructs coreTAP1-2A-ICP47-coreTAP2, ICP47-coreTAP2-2A-coreTAP1, and coreTAP1-2A-coreTAP2. CoreTAP2, coreTAP2/ICP47 and mVenus (Mock) served as controls. MHC I surface expression was monitored by flow cytometry using an APC/Cy7-labeled MHC I-specific antibody (left). The mean APC/Cy7 fluorescence (right) was calculated for transfected cells (mVenus positive). The mean (±SD) fluorescence of MHC I presented on the cell surface of TAP2-deficient cells transfected with a construct coding for coreTAP2 without ICP47 was normalized to 100% (n=6).

Due to the fact that the inhibitory function of ICP47 in F2A constructs appeared to be inferior compared to free ICP47 co-expressed with coreTAP, it was analyzed whether the F2A constructs were correctly expressed and processed. To facilitate handling and transfection conditions, HEK cells were used instead of TAP-deficient cells. These cells were transfected with a construct coding for coreTAP1/2 and the two F2A constructs containing ICP47 (ICP47-coreTAP2-2A-coreTAP1 and coreTAP1-2A-ICP47-coreTAP2). Subsequently, the coreTAP complexes were orthogonally purified, first by His_{10}-tag and second by SBP-tag.

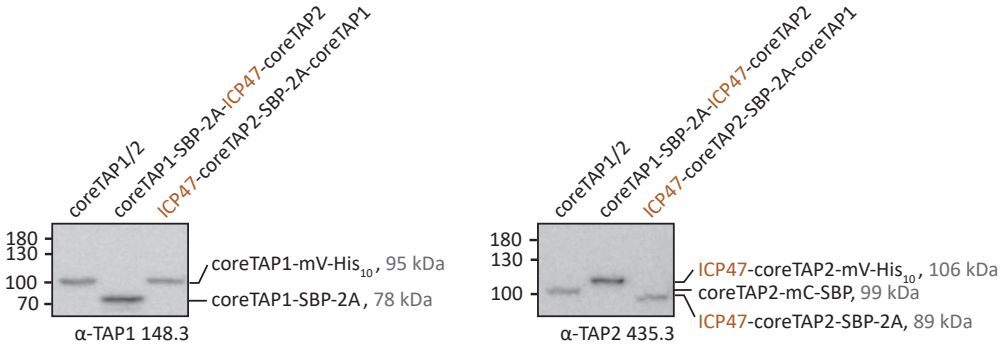

Figure 3.19: ICP47-coreTAP with F2A site is correctly processed in HEK293-F cells. coreTAP1/2, ICP47-coreTAP2-C3-myc-SBP-2A-coreTAP1-C3-mVenus-C8-His_{10} and coreTAP1-myc-SBP-2A-ICP47-coreTAP2-C3-mVenus-C8-His_{10} were expressed in HEK293-F cells. The coreTAP complexes were orthogonally purified via His_{10}- and SBP-tag. Elution samples were loaded onto an SDS-Page and blotted overnight on PVDF-Membrane. CoreTAP1 and coreTAP2 variations were detected by α-TAP1 148.3 and α-TAP2 435.3, respectively.

Both 2A complexes were correctly processed and all three coreTAP variations were purified in comparable amounts (Fig. 3.19). This demonstrated that the cleavage by F2A site was effective and can be utilized to express both coreTAP subunits on one vector under the control of one promoter. The cause for elevated MHC I surface presentation could not be explained by incorrect expression or processing of the coreTAP subunits, and requires further analysis.

3.2.3 The melting temperature of ICP47-coreTAP is affected by the position of F2A site

The previous experiments demonstrated that the orthogonal purification yielded correctly cleaved coreTAP subunits in similar amounts. Moreover, both positions of ICP47 led to an arrested coreTAP transporter, allowing to further examine the suitability of these constructs for structural analysis. In order to monitor the stabilization by ICP47, the previously purified ICP47-coreTAP complexes with F2A cleavage site were utilized for melting temperature determination (Fig. 3.20).

Whereas the positioning of ICP47 in front of the F2A site did not affect the melting temperature of ICP47-coreTAP (46.5 °C), placing the viral inhibitor at the C-terminus of the F2A site strongly influenced the melting temperature, which dropped to 38.4 °C (Fig. 3.20). This difference in melting temperature suggests, as also indicated by the ICP47/TAP structure [33] that the N-terminus of ICP47 (active domain) is highly specific and should not be modified. However, the utilization of an 2A site will inevitably alter the N-terminus of any protein encoded behind the 2A site, independently of which organism the 2A site originates from. When Asn-Pro-Gly-Pro sequence is recognized during protein

biosynthesis, ribosome skipping occurs. The sequence gets cleaved in between glycine and proline [158, 159], always leaving a N-terminal proline residue, which can interfere with the correct interaction of ICP47 and TAP.

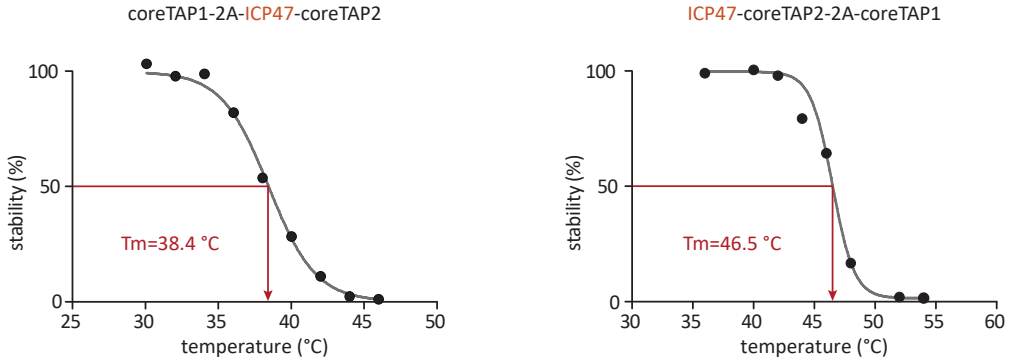

Figure 3.20: The position of F2A site in ICP47-coreTAP constructs influences the melting temperature. ICP47-coreTAP2-2A-coreTAP1 and coreTAP1-2A-ICP47-coreTAP2 were expressed in HEK293-F cells. After orthogonal purification via His_{10}- and SBP-tag the melting temperatures (red arrow) were determined via FSEC.

3.3 CoreTAP subunits connected by flexible linkers

3.3.1 Design of single-chain coreTAP constructs

Another strategy to ensure a 1:1 stoichiometry of the coreTAP subunits during expression is to combine both coding sequences in a single open reading frame to express TAP as single-chain construct. ABCB1 (P-glycoprotein) for instance, has a natural, 60-70 residues long linker domain that joins the end of the first NBD with the elbow helix of the second TMD and is possibly involved in the regulation of NBD dimerization [172]. It was recently shown, that shortening the P-glycoprotein linker does not interfere with the melting temperature and structural integrity of P-glycoprotein [173]. Therefore, artificially joining the two TAP subunits could also help to stabilize the highly flexible coreTAP transporter.

To bridge the distance between the two coreTAP subunits, three different glycine-serine linkers of 40, 50 and 60 amino acid residues were used. The linkers consisted of $(G_4S)G_4$ repeats, flanked N- and C-terminally by C3-protease cleavage sites (Fig. 3.21A). Since the orientation of the two subunits can influence the expression and functionality of coreTAP, both variations were tested (coreTAP1-Linker-coreTAP2 or coreTAP2-Linker-coreTAP1). All constructs were C-terminally flanked by C3-eGFP-myc-SBP tag for detection and purification. For proof of principle these constructs were designed without the viral inhibitor ICP47.

Unfortunately all six coreTAP-Linker-coreTAP construct combinations had expression

levels reduced by more than 50% compared to coreTAP1 in HEK cells and could be visualized only by in-gel fluorescence (Fig. 3.21B). Detection by immunoblot utilizing α-TAP antibodies 148.3 or 435.3 failed repeatedly and independently of the cells used for expression. Yet, based on in-gel fluorescence, all variants had similar expression levels and run at the calculated molecular weight of ~170 kDa.

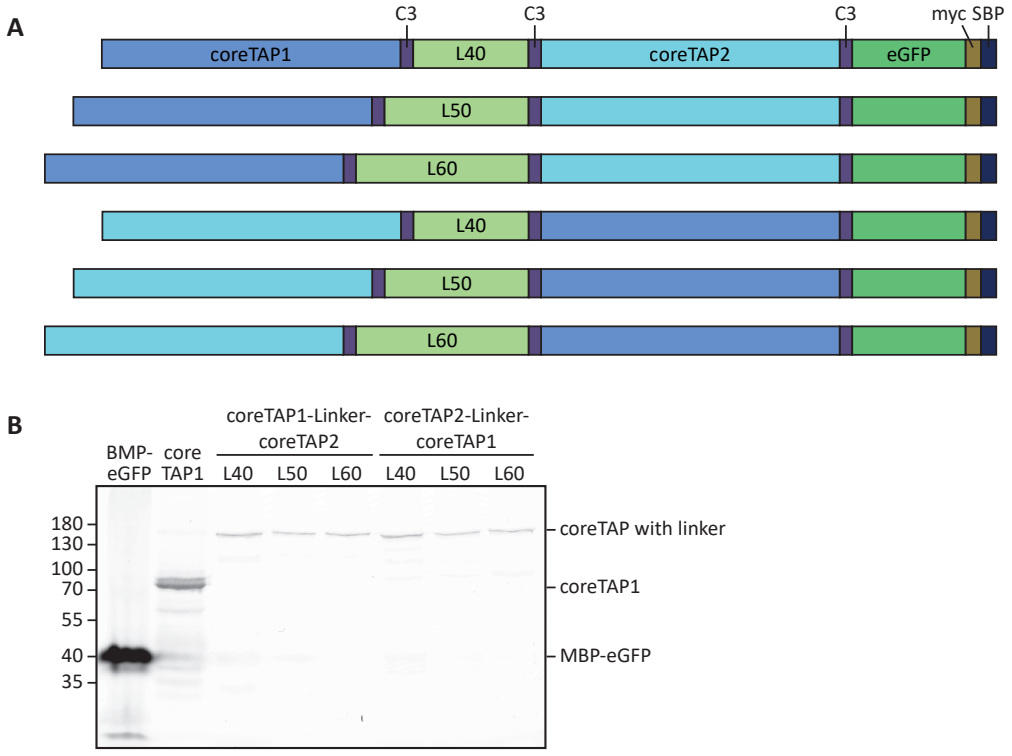

Figure 3.21: Expression analysis of single-chain coreTAP constructs.
(A) Three different glycine-serine (GS) linkers of 40, 50 and 60 amino acid residues were used to join the two coreTAP subunits in different orientations. The linkers consisted of $(G_4S)G_4$ repeats, flanked N- and C-terminally by C3-protease cleavage sites. The constructs were C-terminally flanked by C3-eGFP-myc-SBP tag for detection and purification. (B) The coreTAP-Linker-coreTAP variants, coreTAP1 and eGFP fused to maltose binding protein (MBP) were expressed in HEK293-T cells and monitored by in-gel fluorescence (eGFP). Adapted from my Master thesis [3].

3.3.2 Orientation of coreTAP subunits and linker length affect TAP function

The function of single-chain coreTAP constructs was determined by analyzing the MHC I surface expression in TAP-deficient cells. To ensure that endogenous TAP cannot affect the MHC I surface presentation, MelJuSo cells were used, which have both TAP subunits knocked out [162]. TAP-deficient cells transfected with a construct coding for eGFP-MBP only (mock control) displayed a background level of MHC I surface expression (Fig. 3.22). CoreTAP1/2 with a F2A site was used as positive control and was normalized

to 100%. The three variants with N-terminal coreTAP1 show approximately 75-80% MHC I surface expression, whereas the variants with C-terminal coreTAP1 show a stepwise increased MHC I surface expression in the range of 40-60% with increasing linker length. These differences in surface expression indicate that the preferred orientation for a single-chain coreTAP is coreTAP1-Linker-coreTAP2, although all variants did not show an optimal MHC I surface expression. Since a stable TAP complex only forms in case a newly synthesized TAP2 finds a preexisting TAP1 [97], the constructs with N-terminally positioned coreTAP2 could have difficulties to form a functional coreTAP complex. Furthermore, the connecting linker can alter the interface between the two subunits and restrict the range of motion . All these alterations may affect the proper TAP function and lead to reduced MHC I surface presentation.

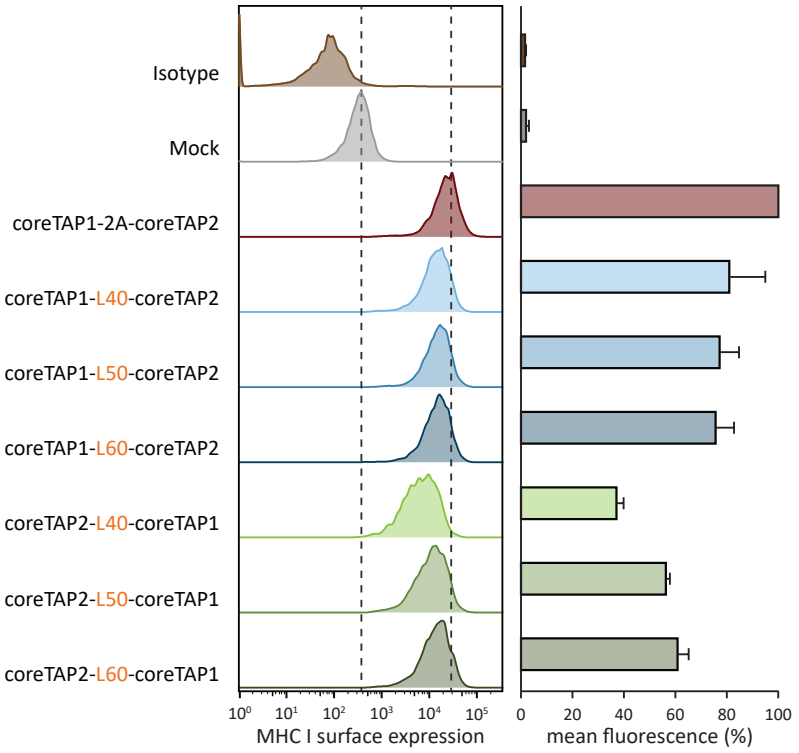

Figure 3.22: Single-chain coreTAP is functional in TAP-deficient cells. coreTAP-Linker-coreTAP variants, coreTAP1-2A-coreTAP2 and eGFP-MBP were expressed in $TAP^{-/-}$-deficient MelJuSo cells [162]. MHC I surface expression was monitored by flow cytometry using a PE-labeled MHC I-specific antibody (left). The mean PE fluorescence (right) was calculated for transfected cells (eGFP positive). The mean (±SD) fluorescence of MHC I presented on the cell surface of MelJuSo cells transfected with a construct coding for coreTAP1-2A-coreTAP2 was normalized to 100% (n=3).

3.3.3 Expression of single-chain coreTAP in *P. pastoris*

Since the expression in human cells was low, coreTAP1-L60-coreTAP2 was transferred to a pPICZ vector carrying a mVenus-His_{10}-tag. The expression in yeast is not an overexpression; however, it is possible to compensate a low expression level with high cell mass amounts. *P. pastoris* cells with constructs coding for coreTAP1-L60-coreTAP2-mVenus-His_{10} were used to pick the clone with highest mVenus fluorescence, which was subsequently utilized for fermentation. Unfortunately, the prepared *P. pastoris* membranes yielded only ∼0.33% of purified coreTAP complexes of total protein amount. Moreover, the His_{10}-tag purified solution contained impurities due to the unfeasible orthogonal purification (Fig. 3.23).
Although coreTAP1-L60-coreTAP2 proved to be functional in regard of MHC I surface expression in TAP-deficient cells, it was rejected for structural studies due to its low yield and low purity. As a consequence, these coreTAP-Linker-coreTAP constructs were not fused to ICP47 and were not further characterized.

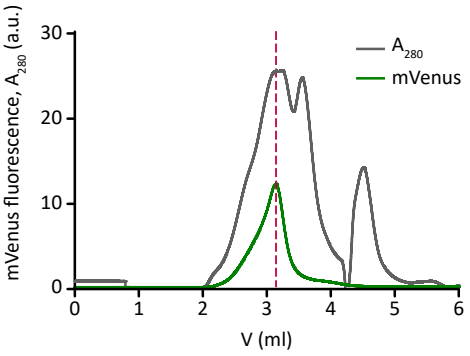

Figure 3.23: CoreTAP1-L60-coreTAP2 expressed in *P. pastoris*.
coreTAP1-L60-coreTAP2-mVenus-His_{10} was expressed in *P. pastoris* by fermentation and purified by His_{10}-tag. 50 μg of protein solution were analyzed by FSEC. mVenus fluorescence is displayed in green, absorbance at 280 nm is displayed in gray. The dotted red line serves as reference and shows the main peak of coreTAP.

3.4 TmrAB: A functional bacterial substitute for TAP

3.4.1 Design of TAP-TmrAB hybrids

TmrAB, the only type I ABC exporter in *Thermus thermophilus*, belongs to the multidrug resistance transporters and has a broad range of substrate specificity. It was demonstrated that Hoechst 33342 can be transported, while verapamil inhibits the transport complex [87]. Furthermore, it was shown, that TmrAB binds and releases phosphoglycolipids upon ATP hydrolysis [107]. Since it was recently discovered that TmrAB has an overlapping substrate specificity with TAP [2, 174], it was investigated whether this transporter

could also be a functional substitute for TAP. However, at the first glance it appeared quite unlikely that a bacterial ABC transporter expressed in human cells will localize exclusively at the ER membrane. As the TMD0 is the first domain of TAP inserted into the ER membrane during protein synthesis, it is conceivable that the TMD0s can also facilitate the insertion of TmrAB into the ER membrane. Although the TMD0s do not contain any ER retention signal, they are needed for complex formation with the PLC [99]. Since TmrAB has no TMD0 domains, hybrid complexes of TAP and TmrAB were created to increase the probability of localizing TmrAB at the ER membrane.
The coding sequence for wildtype TmrAB ($TmrAB^{wt}$) was first transferred to a mammalian expression vector, thereafter the A and B subunits were separated from each other by cutting out one subunit each. The constructs were designed as such that TmrA was fused to C3-mVenus-C8-His_{10} tag, whereas TmrB stayed without tags. Subsequently, the TMD0 of TAP1 (residues 1-164) and of TAP2 (residues 1-127), denominated here TMD01 and TMD02 respectively, were seamlessly fused to the N-terminus of TmrA and TmrB (Fig. 3.24A). The resulting half-transporters were combined to form nine different TmrA/B complexes with two, one, or no TMD0 fused, respectively (Fig. 3.24B).

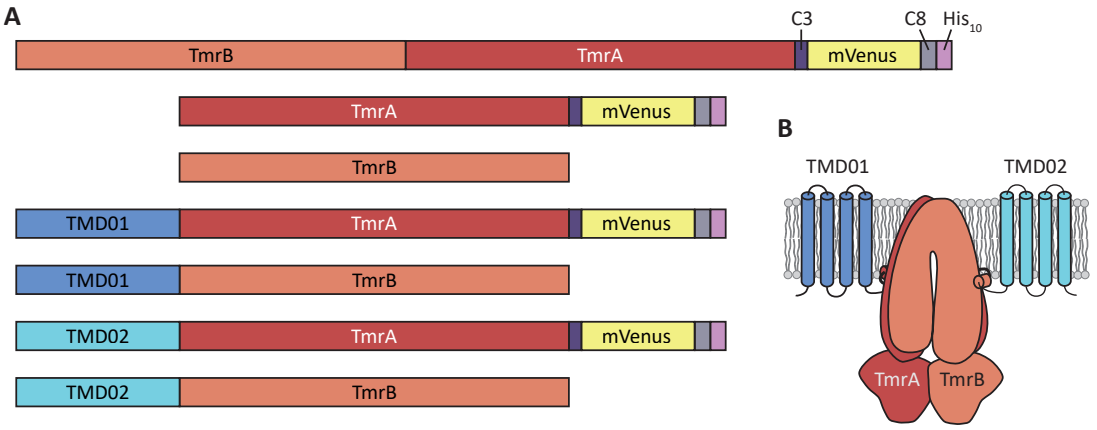

Figure 3.24: Schematic representation of TMD0-TmrAB hybrids.
The coding sequences of the two $TmrAB^{wt}$ subunits were transferred into a mammalian expression vector and then separated from each other. The TMD0 of TAP1 (residues 1-164) and of TAP2 (residues 1-127), denominated here TMD01 and TMD02 respectively, were seamlessly fused to the N-terminus of TmrA and TmrB (A). These half-transporter can be combined in nine different ways. The combination TMD01-TmrA/TMD02-TmrB is exemplarily shown (B).

3.4.2 Functional similarities to the TAP complex

As previously described, the optimization of TmrAB^{wt} for mammalian expression comprised the separation of the A and B subunits and the fusion to the TMD0s of TAP. CoreTAP1/TAP2, TmrA/B, and TMD0-TmrAB hybrids were expressed in TAP1-deficient BRE-169 cells. TmrA with mVenus was visualized by in-gel fluorescence (Fig. 3.25). Since in all combinations TmrA was expressed in comparable amounts to coreTAP1, the complexes were tested for the ability to restore MHC I surface expression in BRE-169 cells. The six half-transporters were combined in nine different ways to find the hybrid

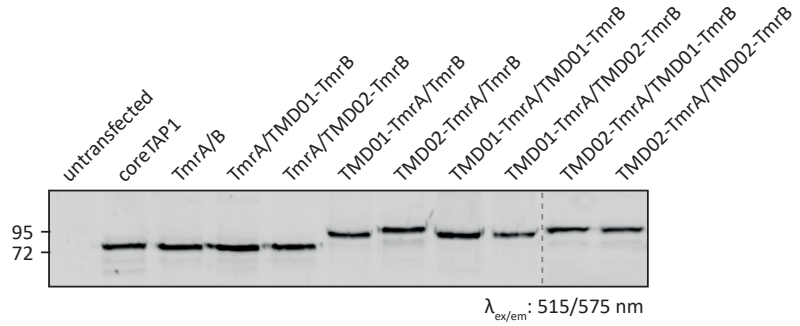

Figure 3.25: TMD0-TmrAB hybrids can be expressed in human cells.
Separated TmrA/B subunits, TMD0-TmrAB hybrids and coreTAP1 as control were expressed in TAP1-deficient BRE-169 cells and visualized by in-gel fluorescence ($\lambda_{ex/em}$=515/575 nm). The samples were loaded on two gels (indicated by the dotted line), and analyzed at the same time.

complex with highest functional similarity to TAP. BRE-169 cells transfected with a construct coding for mVenus only (mock control) displayed a background level of MHC I surface expression (Fig. 3.26). CoreTAP1 and ICP47-coreTAP1 served as positive and negative controls, respectively. The distribution of MHC I positive cells of the chimeric complexes appeared to be relatively broad, indicating the presence of a mixed active and inactive cell population in regard to MHC I surface expression. This is possibly due to folding issues and partial mislocalization of the complexes.

The ability of the hybrid TMD0-TmrAB complexes to restore the MHC I surface expression ranged from ∼30% to ∼80%, depending on which TMD0 was fused to which subunit (Fig. 3.26). The hybrid complex that induced the most pronounced MHC I upshift of ∼80% was TmrA/TMD02-TmrB, followed by TMD02-TmrA/TmrB with ∼70% and then by TMD01-TmrA/TMD02-TmrB and TMD02-TmrA/TMD02-TmrB with ∼60%. Interestingly, all these hybrids contained the TMD0 of TAP2, although a duplicate TMD02 on both subunits did not improve the MHC I surface expression. Furthermore, a slight preference for asymmetric complexes with only one TMD02 was observed. An ATPase inactive TmrA/TMD02-TmrB with E523Q (EQ) mutation in the A subunit [87] was used as control and displayed a background level of MHC I surface expression

(Fig. 3.26). This demonstrated that the TAP function, regarding the transport of antigenic peptides into the ER lumen can be taken on by TmrA/B fused to the TMD0 of TAP2.

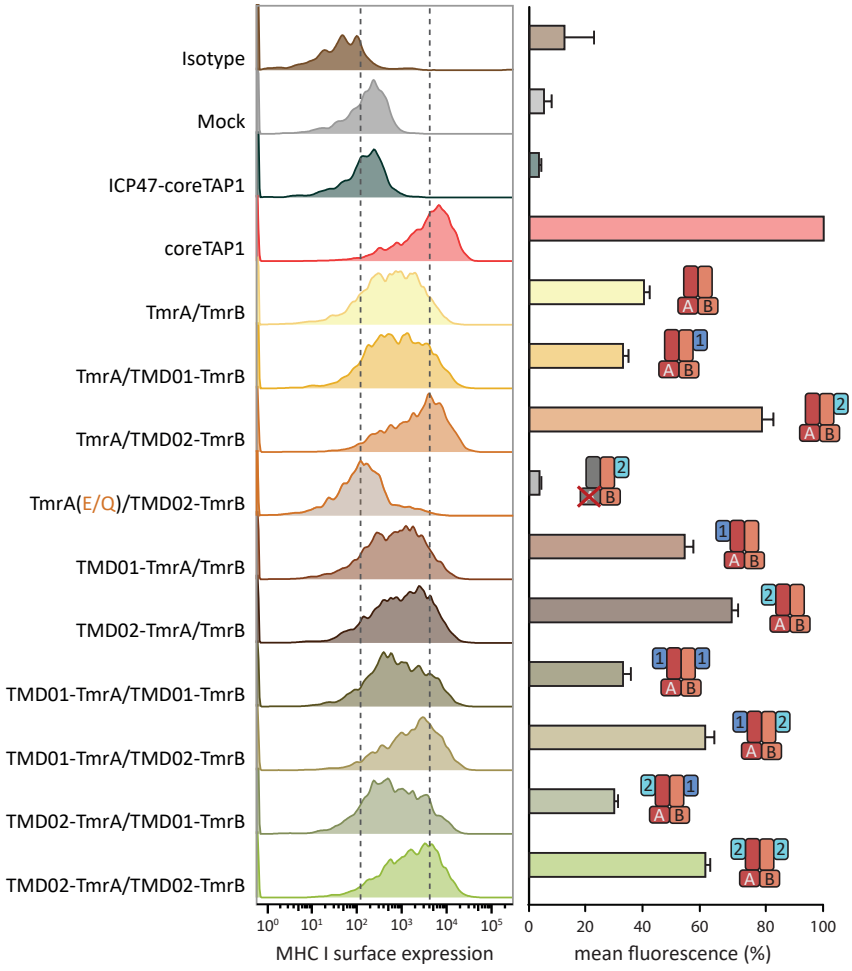

Figure 3.26: TMD0-TmrAB hybrids can take over TAP function.
Functionality of TMD0-TmrAB hybrids was tested in TAP1-deficient BRE-169 cells by monitoring the MHC I surface expression by flow cytometry. Surface presented MHC I complexes were stained using a PE-labeled MHC I-specific antibody (left). The mean PE-fluorescence (right) was calculated for transfected cells (mVenus positive). The mean (±SD) fluorescence of MHC I presented on the cell surface of BRE-169 cells transfected with a construct coding for coreTAP1 was normalized to 100% (n=2).

3.4.3 Expression and localization of TmrA/B in human cells

The previous MHC I surface expression analysis proved that TmrA/B can take over TAP function. Thereby I assumed that TmrA/TMD02-TmrB was mainly localized at the ER membrane. Since TmrA/B without a TMD0 also showed a reasonable MHC I surface presentation, I analyzed whether this difference in function correlates with the mislocalization of TmrA/B without TMD0 to other compartments than the ER. TmrA/TMD02-TmrB, TmrA/B and coreTAP1/2 as control for a ER-localized membrane protein were expressed in TAP1-deficient BRE-169 cells.

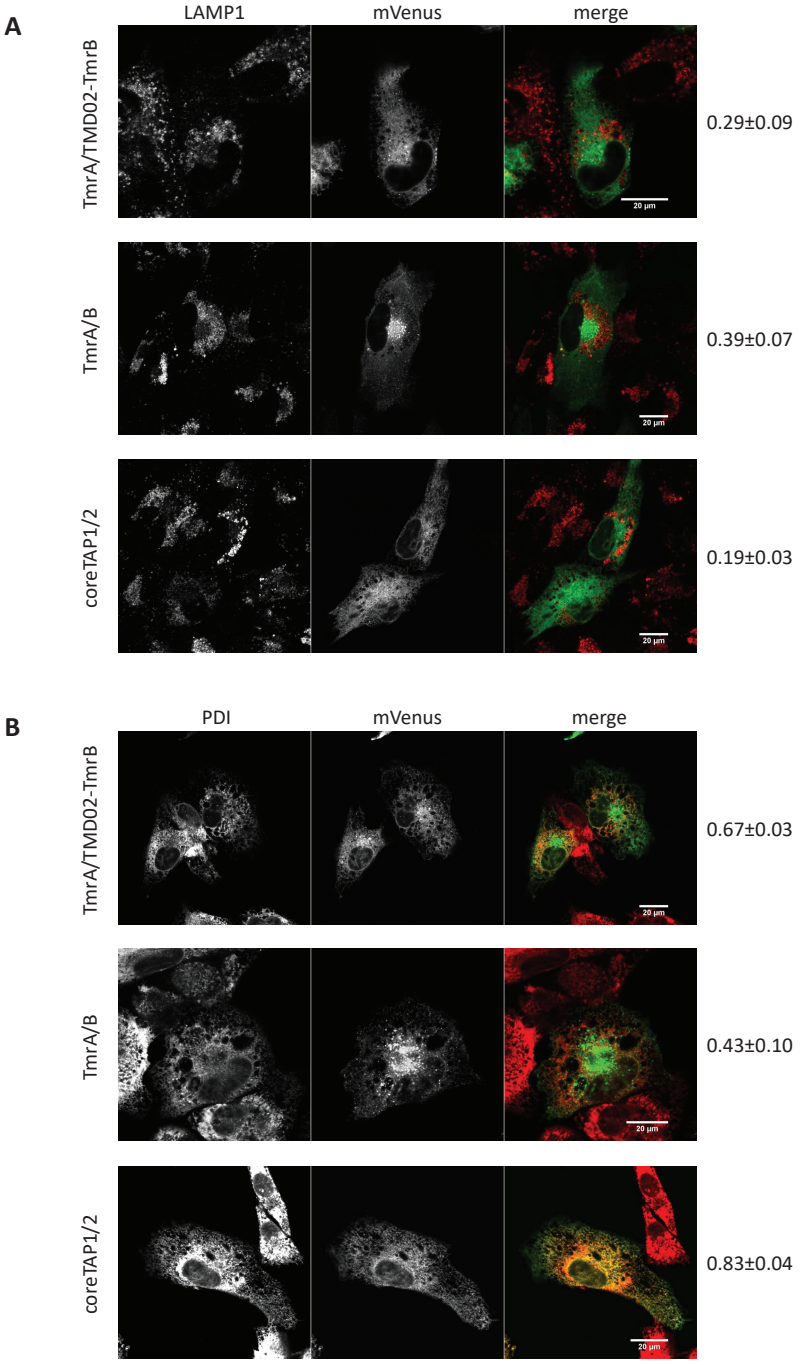

Figure 3.27: TmrA/TMD02-TmrB partially colocalizes with ER marker PDI. TAP1-deficient BRE-169 cells were transfected with constructs coding for TmrA/TMD02-TmrB, TmrA/B and coreTAP1/2 as control for a ER-localized membrane protein (all carrying mVenus). Cells were stained 24 h after transfection with antibodies against ER-marker PDI or lysosomal marker LAMP1 and imaging was performed after fixation. The scale bar indicates 20 μm. Pearson's correlation coefficient was calculated for 4-5 cells (PDI) and 2 cells (LAMP1).

After 24 h, the cells were stained with antibodies against the ER-resident protein disulfide-isomerase (PDI), and lysosomal-associated membrane protein 1 (LAMP1) as negative control. Unfortunately, the staining procedure was not optimized for this particular fibroblastic cell line, causing the formation of holes in the cell membrane. With the LAMP1 staining, a background colocalization with Pearson's correlation coefficients of approximately 0.2 to 0.4 was measured (Fig. 3.27A). Staining of the ER-marker PDI revealed that the highest colocalization was achieved with coreTAP1 (0.83±0.04), followed by TmrA/TMD02-TmrB (0.67±0.03) and then by TmrA/B (0.43±0.10), slightly above background (Fig. 3.27B). These findings indicated that the TMD0 of TAP2 effectively helped to express and retain the bacterial TmrA/B at the ER membrane, although TAP could not be completely replaced by an optimized TmrA/B. Judging by the partial restoration of antigen processing observed for TmrA/B (Fig. 3.26), a Pearson's coefficient above background would have been expected. Hence, this low value and the broad distribution of MHC I surface expression suggest that TmrA/B without TMD02 has difficulties to become properly inserted in the ER membrane.

3.4.4 Interaction of TmrAB with the PLC

It was shown that a TMD0-TmrAB hybrid co-localized with the ER membrane marker PDI and took over TAP function, while TmrA/B without a fused TMD0 of TAP was only partially localized at the ER membrane and consequently provided a low restoration of MHC I surface expression. Thus, I deduced that the TMD0 is needed to retain TmrA/B at the ER membrane, where it operates as transporter for antigenic peptides. However, it remains to be clarified whether the TAP-TmrAB chimera can interact with PLC components via the TMD0 or even take over the position of TAP.

HeLa Kyoto cells treated with interferon-γ were transfected with constructs coding for coreTAP1/TAP2, TmrA/TmrB, and TmrA/TMD02-TmrB. After membrane preparation, the three complexes were pulled down via their His_{10}-tag to detect attached PLC components by immunoblot. Dynabeads for His-tag pulldown were utilized since they reduced background interactions with the bead material. The solubilisate was utilized to detect endogenous TAP1 (Fig. 3.28A) as loading control for the starting material. Since all samples contained comparable amounts of endogenous TAP1, and were treated the same way during transfection and pulldown, the amounts of detected PLC components can be compared with each other. TmrA was detected via in-gel fluorescence (Fig. 3.28B). CoreTAP1 and full length TAP2 were also detected by in-gel fluorescence, whereas TAP2 appeared to be less abundant (Fig. 3.28B). However, the intensities of the bands cannot be directly compared, since the two subunits are fused

to different GFP derivatives. CoreTAP1 was further specifically visualized by α-TAP1 antibody (clone 148.3) (Fig. 3.28C). The amount of co-purified tapasin was strongly reduced for TmrA/B (Fig. 3.28D), confirming that the presence of a TMD0 is required for interaction with tapasin. In turn, calreticulin, MHC I, and ERp57 were present in comparable amounts, regardless of the presence of a TMD0 (Fig. 3.28E-G). As mentioned above, the background for these three PLC components could only be reduced by the use of Dynabeads, but not completely eliminated. A careful optimization of the pulldown conditions may ameliorate and prevent the unspecific binding. Yet, the presence of TAP and TmrAB increased the amounts of co-purified calreticulin, MHC I, and ERp57 by more than 50% compared to the background (Fig. 3.28H).

Combined with the significantly reduced amount of co-purified tapasin for the sample

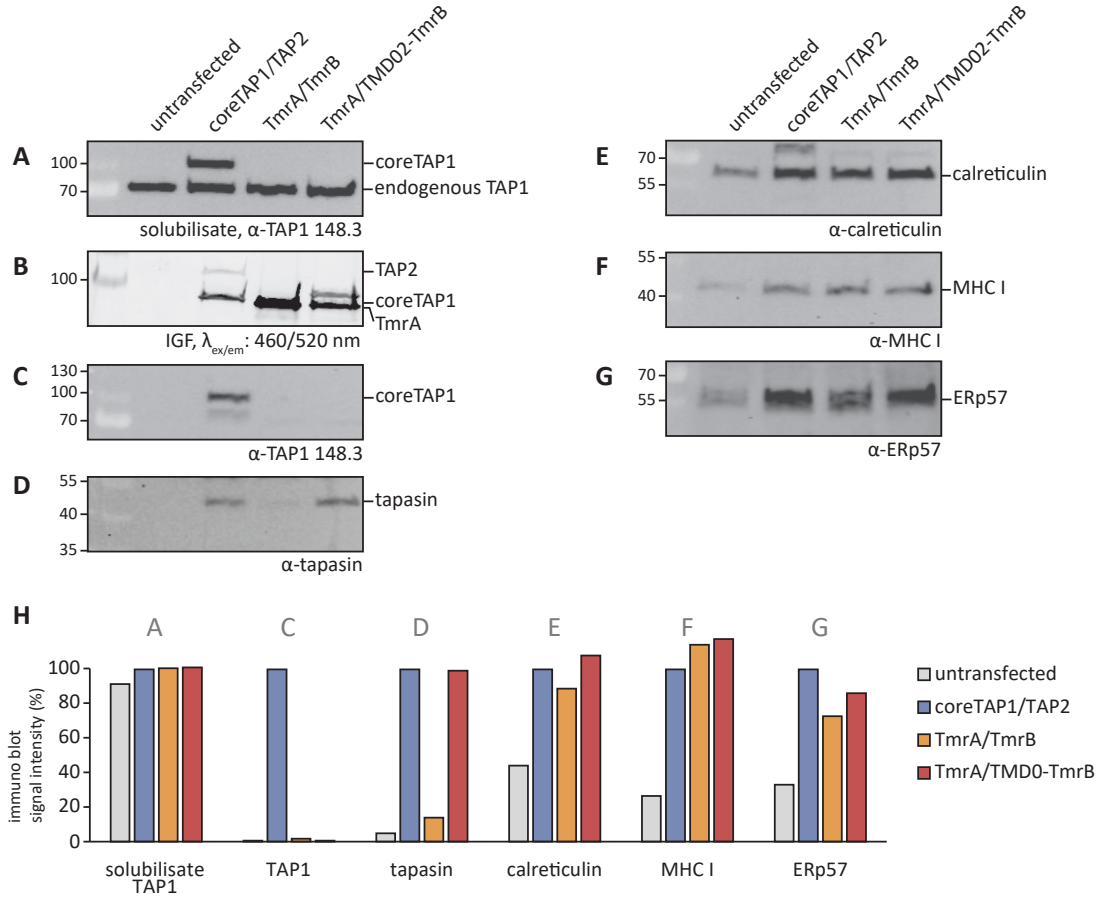

Figure 3.28: TMD0-TmrAB interacts with tapasin.
HeLa Kyoto cells were treated with human interferon-γ and were transfected with constructs coding for coreTAP1/TAP2, TmrA/B, and TmrA/TMD02-TmrB. The membranes were prepared and used for His-tag pulldown with Dynabeads. (A) Detection of endogenous TAP1 in the solubilisate as loading control for the starting material. (B) In-gel fluorescence to visualize coreTAP1 (mVenus), full length TAP2 (mCerulean), and TmrA (mVenus). (C-G) coreTAP1, tapasin, calreticulin, MHC I and ERp57 detected in the eluate of the His-tag pulldown. (H) Comparison of intensities of the immunoblots A and C-G, normalized to the coreTAP1/TAP2 sample (blue).

lacking the TMD0, these results suggest that only a TAP-TmrAB chimera is able to take over the TAP function and possibly also its position in the PLC. Tapasin acts as essential bridge between the TMD0 of TAP and MHC I, and ensures a correct functioning of the PLC [99]. Due to the comparable amounts of calreticulin, MHC I, and ERp57 co-purified with complexes containing and lacking the TMD0, I speculate that one or more of these PLC component is able to directly interact with TmrAB. Despite the presence of a human TAP TMD0, TmrAB may have assembly and folding difficulties that the cell seeks to overcome by recruiting chaperones. Nevertheless, the results of this last experiment could be improved by finding the optimal pulldown conditions to remove background signals and to clarify interactional relationships.

Chapter 4

Discussion

4.1 ICP47 as tool for the inhibition of TAP function

Of the five known TAP inhibitors, ICP47 is the only one that is not anchored in the ER membrane and has a nanomolar affinity to TAP. These properties and its specific architecture make it an interesting protein engineering tool that can be used in a variety of ways to generate functionally arrested TAP complexes for functional and structural studies. This Thesis reports on the identification of functionally arrested coreTAP complexes with high thermostability, generated by fusing herpesviral ICP47 to TAP. Different lengths of ICP47 and GS linkers were chosen to map the optimal distance between the binding pocket and the N-terminal elbow helix of either TAP1 or TAP2. It was demonstrated that the interaction of fused ICP47 with coreTAP inhibited antigen presentation via MHC I. Interestingly, the loss of MHC I surface expression only depended on the presence of the active domain and not on the length of the fused ICP47 fragments. The replacement of ICP47 residues 35-88 by three different GS linkers also arrested the TAP function. The utilization of a self-cleaving 2A site to separate the TAP subunits in ICP47-coreTAP constructs did slightly increase the amount of surface expressed MHC I, although the majority of cells presented low MHC I surface expression. Summarizing it can be said that TAP complexes containing an intact active domain of ICP47 successfully suppressed MHC I surface expression. Furthermore, these findings confirmed the two previous studies, demonstrating that ICP47 residues 2-35 have the same inhibitory capacity as the full-length polypeptide [4, 5]. Contrarily, coreTAP complexes containing a fused inactive ICP47 (ΔH1 and ΔH2) restored the surface expression of MHC I by 50-100%. The ΔH2 fragment fused to coreTAP1 led to apparently two cell populations with low and high surface expressed MHC I respectively. The cause of this variation has not been investigated in more detail, but could be due to unfavorable sequence shifts. Based on the data obtained by these experiments, I assumed that the ICP47 residues

36-88 are dispensable. As a consequence, the optimal construct appeared to be ICP47(1-35) fused to the TAP subunits. An eventual substitution of the eliminated residues by GS linkers could favor the positioning of the active domain into the peptide binding pocket of TAP. However, MHC I surface expression in the use of free ICP47 fragments revealed that the active domain may not be sufficient for TAP inhibition in situ. All free constructs, except the one that contained exclusively the active domain (1-35), were able to fully arrest peptide translocation, while the fragment 1-35 partially restored MHC I surface expression. This suggested for the first time in this study that more residues might contribute to the interaction with TAP.

4.2 Thermostabilization by herpesviral ICP47

Further characterization of the ICP47-coreTAP fusion complexes comprised the determination of their thermostability and melting temperatures. The utilization of HEK293-Freestyle cells for transient transfection allowed to generate sufficient cells to purify small but adequate amounts of the complexes without having to generate stable *P. pastoris* clones by a long-winded process.

The ICP47-coreTAP fusion complexes revealed a preferred orientation for ICP47. The ICP47(1-65) fragment led to a stable complex only if fused to TAP2, highlighting an interesting asymmetry at the TAP1/TAP2 binding interface and suggesting a shorter distance of the C-terminus of the stabilization region to the elbow helix of TAP2 than of TAP1. The shorter fragments 1-35 and 1-50, and the ICP47-linker fragments, which inhibited, but did not trigger any thermostabilizing effects on TAP, revealed a second hint for the presence of other residues important for the ICP47/TAP interaction. However, this method proved to be too inaccurate to determine the precise thermostability of TAP complexes and especially the subtle differences between the various fragments could not be resolved.

To define the thermostability more accurately the melting temperature of complexes with fused or freely bound ICP47 fragments was determined. Short fused fragments of ICP47 (residues 1-35 or 1-50) did not fully stabilize the TAP complex. Only ICP47 fragments longer than residues 1-50 raised the melting temperature to the full extent and led to a completely stabilized complex. Interestingly, with this assay it was not possible to visualize the difference between ICP47(1-65) fused to coreTAP1 (T_M=44.2 °C) or to coreTAP2 (T_M=45.7 °C) as clearly as the determination of thermostability did. This suggests that the critical melting temperature, which determines whether a complex is fully stabilized or not, is about 44-45 °C and only the combination with the prolonged exposure to a high temperature can shed light on all thermostabilizing properties of the ICP47 C-terminus.

Furthermore, free viral fragments in complex with coreTAP revealed ICP47(1-55) as the shortest fragment that stabilizes TAP, while shorter fragments destabilized the complex. This destabilization is also reflected by MHC I surface expression, where only free fragments of at least residues 1-55 prevented MHC I surface expression to its full extent. While the affinity constants of fully inhibiting ICP47 fragments are similar [4], they presumably modulate the structure of the TAP transporter in different ways. Surprisingly, the active domain alone, which was used to study TAP function [95, 129, 175], decreased thermostability, while the fused active domain alone led to a slight increase in stability. Contrarily, the active domain fused by a GS linker did not alter the melting temperature. This can be caused by the high flexibility of the linker, which holds the active domain in close proximity to TAP, but prevents it from being firmly bound. The excessive flexibility can also lead to the active domain not being able to interact with TAP at all and can therefore prevent the formation of a functional PLC. ICP47 interacts via a large interface with TAP, involving most of the residues of the active domain of ICP47 [5, 33]. Therefore, I assumed that a fused active domain, which does not reach the optimal position inside the binding cavity, can still impair the function of the TAP complex. Consequently, non-ideally positioned fused ICP47 can be outcompeted by free full-length ICP47. The functional arrest is demonstrated by the inability of an ICP47-coreTAP complex to bind free US6.

4.3 The dual inhibition mechanism of ICP47

More than 20 years ago, the active domain of ICP47 (residues 3-34) was defined to be the shortest region with the same inhibitory activity as full-length ICP47. Despite a high conservation of residues following the active domain (residues 35-55), no function could be assigned to that region [4, 5]. The comparison of ICP47 sequences derived from human HSV1 and HSV2 shows that residues 1-55 are highly conserved with a sequence identity of 67%, while residues 56-88 are not significantly conserved (Fig. 4.1). A further comparison of different ICP47s from the herpesviral clade reveals a high number of charged residues, a short alanine-rich sequence, and a proline-rich PxxPLLxPP sequence in the C-terminal region (Fig. 4.1). Since proline-rich motifs are known to be involved in protein-protein interactions [176, 177], it can be hypothesized that a similar motif has also evolved in the ICP47/TAP interaction to lock the transporter in a peptide-repellent conformation. By exchanging amino acid triplets in the stabilizing region, the importance of the charged residues as well as the alanine- and proline-rich sequences was proved. It was further demonstrated that the most conserved residues are the most critical for a complete stabilization of the TAP complex. Unfortunately, the ICP47 from human HSV1 used in this study is the only one in the herpesviral

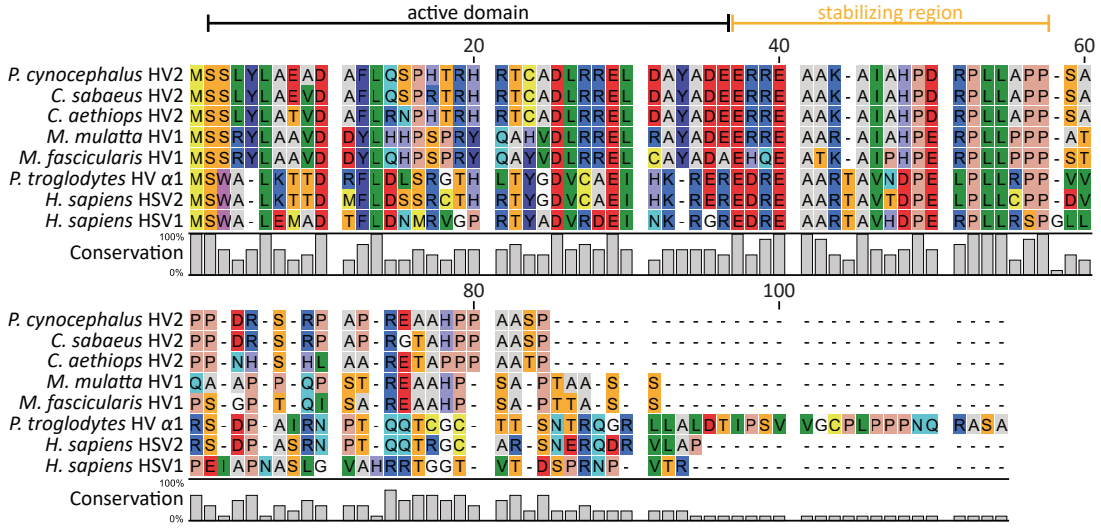

Figure 4.1: ICP47 proteins encoded by different herpes viruses share conserved sequences. When comparing different ICP47s from the herpesviral clade with human ICP47, a high conservation can be found for the residues 1-55. The PxxPLLxPP motif, corresponding to the residues 50-55 of human HSV2, can be found in all ICP47 proteins, except for human HSV1. Alignments were created with CLC Sequence Viewer 7.6.1. and skylign (skylign.org). NCBI accession. version: *P.c.* HV2, YP_443919.1; *C.s.* HV2, AAW78015.1; *C.a.* HV2, YP_164515.1; *M.m.* HV1, NP_851932.1; *M.f.* HV1, AIA09566.1; *P.t.* HV α1, YP_009011060.1; *H.s.* HSV1, AMB65879.1; *H.s.* HSV2, AMB66178.1.

clade with a serine at position 54 instead of a conserved proline. Although the triplet 53-55 did not significantly alter the ICP47/coreTAP stability it cannot be excluded that these residues hold important stabilizing properties in ICP47 inhibitors from other species, where the consensus sequence xPP (x=R, C, P or A) is highly conserved. Based on sequence identity and the thermostabilizing contribution of several residues the stabilizing region was defined to comprise the residues 35-55 of human HSV1 ICP47.

In summary, these findings reveal a dual inhibition mechanism of ICP47. While the active domain of ICP47 is wedged at the TAP1/2 interface and arrests the complex in an open-inward facing conformation, the highly conserved C-terminal region stabilizes the ICP47/TAP interaction and generates a thermostabilized TAP complex. Recent progresses in using stabilizing interaction partners for structure determination by single particle cryo-EM, revealed a 4.0 Å reconstruction of the human coreTAP complex arrested by ICP47 [33] and strongly supported these findings. It was furthermore visualized by this structure that the proline at position 55 is the last ordered residue of ICP47 and interacts with Y477 of TAP2, which is usually involved in ATP binding. Moreover ICP47 appeared to interact preferentially with the TAP2 subunits [33], supporting the here presented thermostability analysis.

Another recent study [178] confirmed the preferred interaction with TAP2 and suggested that the highly conserved ICP47 residues 50-52 (PLL) are important for TAP inhibition.

However, this assumption based mainly on one of the above mentioned first studies made on the ICP47/TAP interaction, which determined the affinities of different ICP47 fragments to TAP [4]. There, the comparison of ICP47 fragments 1-48 and 1-53 led to the slightly different K_d values of 126±14 and 50±12 nM, respectively (while the K_d for full length ICP47 was defined to be 42±2 nM and is quite similar to the 45±5 nM K_d of the 1-40 fragment). The authors of the recent publication [178] concluded that the conserved PLL sequence present in the 1-53 fragment with lower K_d value is mainly responsible for the interaction with TAP. Without doubt they have proven the importance of the PLL sequence, yet they did not analyze other highly conserved residues. Further, the use of K_d values, which obviously fluctuate in a range of ∼80 nM do not appear to be the best explanation. Thus, it may well be that, as shown also by the cryo-EM structure [33], only the interaction of several residues triggers the full inactivation and that quite possibly other highly conserved residues may be involved, as shown in this study.

4.4 Validation of the melting temperature assay

For many years the CPM assay was used as standard and is only recently replaced by nanoDSF analysis for melting temperature determination of proteins. The first approach requires the presence of cysteines embedded in the interior of a protein, which become exposed to a fluorochrome upon unfolding, whereas the technology of the second relies on tryptophane fluorescence, without a dye being involved. Both methods require special technical equipment, usually not present in a common biochemistry laboratory. Furthermore, the CPM assay often requires relatively large protein amounts, depending on the number of available cysteines, while nanoDSF can operate with few μl and low concentrations. However, both methods necessitate condition optimization before they can be reliably applied, especially regarding the sample concentration.
The method used here for the determination of melting temperatures, previously published by Hattori *et al.* [167], requires only purified protein, a device to incubate the samples at defined temperatures, and a high-performance liquid chromatography system, possibly with fluorescence detector. Similar to nanoDSF the unfolding process is not monitored by an external dye and relies on the intrinsic properties of the protein. The limitation of T_M determination via FSEC is the T_M of the reporter GFP, which was determined to be approximately 83 °C [179] and is significantly higher than the T_M of mammalian membrane proteins. The protein sample has not to be highly concentrated, and small quantities are sufficient, as long as the target protein can be fused to a fluorescent reporter protein. I did not test whether the assay can be carried out utilizing the absorbance at 280 nm instead of fluorescence detection, but in principle this should be possible as long as the absorbance at 280 nm of the protein of interest can be detected.

Furthermore, it has to be mentioned that the stability profiles of the TAP complexes were only recorded in a ∼15 °C temperature range. Typical initial temperatures were chosen to be 3-5 °C below the temperature where stability started to drop. The last measuring point was reached as soon as the stability did not significantly drop any further in a temperature range of 5-8 °C. It is very likely that the samples will continue to denature as temperature continues to rise. Nevertheless, the measured T_M values remain comparable in the temperature range mentioned above and could be reproduced with high reliability.
The TAP variants used in this study did not allow to use the CPM assay, since all cysteines except for C213 in TAP2 were replaced. The melting temperature of ICP47-coreTAP complexes was validated only by nanoDSF without optimizing the measurement conditions. Although only few samples were analyzed, the T_M values previously determined by FSEC were confirmed with approximately 2 °C variance. This proved that T_M determination via FSEC can be applied in case other more common methods fail or can not be carried out for various reasons. Yet this alternative method is unlikely to compete with nanoDSF for high throughput screenings as it is quite time consuming.

4.5 Various possibilities of coreTAP expression

The fusion of ICP47 to the single coreTAP subunits allowed to create thermostable TAP complexes, which were meant to be used for structural determination of TAP. Unfortunately, during this study the cryo-EM structure of coreTAP inhibited by free full-length ICP47 was solved at 4.0 Å resolution by the group of Jue Chen at The Rockefeller University, New York [32, 33]. Although in this structure a third of the TMD was not resolved, it is unlikely to achieve a significantly higher or near-atomic resolution of this relatively small membrane protein by cryo-EM. However, the presented ICP47/TAP complex is trapped in an off-path, which represents a conformational state relevant in the antigen transport cycle and it would be of great use to completely solve the structure. Classical X-ray crystallization or lipidic cubic phase could offer alternative options, but they require completely immobile protein and furthermore high amounts of purified protein. The fusion of ICP47 to TAP strongly limits the flexibility of the ICP47 C-terminus so that these constructs could serve for crystallization. It was shown in this work that several residues at the C-terminus of ICP47 are dispensable since they do not significantly alter the melting temperature of the ICP47/TAP complex. As a result the range of fusion complexes that can be used as crystallization candidates becomes expanded. A relatively cheap and common expression system for the generation of large quantities of cell mass is *P. pastoris*. Yeasts in general offer a cellular environment quite similar to mammalian cells and they do not have very high demands on their culture

medium. However, it is not possible to achieve a true overexpression, as would be possible in HEK or insect cells.

The challenging part with TAP expression in *P. pastoris* is the generation of a clone that produces TAP1 and TAP2 in a 1:1 stoichiometry, possibly with high expression levels. Several clones of coreTAP1/ICP47-coreTAP2 were generated and tested for expression, but after fermentation and orthogonal purification it was not possible to obtain higher amounts of purified protein. The purified TAP complexes were visualized by negative-stain EM, although the protein quality could probably be further increased by SEC purification. This demonstrates at least that the expression in *P. pastoris* yields usable TAP complexes and that the obtained protein amounts are in general sufficient for negative-stain EM. However, an alternative TAP expression procedure was needed to deliver higher amounts of protein.

Theoretically, two target constructs on only one plasmid can be expressed in *P. pastoris*, but previous attempts failed. I followed two alternative strategies: The first comprised the fusion of the coreTAP subunits by flexible GS-linkers, while the second involved a self-cleaving 2A site placed in between the two subunits. The first strategy revealed a preferred coreTAP1-linker-coreTAP2 orientation of the subunits to generate functional coreTAP complexes. The linker length of 40 aa proved to be sufficient, but as previously demonstrated, there are several aspects that must be considered when determining the function of a TAP complex. Due to the single-chain design, an orthogonal purification of the subunits, as it was done for classical TAP, could not be carried out and was reflected by impurities after His_{10}-tag purification. Most importantly, the expression of coreTAP linker constructs in mammalian cells was considerably lower than conventional coreTAP, which impeded also the determination of melting temperatures. As a consequence, these constructs were not further characterized, including their analysis after a potential fusion to ICP47. In future studies other purification tags, like SBP or various tandem-affinity tags could be tested.

For the second strategy involving a 2A site, only the coreTAP1-2A-coreTAP2 orientation was tested, since the previous experiment revealed a preferred orientation with N-terminal coreTAP1. The insertion of ICP47, however, made it necessary to swap the subunits to find the most thermostable construct. As a result coreTAP1-2A-ICP47-coreTAP2 and ICP47-coreTAP2-2A-coreTAP1 were generated. The function of coreTAP without ICP47 proved to be comparable to conventional coreTAP, while the ICP47 variants behaved slightly different than their non-2A counterparts. The ability to prevent MHC I surface expression was slightly reduced for both constructs with ICP47, but more importantly a preferred orientation having ICP47-coreTAP2 at the N-terminus of the 2A constructs was revealed by analyzing the melting temperatures. Small-scale expression showed similar expression levels for conventional and 2A-site coreTAP complexes. Although these constructs have been tested only for small scale expression in *P. pastoris*, it can be assumed that they will at least solve the issue of proper 1:1 stoichiometry during

the generation of *P. pastoris* clones. Furthermore, the 2A site generates two separated subunits, enabling orthogonal purification of TAP. It still has to be determined whether it is possible to find a *P. pastoris* clone with these constructs yielding higher TAP expression levels during fermentation.

4.6 TmrAB: A bacterial substitute for coreTAP

Based on sequence comparison, the bacterial ABC transporter TmrAB was identified to be part of the same ABC subfamily as TAP [87]. Recently it was demonstrated that TmrAB has a broader substrate specificity, covering the substrate spectrum of TAP [2, 174]. But it still had to be clarified whether TmrAB could replace the function of TAP and possibly its place in the PLC. The generation of chimeras, composed of the TMD0s of TAP and the TmrAB subunits, made it possible to study the function of TmrAB in human cells. Interestingly, not all complexes had the ability to restore MHC I surface expression, whereas all of the most functional constructs had at least one TMD0 derived from TAP2. However, the presence of two TMD0s of TAP2 did not improve the function any further. It was demonstrated that TmrA/TMD02-TmrB is mainly co-localized with the ER membrane marker PDI, while only small amounts of TmrA/B co-localize with PDI. Since the TMD0 is naturally residing in the ER membrane, this was an expected result. A specific interaction of TMD02-TmrA/TmrB could be demonstrated only for the PLC component tapasin, whereas the interaction with calreticulin, MHC I, and ERp57 occurred independently from the fusion to the TMD0. Hence, it remains elusive whether the interaction with tapasin supports the recovery of MHC I surface expression. Since coreTAP without TMD0 is able to partially restore MHC I surface expression [99] without interacting with the PLC, it is possible that a TmrAB localized at the ER membrane operates the same way. Nevertheless, TmrAB appears to be homologous to coreTAP, not only in terms of sequence and structure, but also in terms of function. It is furthermore quite remarkable that a bacterial protein, sharing only 27-30% sequence identity with human TAP [2] is able to take over a key function of our adaptive immune system. Despite the presence of a human TAP TMD0, it should not be forgotten that TmrAB originates from a hyperthermophilic bacterium and has only ∼20% transport activity at 37 °C (unpublished data, Philipp Höllthaler, R. Tampé lab). In addition, TmrAB may have assembly and folding difficulties that the human cell seeks to overcome by recruiting chaperones, including calreticulin and ERp57. Further experiments will be necessary to analyze the interaction of TmrAB with the PLC components in more detail. It could also be of interest to determine whether TAPL or other multidrug resistance proteins like P-glycoprotein and its homologs could also take over TAP function if fused to a TMD0 of TAP.

4.7 Conclusion and future perspectives

This study demonstrated that the utilization of protein engineering can be a powerful tool to create chimeric proteins with new properties. The fusion of the viral inhibitor ICP47 to coreTAP led to the discovery of a stabilizing region in ICP47 that had gone unnoticed until now. Although the combination with the recent cryo-EM structure of ICP47/coreTAP [33] allows a deeper understanding of the residues involved in the interaction, the specific function of several residues remained undefined. Moreover, all of the recent studies mentioned refer to ICP47 derived from human HSV1, which has the least sequence identity with the other ICP47 variants. It cannot be excluded that for example ICP47 from human HSV2 could induce a higher thermostabilization of coreTAP, which could lead to a more rigid protein suited for X-ray crystallization. The same could apply to the other ICP47 variants and their respective TAP complexes. It was furthermore shown that a full-length ICP47 slightly increased the melting temperature compared to the other fragments, which included the residues 1-55. These findings indicate that there might be few other residues essential for a complete interaction. Although the highest sequence conservation can be observed for consensus sequence 37-58, followed by the active domain (Fig. 4.1), the remaining sequence owns some conserved residues, such as P61, P65, R69, and the region around residues 74-84. The repeated occurrence of prolines, already starting at residue 49 in the stabilizing region, suggests a linear structure of the C-terminal ICP47. Since the residue P55 has already been assigned an anchoring function [33], it is conceivable that the remaining residues could further fortify the interaction. The viral inhibitor fused by a rigid natural linker to the TAP complex has the advantage of inhibiting TAP directly after synthesis and furthermore reduces the probability of a dissociation from TAP. If, in the future, a possibility is found to express ICP47-coreTAP in large quantities, it would be of interest to crystallize this complex in order to potentially improve the resolution of the structure and to describe the full inhibition mechanism of ICP47.

Another part of this work revealed that the fusion of two ABC transporters, the human TAP and the bacterial TmrAB, resulted in a new hybrid transporter, which adopts the function of TAP. However, it would have to be clarified by further experiments if and how the TAP-TmrAB hybrids and TmrAB interact with the single components of the PLC. The fusion demonstrated that appropriate modifications of a potential bacterial TAP ancestor enabled functional comparison of these two transporters in mammalian cells. Unfortunately, this technique is not applicable to many other ABC transporters mainly due to two reasons: Firstly, knowledge about other homologs of ABC transporters is limited. Secondly, the special architecture of TAP having extra domains, in addition to the core complex, allows their fusion to other ABC transporters. In case of TmrAB, fusing the TMD0 of TAP2 resulted in the acquisition of TAP function. Nevertheless, it

might be possible to create other types of fusion constructs, depending on the architecture of the target ABC transporters.

Besides the generation of chimeric ABC transporters, various TAP constructs were engineered to enhance expression and in some cases also stability. Unfortunately, the single-chain TAP approach in which the two TAP subunits were fused together similar to those of P-glycoprotein did not show high expression levels and yielded insufficiently pure protein. In contrast, the generation of coreTAP subunits using the 2A-site proved to be very promising. Although, it has yet to be determined whether higher expression rates can be achieved by fermentation in *P. pastoris*, the constructs could be also very helpful in other applications. Experiments involving the co-expression of TAP with one or more proteins may particularly rely on the two TAP subunits being in a 1:1 stoichiometry. The utilization of a 2A-site has many advantages and is easy to use, creating plenty of new possibilities for the co-expression of heterodimeric ABC transporters. An alternative procedure, which was not addressed in this work, comprises the utilization of lentiviral transduction to generate human cells stably expressing TAP variations. Under the control of an inducible promoter, this method allows to produce TAP in comparable amounts to a transient transfection. However, the generation of such cell lines is time consuming and the subsequent cultivation is expensive due to special culture media requisitions.

Since it was not possible to produce the human TAP transporter in sufficient quantities for crystallization utilizing human or yeast cells, it might be necessary to test other expression systems. Bacterial expression was tested by previous members of the laboratory but failed due to very low or non-detectable TAP expression. The production of membrane proteins in insect cells represents a more common expression system, but here the amounts of produced TAP often vary depending on the quality of the baculovirus used to infect the cells. In recent years a new method for membrane protein production based on the *Leishmania tarentolae* parasites was developed and also used for expression of ABCs transporters [180]. The system is capable to create mammalian-like N-glycosylation pattern and to express proteins at high levels. It is further described as interesting alternative for structural studies since it provides high quality proteins at low costs. A more exotic expression system is represented by *Rhodobacter sphaeroides*, a photosynthetic bacterium that owns an extensive network of intracellular photosynthetic membranes, which can accommodate large quantities of membrane proteins [181]. Although this method was tested for different membrane proteins, it is anything but known, and would have to be checked thoroughly for the expression of TAP. Which constructs finally yield the best results in which expression system can not be foreseen and can only be found out by examining the individual systems.

Chapter 5

Appendix

5.1 Sequences of used constructs

coreTAP1

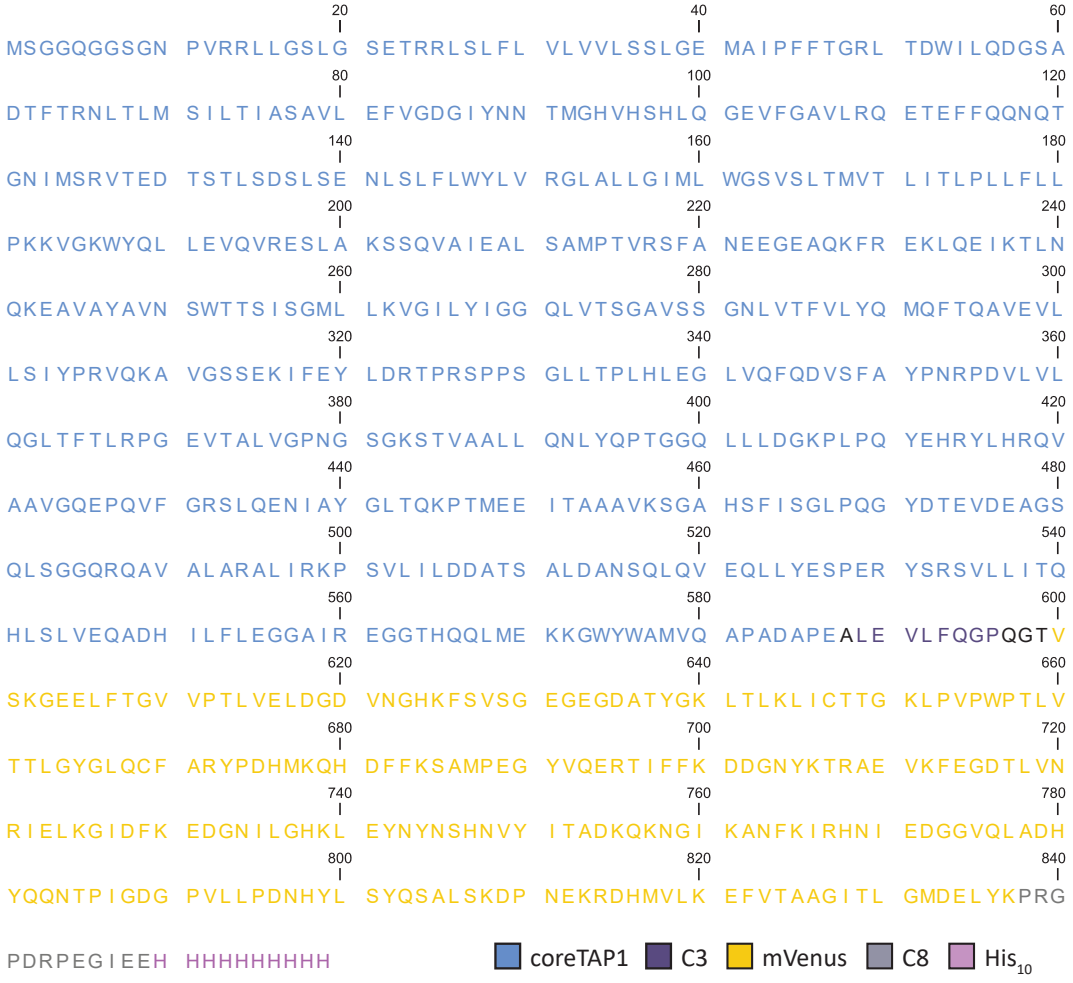

coreTAP2

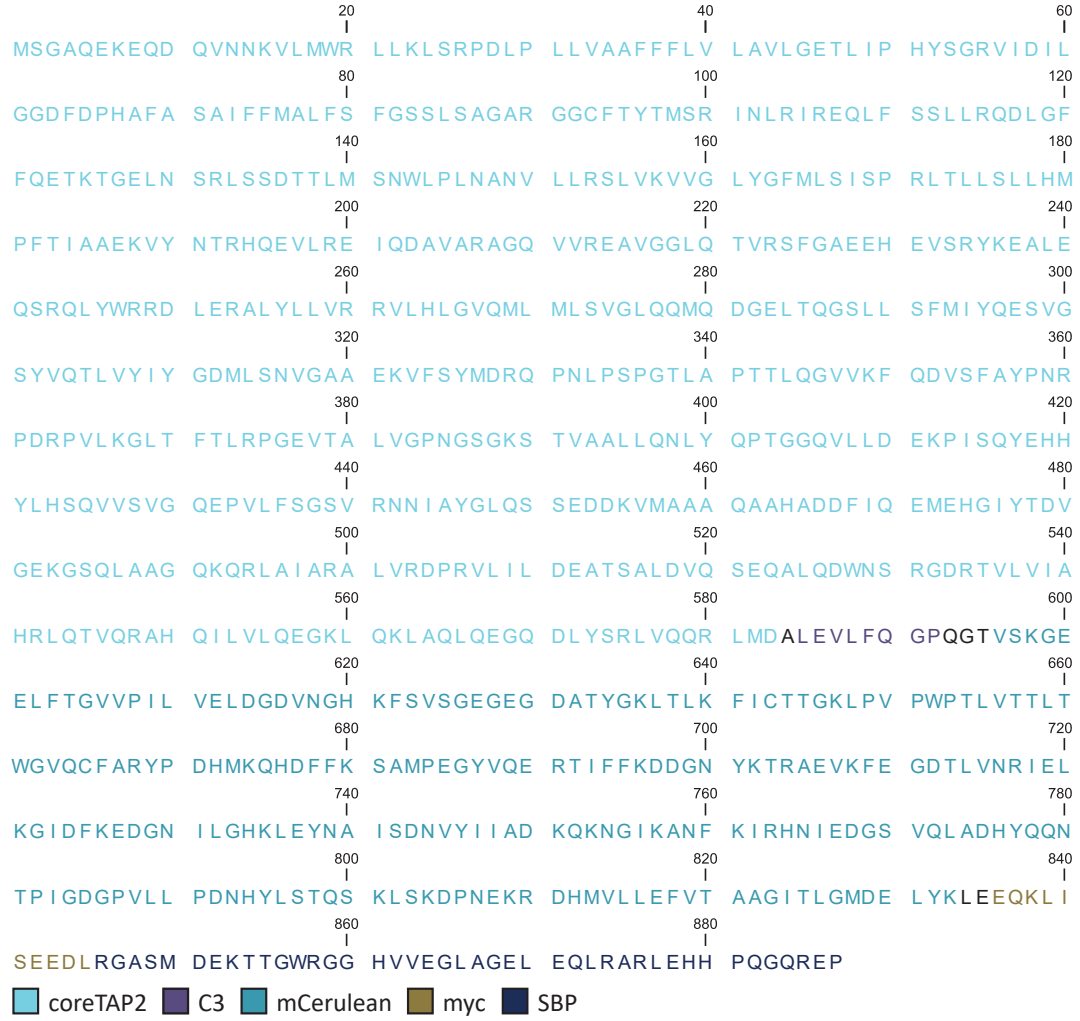

ICP47

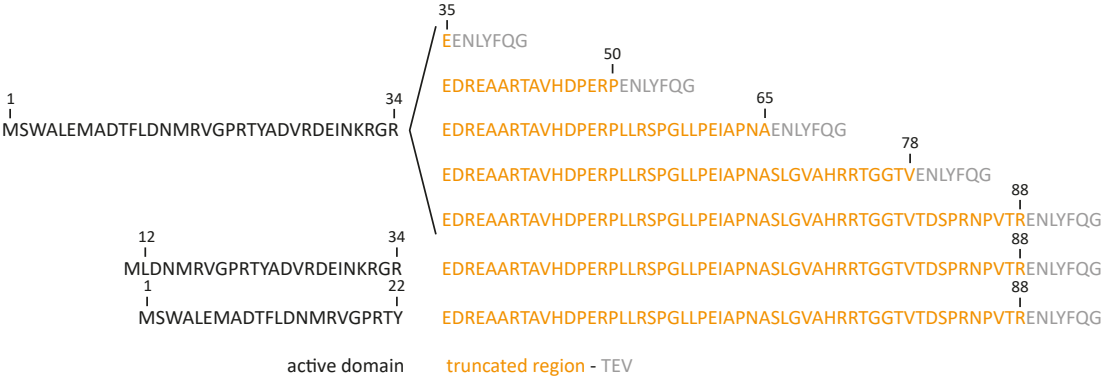

TMD01

```
                         20                        40                        60
                         |                         |                         |
MSMASSRCPA PRGCRCLPGA SLAWLGTVLL LLADWVLLRT ALPRIFSLLV PTALPLLRVW
                         80                        100                       120
                         |                         |                         |
AVGLSRWAVL WLGACGVLRA TVGSKSENAG AQGWLAALKP LAAALGLALP GLALFRELIS
                        140                       160
                         |                         |
WGAPGSADST RLLHWGSHPT AFVVSYAAAL PAAALWHKLG SLWVP
```

TMD02

```
                         20                        40                        60
                         |                         |                         |
MMRLPDLRPW TSLLLVDAAL LWLLQGPLGT LLPQGLPGLW LEGTLRLGGL WGLLKLRGLL
                         80                        100                       120
                         |                         |                         |
GFVGTLLLPL CLATPLTVSL RALVAGASRA PPARVASAPW SWLLVGYGAA GLSWSLWAVL

SPPGAQEK
```

TmrA

```
                         20                        40                        60
                         |                         |                         |
MVTEDTYSKA FDRALFARIL RYVWPYRLQV VLALLFLLVV TLAAAATPLF FKWAIDLALV
                         80                        100                       120
                         |                         |                         |
PTEPRPLAER FHLLLWISLG FLAVRAVHFA ATYGETYLIQ WVGQRVLFDL RSDLFAKLMR
                        140                       160                       180
                         |                         |                         |
LHPGFYDRNP VGRLMTRVTS DVDAINQFIT GGLVGVIADL FTLVGLLGFM LFLSPKLTLV
                        200                       220                       240
                         |                         |                         |
VLLVAPVLLA VTTWVRLGMR SAYREMRLRL ARVNAALQEN LSGVETIQLF VKEREREEKF
                        260                       280                       300
                         |                         |                         |
DRLNRDLFRA WVEIIRWFAL FFPVVGFLGD FAVASLVYYG GGEVVRGAVS LGLLVAFVDY
                        320                       340                       360
                         |                         |                         |
TRQLFQPLQD LSDKFNLFQG AMASAERIFG VLDTEEELKD PEDPTPIRGF RGEVEFRDVW
                        380                       400                       420
                         |                         |                         |
LAYTPKGVEP TEKDWVLKGV SFRVRPGEKV ALVGATGAGK TSVVSLIARF YDPQRGCVFL
                        440                       460                       480
                         |                         |                         |
DGVDVRRYRQ EELRRHVGIV LQEPFLFSGT VLDNLRLFDP SVPPERVEEV ARFLGAHEFI
                        500                       520                       540
                         |                         |                         |
LRLPKGYQTV LGERGAGLST GEKQLLALVR ALLASPDILL ILDEATASVD SETEKRLQEA
                        560                       580                       600
                         |                         |                         |
LYKAMEGRTS LIIAHRLSTI RHVDRILVFR KGRLVEEGSH EELLAKGGYY AALYRLQFQE

A
```

TmrB

```
                        20                        40                        60
                        |                         |                         |
MSTGRSAAPL LRRLWPYVGR YRWRYLWAVL AGLVSIFFFV LTPYFLRLAV DAVQAGRGFG
                        80                       100                       120
                        |                         |                         |
VYALAIVASA ALSGLLSYAM RRLAVVASRQ VEYDLRRDLL HHLLTLDRDF YHKHRVGDLM
                       140                       160                       180
                        |                         |                         |
NRLNTDLSAV REMVGPGILM GSRLSFLVLL AFLSMYAVNA RLAFYLTLIL PGIFLAMRFL
                       200                       220                       240
                        |                         |                         |
LRLIDRRYRE AQEVFDRIST LAQEAFSGIR VVKGYALERR MVAWFQDLNR LYVEKSLALA
                       260                       280                       300
                        |                         |                         |
RVEGPLHALL GFLMGFAFLT VLWAGGAMVV RGELSVGELV QFNAYLAQLT WPILGLGWVM
                       320                       340                       360
                        |                         |                         |
ALYQRGLTSL RRLFELLDEK PAIRDEDPLP LALEDLSGEV RFEGVGLKRD GRWLLRGLTL
                       380                       400                       420
                        |                         |                         |
TIPEGMTLGI TGRTGSGKSL LAALVPRLLD PSEGRVYVGG HEARRIPLAV LRKAVGVAPQ
                       440                       460                       480
                        |                         |                         |
EPFLFSETIL ENIAFGLDEV DRERVEWAAR LAGIHEEILA FPKGYETVLG ERGITLSGGQ
                       500                       520                       540
                        |                         |                         |
RQRVALARAL AKRPKILILD DALSAVDAET EARILQGLKT VLGKQTTLLI SHRTAALRHA
                       560
                        |
DWIIVLDGGR IVEEGTHESL LQAGGLYAEM DRLQKEVEA
```

5.2 Fermentation sequence

The fermentation program for expression in *P. pastoris* with the Labfors 3 bioreactor was developed by David Parcej.

#0,Startup, 10
// Allow the cells to start growing. Monitor oxygen consumption.
pO2.sp=30
stirrer.sp=800
Temp.sp=30
Mass_Flow.sp=5.7
pH.sp=4.5
Gycerol.sp=0
Feed_Pump.sp=0
Sequence.v=0
MeOHconc.sp=0
MeOHconc.v=(exp((MetOH.v-5.9514)/1.195))
if((pO2.v<pO2.sp+40)AND(Gas_Mix.v>28)AND(seq_time>time(6:00))){seq=1}

#1, Glycerol_batch, 20
// Wait untill glycerol in medium is exhausted. O_2 consumtion drops
stirrer.sp=1000
rampc(pH,5.0,pO2.v>20,0.001)
MeOHconc.v=(exp((MetOH.v-5.9514)/1.195))
if((Gas_mix.v<25)AND(pO2.v>pO2.sp+30)AND(pH.v>pH.sp+0.0)){seq=2}

if(Mass_Flow.v<1){pO2.sp=0}else{pO2.sp=30}
Sequence.v=1

#2, Gly_feed_1,20
// FOR DUTY CYCLE 30s !!!
// Start glycerol feed
// Ideally would like exponential feed, but for now do in steps
// seting is % pump duty cycle
stirrer.sp=1000
if(Mass_Flow.v<1){pO2.sp=0}else{pO2.sp=30}
Gycerol.sp=LIM(Gycerol.sp,0,2)
MeOHconc.v=(exp((MetOH.v-5.9514)/1.195))
if((pO2.v<pO2.sp-5)AND(Gas_Mix.v>80)){Gycerol.sp=Gycerol.sp-1}else{Gycerol.sp= Gycerol.sp+1}
if(seq_time>time(1:00)){seq=3}
Sequence.v=2

#3,Gly_feed 2,20
if(Mass_Flow.v<1){pO2.sp=0}else{pO2.sp=30}
MeOHconc.sp=0
Gycerol.sp=LIM(Gycerol.sp,0,3)
MeOHconc.v=(exp((MetOH.v-5.9514)/1.195))
if((pO2.v<pO2.sp-5)AND(Gas_Mix.v>80)){Gycerol.sp=Gycerol.sp-1}else{Gycerol.sp=Gycerol.sp+1}
if(seq_time>time(1:00)){seq=4}
Sequence.v=3

#4,Gly_feed 3,20
if(Mass_Flow.v<1){pO2.sp=0}else{pO2.sp=30}
MeOHconc.sp=0
Gycerol.sp=LIM(Gycerol.sp,0,4)
MeOHconc.v=(exp((MetOH.v-5.9514)/1.195))
if((pO2.v<pO2.sp-5)AND(Gas_Mix.v>80)){Gycerol.sp=Gycerol.sp-1}else{Gycerol.sp= Gycerol.sp+1}
if(seq_time>time(4:00)){seq=5}
Sequence.v=4

#5,Gly_feed 4,20
if(Mass_Flow.v<1){pO2.sp=0}else{pO2.sp=30}
MeOHconc.sp=0
Gycerol.sp=LIM(Gycerol.sp,0,6)
MeOHconc.v=(exp((MetOH.v-5.9514)/1.195))
if((pO2.v<pO2.sp-5)AND(Gas_Mix.v>80)){Gycerol.sp=Gycerol.sp-1}else{Gycerol.sp= Gycerol.sp+1}
if(seq_time>time(2:00)){seq=6}
Sequence.v=5

#6,Gly_feed 5,20
if(Mass_Flow.v<1){pO2.sp=0}else{pO2.sp=30}
MeOHconc.sp=0
Gycerol.sp=LIM(Gycerol.sp,0,10)
MeOHconc.v=(exp((MetOH.v-5.9514)/1.195))
if((pO2.v<pO2.sp-5)AND(Gas_Mix.v>80)){Gycerol.sp=Gycerol.sp-1}else{Gycerol.sp= Gycerol.sp+1}
if(seq_time>time(2:00)){seq=7}
Sequence.v=6

#7,Gly_feed 6,20
if(Mass_Flow.v<1){pO2.sp=0}else{pO2.sp=30}
MeOHconc.sp=0
Gycerol.sp=LIM(Gycerol.sp,0,12)
MeOHconc.v=(exp((MetOH.v-5.9514)/1.195))
if((pO2.v<pO2.sp-5)AND(Gas_Mix.v>80)){Gycerol.sp=Gycerol.sp-1}else{Gycerol.sp= Gycerol.sp+1}
if(seq_time>time(10:00)){seq=8}
if(Gycerol.v>150000){seq=8}
Sequence.v=7

#8,Gly_feed 7,20
if(Mass_Flow.v<1){pO2.sp=0}else{pO2.sp=30}
MeOHconc.sp=0
Gycerol.sp=LIM(Gycerol.sp,0,8)
MeOHconc.v=(exp((MetOH.v-5.9514)/1.195))
if((pO2.v<pO2.sp-5)AND(Gas_Mix.v>80)){Gycerol.sp=Gycerol.sp-1}else{Gycerol.sp= Gycerol.sp+1}
if(seq_time>time(3:00)){seq=9}
Sequence.v=8

#9,Gly_feed 8,20
if(Mass_Flow.v<1){pO2.sp=0}else{pO2.sp=30}
MeOHconc.sp=0
Gycerol.sp=LIM(Gycerol.sp,0,4)
MeOHconc.v=(exp((MetOH.v-5.9514)/1.195))
if((pO2.v<pO2.sp-5)AND(Gas_Mix.v>80)){Gycerol.sp=Gycerol.sp-1}else{Gycerol.sp= Gycerol.sp+1}
if(seq_time>time(2:00)){seq=10}
Sequence.v=9

#10,Gly_reduce,20
// gradually reduce glycerol feed to de-repress the AOX promoter
if(Mass_Flow.v<1){pO2.sp=0}else{pO2.sp=35}
Gycerol.sp=rampc(Gycerol,0,pO2.v>1,0.05)
if((Gycerol.sp<=0)AND(seq_time>time(1:00))){seq=11}
MeOHconc.v=(exp((MetOH.v-5.9514)/1.195))
MeOHconc.sp=0
if(((Gas_Mix.v>80)AND(pO2.v <30))OR(MeOHconc.v > MeOHconc.sp*0.9)OR(temp.v >31))

{Feed_pump.sp=0}ELSE{Feed_Pump.sp=10}
Sequence.v=10

#11,MeOH_adapt,10
//Let the cells adapt to Methanol
stirrer.sp=1000
Gycerol.sp=0
temp.sp=30
if(Mass_Flow.v<1){pO2.sp=0}else{pO2.sp=35}
MeOHconc.v=(exp((MetOH.v-5.9514)/1.195))
MeOHconc.sp=0.2
if(((Gas_Mix.v>85)AND(pO2.v <30))OR(MeOHconc.v > MeOHconc.sp*0.9)OR(temp.v >31))
{Feed_pump.sp=0}ELSE{Feed_Pump.sp=10}
if(seq_time>time(3:00)){seq=12}
Sequence.v=11

#12,Induction 1, 10
if(Mass_Flow.v<1){pO2.sp=0}else{pO2.sp=35}
temp.sp=30
MeOHconc.v=(exp((MetOH.v-5.9514)/1.195))
MeOHconc.sp=0.5
MeOHconc.sp=rampc(MeOHconc,0.5,((pO2.v>35)AND(Gas_mix.v<85)),0.01)
if(((Gas_Mix.v>95)AND(pO2.v <25))OR(MeOHconc.v > MeOHconc.sp*0.9)OR(temp.v >31))
{Feed_pump.sp=0}ELSE{Feed_Pump.sp=10}
if(seq_time>time(5:00)){seq=13}
Sequence.v=12

#13,Induction 2,60
temp.sp=30
MeOHconc.v=(exp((MetOH.v-5.9514)/1.195))
MeOHconc.sp=rampc(MeOHconc,1,((pO2.v>25)AND(Gas_mix.v<85)),0.05)
if(((Gas_Mix.v>95)AND(pO2.v <25))OR(MeOHconc.v > MeOHconc.sp*0.9)OR(temp.v >31))
{Feed_pump.sp=0}ELSE{Feed_Pump.sp=20}
if(pO2.sp<20){seq=20}
Sequence.v=13

#20 Emergency 1,20
// if oxygen gets too low during induction, wait for a while
Feed_pump.sp=0
if((pO2.v>pO2.sp)AND(Gas_Mix.sp<70)AND(Temp.v<30)){seq=13}
Sequence.v=20

Abbreviations

aa	amino acid
ABC	ATP-binding cassette
ATP	adenosine triphosphate
C3	C3 protease
C8	purification tag for α-C8 antibody purified from Chessie 8 supernatant
CPM	N-[4-(7-diethylamino-4-methyl-3-coumarinyl)phenyl]maleimide
DDM	n-dodecyl β-D-maltoside
dH_2O	distilled, filtered water
DMEM	dulbecco's modified eagle's medium
DNA	deoxyribonucleic acid
dNTP	deoxynucleoside triphosphate
EM	electron microscopy
ER	endoplasmic reticulum
ERAP	ER-associated amino peptidase
ERp57	ER thiol oxidoreductase
FACS	fluorescence activated cell sorting
FCS	fetal calf serum
FSEC	fluorescence detection size-exclusion chromatography
g	gramm or gravitational constant
GDN	glyco-diosgenin
GFP	green fluorescent protein
GS	glycine-serine
h	hour
HEK	human embryonal kidney
HEPES	hydroxyethyle piperazinyle ethanesulfonic acid
HGNC	HUGO (human genome organization) gene nomenclature commitee
His	histidine
HLA	human leukocyte antigen
ICP47	infected cell polypeptide 47
kDa	kilo Dalton
kg	kilo gramm

LB	lysogeny broth
M	molar
mCerulean	monomeric enhanced cyan fluorescent protein
MC-FSEC	multicolor fluorescence-detection size-exclusion chromatography
MHC I	major histocompatibility complex class I
min	minute
ml	milliliter
mVenus	monomeric enhanced yellow fluorescent protein
μ	micro
myc	myc tag, derived from the c-Myc protein
n	nano
nanoDSF	nano dierential scanning uorimetry
NBD	nucleotide binding domain
PAGE	polyacrylamide gel electrophoresis
PBS	phosphate-buffered saline
PCR	polymerase chain reaction
PEI	polyethylenimine
PLC	peptide loading complex
PMSF	phenylmethylsulfonyl fluoride
rpm	revolutions per minute
s	second
SBP	streptavidin binding protein
SDS	sodium dodecyl sulfate
SDS-PAGE	sodium dodecyl sulfate polyacrylamide gel electrophoresis
SEC	size exclusion chromatography
SR	stabilizing region of ICP47
TAP	transporter associated with antigen processing
TEMED	tetramethylethylenediamine
TEV	tobacco etch virus
TMD	transmembrane domain
TMD0	transmembrane domain 0
TmrAB	*Thermus thermophilus* multidrug resistance protein AB
Tris	tris(hydroxymethyl)amino methane
US6	unique short region 6
v/v	volume/volume
w/v	weight/volume

Bibliography

[1] V. Herbring, A. Bäucker, S. Trowitzsch, and R. Tampé. A dual inhibition mechanism of herpesviral ICP47 arresting a conformationally thermostable TAP complex. *Scientific Reports*, 6:36907, 2016.

[2] A. Nöll, C. Thomas, V. Herbring, T. Zollmann, K. Barth, A. R. Mehdipour, T. M. Tomasiak, S. Brüchert, B. Joseph, R. Abele, V. Oliéric, M. Wang, K. Diederichs, G. Hummer, R. M. Stroud, K. M. Pos, and R. Tampé. Crystal structure and mechanistic basis of a functional homolog of the antigen transporter TAP. *Proceedings of the National Academy of Sciences of the United States of America*, 114:E438–E447, 2017.

[3] V. Herbring. *Funktionale Stabilisierung des Antigentranslokationskomplexes TAP*. Technische Universität Darmstadt, 2014. Master Thesis.

[4] L. Neumann, W. Kraas, S. Uebel, G. Jung, and R. Tampé. The active domain of the Herpes Simplex Virus protein ICP47: A potent inhibitor of the transporter associated with antigen processing (TAP). *Journal of Molecular Biology*, 272:484–492, 1997.

[5] B. Galocha, A. Hill, B. C. Barnett, A. Dolan, A. Raimondi, R. F. Cook, J. Brunner, D. J. McGeoch, and H. L. Ploegh. The active site of ICP47, a Herpes Simplex Virus–encoded inhibitor of the Major Histocompatibility Complex (MHC)-encoded peptide transporter associated with antigen processing (TAP), maps to the NH_2-terminal 35 residues. *Journal of Experimental Medicine*, 185: 1565–1572, 1997.

[6] C. F. Higgins. ABC transporters: from microorganisms to man. *Annual Review of Cell Biology*, 8: 67–113, 1992.

[7] T. Eitinger, D. A. Rodionov, M. Grote, and E. Schneider. Canonical and ECF-type ATP-binding cassette importers in prokaryotes: diversity in modular organization and cellular functions. *FEMS Microbiology Reviews*, 35:3–67, 2011.

[8] L. Silverton, M. Dean, and K. Moitra. Variation and evolution of the ABC transporter genes ABCB1, ABCC1, ABCG2, ABCG5 and ABCG8: implication for pharmacogenetics and disease. *Drug Metabolism and Drug Interactions*, 26:169–179, 2011.

[9] J. Zimmer, E. Andrès, L. Donato, D. Hanau, F. Hentges, and H. de La Salle. Clinical and immunological aspects of HLA class I deficiency. *QJM : Monthly Journal of the Association of Physicians*, 98:719–727, 2005.

[10] D. Parcej and R. Tampé. ABC proteins in antigen translocation and viral inhibition. *Nature Chemical Biology*, 6:572–580, 2010.

[11] E. Biemans-Oldehinkel, M. K. Doeven, and B. Poolman. ABC transporter architecture and regulatory roles of accessory domains. *FEBS Letters*, 580:1023–1035, 2006.

[12] A. J. Rice, A. Park, and H. W. Pinkett. Diversity in ABC transporters: type I, II and III importers. *Critical Reviews in Biochemistry and Molecular Biology*, 49:426–437, 2014.

[13] M. Lee, Y. Choi, B. Burla, Y. Kim, B. Jeon, M. Maeshima, J. Yoo, E. Martinoia, and Y. Lee. The ABC transporter AtABCB14 is a malate importer and modulates stomatal response to CO_2. *Nature Cell Biology*, 10:1217–1223, 2008.

[14] F. Quazi, S. Lenevich, and R. S. Molday. ABCA4 is an N-retinylidene-phosphatidylethanolamine and phosphatidylethanolamine importer. *Nature Communications*, 3:925, 2012.

[15] N. S. Kadaba, J. T. Kaiser, E. Johnson, A. Lee, and D. C. Rees. The high affinity *E. coli* methionine ABC transporter: structure and allosteric regulation. *Science*, 321:250–253, 2008.

[16] M. L. Oldham and J. Chen. Crystal structure of the maltose transporter in a pretranslocation intermediate state. *Science*, 332:1202–1205, 2011.

[17] O. Jardetzky. Simple allosteric model for membrane pumps. *Nature*, 211:969–970, 1966.

[18] F. A. Quiocho and P. S. Ledvina. Atomic structure and specificity of bacterial periplasmic receptors for active transport and chemotaxis: variation of common themes. *Molecular Microbiology*, 20: 17–25, 1996.

[19] G. B. Henderson, E. M. Zevely, and F. M. Huennekens. Mechanism of folate transport in *Lactobacillus casei*: evidence for a component shared with the thiamine and biotin transport systems. *Journal of Bacteriology*, 137:1308–1314, 1979.

[20] D. A. Rodionov, P. Hebbeln, A. Eudes, J. ter Beek, I. A. Rodionova, G. B. Erkens, D. J. Slotboom, M. S. Gelfand, A. L. Osterman, A. D. Hanson, and T. Eitinger. A novel class of modular transporters for vitamins in prokaryotes. *Journal of Bacteriology*, 191:42–51, 2009.

[21] A. Crow, N. P. Greene, E. Kaplan, and V. Koronakis. Structure and mechanotransmission mechanism of the MacB ABC transporter superfamily. *Proceedings of the National Academy of Sciences of the United States of America*, 114:12572–12577, 2017.

[22] C. Thomas and R. Tampé. Multifaceted structures and mechanisms of ABC transport systems in health and disease. *Current Opinion in Structural Biology*, 51:116–128, 2018.

[23] R. N. Hvorup, B. A. Goetz, M. Niederer, K. Hollenstein, E. Perozo, and K. P. Locher. Asymmetry in the structure of the ABC transporter-binding protein complex BtuCD-BtuF. *Science*, 317: 1387–1390, 2007.

[24] K. Xu, M. Zhang, Q. Zhao, F. Yu, H. Guo, C. Wang, F. He, J. Ding, and P. Zhang. Crystal structure of a folate energy-coupling factor transporter from Lactobacillus brevis. *Nature*, 497: 268–271, 2013.

[25] N. M. I. Taylor, I. Manolaridis, S. M. Jackson, J. Kowal, H. Stahlberg, and K. P. Locher. Structure of the human multidrug transporter ABCG2. *Nature*, 546:504–509, 2017.

[26] Q. Luo, X. Yang, S. Yu, H. Shi, K. Wang, X. Le, G. Zhu, C. Sun, T. Li, D. Li, X. Zhang, M. Zhou, and Y. Huang. Structural basis for lipopolysaccharide extraction by ABC transporter LptB2FG. *Nature Structural & Molecular Biology*, 24:469–474, 2017.

[27] U. Okada, E. Yamashita, A. Neuberger, M. Morimoto, H. W. van Veen, and S. Murakami. Crystal structure of tripartite-type ABC transporter MacB from Acinetobacter baumannii. *Nature Communications*, 8:1336, 2017.

[28] B. Wang, M. Dukarevich, E. I. Sun, M. R. Yen, and M. H. Saier. Membrane porters of ATP-binding cassette transport systems are polyphyletic. *The Journal of Membrane Biology*, 231:1–10, 2009.

[29] M. H. Saier Jr. Transporter classification database. URL http://www.tcdb.org.

[30] R. J. P. Dawson and K. P. Locher. Structure of a bacterial multidrug ABC transporter. *Nature*, 443:180–185, 2006.

[31] M. Hohl, C. Briand, M. G. Grütter, and M. A. Seeger. Crystal structure of a heterodimeric ABC transporter in its inward-facing conformation. *Nature Structural & Molecular Biology*, 19:395–402, 2012.

[32] M. L. Oldham, R. K. Hite, A. M. Steffen, E. Damko, Z. Li, T. Walz, and J. Chen. A mechanism of viral immune evasion revealed by cryo-EM analysis of the TAP transporter. *Nature*, 529:537–540, 2016.

[33] M. L. Oldham, N. Grigorieff, and J. Chen. Structure of the transporter associated with antigen processing trapped by herpes simplex virus. *eLife*, 5:e21829, 2016.

[34] J. F. Fay, L. A. Aleksandrov, T. J. Jensen, L. L. Cui, J. N. Kousouros, L. He, A. A. Aleksandrov, D. S. Gingerich, J. R. Riordan, and J. Z. Chen. Cryo-EM visualization of an active high open probability CFTR anion channel. *Biochemistry*, 57:6234–6246, 2018.

[35] J. Y. Lee, L. N. Kinch, D. M. Borek, J. Wang, J. Wang, I. L. Urbatsch, X. S. Xie, N. V. Grishin, J. C. Cohen, Z. Otwinowski, H. H. Hobbs, and D. M. Rosenbaum. Crystal structure of the human sterol transporter ABCG5/ABCG8. *Nature*, 533:561–564, 2016.

[36] C. Perez, S. Gerber, J. Boilevin, M. Bucher, T. Darbre, M. Aebi, J. L. Reymond, and K. P. Locher. Structure and mechanism of an active lipid-linked oligosaccharide flippase. *Nature*, 524:433–438, 2015.

[37] H. Qian, X. Zhao, P. Cao, J. Lei, N. Yan, and X. Gong. Structure of the Human Lipid Exporter ABCA1. *Cell*, 169:1228–1239, 2017.

[38] J. ter Beek, A. Guskov, and D. J. Slotboom. Structural diversity of ABC transporters. *The Journal of General Physiology*, 143:419–435, 2014.

[39] H. Dong, Z. Zhang, X. Tang, N. G. Paterson, and C. Dong. Structural and functional insights into the lipopolysaccharide ABC transporter LptB2FG. *Nature Communications*, 8:222, 2017.

[40] D. J. Sherman, R. Xie, R. J. Taylor, A. H. George, S. Okuda, P. J. Foster, D. J. Needleman, and D. Kahne. Lipopolysaccharide is transported to the cell surface by a membrane-to-membrane protein bridge. *Science*, 359:798–801, 2018.

[41] P. Hinchliffe, M. F. Symmons, C. Hughes, and V. Koronakis. Structure and operation of bacterial tripartite pumps. *Annual Review of Microbiology*, 67:221–242, 2013.

[42] N. Kobayashi, K. Nishino, and A. Yamaguchi. Novel macrolide-specific ABC-type efflux transporter in *Escherichia coli*. *Journal of Bacteriology*, 183:5639–5644, 2001.

[43] HGNC (HUGO Gene Nomenclature Committee). URL http://www.genenames.org.

[44] T. Annilo, Z. Q. Chen, S. Shulenin, J. Costantino, L. Thomas, H. Lou, S. Stefanov, and M. Dean. Evolution of the vertebrate ABC gene family: analysis of gene birth and death. *Genomics*, 88: 1–11, 2006.

[45] M. Dean, A. Rzhetsky, and R. Allikmets. The human ATP-binding cassette (ABC) transporter superfamily. *Genome Research*, 11:1156–1166, 2001.

[46] F. P. M. Cremers, D. J. R. van de Pol, M. van Driel, A. I. den Hollander, F. J. J. van Haren, N. V. A. M. Knoers, N. Tijmes, A. A. B. Bergen, K. Rohrschneider, A. Blankenagel, A. J. L. G. Pinckers, A. F. Deutman, and C. B. Hoyng. Autosomal recessive retinitis pigmentosa and cone-rod dystrophy caused by splice site mutations in the Stargardt's disease gene ABCR. *Human Molecular Genetics*, 7:355–362, 1998.

[47] R. Allikmets, N. F. Shroyer, N. Singh, J. M. Seddon, R. A. Lewis, P. S. Bernstein, A. Peiffer, N. A. Zabriskie, Y. Li, A. Hutchinson, M. Dean, J. R. Lupski, and M. Leppert. Mutation of the stargardt disease gene (ABCR) in age-related macular degeneration. *Science*, 277:1805–1807, 1997.

[48] C. A. Scott, S. Rajpopat, and W. L. Di. Harlequin ichthyosis: ABCA12 mutations underlie defective lipid transport, reduced protease regulation and skin-barrier dysfunction. *Cell and Tissue Research*, 351:281–288, 2013.

[49] M. Akiyama. The roles of ABCA12 in keratinocyte differentiation and lipid barrier formation in the epidermis. *Dermato-Endocrinology*, 3:107–112, 2011.

[50] Y. J. Kim and J. Chen. Molecular structure of human P-glycoprotein in the ATP-bound, outward-facing conformation. *Science*, 359:915–919, 2018.

[51] F. Seyffer and R. Tampé. ABC transporters in adaptive immunity. *Biochimica et Biophysica Acta*, 1850:449–460, 2015.

[52] A. J. Smith, J. L. P. M. Timmermans-Hereijgers, B. Roelofsenc, K. W. A. Wirtz, W. J. van Blitterswijk, J. J. M. Smit, A. H. Schinkel, and P. Borst. The human MDR3 P-glycoprotein promotes translocation of phosphatidylcholine through the plasma membrane of fibroblasts from transgenic mice. *FEBS Letters*, 354:263–266, 1994.

[53] A. van Helvoort, A. J. Smith, H. Sprong, I. Fritzsche, A. H. Schinkel, P. Borst, and G. van Meer. MDR1 P-glycoprotein is a lipid translocase of broad specificity, while MDR3 P-glycoprotein specifically translocates phosphatidylcholine. *Cell*, 87:507–517, 1996.

[54] J. Noé, B. Stieger, and P. J. Meier. Functional expression of the canalicular bile salt export pump of human liver. *Gastroenterology*, 123:1659–1666, 2002.

[55] K. G. Chen, G. Szakács, J. P. Annereau, F. Rouzaud, X. J. Liang, J. C. Valencia, C. N. Nagineni, J. J. Hooks, V. J. Hearing, and M. M. Gottesman. Principal expression of two mRNA isoforms (ABCB5α and ABCB5β) of the ATP-binding cassette transporter gene ABCB5 in melanoma cells and melanocytes. *Pigment Cell Research*, 18:102–112, 2005.

[56] N. Y. Frank, A. Margaryan, Y. Huang, T. Schatton, A. M. Waaga-Gasser, M. Gasser, M. H. Sayegh, W. Sadee, and M. H. Frank. ABCB5-mediated doxorubicin transport and chemoresistance in human malignant melanoma. *Cancer Research*, 65:4320–4333, 2005.

[57] R. Abele and R. Tampé. The ABCs of immunology: structure and function of TAP, the transporter associated with antigen processing. *Physiology*, 19:216–224, 2004.

[58] H. de La Salle, D. Hanau, D. Fricker, A. Urlacher, A. Kelly, J. Salamero, S. H. Powis, L. Donato, H. Bausinger, M. Laforet, M. Jeras, D. Spehner, T. Bieber, A. Falkenrodt, J. P. Cazenave, J. Trowsdale, and M. M. Tongio. Homozygous human TAP peptide transporter mutation in HLA class I deficiency. *Science*, 265:237–241, 1994.

[59] H. de La Salle, J. Zimmer, D. Fricker, C. Angenieux, J. P. Cazenave, M. Okubo, H. Maeda, A. Plebani, M. M. Tongio, A. Dormoy, and D. Hanau. HLA class I deficiencies due to mutations in subunit 1 of the peptide transporter TAP1. *The Journal of Clinical Investigation*, 103:R9–R13, 1999.

[60] T. Zollmann, C. Bock, P. Graab, and R. Abele. Team work at its best – TAPL and its two domains. *Biological Chemistry*, 396:967–974, 2015.

[61] A. Zutz, S. Gompf, H. Schägger, and R. Tampé. Mitochondrial ABC proteins in health and disease. *Biochimica et Biophysica Acta*, 1787:681–690, 2009.

[62] J. R. Riordan, J. M. Rommens, B. S. Kerem, N. Alon, R. Rozmahel, Z. Grzelczak, J. Zielenski, S. Lok, N. Plavsic, J. L. Chou, M. L. Drumm, M. C. Iannuzzi, F. S. Collins, and L. C. Tsui. Identification of the cystic fibrosis gene: cloning and characterization of complementary DNA. *Science*, 245:1066–1073, 1989.

[63] J. Riordan. The cystic fibrosis transmembrane conductance regulator. *Annual Review of Physiology*, 55:609–630, 1993.

[64] J. Bryan, A. Muñoz, X. Zhang, M. Düfer, G. Drews, P. Krippeit-Drews, and L. Aguilar-Bryan. ABCC8 and ABCC9: ABC transporters that regulate K^+ channels. *Pflugers Archiv : European Journal of Physiology*, 453:703–718, 2007.

[65] UniProt (universal protein database). URL http://www.uniprot.org.

[66] J. Gärtner, H. Moser, and D. Valle. Mutations in the 70K peroxisomal membrane protein gene in Zellweger syndrome. *Nature Genetics*, 1:16–23, 1992.

[67] A. Holzinger, S. Kammerer, and A. A. Roscher. Primary structure of human PMP69, a putative peroxisomal ABC-transporter. *Biochemical and Biophysical Research Communications*, 237:152–157, 1997.

[68] G. Lombard-Platet, S. Savary, C. O. Sarde, J. L. Mandel, and G. Chimini. A close relative of the adrenoleukodystrophy (ALD) gene codes for a peroxisomal protein with a specific expression pattern. *Proceedings of the National Academy of Sciences of the United States of America*, 93: 1265–1269, 1996.

[69] J. Mosser, A. M. Douar, C. O. Sarde, P. Kioschis, R. Feil, H. Moser, A. M. Poustka, J. L. Mandel, and P. Aubourg. Putative X-linked adrenoleukodystrophy gene shares unexpected homology with ABC transporters. *Nature*, 361:726–730, 1993.

[70] A. Netik, S. Forss-Petter, A. Holzinger, B. Molzer, G. Unterrainer, and J. Berger. Adrenoleukodystrophy-related protein can compensate functionally for adrenoleukodystrophy protein deficiency (X-ALD): implications for therapy. *Human Molecular Genetics*, 8:907–913, 1999.

[71] P. Roerig, P. Mayerhofer, A. Holzinger, and J. Gärtner. Characterization and functional analysis of the nucleotide binding fold in human peroxisomal ATP binding cassette transporters. *FEBS Letters*, 492:66–72, 2001.

[72] S. Ferdinandusse, G. Jimenez-Sanchez, J. Koster, S. Denis, C. W. van Roermund, I. Silva-Zolezzi, A. B. Moser, W. F. Visser, M. Gulluoglu, O. Durmaz, M. Demirkol, H. R. Waterham, G. Gökcay, R. J. A. Wanders, and D. Valle. A novel bile acid biosynthesis defect due to a deficiency of peroxisomal ABCD3. *Human Molecular Genetics*, 24:361–370, 2015.

[73] K. Kawaguchi, T. Okamoto, M. Morita, and T. Imanaka. Translocation of the ABC transporter ABCD4 from the endoplasmic reticulum to lysosomes requires the escort protein LMBD1. *Scientific Reports*, 6:30183, 2016.

[74] E. Nürenberg and R. Tampé. Tying up loose ends: ribosome recycling in eukaryotes and archaea. *Trends in Biochemical Sciences*, 38:64–74, 2013.

[75] S. Paytubi, X. Wang, Y. W. Lam, L. Izquierdo, M. J. Hunter, E. Jan, H. S. Hundal, and C. G. Proud. ABC50 promotes translation initiation in mammalian cells. *The Journal of Biological Chemistry*, 284:24061–24073, 2009.

[76] J. Klucken, C. Buchler, E. Orso, W. E. Kaminski, M. Porsch-Ozcurumez, G. Liebisch, M. Kapinsky, W. Diederich, W. Drobnik, M. Dean, R. Allikmets, and G. Schmitz. ABCG1 (ABC8), the human homolog of the Drosophila white gene, is a regulator of macrophage cholesterol and phospholipid transport. *Proceedings of the National Academy of Sciences of the United States of America*, 97: 817–822, 2000.

[77] A. M. Vaughan and J. F. Oram. ABCA1 and ABCG1 or ABCG4 act sequentially to remove cellular cholesterol and generate cholesterol-rich HDL. *Journal of Lipid Research*, 47:2433–2443, 2006.

[78] J. Cserepes, Z. Szentpétery, L. Seres, C. Ozvegy-Laczka, T. Langmann, G. Schmitz, H. Glavinas, I. Klein, L. Homolya, A. Váradi, B. Sarkadi, and N. B. Elkind. Functional expression and characterization of the human ABCG1 and ABCG4 proteins: indications for heterodimerization. *Biochemical and Biophysical Research Communications*, 320:860–867, 2004.

[79] J. E. Diestra, G. L. Scheffer, I. Català, M. Maliepaard, J. H. M. Schellens, R. J. Scheper, J. R. Germà-Lluch, and M. A. Izquierdo. Frequent expression of the multi-drug resistance-associated protein BCRP/MXR/ABCP/ABCG2 in human tumours detected by the BXP-21 monoclonal antibody in paraffin-embedded material. *The Journal of Pathology*, 198:213–219, 2002.

[80] G. A. Graf, L. Yu, W. P. Li, R. Gerard, P. L. Tuma, J. C. Cohen, and H. H. Hobbs. ABCG5 and ABCG8 are obligate heterodimers for protein trafficking and biliary cholesterol excretion. *The Journal of Biological Chemistry*, 278:48275–48282, 2003.

[81] K. E. Berge, H. Tian, G. A. Graf, L. Yu, N. V. Grishin, J. Schultz, P. Kwiterovich, B. Shan, R. Barnes, and H. H. Hobbs. Accumulation of dietary cholesterol in sitosterolemia caused by mutations in adjacent ABC transporters. *Science*, 290:1771–1775, 2000.

[82] Anthony M. George, editor. *ABC Transporters - 40 Years on*. Springer International Publishing, 1st ed. 2016 edition, 2016.

[83] D. C. Yang, N. T. Peters, K. R. Parzych, T. Uehara, M. Markovski, and T. G. Bernhardt. An ATP-binding cassette transporter-like complex governs cell-wall hydrolysis at the bacterial cytokinetic ring. *Proceedings of the National Academy of Sciences of the United States of America*, 108: E1052–60, 2011.

[84] Z. Zhou, K. A. White, A. Polissi, C. Georgopoulos, and C. R. H. Raetz. Function of *Escherichia coli* MsbA, an essential ABC family transporter, in lipid A and phospholipid biosynthesis. *Journal of Biological Chemistry*, 273:12466–12475, 1998.

[85] P. D. W. Eckford and F. J. Sharom. The reconstituted *Escherichia coli* MsbA protein displays lipid flippase activity. *The Biochemical Journal*, 429:195–203, 2010.

[86] G. Reuter, T. Janvilisri, H. Venter, S. Shahi, L. Balakrishnan, and H. W. van Veen. The ATP binding cassette multidrug transporter LmrA and lipid transporter MsbA have overlapping substrate specificities. *The Journal of Biological Chemistry*, 278:35193–35198, 2003.

[87] A. Zutz, J. Hoffmann, U. A. Hellmich, C. Glaubitz, B. Ludwig, B. Brutschy, and R. Tampé. Asymmetric ATP hydrolysis cycle of the heterodimeric multidrug ABC transport complex TmrAB from Thermus thermophilus. *The Journal of Biological Chemistry*, 286:7104–7115, 2011.

[88] Jardetzky O. Simple allosteric model for membrane pumps. *Nature*, 211:969–970, 1966.

[89] K. P. Locher. Mechanistic diversity in ATP-binding cassette (ABC) transporters. *Nature Structural & Molecular Biology*, 23:487–493, 2016.

[90] N. Grossmann, A. Vakkasoglu, S., S. Hulpke, R. Abele, R. Gaudet, and R. Tampé. Mechanistic determinants of the directionality and energetics of active export by a heterodimeric ABC transporter. *Nature Communications*, 5:5419, 2014.

[91] E. Procko, M. L. O'Mara, W. F. D. Bennett, D. P. Tieleman, and R. Gaudet. The mechanism of ABC transporters: general lessons from structural and functional studies of an antigenic peptide transporter. *FASEB Journal*, 23:1287–1302, 2009.

[92] K. Bountra, G. Hagelueken, H. G. Choudhury, V. Corradi, K. El Omari, A. Wagner, I. Mathavan, S. Zirah, W. Yuan Wahlgren, D. P. Tieleman, O. Schiemann, S. Rebuffat, and K. Beis. Structural basis for antibacterial peptide self-immunity by the bacterial ABC transporter McjD. *The EMBO Journal*, 36:3062–3079, 2017.

[93] J. Trowsdale, I. Hanson, I. Mockridge, S. Beck, A. Townsend, and A. Kelly. Sequences encoded in the class II region of the MHC related to the 'ABC' superfamily of transporters. *Nature*, 348: 741–744, 1990.

[94] E. V. Deverson, I. R. Gow, W. J. Coadwell, J. J. Monaco, G. W. Butcher, and J. C. Howard. MHC class II region encoding proteins related to the multidrug resistance family of transmembrane transporters. *Nature*, 348:738–741, 1990.

[95] J. Koch, R. Guntrum, S. Heintke, C. Kyritsis, and R. Tampé. Functional dissection of the transmembrane domains of the transporter associated with antigen processing (TAP). *The Journal of Biological Chemistry*, 279:10142–10147, 2004.

[96] J. Koch and R. Tampé. The macromolecular peptide-loading complex in MHC class I-dependent antigen presentation. *Cellular and Molecular Life Sciences*, 63:653–662, 2006.

[97] K. Keusekotten, R. M. Leonhardt, S. Ehses, and M. R. Knittler. Biogenesis of functional antigenic peptide transporter TAP requires assembly of pre-existing TAP1 with newly synthesized TAP2. *The Journal of Biological Chemistry*, 281:17545–17551, 2006.

[98] P. M. van Endert, R. Tampé, T. H. Meyer, R. Tisch, J.-F. Bach, and H. O. McDevitt. A sequential model for peptide binding and transport by the transporters associated with antigen processing. *Immunity*, 1:491–500, 1994.

[99] A. Blees, K. Reichel, S. Trowitzsch, O. Fisette, C. Bock, R. Abele, G. Hummer, L. V. Schäfer, and R. Tampé. Assembly of the MHC I peptide-loading complex determined by a conserved ionic lock-switch. *Scientific Reports*, 5:17341, 2015.

[100] M. J. Androlewicz and P. Cresswell. Human transporters associated with antigen processing possess a promiscuous peptide-binding site. *Immunity*, 1:7–14, 1994.

[101] S. Uebel, T. H. Meyer, W. Kraas, S. Kienle, G. Jung, K. H. Wiesmüller, and Tampé, R. Requirements for peptide binding to the human transporter associated with antigen processing revealed by peptide scans and complex peptide libraries. *Journal of Biological Chemistry*, 270:18512–18516, 1995.

[102] S. Uebel, W. Kraas, S. Kienle, K.-H. Wiesmuller, G. Jung, and R. Tampé. Recognition principle of the TAP transporter disclosed by combinatorial peptide libraries. *Proceedings of the National Academy of Sciences of the United States of America*, 94:8976–8981, 1997.

[103] E. Lehnert, J. Mao, A. R. Mehdipour, G. Hummer, R. Abele, C. Glaubitz, and R. Tampé. Antigenic peptide recognition on the human ABC transporter TAP resolved by DNP-enhanced solid-state NMR spectroscopy. *Journal of the American Chemical Society*, 138:13967–13974, 2016.

[104] E. Procko, I. Ferrin-O'Connell, S.-L. Ng, and R. Gaudet. Distinct structural and functional properties of the ATPase sites in an asymmetric ABC transporter. *Molecular Cell*, 24:51–62, 2006.

[105] T. Oshima and K. Imahori. Description of *Thermus thermophilus* (Yoshida and Oshima) comb. nov., a nonsporulating thermophilic bacterium from a japanese thermal spa. *International Journal of Systematic Bacteriology*, 24:102–112, 1974.

[106] J. Kim, S. Wu, T. M. Tomasiak, C. Mergel, M. B. Winter, S. B. Stiller, Y. Robles-Colmanares, R. M. Stroud, R. Tampé, C. S. Craik, and Y. Cheng. Subnanometre-resolution electron cryomicroscopy structure of a heterodimeric ABC exporter. *Nature*, 517:396–400, 2015.

[107] C. Bechara, A. Nöll, N. Morgner, M. T. Degiacomi, R. Tampé, and C. V. Robinson. A subset of annular lipids is linked to the flippase activity of an ABC transporter. *Nature Chemistry*, 7: 255–262, 2015.

[108] C. A. Janeway, P. Travers, M. Walport, and M. Shlomchik. *Immunobiology - The immune system in health and disease*. Garland Publishing, New York , 2001.

[109] G. E. Hammer, F. Gonzalez, E. James, H. Nolla, and N. Shastri. In the absence of aminopeptidase ERAAP, MHC class I molecules present many unstable and highly immunogenic peptides. *Nature Immunology*, 8:101–108, 2007.

[110] D. R. Peaper and P. Cresswell. Regulation of MHC class I assembly and peptide binding. *Annual Review of Cell and Developmental Biology*, 24:343–368, 2008.

[111] A. Blees, D. Januliene, T. Hofmann, N. Koller, C. Schmidt, S. Trowitzsch, A. Moeller, and R. Tampé. Structure of the human MHC-I peptide-loading complex. *Nature*, 551:525–528, 2017.

[112] A. P. Williams, C. A. Peh, A. W. Purcell, J. McCluskey, and T. Elliott. Optimization of the MHC class I peptide cargo is dependent on tapasin. *Immunity*, 16:509–520, 2002.

[113] M. Howarth, A. Williams, A. B. Tolstrup, and T. Elliott. Tapasin enhances MHC class I peptide presentation according to peptide half-life. *Proceedings of the National Academy of Sciences of the United States of America*, 101:11737–11742, 2004.

[114] G. Fleischmann, O. Fisette, C. Thomas, R. Wieneke, F. Tumulka, C. Schneeweiss, S. Springer, L. V. Schäfer, and R. Tampé. Mechanistic basis for epitope proofreading in the peptide-loading complex. *Journal of Immunology*, 195:4503–4513, 2015.

[115] T. Saric, S.-C. Chang, A. Hattori, I. A. York, S. Markant, K. L. Rock, M. Tsujimoto, and A. L. Goldberg. An IFN-gamma-induced aminopeptidase in the ER, ERAP1, trims precursors to MHC class I-presented peptides. *Nature Immunology*, 3:1169–1176, 2002.

[116] G. E. Hammer, F. Gonzalez, E. James, H. Nolla, and N. Shastri. In the absence of aminopeptidase ERAAP, MHC class I molecules present many unstable and highly immunogenic peptides. *Nature Immunology*, 8:101–108, 2007.

[117] D. R. Peaper, P. A. Wearsch, and P. Cresswell. Tapasin and ERp57 form a stable disulfidelinked dimer within the MHC class I peptideloading complex. *The EMBO Journal*, 24:3613–3623, 2005.

[118] S. Springer. Transport and quality control of MHC class I molecules in the early secretory pathway. *Current Opinion in Immunology*, 34:83–90, 2015.

[119] L. H. Boyle, C. Hermann, J. M. Boname, K. M. Porter, P. A. Patel, M. L. Burr, L. M. Duncan, M. E. Harbour, D. A. Rhodes, K. Skjødt, P. J. Lehner, and J. Trowsdale. Tapasin-related protein TAPBPR is an additional component of the MHC class I presentation pathway. *Proceedings of the National Academy of Sciences of the United States of America*, 110:3465–3470, 2013.

[120] C. Thomas and R. Tampé. Structure of the TAPBPR-MHC I complex defines the mechanism of peptide loading and editing. *Science*, 358:1060–1064, 2017.

[121] A. Neerincx, C. Hermann, R. Antrobus, A. van Hateren, H. Cao, N. Trautwein, S. Stevanović, T. Elliott, J. E. Deane, and L. H. Boyle. TAPBPR bridges UDP-glucose:glycoprotein glucosyltransferase 1 onto MHC class I to provide quality control in the antigen presentation pathway. *eLife*, 6: e23049, 2017.

[122] P. U. Mayerhofer and R. Tampé. Antigen translocation machineries in adaptive immunity and viral immune evasion. *Journal of Molecular Biology*, 427:1102–1118, 2015.

[123] D. Alzhanova, D. M. Edwards, E. Hammarlund, I. G. Scholz, D. Horst, M. J. Wagner, C. Upton, E. J. Wiertz, M. K. Slifka, and K. Früh. Cowpox virus inhibits the transporter associated with antigen processing to evade T cell recognition. *Cell Host & Microbe*, 6:433–445, 2009.

[124] M. E. Ressing, R. D. Luteijn, D. Horst, and E. J. Wiertz. Viral interference with antigen presentation: trapping TAP. *Molecular Immunology*, 55:139–142, 2013.

[125] A. Hinz and R. Tampé. ABC transporters and immunity: mechanism of self-defense. *Biochemistry*, 51:4981–4989, 2012.

[126] R. J. Whitley, D. W. Kimberlin, and B. Roizman. Herpes simplex viruses. *Clinical Infectious Diseases*, 26:541–555, 1998.

[127] R. W. Honess and B. Roizman. Proteins specified by herpes simplex virus. *Journal of Virology*, 12: 1347–1365, 1973.

[128] R. J. Watson, C. M. Preston, and B. Clements. Separation and characterization of herpes simplex virus type 1 immediate-early mRNA's. *Journal of Virology*, 31:42–52, 1979.

[129] C. Aisenbrey, C. Sizun, J. Koch, M. Herget, R. Abele, B. Bechinger, and R. Tampé. Structure and dynamics of membrane-associated ICP47, a viral inhibitor of the MHC I antigen-processing machinery. *The Journal of Biological Chemistry*, 281:30365–30372, 2006.

[130] A. Hill, P. Jugovic, I. York, G. Russ, J. Bennink, J. Yewdell, H. Ploegh, and D. Johnson. Herpes simplex virus turns off the TAP to evade host immunity. *Nature*, 375:411–415, 1995.

[131] I. A. York, C. Roop, D. W. Andrews, S. R. Riddell, F. L. Graham, and D. C. Johnson. A cytosolic herpes simplex virus protein inhibits antigen presentation to $CD8^+$ T lymphocytes. *Cell*, 77: 525–535, 1994.

[132] E. A. Hughes, C. Hammond, and P. Cresswell. Misfolded major histocompatibility complex class I heavy chains are translocated into the cytoplasm and degraded by the proteasome. *Proceedings of the National Academy of Sciences of the United States of America*, 94:1896–1901, 1997.

[133] D. Beinert, L. Neumann, S. Uebel, and R. Tampé. Structure of the viral TAP-inhibitor ICP47 induced by membrane association. *Biochemistry*, 36:4694–4700, 1997.

[134] R. Pfänder, L. Neumann, M. Zweckstetter, C. Seger, T. A. Holak, and R. Tampé. Structure of the active domain of the herpes simplex virus protein ICP47 in water/sodium dodecyl sulfate solution determined by nuclear magnetic resonance spectroscopy. *Biochemistry*, 38:13692–13698, 1999.

[135] R. Tomazin, N. E. van Schoot, K. Goldsmith, P. Jugovic, P. Sempé, K. Früh, and D. C. Johnson. Herpes simplex virus type 2 ICP47 inhibits human TAP but not mouse TAP. *Journal of Virology*, 72:2560–2563, 1998.

[136] K. Ahn, A. Gruhler, B. Galocha, T. R. Jones, E. J. H. J. Wiertz, H. L. Ploegh, P. A. Peterson, Y. Yang, and K. Früh. The ER-luminal domain of the HCMV glycoprotein US6 inhibits peptide translocation by TAP. *Immunity*, 6:613–621, 1997.

[137] H. Hengel, J.-O. Koopmann, T. Flohr, W. Muranyi, E. Goulmy, G. J. Hämmerling, U. H. Koszinowski, and F. Momburg. A viral ER-resident glycoprotein inactivates the MHC-encoded peptide transporter. *Immunity*, 6:623–632, 1997.

[138] P. J. Lehner, J. T. Karttunen, G. W. G. Wilkinson, and P. Cresswell. The human cytomegalovirus US6 glycoprotein inhibits transporter associated with antigen processing-dependent peptide translocation. *Proceedings of the National Academy of Sciences of the United States of America*, 94: 6904–6909, 1997.

[139] E. W. Hewitt, S. S. Gupta, and P. J. Lehner. The human cytomegalovirus gene product US6 inhibits ATP binding by TAP. *The EMBO Journal*, 20:387–396, 2001.

[140] C. Kyritsis, S. Gorbulev, S. Hutschenreiter, K. Pawlitschko, R. Abele, and R. Tampé. Molecular mechanism and structural aspects of transporter associated with antigen processing inhibition by the cytomegalovirus protein US6. *The Journal of Biological Chemistry*, 276:48031–48039, 2001.

[141] A. Halenius, F. Momburg, H. Reinhard, D. Bauer, M. Lobigs, and H. Hengel. Physical and functional interactions of the cytomegalovirus US6 glycoprotein with the transporter associated with antigen processing. *The Journal of Biological Chemistry*, 281:5383–5390, 2006.

[142] M. C. Verweij, A. D. Lipinska, D. Koppers-Lalic, W. F. van Leeuwen, J. I. Cohen, P. R. Kinchington, I. Messaoudi, K. Bienkowska-Szewczyk, M. E. Ressing, F. A. M. Rijsewijk, and E. J. H. J. Wiertz. The capacity of UL49.5 proteins to inhibit TAP is widely distributed among members of the genus Varicellovirus. *Journal of Virology*, 85:2351–2363, 2011.

[143] D. Koppers-Lalic, E. A. J. Reits, M. E. Ressing, A. D. Lipinska, R. Abele, J. Koch, M. Marcondes Rezende, P. Admiraal, D. van Leeuwen, K. Bienkowska-Szewczyk, T. C. Mettenleiter, F. A. M. Rijsewijk, R. Tampé, J. Neefjes, and E. J. H. J. Wiertz. Varicelloviruses avoid T cell recognition by UL49.5-mediated inactivation of the transporter associated with antigen processing. *Proceedings of the National Academy of Sciences of the United States of America*, 102:5144–5149, 2005.

[144] D. Koppers-Lalic, M. C. Verweij, A. D. Lipińska, Y. Wang, E. Quinten, E. A. Reits, J. Koch, S. Loch, M. Marcondes Rezende, F. Daus, K. Bieńkowska-Szewczyk, N. Osterrieder, T. C. Mettenleiter, M. H. M. Heemskerk, R. Tampé, J. J. Neefjes, S. I. Chowdhury, M. E. Ressing, F. A. M. Rijsewijk, and E. J. H. J. Wiertz. Varicellovirus UL 49.5 proteins differentially affect the function of the transporter associated with antigen processing, TAP. *PLoS Pathogens*, 4:e1000080, 2008.

[145] S. Loch, F. Klauschies, C. Schölz, M. C. Verweij, E. J. H. J. Wiertz, J. Koch, and R. Tampé. Signaling of a varicelloviral factor across the endoplasmic reticulum membrane induces destruction of the peptide-loading complex and immune evasion. *The Journal of Biological Chemistry*, 283: 13428–13436, 2008.

[146] M. E. Ressing, S. E. Keating, D. van Leeuwen, D. Koppers-Lalic, I. Y. Pappworth, E. J. H. J. Wiertz, and M. Rowe. Impaired transporter associated with antigen processing-dependent peptide transport during productive EBV infection. *The Journal of Immunology*, 174:6829–6838, 2005.

[147] D. Horst, D. van Leeuwen, N. P. Croft, M. A. Garstka, A. D. Hislop, E. Kremmer, A. B. Rickinson, E. J. H. J. Wiertz, and M. E. Ressing. Specific targeting of the EBV lytic phase protein BNLF2a to the transporter associated with antigen processing results in impairment of HLA class I-restricted antigen presentation. *Journal of Immunology*, 182:2313–2324, 2009.

[148] N. P. Croft, C. Shannon-Lowe, A. I. Bell, D. Horst, E. Kremmer, M. E. Ressing, E. J. H. J. Wiertz, J. M. Middeldorp, M. Rowe, A. B. Rickinson, and A. D. Hislop. Stage-specific inhibition of MHC class I presentation by the Epstein-Barr virus BNLF2a protein during virus lytic cycle. *PLoS Pathogens*, 5:e1000490, 2009.

[149] A. I. Wycisk, J. Lin, S. Loch, K. Hobohm, J. Funke, R. Wieneke, J. Koch, W. R. Skach, P. U. Mayerhofer, and R. Tampé. Epstein-Barr viral BNLF2a protein hijacks the tail-anchored protein insertion machinery to block antigen processing by the transport complex TAP. *The Journal of Biological Chemistry*, 286:41402–41412, 2011.

[150] D. Horst, V. Favaloro, F. Vilardi, H. C. van Leeuwen, M. A. Garstka, A. D. Hislop, C. Rabu, E. Kremmer, A. B. Rickinson, S. High, B. Dobberstein, M. E. Ressing, and E. J. H. J. Wiertz. EBV protein BNLF2a exploits host tail-anchored protein integration machinery to inhibit TAP. *Journal of Immunology*, 186:3594–3605, 2011.

[151] D. Horst, S. R. Burrows, D. Gatherer, B. van Wilgenburg, M. J. Bell, I. G. J. Boer, M. E. Ressing, and E. J. H. J. Wiertz. Epstein-Barr virus isolates retain their capacity to evade T cell immunity through BNLF2a despite extensive sequence variation. *Journal of Virology*, 86:572–577, 2012.

[152] M. Byun, M. C. Verweij, D. J. Pickup, E. J. H. J. Wiertz, T. H. Hansen, and W. M. Yokoyama. Two mechanistically distinct immune evasion proteins of cowpox virus combine to avoid antiviral CD8 T cells. *Cell Host & Microbe*, 6:422–432, 2009.

[153] N. Lerner-Marmarosh, K. Gimi, I. L. Urbatsch, P. Gros, and A. E. Senior. Large scale purification of detergent-soluble P-glycoprotein from *Pichia pastoris* cells and characterization of nucleotide binding properties of wild-type, Walker A, and Walker B mutant proteins. *Journal of Biological Chemistry*, 274:34711–34718, 1999.

[154] E. R. Geertsma and R. Dutzler. A versatile and efficient high-throughput cloning tool for structural biology. *Biochemistry*, 50:3272–3278, 2011.

[155] A. Hinz, J. Jedamzick, V. Herbring, H. Fischbach, J. Hartmann, D. Parcej, J. Koch, and R. Tampé. Assembly and function of the major histocompatibility complex MHC I peptide-loading complex are conserved across higher vertebrates. *Journal of Biological Chemistry*, 289:33109–33117, 2014.

[156] C. M. Armstrong and F. Bezanilla. Inactivation of the sodium channel: II. Gating current experiments. *The Journal of General Physiology*, 70:R9–R13, 1977.

[157] A. Bäucker (née Swistek). *Generierung eines durch virale Faktoren konformationell arretierten Antigen-Translokationskomplexes TAP*. Goethe Universität Frankfurt am Main, 2013. Bachelor Thesis.

[158] M. D. Ryan, A. M. Q. King, and G. P. Thomas. Cleavage of foot-and-mouth disease virus polyprotein is mediated by residues located within a 19 amino acid sequence. *Journal of General Virology*, 72:2727–2732, 1991.

[159] A. Castelló, E. Alvarez, and L. Carrasco. The multifaceted poliovirus 2A protease: regulation of gene expression by picornavirus proteases. *Journal of Biomedicine & Biotechnology*, 2011:369648, 2011.

[160] E. Minskaia, J. Nicholson, and M. D. Ryan. Optimisation of the foot-and-mouth disease virus 2A co-expression system for biomedical applications. *BMC Biotechnology*, 13:67, 2013.

[161] C. Rehwald. *Klonierung, Expression und Isolierung von verschiedenen Fusionsproteinen des Antigentransportkomplexes TAP.* Goethe Universität Frankfurt am Main, 2013. Bachelor Thesis.

[162] P. Praest, R. D. Luteijn, I. G. J. Brak-Boer, J. Lanfermeijer, H. Hoelen, L. Ijgosse, A. I. Costa, R. D. Gorham, R. J. Lebbink, and E. J. H. J. Wiertz. The influence of TAP1 and TAP2 gene polymorphisms on TAP function and its inhibition by viral immune evasion proteins. *Molecular Immunology*, 101:55–64, 2018.

[163] Y. H. Abacioglu, T. R. Fouts, J. D. Laman, E. Claassen, S. H. Pincus, J. P. Moore, C. A. Roby, R. Kamin-Lewis, and G. K. Lewis. Epitope mapping and topology of baculovirus-expressed hiv-1 gp160 determined with a panel of murine monoclonal antibodies. *Aids Research and Human Retroviruses*, 10:371–381, 1994.

[164] U. K. Leammli. Cleavage of structural proteins during the assembly of the head of bacteriophage T4. *Nature*, 227:680–685, 1970.

[165] J. Kyhse-Andersen. Electroblotting of multiple gels: a simple apparatus without buffer tank for rapid transfer of proteins from polyacrylamide to nitrocellulose. *Journal of Biochemical and Biophysical Methods*, 10:203–209, 1984.

[166] D. Parcej, R. Guntrum, S. Schmidt, A. Hinz, and R. Tampé. Multicolour fluorescence-detection size-exclusion chromatography for structural genomics of membrane multiprotein complexes. *PloS ONE*, 8:e67112, 2013.

[167] M. Hattori, R. E. Hibbs, and E. Gouaux. A fluorescence-detection size-exclusion chromatography-based thermostability assay for membrane protein precrystallization screening. *Structure*, 20: 1293–1299, 2012.

[168] A. I. Alexandrov, M. Mileni, E. Y. T. Chien, M. A. Hanson, and R. C. Stevens. Microscale fluorescent thermal stability assay for membrane proteins. *Structure*, 16:351–359, 2008.

[169] J. R. Lakowicz. *Principles of Fluorescence Spectroscopy.* Springer Science + Business Media, 3. edition, 2006.

[170] G. G. Privé. Detergents for the stabilization and crystallization of membrane proteins. *Methods*, 41:388–397, 2007.

[171] T. Zollmann. *Single-liposome based mechanistic studies of peptide translocation by the lysosomal ABC transporter TAPL.* Goethe Universität Frankfurt am Main, 2015. Dissertation.

[172] N. Thongin, R. F. Collins, A. Barbieri, T. Shafi, A. Siebert, and R. C. Ford. Novel features in the structure of P-glycoprotein (ABCB1) in the post-hydrolytic state as determined at 7.9Å resolution. *bioRixiv*, 2018.

[173] L. Esser, F. Zhou, K. M. Pluchino, J. Shiloach, J. Ma, W. Tang, C. Gutierrez, A. Zhang, S. Shukla, J. P. Madigan, T. Zhou, P. D. Kwong, S. V. Ambudkar, M. M. Gottesman, and D. Xia. Structures of the multidrug transporter P-glycoprotein reveal asymmetric ATP binding and the mechanism of polyspecificity. *Journal of Biological Chemistry*, 292:446–461, 2017.

[174] C. Bock. *Dimerisation of the TMD0 of the lysosomal ABC-Transporter TAPL (ABCB9) and labeling of single cysteine mutants for NMR measurements.* Goethe Universität Frankfurt am Main, 2013.

[175] S. Eggensperger, O. Fisette, D. Parcej, L. V. Schäfer, and R. Tampé. An annular lipid belt is essential for allosteric coupling and viral inhibition of the antigen translocation complex TAP (transporter associated with antigen processing). *The Journal of Biological Chemistry*, 289:33098–33108, 2014.

[176] B. K. Kay, M. P. Williamson, and M. Sudol. The importance of being proline: the interaction of proline-rich motifs in signaling proteins with their cognate domains. *FASEB Journal*, 14:231–241, 2000.

[177] L. J. Ball, R. Kühne, J. Schneider-Mergener, and H. Oschkinat. Recognition of proline-rich motifs by protein-protein-interaction domains. *Angewandte Chemie*, 44:2852–2869, 2005.

[178] T. Matschulla, R. Berry, C. Gerke, M. Döring, J. Busch, J. Paijo, U. Kalinke, F. Momburg, H. Hengel, and A. Halenius. A highly conserved sequence of the viral TAP inhibitor ICP47 is required for freezing of the peptide transport cycle. *Scientific Reports*, 7(1):2933, 2017.

[179] A. Nagy, A. Málnási-Csizmadia, B. Somogyi, and D. Lőrinczy. Thermal stability of chemically denatured green fluorescent protein (GFP): A preliminary study. *Thermochimica Acta*, 410:161–163, 2004.

[180] L. Gonzalez-Lobato, V. Chaptal, J. Molle, and Falson P. *Leishmania tarentolae as a promising tool for expressing polytopic and multi-transmembrane spans eukaryotic membrane proteins: The case of the ABC pump ABCG6. In: Mus-Veteau I. (eds) Heterologous expression of membrane proteins. Methods in molecular biology.* Humana Press, 2016.

[181] M. Erbakan, B. S. Curtis, B. T. Nixon, M. Kumar, and W. R. Curtis. Advancing *Rhodobacter sphaeroides* as a platform for expression of functional membrane proteins. *Protein Expression and Purification*, 115:109–117, 2015.

Danksagung

- Prof. Dr. Robert Tampé möchte ich an erster Stelle für all meine interessanten und spannenden Projekte danken. Danke für die Unterstützung seit meiner Masterabreit und für die stets anregenden und weiterführenden Disskussionen. Ich möchte mich auch dafür bedanken, dass ich oft die Freiheit hatte eigene Ideen in meine Experimente einzubringen, dies war meistens sehr lehrreich.

- Jun. Prof. Dr. Inga Hänelt danke ich für das Bewerten meiner Arbeit als Zweitgutachterin und für die Tätigkeit als TRAM-Mentorin. Danke für alle konstruktiven Anregungen und danke, dass du stets ein Auge darauf hattest, dass meine Projekte nicht vom Kurs abkamen.

- Ein Dank geht auch an meinen TRAM-Mentor Jun. Prof. Dr. Eric Geertsma, der mir ebenfalls mit stets neuen Ideen zur Seite stand.

- All meinen Kollegen der Tampé-, Abele-, Hänelt- und Ernst-Labore, vor allem den aktuellen und ehemaligen Doktoranden des Labors 1.23, danke ich für die schöne Zeit im, aber auch außerhalb des Labors. Ein großes Dankeschön auch an alle, die mitgeholfen haben die Pizzabackabende auf die Beine zu stellen!

- Nicole Koller und Philipp Graab danke ich für die Unterstützung und Geduld bei Mikroskopie-Experimenten.

- Ich möchte mich bei Prof. Dr. Werner Kühlbrandt am Max-Planck-Institut für Biophysik in Frankfurt für die Bereitstellung der *negative-stain* EM-Ausstattung bedanken. Susanne Hofmann danke ich für die *negative-stain* EM Analyse meiner Proben.

- Henri de la Salle (Straßburg, Frankreich) danke ich für das Bereitstellen der TAP-defizienten Zelllinien BRE-169 und STF1-169.

- Prof. Dr. Emmanuel Wiertz (Utrecht, Niederlande) danke ich für die TAP-defiziente MelJuSo Zelllinie, die hoffentlich auch zukünftige Experimente vereinfachen wird.

- Ein großer Dank geht auch an all meine Praktikanten und HiWis. Besonders möchte ich mich bei Anja Bäucker, Martina Barends, Carolina Kuge und Esteban Günther Castillo für die Unterstützung meiner Projekte bedanken.

- Ich danke Martin, Barbara, Martina und meiner Mutter, die sich bereit erklärt haben meine Arbeit korrekturzulesen. Ein besonderer Dank geht allerdings an Dr. Simon Trowitzsch, der zusätzlich dabei geholfen hat die Arbeit an diversen Stellen zurechtzurücken.

- Zuletzt möchte ich noch meiner Familie und Martin für die Unterstützung, vor allem in der letzten Phase meiner Arbeit danken.

Curriculum vitae

Personal data

Name	Valentina Herbring
Date of birth	02.06.1989
Place of birth	Münster (NRW), Germany
Nationality	German, Italian

Academic qualifications

05/2014 - present	**PhD student in Biochemistry**, Goethe University Frankfurt Institute of Biochemistry, Prof. Robert Tampé
10/2011 - 04-2014	**Master of Science in Biomolecular Engineering**, TU Darmstadt
10/2013 - 04-2014	**Master thesis** in the group of Prof. Robert Tampé, Goethe University Frankfurt: "Functional stabilization of the transporter associated with antigen processing TAP"
10/2008 - 09/2011	**Bachelor of Science in Biomolecular Engineering**, TU Darmstadt
04/2011 - 06/2011	**Bachelor thesis** in the group of Prof. Ralf Kaldenhoff, TU Darmstadt: "Charakterisierung eines codon-optimierten Aquaporins in Hefe"
06/2008	**Allgemeine Hochschulreife**, Elisabeth von Thadden Schule Heidelberg

Scholarships

01/2015 - 12/2016	IMPRS graduate program fellowship of the Max Planck Institutes
05/2014 - 11/2014	PhD fellowship of the MGK - Integrated research training group "TRAM"of the CRC 807

Conferences

2012 - 2017	Mosbacher Kolloquium of the German Society for Biochemistry and Molecular Biology (GBM), Mosbach, Germany Activity: **Poster presentations**
2014 - 2017	International Summer School of the Institute of Biochemistry, Goethe University Frankfurt, Hirschegg, Austria Activity: **Oral presentations**
2011	Molecular Life Sciences (GBM), Frankfurt a. M.
2014	Biophysics of channels and transporters (FEBS/EMBO Lecture Course), Ettore Majorana Foundation and Centre, Erice Sicily Activity: **Poster presentation**
2014, 2017	Membrane Transport and Communication (CRC 807 International Symposium), Frankfurt a.M., Germany Activity: **Poster presentation**
2016, 2018	ABC 2016: ATP-Binding Cassette (ABC) Proteins: From Multidrug Resistance to Genetic Diseases, Innsbruck, Austria Activity: **Poster and oral presentations**

Memberships

2011 - present	Member of the society for biochemistry and molecular biology (GBM)
2014 - present	Integrated research training group of the collaborative research center 807
2015 - present	IMPRS graduate program of the Max Planck institutes